NASA TECHNICAL MEMORANDUM NASA TM-76731

LIGHT FIELDS IN THE OCEAN

V. N. Pelevin, M.V. Kozlyaninov

(NASA-TM-76731) LIGHT FIELDS IN THE OCEAN (National Aeronautics and Space Administration) 267 p HC A12/MF A01 N82-14790

CSCL 08C Unclas
G3/48 08604

Translation of "Svetovyye polya v okeane". Moscow, P.P. Shirshov Institute of Oceanology, USSR Academy of Sciences, Moscow, 1979, pp 1 - 232 and pp 243 - 258

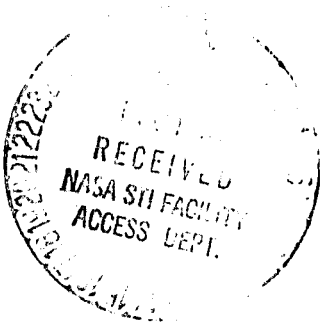

NATIONAL AERONAUTICS AND SPACE ADMINISTRATION
WASHINGTON D.C. 20546 NOVEMBER 1981

STANDARD TITLE PAGE

1. Report No. NASA TM-76731	2. Government Accession No.	3. Recipient's Catalog No.
4. Title and Subtitle: LIGHT FIELDS IN THE OCEAN		5. Report Date NOVEMBER 1981
		6. Performing Organization Code
7. Author(s) V. N. Pelevin, M. V. Kozlyaninov		8. Performing Organization Report No.
		10. Work Unit No.
9. Performing Organization Name and Address SCITRAN Box 5456 Santa Barbara, CA 93108		11. Contract or Grant No. NASw-3542
		13. Type of Report and Period Covered Translation
12. Sponsoring Agency Name and Address National Aeronautics and Space Administration Washington, D.C. 20546		14. Sponsoring Agency Code

15. Supplementary Notes

Translation of "Svetovyye Polya v Okeane", Moscow, P. P. Shirshov Institute of Oceanology, USSR Academy of Sciences, Moscow, 1979, pp. 1-232 and 243-258.

16. Abstract

This book is a study of light fields in the ocean. This is a basic problem of ocean optics. For this purpose, these twenty six separate studies have been collected. The material has been grouped into three sections:

1) Theoretical and experimental studies of the field of solar radiation in the ocean.
2) Study of stationary and nonstationary light fields created in the sea by artificial sources.
3) Use of optical methods to study biological and hydrodynamic characteristics of the sea.

17. Key Words (Selected by Author(s))	18. Distribution Statement: Unclassified - Unlimited		
19. Security Classif. (of this report) Unclassified	20. Security Classif. (of this page) Unclassified	21. No. of Pages 267	22. Price

Table of Contents

LIGHT FIELDS IN THE OCEAN

Edited by

Doctor of Physical and Mathematical Sciences V. N. Pelevin
and Candidate of Geographical
Sciences M. V. Kozlyaninov*

FOREWORD /5**

Study of light fields in the ocean is a basic problem of ocean optics. Although a light field in a turbid medium with assigned conditions of irradiation and primary hydro-optical characteristics can be computed formally and completely, this calculation for the case of seawater actually encounters great difficulties. This is not only associated with the fact that there is currently no effective method for solving the equations of transport for a very extended indicatrix and nonuniform turbid medium. The main reason is that in order to compute light fields in the sea with applicable accuracy and detail, it is necessary to know the primary hydro-optical characteristics and wave action with accuracy that is not currently accessible. The situation is complicated even more by the fact that we have a poor knowledge of the polarization matrix of the scattering in the ocean, and without its consideration it is impossible to accurately determine not only the condition of

*P. P. Shirshov Institute of Oceanology, USSR Academy of Sciences.
**Numbers in margin indicate pagination in original foreign text.

polarization of the light beam, but also its energetics. Direct measurements of the brightness and polarization characteristics of the light field in the ocean, processes of transformation of the light stream on the surface of the ocean, analysis of these phenomena in relation to the factors which form them are therefore of great importance. This collection refers precisely to this circle of questions. It contains results of theoretical and experimental studies of light dispersion in ocean water and on the boundary between the ocean and the atmosphere. The articles were written by colleagues from the P. P. Shirshov Institute of Oceanology of the USSR Academy of Sciences, the Marine Hydrophysical Institute of the USSR Academy of Sciences, the V. I. Lenin All-Union Electrical Engineering Institute, and other organizations involved in questions of ocean optics.

The material has been grouped into three sections.

1. Theoretical and experimental studies of the field of solar radiation in the ocean.

2. Study of stationary and nonstationary light fields created in the sea by artificial sources.

3. Use of optical methods to study biological and hydrodynamic characteristics of the sea.

This collection is of undoubted importance not only for scientific workers, /6
engineers, graduate students and students involved in ocean optics, optics of turbid media, long-range methods of studying natural waters, but also for all individuals interested in oceanography and its numerous applications.

K. S. Shifrin, Head of the Laboratory of Optics of the Ocean and Atmosphere, Professor, Doctor of Physical and Mathematical Sciences

1. THEORETICAL AND EXPERIMENTAL STUDY OF THE FIELD OF SOLAR RADIATION IN THE OCEAN (GENERAL AND REGIONAL ASPECTS)

ASYMPTOTIC DISTRIBUTION OF BRIGHTNESS IN A MEDIUM WITH EXTENDED SCATTERING INDICATRIX.

A. V. BYALKO

This work obtains an approximate analytical solution to the transport equation for a deep-sea regime. It is used as the basis to find an expression for the nonstationary distribution of brightness in a medium when it is illuminated by a momentary light pulse.

1. INTRODUCTION

For certain media, in particular, for aerosols and seawater, the volumetric scattering function $\sigma(\gamma)$ is distinguished by excessive extension forward, governed diffraction on large particles. The $\sigma(0)/\sigma(\pi)$ ratio in the sea has an order of 10^4 [1]. This circumstance impairs the application of standard methods for solving the transport equation [2] which use expansion according to Legendre polynomials, since in this case harmonics with very high numbers must be taken into account.

Precise analytical solution to the transport equation is apparently impossible. With the current development of computer equipment there is no basic difficulty in obtaining precise numerical solutions. However, an inevitable shortcoming in these solutions in this case is their limited generality, associated with the large number of functions and parameters of the task. In fact, we will determine the dimensionality of the complete transport problem in a uniform semi-infinite medium, that is the number of variables on which the brighness of radiation depends. These are depth z, zenith angle θ, azimuth ϕ, wavelength γ, and boundary condition, the initial angle of radiation incidence θ_0, a total of five for the stationary problem, and together with time, a total of six for the nonstationary. This high dimensionality of the task plus the need to fix one function, the scattering indicatrix of the medium, in the numerical calculation makes it very difficult to extract practical information from individual accurate numerical solutions.

This same circumstance to a considerable measure depreciates the approximate solutions whose result is complicated and requires the use of computers for comparison with the experiment.

These difficulties result in the need to simplify the task and reduce the number of variables through reducing the generality. It is well known [2] that the /8 transport equation has an asymptotic solution for the case of a deep-sea regime. This solution does not depend on the boundary conditions, that is, on the angle of incidence. It possesses a cylindrical symmetry, that is, does not depend on the azimuth ϕ. Thus, the dimensionality of the task is reduced to three in the stationary, and four in the nonstationary cases. In addition, the variable z is separated from 0. The wavelength λ is usually a functional parameter of the task, since in calculating radiation transport in the sea, the scattering processes with change in wavelength (fluorescence) are generally ignored. There are accurate numerical solutions for model extended indicatrixes [3, 4], and an approximate analytical solution [5] for a random extended indicatrix. The solution that will be found in this work, is similar in degree of approximation of the solution of V. V. Sobolev [5], but it differs in form, having further application in mind. According to the theorem of Minin, a temporal Laplace transform from nonstationary response to a momentary impulse can be obtained for a certain stationary solution. Conversion of the Laplace transform is really only possible for a limited set of analytical functions. There are currently no reliable methods for numerical conversion. The asymptotic solution of the transport equation which will be found here makes it possible to use Minin's method to obtain a fairly simple analytical solution to the nonstationary task in a deep-sea regime. The accuracy of the stationary solution will be evaluated by comparing it with certain numerical solutions for model indicatrixes [3, 4]. The physical meaning and degree of approximateness of the nonstationary solution are discussed in the conclusion.

2. APPROXIMATE SOLUTION TO THE TRANSPORT EQUATION FOR AN EXTENDED SCATTERING INDICATRIX

The transport equation for radiation brightness B(z, n) without consideration for polarization and the fluorescence phenomena looks like:

$$(en)\frac{\partial B}{\partial z} = -(\sigma+\varkappa)B + \int \sigma(\gamma)B(z, n')do' \qquad (2.1)$$

Here $\sigma = \int \sigma(\gamma)do$ and $\varkappa$--respectively the indicators of scattering and absorption--functions of length, e--single vector directed on the z-axis, $\gamma = \arccos(nn')$--scattering angle. In the case of cylindrical symmetry, brightness B depends on the zenith angle $\Theta = \arccos(ne)$.

M. Wang and E. Guth [6] have obtained from this equation differential equation of the Fokker-Planck type, by using expansion according to smallness of the scattering angle γ.

$$\frac{1}{\sigma+\varkappa}\mu\frac{\partial B}{\partial z} + \frac{\varkappa}{\sigma}B = q\frac{\partial}{\partial\mu}\left[(1-\mu^2)\frac{\partial B}{\partial\mu}\right] \qquad (2.2)$$

Here $\mu = \cos\Theta = ne$; $q = \frac{2\pi}{\sigma}\int \sigma(\gamma)\sin^2\gamma/2\sin\gamma d\gamma$ /9

A necessary condition for the applicability of this approximation is the smallness of the parameter q. Its physical meaning for the extended indicatrixes is the average square of the scattering angle $q \simeq \langle\gamma^2\rangle/4$.

For real indicatrixes of seawater, because of their drastic extension forward, q has an order of 10^{-2}.

We will discuss the question of the steady-state deep-sea distribution of brightness, if the indicatrix is sharply extended forward. With each act of scattering, redistribution of the brightness body occurs, diffusion of radiation over the angles. In this case, the average square of the angle within which distribution was established which is close to equilibrium, rises linearly, increasing with each act of

scattering with a quantity on the order of $\langle\gamma^2\rangle \sim q$, therefore, the deep-sea regime for all directions occurs with a number of acts of scattering greater than q^{-1}, and correspondingly, the depth at which the asymptotic regime is implemented, must satisfy the inequality $z \gg (\sigma q)^{-1}$ (2.3)

With an acutely-directed indicatrix, that is, with small q, as will be seen below, the deep-sea body of brightness is very extended. This makes it possible to consider that the asymptotic distribution within the zenith angle θ was established after $n \sim \theta^2 q^{-1}$ acts of scattering, that is at depth $z > z_n \simeq \theta^2 (q\sigma)^{-1}$. The distribution which was established at smaller angles, will further be weakly distorted, since the relative quantity of light energy that is redistributed at great depth in a direction close to the nadir is small.

We will search for the asymptotic solution to equation (2.2) in the form

$$B(z, \mu) = S(x) \exp(-\alpha z) \sim \text{const} \exp(-\alpha z + \psi(x)),$$

here $x = \cos\Theta/2$; $\mu = 2x^2 - 1$ and α --still unknown deep-sea indicator of attenuation, a certain function of the parameters of the task q, σ and $\varkappa$. In order to find α, we can use the precise correlation which is easily obtained by integrating for the angles of the original equation (2.1):

$$\alpha = \varkappa \int B(z, \mu)\, d\mu / \int B(z, \mu)\, \mu d\mu. \quad (2.4)$$

We hypothesize (and this is confirmed after the solution is obtained) that the characteristic change in this function $\psi(x)$ by magnitude is much greater than one. This means that the "asymptotic brightness body" is very extended.

We will make the substitution $\psi(x) = G\int_1^x f(x)\, dx$ into equation (1.2); we then obtain /10 the following equation for the function f(x)

$$\left| \frac{\alpha}{\sigma} \quad \frac{\varkappa(2x^2-1)}{\sigma} \right| \frac{4}{G^2 q (1-x^2)} \quad f^2 + \frac{1}{G} \frac{\varkappa}{2x} + \frac{1}{G} f \quad \frac{1-3x^2}{x(1-x^2)} \quad (2.5)$$

We will now consider that the large quantity of the function $\psi(x)$ is defined as the parameter G which is large as compared to one, while the characteristic quantity $f(x)$ and its derivative are on the order of one . Then in the right side of equation (2.5), the first term is on the order of one , the others are small, while the left side in the denominator contains the product G^2q, which we will consider to be equal to one.

We will select the value of parameter G such that in the left side of equation (2.5) the part which is whole for x will be equal in accuracy to one:

$$G^2 = \frac{8a}{aq} \tag{2.6}$$

Since the function $\psi(x)$ was expressed as the product of two new unknowns, the unambiguity of the determination is introduced only by condition (2.6). At this stage, G is expressed through the unknown deep-sea indicator α. However, after solving the equation, α with the help of (2.4) will be found in the form of an expansion of G^{-1}. This will make it possible to compute the actual parameter G through primary hydro-optical characteristics.

We will present the quantity $\frac{a-x}{2a}$, , with regard for (2.4) as an expansion of the small parameter G^{-1} with indefinite coefficients

$$\frac{a-x}{2a} = \int_0^1 \frac{x(1-x)\exp(\psi(x))\,dx}{\int_0^1 x(1-x)\exp(\psi(x))\,dx} \qquad \frac{a_1}{G} - \frac{a_2}{G^2} \quad \cdots \tag{2.7}$$

After substituting expansion (2.7), with regard for (2.6) into equation (2.5), it will adopt the appearance.

$$f^2 + \frac{1}{G}\frac{df}{dx} + \frac{1}{G}f^3 \frac{3x^2}{x(1-x^2)} = 1 \qquad \frac{a_1}{G(1-x^2)} \tag{2.8}$$

Here terms on the order of G^{-1} are omitted, therefore the solution to this equation must be sought in the form of an exponential series G^{-1}, limited to the first order:

$$f(x) = f_0(x) + G f_1(x) + \ldots$$

In the zero approximation we have $f_0^2 = 1$; $f_0 = 1$. The solution with negative sign results in a negative value of α, which is not of interest for the semi-infinite medium.

After substituting the zero approximation into correlation (2.7)--($\psi(x) = \text{Const} + x$), we compute the coefficient with the first term of the expansion: $a_1 = 2$. By using this value in (2.8), we find the following approximation for $f(x)$: /11

$$f_1(x) = \frac{1}{1+x} - \frac{1}{2x}.$$

The area of applicability for x of the obtained solution is found from the requirement of smallness of the first term in the expansion as compared to zero:

$$Gx = G\cos\frac{\theta}{2} \ll 1 \qquad (2.9)$$

Thus, the solution is correct for a fairly large region of angles and is inapplicable only for the directions close to the nadir. Returning to the distribution of brightness, that is, by computing the indefinite integral for the function $\psi(x)$, we obtain:

$$B(z,\Theta) = \frac{\text{Const}}{\left(1+\cos\frac{\Theta}{2}\right)\sqrt{\cos\frac{\Theta}{2}}} \exp\left\{-G\left(1-\cos\frac{\theta}{2}\right)\alpha z\right\}. \qquad (2.10)$$

By using function $f_1(x)$ we can compute the coefficient a_2 in the expansion (2.7) $a_1 = 4$. This yields the following link between G and α: $\frac{\alpha}{\varkappa}\left(1-\frac{2}{G}\right)^2$.

After uniting this formula with the definition of G (2.6), we will express G, α and consequently, the solution to (2.10) of the transport equation through the primary hydro-optical characteristics:

$$G = \sqrt{\frac{8(1-\Lambda)}{\Lambda q}} + 2, \qquad (2.11)$$

$$\alpha = \varkappa\left|1 + \sqrt{\frac{2\Lambda q}{1-\Lambda}} + \frac{\Lambda q}{2(1-\Lambda)}\right|$$

here $\Lambda = \frac{\sigma}{\sigma + \varkappa}$ --parameter of survival of the quantum.

It was thus found that in the small-angular approximation, distribution of brightness in the deep-sea regime, and the deep-sea indicator of attenuation α depend on one combination of primary hydro-optical characteristics $q\Lambda/1-\Lambda = \sigma\langle\gamma^2\rangle/4\varkappa$. It is important that precisely this parameter was empirically introduced [7] as the combination of constants which determines the light field in the deep-sea regime, as well as the field of the isotropic source.

The parameter G in the case $\Lambda \neq 1$, is actually much larger than one because of the smallness of q for very extended indicatrixes. The derivative of the function /12 $\psi(x)$ in this case is therefore a large quantity, that is, the asymptotic form of the brightness body is actually very extended, as was assumed in obtaining the solution.

3. COMPARISON OF THE OBTAINED SOLUTION WITH OTHER THEORETICAL SOLUTIONS FOR MODEL INDICATRIXES

We will compare the solution (2.10) depending on (2.11) with certain results of numerical calculations for model extended indicatrixes. The work of V. Sobolev [3] has obtained a solution for indicatrixes of the type

$$\frac{4\pi\sigma(\gamma)}{\sigma} = \frac{n+1}{2}(1+\cos\gamma)^n. \tag{3.1}$$

The most expended of the calculated indicatrixes has the parameter n = 4. Publication [3] solved the inverse problem: the values of the parameter of the deep-sea regime $\Gamma = (1-\Lambda)\frac{1}{\varkappa}$ were initial, but they were used to compute the probability of survival of the photon Λ and the coefficients in Legendre's polynomials. In particular, it was found for $\Gamma = 0.4$ that $\Lambda = 0.856$ and the distribution of brightness in the deep-sea regime looked like:

$$S(\Theta) = \frac{1+0.72\cos\Theta+0.185\,P_2(\cos\Theta)+0.06\,P_3(\cos\Theta)}{1-0.4\cos\Theta}. \tag{3.2}$$

We obtain the quantities of parameters for the solution to this work for the same value Λ:

$$q = \frac{1}{n+2} = 0{,}167;\ G = 4{,}842;\ \frac{a}{\varkappa} = 2{,}903.$$

Comparison of the brightness distribution of (3.2) and (2.10) with G = 4.842 demonstrated that discrepancy between the precise solution and the given approximation in the entire range of angles $G\cos\frac{\theta}{2} < 1$ is in limits of theoretical error G^{-1} = 20%. Computation of the parameter of deep-sea regime

$$\Gamma = (1-\Lambda)\frac{a}{\varkappa} = 1 - \Lambda + \sqrt{2q\Lambda(1-\Lambda)} + q\frac{\Lambda}{2}. \qquad (3.3)$$

for this same indicatrix results in the value Γ = 0.418 instead of the precise 0.4.

In order to be convinced that the error in formula (3.3) which was obtained based on the solution to (2.11) of this work, is uniform in the entire range of change in Λ, this relationship was compared with results of accurate calculations for Haney -Greenstein indicatrixes [4]: /13

$$\frac{4\pi\sigma(\gamma)}{\sigma} = \frac{1-g^2}{(1-2g\cos\gamma+g^2)^{3/2}}. \qquad (3.4)$$

The most extended of the calculated indicatrixes corresponds to the parameter q = 0.95. The value q for the indicatrix (3.4) equals $q = \frac{1-g}{2} = 0{,}025$. Comparison of the relationship (3.3) with the results of these calculations shows that the relative error in formula (3.3) is uniform in the entire range $0 < \Lambda < 1$.

Thus, both formula (2.10) for brightness distribution and formula (2.11) for the deep-sea indicator of attenuation are approximate analytical expressions which have relative error on the order G^{-1}. The basically possible refinement of these formulas, that is, finding the following terms in the expansion for G^{-2}, is hardly justified, since the formulas in this case will become so cumbersome that the possibility of rapid assessment is lost.

4. TEMPORAL DISTRIBUTIONS OF BRIGHTNESS

The brightness distributions during irradiation of the medium by a stream of radiation that varies in time are provided by solution to the nonstationary transport equation. We will introduce the dimensionless depth- optical thickness $\tau = z(\sigma+\varkappa)$ and the dimensionless time $u = ct(\sigma+\varkappa)/c$--speed of light in the medium). The nonstationary transport equation of these variables looks like:

$$\left(1+\frac{\partial}{\partial u}+\cos\Theta\frac{\partial}{\partial\tau}\right)B(u,\tau,\Theta)=\Lambda\int B(u,\tau,\Theta')\frac{\gamma(\lambda)}{\gamma}d\omega'. \tag{4.1}$$

If the solution to the stationary task is known, then the solution to the temporal equation with the same geometry which represents a response of the medium to the momentary impulse of radiation, is provided by the theorem of I. N. Minin [8]: in the stationary solution it is necessary to replace τ by $\tau(1+p)$, and Λ by $\Lambda(1+p)^{-1}$. Then the inverse transform of Laplace is made for the parameter p. The function of Green which is thus obtained makes it possible to solve the nonstationary task with random boundary conditions.

We will use the obtained stationary solution to find temporal distributions of brightness of deep-sea regime with acutely-directed indicatrix. We will write the solution to (2.7) for small zenith angles after standardizing it for the incident stream with the use of explicit expressions of the parameter G and the deep indicator of attenuation through the probability of survival of the photon Λ.

$$B(\tau,\Theta)\quad\frac{\Gamma_0\left|6+1\overline{8(1-\Lambda)/\Lambda q}\right|}{\tau(1+\cos\Theta/2)\sqrt{\cos\Theta/2}}\exp\left\{-2(1-\cos\Theta/2)\right. \tag{4.2}$$

$$\left.\left|\overline{8(1-\Lambda)/\Lambda q}(1-\cos\Theta/2)\right.\right.\tau\left|1-\Lambda+\right|2q\Lambda(1-\Lambda)\Big\}.$$

We will make the indicated replacement and will thus obtain the Laplace transform from the response to the momentary impulse: /14

$$B_p(\tau,\Theta)=\Phi_1(\Theta)\left|6+\right|\overline{8(p+1-\Lambda)/\Lambda q}\left|\exp\right\{-\tau(p+1-\Lambda)+$$
$$+R\left|\overline{p+1-\Lambda}\right\}.$$

Here we will introduce the designations

$$\Phi_0(\Theta) = \frac{E_0 \exp\{-2(1-\cos\Theta/2)\}}{4\pi(\beta+\cos\Theta/2)\sqrt{\cos\Theta/2}};$$

$$R(\tau,\Theta) = \sqrt{2\Lambda q} - \sqrt{8/\Lambda q}(\Lambda - \cos\Theta/2);\ \tau \gg (\Lambda q)^{-1}$$

In fulfilling the inverse Laplace transform, we obtain the distributions of brightness which depend on time, with irradiation of the medium by a momentary pulse:

$$B(u,\tau,\Theta) = \frac{\Phi_0(\Theta)}{2\pi}\left|6R + \frac{R^2+\sqrt{8/\Lambda q}}{2(u-\tau)}\right|\frac{1}{(u-\tau)^{3/2}} \times \tag{4.3}$$

$$\times \exp\left\{-(1-\Lambda)u - \frac{R^2}{4(u-\tau)}\right\};\ u-\tau,\ R \gg 1$$

The temporal asymptotics of the solution coincide with the asymptotics for a semi-infinite medium which is found in the diffuse approximation [9]:

$$B \sim (u-\tau)^{3/2}\exp\{-(1-\Lambda)u\}$$

The function $R(\tau,\Theta)$ characterizes the curvature of the anterior front of the arriving impulse and the energy of the received signal. With an increase in depth or zenith angle, the received impulse becomes more gently sloping. The moment of arrival of the maximum signal $u_{max} \approx \tau + R^2/6$.

Formula (3.3) provides the approximate distribution of brightness in the deep-sea regime from the impulse broad light beam. Strictly speaking, in order to justify the use of Minin theorem for the asymptotic deep-sea regime, one should first of all show that the nonstationary equation has a certain asymptotic solution. In this work, this circumstance is a hypothesis. It is important to compare formula (3.3) with the experimental data. In the work of this collection [10], by using the /15
results of measuring the shape of the pulse of underwater irradiation from a laser source, Green's function was computed, that is, the response to the momentary pulse for a broad directed light beam. Integration by angles in order to obtain the underwater irradiation from (3.4) is difficult in a general form. We will use the fact

that for the small angles of θ which make the main contribution to the integral of underwater irradiation, the second term for $R(\tau,\theta)$ is much smaller than the first, and thus, R practically does not depend on the angle θ: $R = 1/2\Lambda q\tau$. Since in [10] the results are presented for norming for the maximum, we will act in a similar manner. Then, returning to the dimensional quantities, we obtain for the underwater irradiation in the deep-sea regime

$$E(t,z) = \text{Const}\ \frac{(\varkappa ct - 2z)z}{(ct-z)^{5/2}}\ \exp\left\{-\varkappa ct - \frac{\sigma q z^2}{2(ct-z)}\right\}.$$

For comparisons with results of [10], the indicators of absorption and scattering were assumed to be the same: $\varepsilon = \sigma + \varkappa = 0{,}14\ \text{м}^{-1}$; $\Lambda = \sigma/\varepsilon = 0{,}75$, the coefficient q was selected as equal to 0.0214 from the condition of coincidence of the moment of the maximum for the depth 100 m. This value q corresponds to $\langle\gamma^2\rangle = 0{,}0857$. This agrees fairly well with the characteristic quantity $\langle\gamma^2\rangle$ 0,1 for the indicatrix of the open part of the Indian Ocean. Graphs of the pulses which were normed for the maximum are presented for depths 50, 75 and 100 m in the figure.

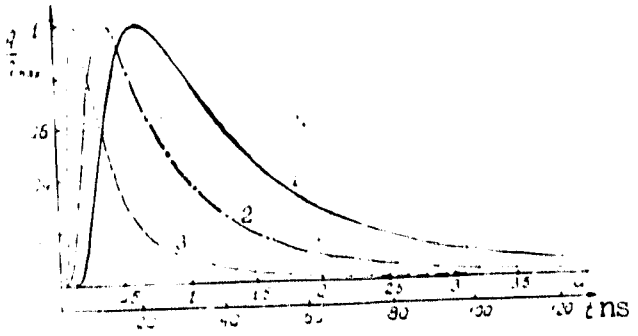

Figure. Approximate Analytical Functions of Green, Momentary Pulse of Broad Directional Beam for Depths: 1--z = 100 m, 2--z = 75 m, 3--z = 50 m, with ε = 0.14 m^{-1}, Λ = 0.75, q = 0.0214 (compare with Figure 6 of publication [10] of this collection). The pulses were normed for the maximum. The time axis is in ns and dimensionless variable $u = \varepsilon ct$.

BIBLIOGRAPHY

1. Yerlov, N. Opticheskaya okeanografiya ["Optical Oceanography"], (translated from English edition, 1968), Moscow, Izd. mir, 1970.

2. Sobolev, V. V. Rasseyaniya sveta v atmosferakh planet ["Light Scatterings in Atmospheres of Planets"], Izd. Nauka, 1972.

3. Sobolev, V. V. Izv. AN SSSR, Ser. geograf. i geofiz, vol 8, 1944, p 273. /16

4. Loskutov, V. M. Vestnik LGU, No 13, 1969.

5. Sobolev, V. V. DAN, vol 177, 1967, p 812.

6. Wang, M. C.; and Guth, E. Phys. Rev., 84, 1951, p 1092.

7. Pelevin, V. N.; and Prokudina, T. M. in Gidrofizicheskiye i gidrooptricheskiye issledovaniya v Atlanticheskom i Tikhom okeanakh ["Hydrophysical and Hydro-Optical Studies in the Atlantic and Pacific Oceans"], Moscow, Izd. Nauka, 1974.

8. Minin, I. N. Teoriya zvezdnykh spektrov ["Theory of Stellar Spectra"], Izd. Nauka, 1966.

9. Zege, E. P.; and Katsev, I. L. Vremennyye asimptoticheskiye resheniya uravneniya perenosa izlucheniya i ikh primeneniye ["Temporal Asymptotic Solutions to Transport Equation of Radiation and their Application"], Minsk, 1973.

10. Pelevin, V. N.; Gol'din, Yu. A.; and Snitov, B. V. "Use of the Method of Superposition to Calculate the Green's Function of a Nonstationary Light Field Created by a Broad Directed Light Beam", this collection.

SPECTRAL CHARACTERISTICS OF THE FIELD OF SOLAR RADIATION IN THE SEA AND ABOVE ITS SURFACE. V. N. PELEVIN

Correlations are established between the spectral characteristics of a light field in the ocean and above its surface. Index of vertical attenuation $\alpha\downarrow\lambda$, coefficient of diffuse reflection $R\lambda$ and coefficient of brightness of the sea surface $\rho\lambda$.

It is shown that knowledge of the optical water type index $m = 100\ \alpha\downarrow_{500}$ is sufficient to evaluate the spectral courses and values of $R\lambda$ and $\rho\lambda$. On the other hand, measurement of one value $R\lambda$ or $\rho\lambda$ in the blue spectrum region or the $\rho\lambda_1/\rho\lambda_2$ ratio (similarily for R_1/R_2) for both radiation wavelengths selected in the short wavelength and long wavelength spectral regions, makes it possible to evaluate the optical water type index m, the spectral attenuation of solar light over the entire spectrum, and other characteristics of light fields in the ocean. The described relationships comprise the basis for constructing a one-parametric model of the field of solar radiation in the ocean and above its surface.

Statistical relationships are found in a number of cases between different optical characteristics of the field of solar radiation in the sea, or values of one quantity, but taken in different parts of the spectrum. These relationships are not very sensitive to the illumination conditions of the sea surface and are mainly governed by the optical properties of sea water together with the substances dissolved and suspended in it. The existence of these relationships afford the possibility of evaluating the importance of a number of unknown characteristics and their expected spectral courses from a limited number of known quantities, sometimes one

numerical quantity. For example, N. Yerlov [1] drew attention to the fact that the values of the vertical attenuation index $\alpha_{\downarrow\lambda}$ [2] for different λ are not interdependent. This permitted him to suggest classification of ocean water according to spectral attenuation of the solar radiation flux [1, 3]. More detailed measurements [4, 5] permitted corrections to be made in the attenuation curves suggested by Yerlov, and in the final analysis, to suggest a new, refined classification of ocean water according to spectral attenuation of solar radiation in the near-surface mass of ocean water [6]. In particular, the drastic discreteness (gradation) was eliminated in the distribution of ocean water according to optical types. An index of water type equal to $\alpha_{\downarrow 500}$ was introduced (with decimal base for $\alpha_{\downarrow\lambda}$). It was used to evaluate the expected course of $\alpha_{\downarrow\lambda}$ for the given water for the entire visible spectrum of radiation according to a nomogram given in [6], with evaluation of dispersion in different parts of the spectrum. Table 13 of [7] presents the /17
values of $\alpha_{\downarrow\lambda}$ for water characterized by the index $m = 100\ \alpha_{\downarrow 500}$. The table completely corresponds to the indicated nomogram. The index values change smoothly over the water area in the Pacific Ocean. The index changes in the interval from 1.1 to 9.0.

Publication [7] gives an evaluation of the spectral distribution of underwater irradiance at different depths, as well as attenuation of the entire flux of solar radiation with depth and thickness of the photosynthetically active layer of sea water depending on the value of the optical index of water type.

This work will examine the spectral distribution of other quantities, the coefficient of diffuse reflection of light by the sea R_λ, and the coefficient of brightness of the sea surface at the nadir ρ_λ [2], as well as the interrelationship of these two quantities with the index of water type according to the mentioned new

classification. Experimental data were used [4, 5] that were obtained by instruments with resolution for the spectrum no less than 6 - 8 nm. Processing of the data indicated that the values of the coefficient R_λ, its spectral course in the surface layer of the ocean water with high sun ($h > 45°$) correlate well with the index of water type. Figure 1 plots the values of R_λ with λ = 430 nm, and for the interval 510 - 530 nm from measurements in different regions of the Pacific, Atlantic and Indian Oceans. The corresponding values of the water type index are plotted on the x-axis. It is apparent from Figure 1 that in the transition from very clean water to more turbid (to an index equal to 3.0) $R_{510-530}$ rises, while R_{430} decreases intensively. For even more turbid waters with an index greater than 3.0, $R_{510-530}$ is maintained unchanged on the average with large dispersion of the R values, while R_{430} (blue area of the spectrum) continues to diminish stably. The curves given in Figure 1 are intersected with a index value 4 - 4.5, in clean waters $R_{430} > R_{510-530}$, while in turbid waters the opposite correlation is observed.

An explanation for these relationships can be seen in the following. The coefficient of diffuse reflection $R_\lambda \sim \frac{\beta_\lambda}{\varkappa_\lambda + \beta_\lambda}$ [9, 8], where β_λ -- index of backscattering into the hemisphere 2π, $\varkappa_\lambda$ --absorption index. In clean water, light absorption $\varkappa_\lambda$ in the blue region of the spectrum is low. This governs the high values of R_λ in this spectral region. Light absorption by clean water in the longer wavelength region of the spectrum rises, while scattering in clean water approaches the Rayleigh, i.e., drastically diminishes with an increase in wavelength. These circumstances jointly result in the fact that $R_{510-530} \ll R_{340}$. [sic].

Increase in the water type index in this water area is associated with the appearance of a noticeable quantity of suspended and dissolved material, primarily of organic origin. In this case absorption in the blue region of the spectrum by chlorophyll, and other pigments of phytoplankton, pheophytin and dissolved substances

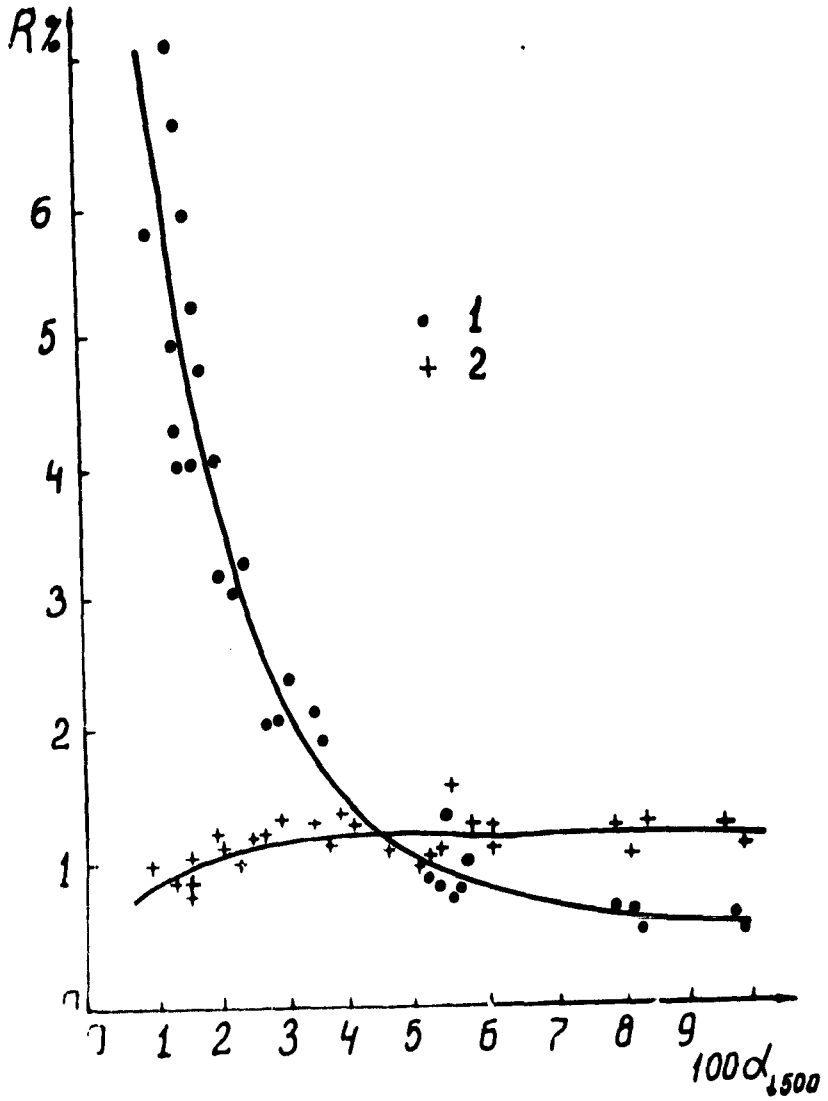

/18

Figure 1. Dependence of Coefficient of Diffuse Reflection R_λ with λ = 430 nm (1) and λ = 510 - 530 nm (2) on Water Type Index $m = 100\alpha_{\downarrow 500}$.

of organic origin ("yellow substance"). As a result R_λ is intensively reduced in the blue spectral region with an increase in the water type index. In the green spectral region, different factors influencing the R_λ value compensate for each other to a considerable degree. Light absorption by pigments of phytoplankton and "yellow substance" in the green region increases to a considerably lower degree than in the blue. At the same time, scattering, and in particular, the back-scattering index β_λ rises over the entire spectrum with an increase in concentration of

/19

suspension, therefore $R_{510-530}$ rises with an increase in the water type index. In very turbid waters, nonselective light absorption by "dirty" or "gray" suspension [10] plays a large role. The different contribution from this factor to the quantity $\varkappa_\lambda$ in different waters governs the high dispersion of $R_{510-530}$ in turbid waters.

In order to evaluate the spectral course of R_λ in a broad interval of λ, the average values of R_λ were computed according to samplings corresponding to narrow intervals of the water type index and referring to the most diverse ocean waters, see Figure 2. For the samplings (each numbering from 8 to 12 spectral curves) the standard deviations in R_λ from the average are plotted on both sides of the figure. The figure caption indicates the corresponding intervals of the water type index $m = 100\ \alpha_{500}$.

It is apparent from Figure 2 how strongly R_λ differs in the blue spectral region (this circumstance is well known, see for example [1]. An important fact that should be taken into consideration is the systematic decrease in the curves R_λ in the spectral zone near 430 nm which is created by the blue band of absorption of chlorophyll and its accompanying pigments (for the first observations and explanation of this phenomenon see [4]).

The values R_λ in the green spectral region differ less for different waters. This corresponds to what has been said above. In the longer wavelength yellow spectral region, a systematic rise in R_λ is observed with an increase in the water type index (see also [11]).

The data presented in Figure 2 makes it possible to fulfill the task set above, to evaluate the values of R_λ in different spectral regions according to the known quantity $m = 100\ \alpha_{500}$, with evaluation of the expected dispersion of the result.

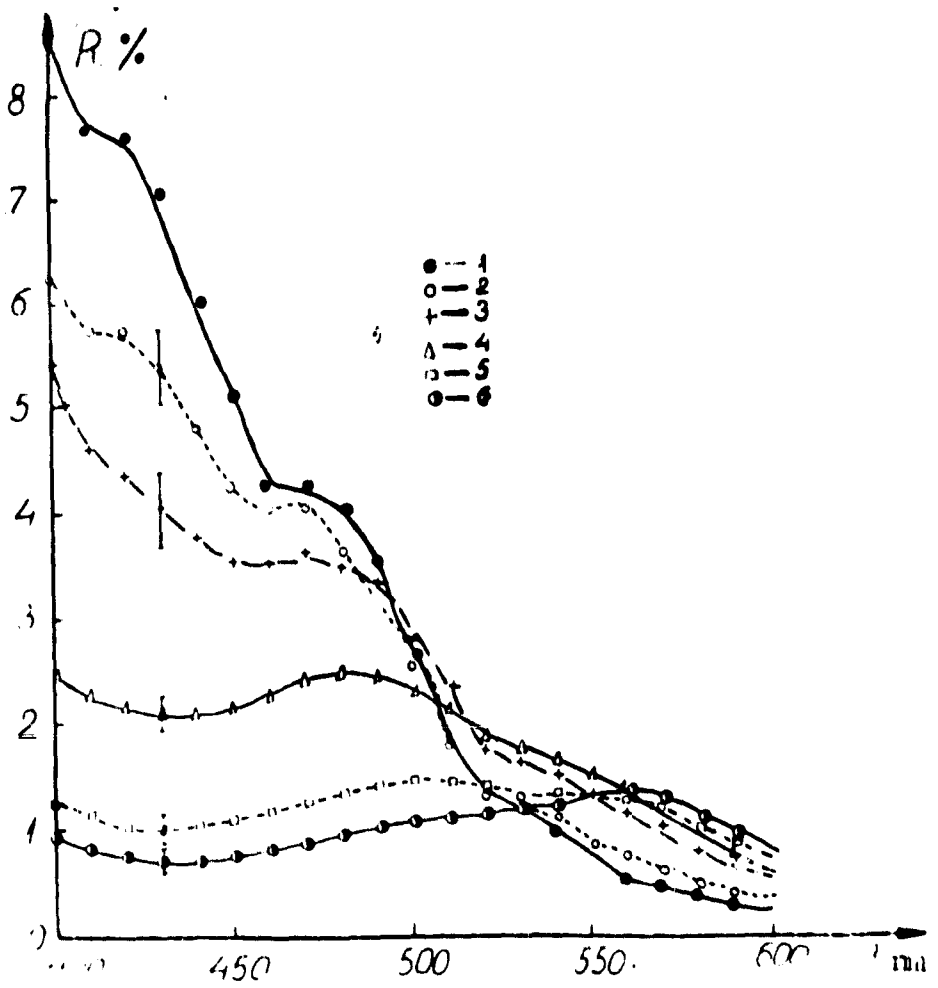

/20

Figure 2. Dependence of $\bar{R}_\lambda$ on λ. Average $\bar{R}_\lambda$ are given from samplings which differ in the values of the water type index m: 1--values of index m = 1.17 - 1.35, 2--1.5 - 1.6, 3--2.0 - 2.5, 4--2.7 - 3.7, 5--5.8 - 6.4, 6--8.8 - 10.5.

By using the same graph, one can solve the inverse task, to evaluate the water type index from the values R_λ in the blue spectral region, or in relation to R_λ measured in two spectral intervals. The necessary further set of experimental data will make it possible to pinpoint the course of the curves in Figure 2 and the values of dispersions.

The spectral course of the brightness coefficient of the sea $\rho_\lambda = \frac{B_{\uparrow m}}{B_0}$, where $B_{\uparrow m}$--brightness of the radiation emerging from the sea mass (during observation above the water surface at the nadir), B_0--brightness of the white horizontal diffuser illuminated by the sun and light of the sky, corresponds in general features to the spectral course of R_λ under the surface of the sea, but these two amounts quantitatively differ. We will use the correlation presented in [8]:

$$\rho_\lambda = 0{,}53\, K^{-1} R_\lambda . \tag{1}$$

where

$$K = \frac{1}{\pi} \int_{(2\pi)} B(\Theta, \varphi) / B(0, 0) \cdot \cos\Theta \, d\omega, \tag{2}$$

In (Θ,ϕ)--subsurface distribution of brightness (integration is done for the lower hemisphere, i.e., for ascending radiation). The coefficient K does not differ strongly from one. With isotropic ascending radiation K = 1. Publication [8] has recommended that the following empirical relationship be used in the interval $0.007 \leq \rho \leq 0.07$ to assess the value of K

$$K = 1 + \frac{0{,}007}{\rho}. \tag{3}$$

The standard deviation of K in calculations for (3) for the available experimental data (16 points) was 8%. The dependence of K on ρ requires further refinement. /21

By using the data for R_λ presented in Figure 2, and correlation (1) one can compute the spectral course of ρ_λ for not too turbid ocean waters (with index 100 $a_{500} < 3$). In more turbid waters, the ρ values go beyond the limits of applicability of (3). The data of this calculation are given in Figure 3. The course of ρ_λ presented in the figure explains the natural color of the sea in different waters: very clean waters--blue, sometimes violet, while with an increase in the quantity of dissolved and suspended substances, the color of the sea becomes green. There is a tendency for further change in color (in the long wavelength region of the spectrum) with an increase in the index of water type. The general spectral course of ρ_λ

which is computed by the indicated method, corresponds to that which was obtained by direct measurements (compare with [8, 11, 12]).

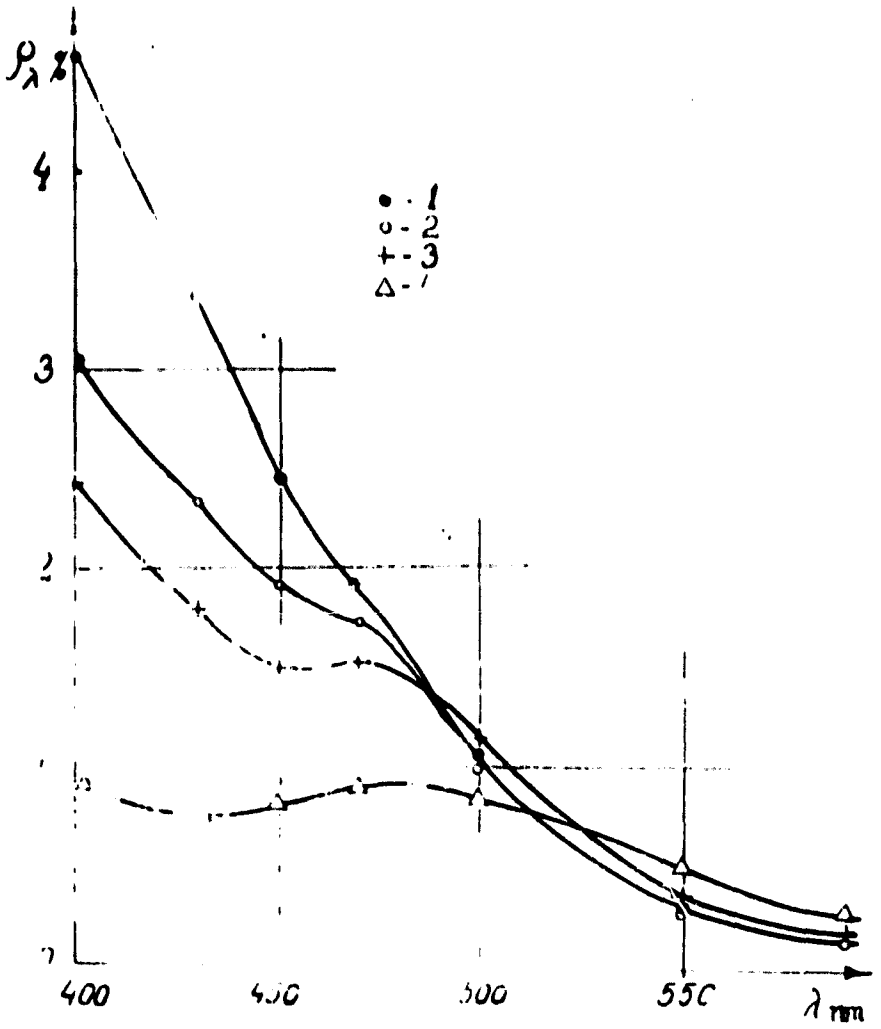

Figure 3. Dependence of Brightness Coefficient of Sea Surface ρ_λ on λ. Average ρ_λ are given from samplings of different values of the index of water type $m = 100\,\alpha_{\lambda 500}$: 1--values of the index $m = 1.17 - 1.35$; 2---1.5 - 1.6; 3---2.0 - 2.5; 4---2.1 - 3.7.

Examination of Figure 3 results in a conclusion regarding the possible evaluation of the optical type of water and the results of noncontact measurements of ρ_λ from a ship, helicopter or airplane. For example, one can estimate the value

of the water type index m from the ratio of brightness coefficients $\rho\lambda_1/\rho\lambda_2$ measured in two spectral sections. It should be noted that the existence of a relationship between $\rho\lambda_1/\rho\lambda_2$ and the values $\alpha_\downarrow$ in the "midregion of the spectrum" was noted for the first time in [13] without indication of wavelength. The authors offered the following regression equation. $\alpha_\downarrow = 0{,}068$

The straight line corresponding to this equation is presented in Figure 4. It also plots the points corresponding to the data of Figures 2 and 3, and as $\alpha_\downarrow$ on the y-axis, $\alpha_{\downarrow\,500}$ was plotted. A good coincidence is visible which confirms the conclusion of publication [13]. It also makes it possible to use this regression relationship for long-range determination of the water type index $m = 100\ \alpha_{\downarrow\,500}$ from the value ρ_{549}/ρ_{432}.

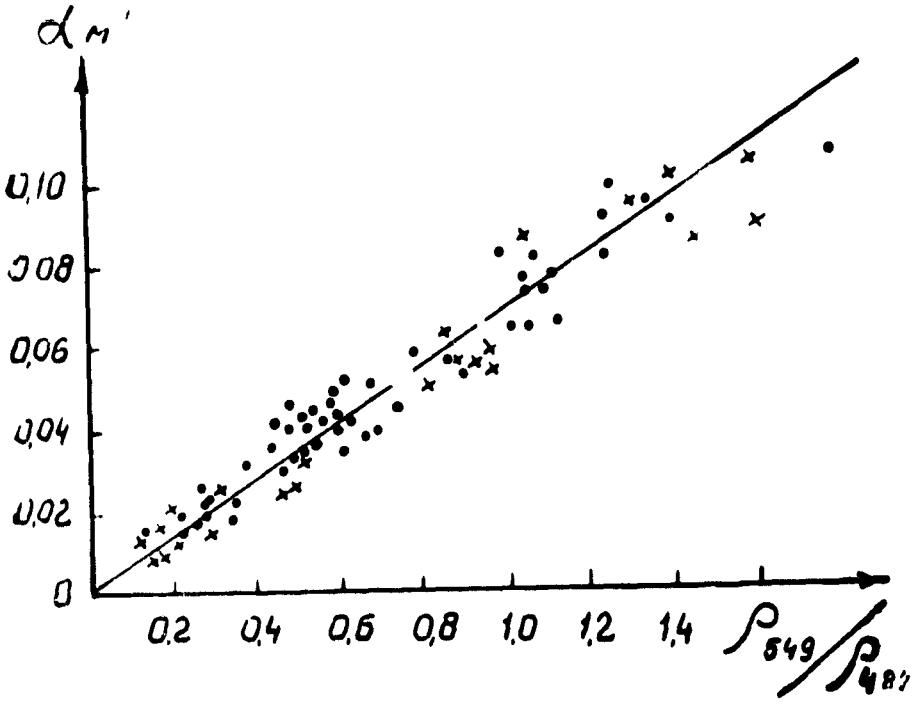

Figure 4. Comparison of Indicator of Vertical Attenuation α in Average Section of Visible Region of Spectrum [13] and Ratio ρ_{549}/ρ_{482}. The crosses indicate the average data taken from Figures 2 and 3, and the value $\alpha_{\downarrow 500}$ was taken as α.

One should note, on the other hand, that selection of the wavelengths 549 and 482 m in publication [13] was random to a considerable degree. It is apparent from Figure 2 that the interval of changes in the $\rho\lambda_1/\rho\lambda_2$ ratio rises if the interval $(\lambda_1 - \lambda_2)$ increases.

Extensive measurements are currently being made of the "color index of water" by Neuymin, et al. [14]. The authors have called the "color index" the ρ_{550}/ρ_{440} ratio which is measured on the ship's course in a shaft passing through the bottom of the ship at a depth of 4 - 6 m. Its values change dynamically in the transition from one type of water to another. They are used by the authors to study the boundaries of the currents, the process of stream separation, and in other hydrological studies. In the latest work of Marine Hydrophysical Inst.the authors seek a correlation between the value of the color index and the chlorophyll concentration in the surface layer of water [15].

In the measurement of ρ_{550}/ρ_{440} the $\lambda_1 - \lambda_2$ difference is greater than [13]. This makes the value of the color index even more suitable for estimating the optical type of water. Processing of the experimental data resulted in the following regression equation which links the quantity $100\ \alpha_{\downarrow}500$ and ρ_{550}/ρ_{440}

$$100\,\alpha_{\downarrow 500} = 1{,}0 + 3{,}7\ \frac{\rho_{550}}{\rho_{440}}, \qquad (4)$$

standard deviation from the average 14%.

It follows from Figures 2 and 3 that the greatest dynamic range of the ratio $\rho\lambda_1/\rho\lambda_2$ is observed with λ_1 = 560 nm and λ_2 = 430 nm. The ratio ρ_{560}/ρ_{430} really changes from 0.05 (with index of the water type 1.35) to 2.75 (with index type 9.1) according to the available data file, i.e., 55 - fold.

Processing of the experimental data resulted in Figure 5 which gives the dependence of the water type index in the ratio ρ_{560}/ρ_{430}.

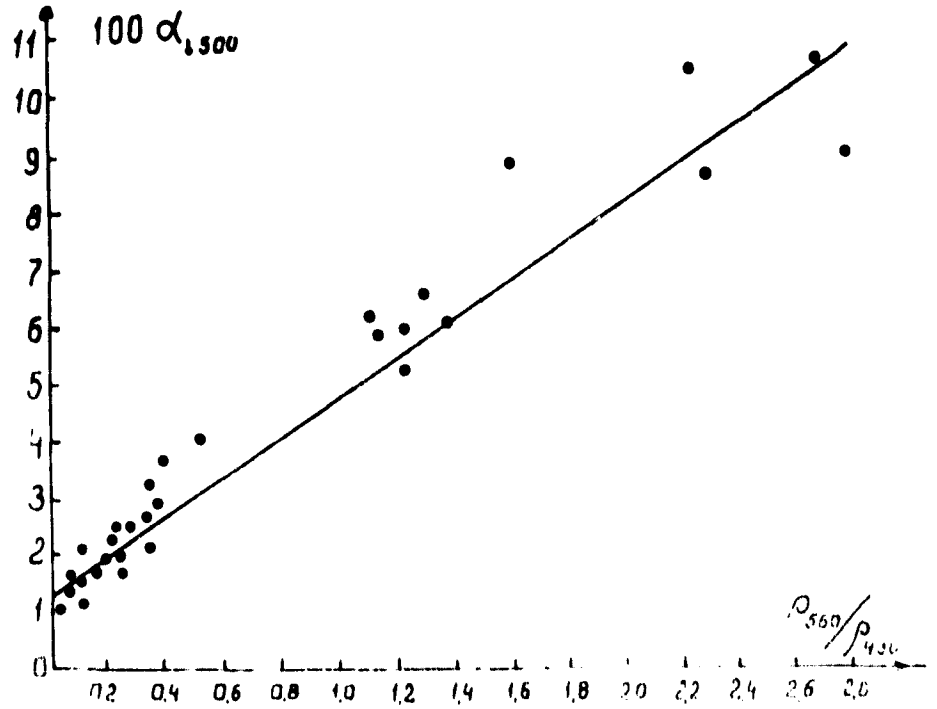

Figure 5. Comparison of Water Type Index 100 $\alpha_{\downarrow 500}$ and Ratio ρ_{560}/ρ_{430}.

The regression equation $$100\,\alpha_{\downarrow 500} = 1{,}3 + 3{,}5\,\frac{\rho_{560}}{\rho_{430}}, \qquad (5)$$

The standard deviation from the average was 20%.

We have presented three different regression relationships to estimate the index /24 of the optical type of water m = 100 $\alpha_{\downarrow 500}$. They can be used depending on what data are available. Equations (4) and (5) seem more preferable to us.

An enticing outlook is thus afforded to use one long-range measured parameter $\rho\lambda_1/\rho\lambda_2$ to evaluate the water type index, and then with regard for the data presented in [7] and in this publication, to assess the absolute values $R\lambda$ and $\rho\lambda$ for the given waters, the spectral composition of light at different depths, the PRE level

and thickness of the photosynthetically active layer. This has brought us right up to the construction of a model for the light field in ocean waters. The relationships presented here may naturally be pinpointed when additional experimental data has been found.

The next important step in constructing the model would be establishment of statistical relationship between the characteristics of the light field and the primary hydro-optical characteristics of the ocean waters which form the light fields.

By having typical spectral a_λ for ocean waters [6, 7] and the corresponding R_λ /25 given here, typical distributions are computed for $\varkappa_\lambda$, as we have previously suggested. On the other hand, since in the two-stream approximation $a \approx \varkappa + \beta$ and $R \approx k\beta/(\varkappa + \beta)$, while this approximation is confirmed in practice, we find that $a_\lambda \times R_\lambda = k\beta_\lambda$, and by having k [8], we obtain the typical course β_λ. The spectral course of β_λ, in turn, correlates with the spectral values of a_λ. The typical a_λ are determined from here, as well as the parameter for survival of the quantum $\Lambda_\lambda = a_\lambda/(a_\lambda + \varkappa)$ --for the corresponding waters which initially are characterized only by the index m. It is natural that processing of extensive experimental material will permit determination of the confidence intervals for these assessments.

The next step may be assessment of the typical concentrations of substances which determine water primary hydro-optical features. It is noted in publication [10] that $\varkappa_\lambda \approx \varkappa_{c\lambda} + \varkappa_{p\lambda} + \varkappa_{y\lambda} + \varkappa_n$ where the first term corresponds to absorption by clean water, the second--by plankton pigments, the third--by dissolved organic materials ("yellow substance"), and the fourth--nonselective absorption by suspensions. The spectral course of these quantities differs drastically. By selecting the concentration of individual substances, the method of least squares is used to determine the curve $\varkappa_\lambda$ which corresponds the most to the previously obtained typical

curve. The quantity and spectral course of β_λ and σ_λ will make it possible to estimate the dispersion and concentration of suspended substances contained in the water.

BIBLIOGRAPHY

1. Yerlov, N. Opticheskaya okeanografiya ["Optical Oceanography"], Moscow, Izd. Mir, 1970.

2. Gidrooptícheskiye kharakteristiki (terminy i opredeleniya) ["Hydro-Optical Characteristics (Terms and Definitions)"], GOST 19210-73, Moscow, Izd. standartov, 1974.

3. Gerlov, N. G. "Optical Studies of Ocean Water" Rep. Of Swedish Deep-Sea Exped., No 3, 1951.

4. Yefimenko, I. D.; Pelevin, V. M.; Svetlykh, A. A.; and Khalemskiy, E. N. "Radiance by Natural Light in Waters of the Indian Ocean," Gidrofizicheskiye i optícheskiye issledovaniya v Indiyskom okeane ["Hydrophysical and Optical Studies in the Indian Ocean"], Moscow, Nauka, 1975.

5. Morel, A.; and Prieur, L. "Spectral Analysis of Diffuse Attenuation, Diffuse Reflection, Absorption and Retro-diffusion For Various Regions, Report 17 July. Vill Franche-sur-mer.

6. Pelevin, V. M.; and Rutkovskaya, V. A. "Optical Classification of Ocean Waters According to Spectral Attenuation of Solar Radiation," Okeanologiya, vol 17, No 1, 1977.

7. Pelevin, V. M.; and Rutkovskaya, V. A. "Attenuation of Photosynthetically Active Solar Radiation in Waters of the Pacific Ocean," Okeanologiya, vol 18, No 4, 1978.

8. Pelevin, V. M. "Evaluation of Concentrations of Suspension and Chlorophyll in the Sea from Spectrum of Outgoing Radiation Measured from a Helicopter," Okeanologiya, vol 18, No 3, 1978.

9. Gamburtsev, A. G. K voprosu o tsvetnosti morya ["Question of the Color of the Sea"], Moscow, 1924. /26

10. Pelevin, V. M.; Pelevina, M. A.; Kel'balikhanov, B. F. "Study of Spectra of Radiation Emerging from the Sea from a Helicopter," Opticheskiye metody izucheniya okeanov i vnutrennikh vodoyemov ["Optical Methods of Studying Oceans and Internal Reservoirs"], Novosibirsk, Nauka, Siberian Department of the USSR Academy of Sciences, 1979.

11. Pelevin, V. M. "Estimate of the Concentration of Suspended Matter in the Sea from Spectral Brightness of Outgoing Radiation," Ekspr. inf. TSNIITEIRKH, No 5, Moscow, 1978.

12. Khalemskiy, E. N. "Spectral Distribution of Brightness Coefficient of Sea in Waters with Different Optical Properties", Optika okeana i atmosfery ["Optics of the Ocean and the Atmosphere"], Leningrad, Izd., Nauka, 1972.

13. Kozlyaninov, M. V.; and Semenchenko, I. V. "Determination of the Indicators of Vertical Attenuation and Absorption Based on Measurement from an Airplane of the Coefficients of Spectral Brightness of the Sea", Izv. AN SSSR, FAO, vol 3, No 10, 1967.

14. Li, M. Ye.; and Martynov, O. V. "Certain Results of Studying the Color Index in the Sea", Morskiye gidrofizicheskiye issledovaniya, No 1 (72), Sevastopol', Izd. MGI AN UkSSR, 1976.

15. Afonin, Ye. I.; Berseneva, G. P.; Krupatkina, D.N.; Li, M. M. Man'kovskiy, V. I.; and Solog'yev, M. V. "Estimate of the Chlorophyll Content in the Upper Layer of the Sea from Measurement of the Color Index", in this collection.

EXPERIMENTAL VERIFICATION OF ONE OF THE METHODS FOR MATHEMATICAL MODELING OF THE LIGHT FIELD IN TURBID MEDIA OF THE SEA WATER TYPE.

V. A. TIMOFEYEVA, M. V. SOLOV'YEV and V. YE. SHEMSHURA

Approximating functions are selected for experimental scattering indicatrixes which drastically differ in shape. In each case, a comparison is made of the calculated and measured angular distributions of brightness as well as certain parameters of the corresponding light fields in a deep-sea regime.

A conclusion is drawn that this method of mathematical modeling of light fields is applicable to natural waters.

There are currently a number of methods for numerical solution to the transport equation of radiation in deep layers of a turbid medium [1-4, 14]. For media of the sea water type which are characterized by a very forward-extended scattering indicatrix $\chi(\gamma)$ (γ--scattering angle) and the presence of random absorption, unfortunately some of the [1, 2, 14] become very complicated and cumbersome. Convenient algorithms for computing the parameter of the deep-sea regime Γ and angular distribution of brightness $B(\theta)$ (θ--vertical angle) have been suggested in [3,4]. The method used by Loskutov [3] is apparently the simplest method for solving this problem. Here the relationship between Γ and the probability of survival of the photon Λ is expressed in the form of a continuous fraction. In this case the calculation is significantly simplified if the experimental indicatrixes $\chi(\gamma)_{exp}$ are represented by functions which are easily distributed into a series according to the Legendre polynomials, for example, the Haney-Greenstein indicatrix.

This indicatrix in principle is a good approximation of the real $\chi(\gamma)_{exp}$, and as noted in [5], in order to attain better approximation, sometimes a combination made of two Haney-Greenstein indicatrixes is used. The possibility of using this /27 combination for sea and ocean $\chi(\gamma)_{exp}$ was shown [6].

By using a similar approximation of certain experimental indicatrixes of scattering, as well as the algorithm for calculating the brightness developed in [3], the authors of [7] studied the effect of the shape of $\chi(\gamma)$ on $B(0)$ in a medium with different values of Λ. They essentially used mathematical modeling of the light field in deep layers of a turbid medium.

The purpose of this work is to experimentally verify this modeling. For this purpose we compare results of a calculation and measurements of the $B(0)$ functions in a deep-sea regime in different turbid media of the sea and ocean water type.

For generality of the findings, experimental data are used which were obtained in media with drastically different shapes of scattering indicatrixes, and namely, in milky (with large particles) and in media with latex L-4 (colloidal). Data on brightness distribution bodies of different Λ and on $\chi(\gamma)_{exp}$ of milky media are presented in [8, 9]. The scattering indicatrix of the medium with latex (λ = 520 nm) was measured by Man'konskiy on an instrument of the Mineralogical Institute [10], while the function $B(0)$ for λ = 566 nm with different Λ were experimentally obtained by us according to the technique described in [11]. We will therefore not dwell on it.

It is unfortunately practically impossible to use full-scale data, since information about one-time measurements of the angular distribution of brightness and optical characteristics $\chi(\gamma)$ and Λ in some sea and ocean waters are currently almost lacking. We succeeded in only finding one case [12], where in addition to natural optical characteristics of the water, the function $B(0)$ is also given in a deep-sea regime for one of the regions of the Black Sea. We thus have data not only of laboratory studies, but also results, although few, of full-scale measurements.

For the scattering indicatrixes of the media mentioned above (Figure 1), the corresponding functions approximating them $\chi(\gamma)_{ap}$ which approximate them were selected in a similar manner to [6]. In both cases (i.e., for $\chi(\gamma)_{ap}$ and $\chi(\gamma)_{exp}$) the following integrated characteristics were computed: the average cosine $\cos\gamma$, asymmetry coefficient k, average angle γ and square of the angle γ^2 of scattering over the entire sphere. The obtained values are presented in Table 1. It also gives the numerical values for the approximation parameters of a, g_1 and g_2 [6] which determine the shape of $\chi(\gamma)_{ap}$. We note that in calculating the integrated characteristics, each examined experimental indicatrix, similarly to [13] was extrapolated to zero on the parabola, while for angles $\gamma > \gamma_o$, it was considered that $\chi(\gamma)_{exp} = \text{Const}$ (γ_o-- greatest angle of measurement of the indicatrix in the posterior hemisphere). It is apparent from Table 1 that the integrated characteristic, as should be expected, change in a fairly broad region, and their values for $\chi(\gamma)_{ap}$ and $\chi(\gamma)_{exp}$ are close /28 to each other. This means that the approximation is successful and one can expect a good coincidence between the calculated and the measured $B(\theta)$.

Figure 2 presents the average experimental $B^H(\theta)_{exp}$ (solid curves) and calculated /29 $B^H(\theta)_{cal}$ (dotted curves) angular distributions of brightness, normed for $\theta = 0°$. The calculation of $B(\theta)$ also used those values of Λ, in which $B(\theta)_{exp}$ were measured most reliably, for milky media, therefore the quantity $\Lambda \geq 0.494$, while for "latex" $\Lambda \geq 0.290$. The quantity $B(0)$ for Black Sea water was computed with $\bar{\Lambda} = 0.82$. It is the average for all values of Λ presented in [12].

It is apparent from Figure 2a that in the case of milky media, the calculated /30 data coincide fairly well with the experimental for all θ angles, especially with $0.7 \leq \Lambda \leq 1.0$ [sic], i.e., with quantities of Λ which are more characteristic for the majority of sea and ocean waters. In this case, the greatest discrepancy in brightnesses reaches ~ 30%.

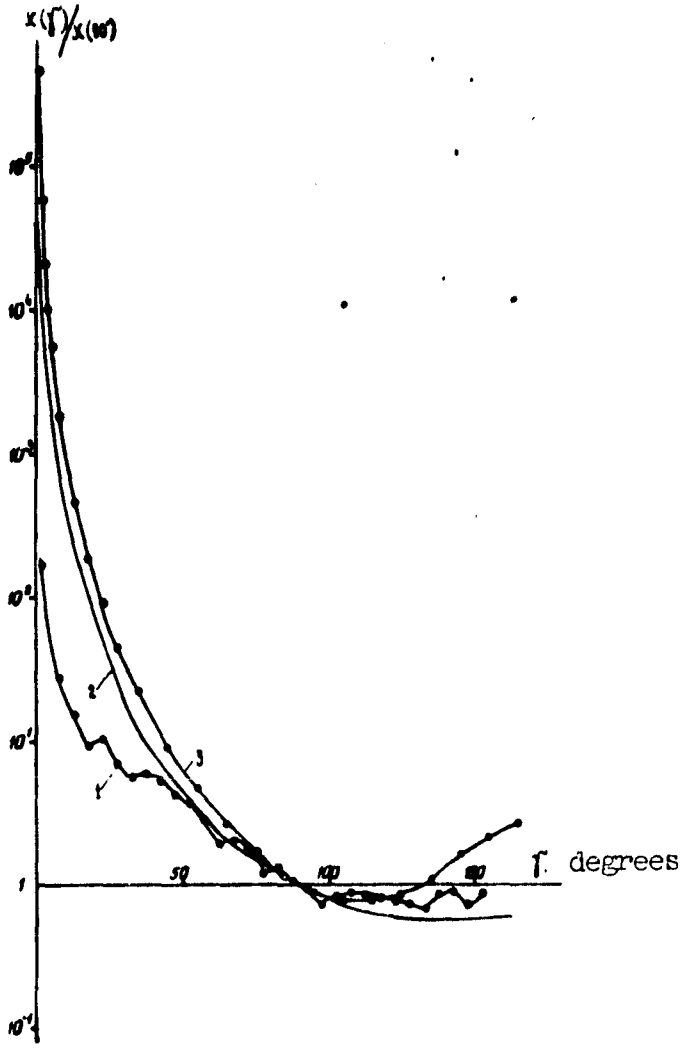

Figure 1. Scattering Indicatrixes: 1-- medium with latex L-4, 2--milky medium, 3-- Black Sea water

For colloidal media (Figure 2b), good coincidence of the calculated and experimental curves is observed to fairly small values of (0.4 Λ 1.0) [sic]. They are, generally speaking, characteristic for very clean ocean waters with slightly forward-extended indicatrixes of scattering. In this case, the greatest discrepancy between $B^{H}(\theta)$ with $\theta < 90°$ is about 40%.

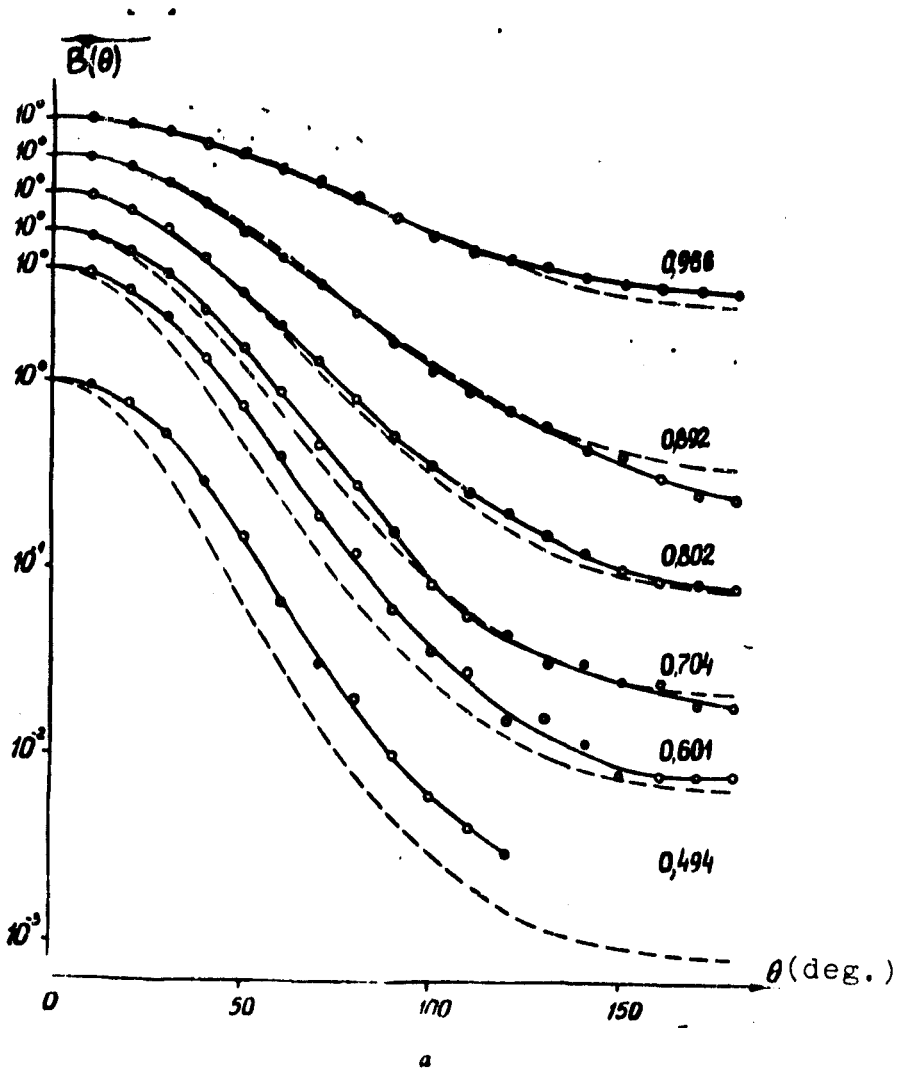

Figure 2. Angular Distribution of Brightness with Different (number on curves) a--milky medium, b--medium with latex, c--Black Sea water.

TABLE 1. Type of Scattering Indicatrix	Indicated Characteristics of Scattering Indicatrix				Approximation Parameters		
	Cos γ	k	γ_{rad}	γ^2_{rad}			
$x(\gamma)_{exp}$ of Black Sea water [12]	0,972	142,5	0,109	0,074	—	—	—
$x(\gamma)_{ap}$	0,972	126,9	0,114	0,079	0,99662	0,977	—0,60
$x(\gamma)_{exp}$ of milky medium [9]	0,927	54,6	0,233	0,187	—	—	—
$x(\gamma)_{ap}$	0,927	56,4	0,242	0,182	0,9977	0,930	0,50
$x(\gamma)_{exp}$ of latex medium	0,542	5,2	0,878	1,24	0,95194		
$x(\gamma)_{ap}$	0,542	5,2	0,892	1,25	—	0,600	0,60

/32

/30

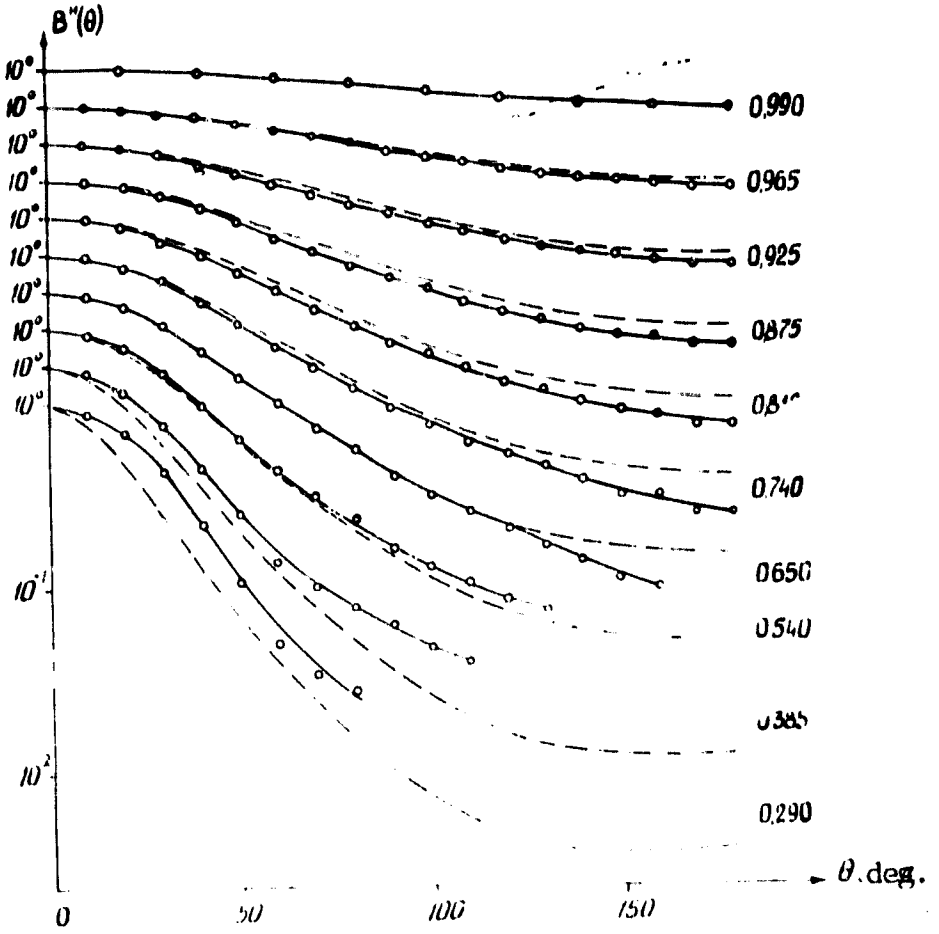

Figure 2b.

/31

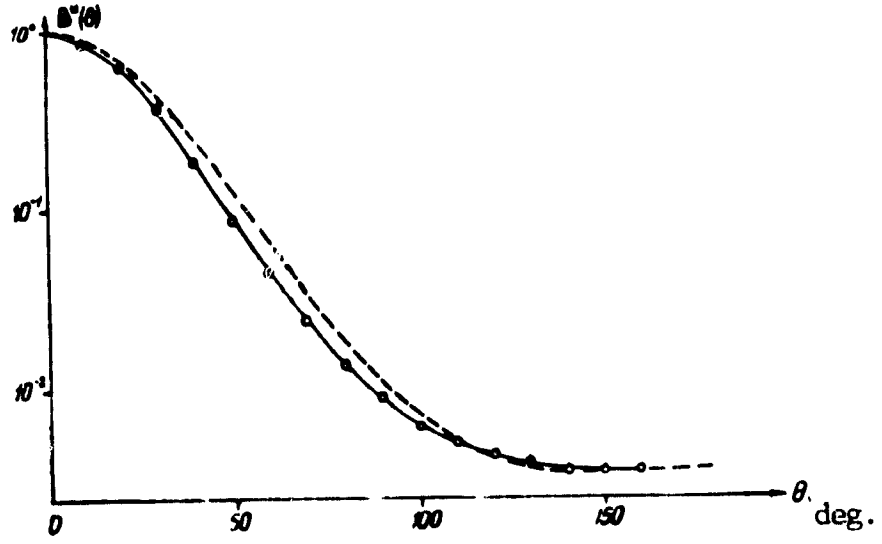

Figure 2c.

Experimental and calculated angular distribution of brightness for the Black Sea water are presented in Figure 2c. In this case, the maximum discrepancy between the experimental and calculated data occurs at the anterior hemisphere and is ~60%. /31

It is common knowledge that in practice, in addition to brightness in a certain direction, it is often necessary to know different integrated parameters of the light field in a deep-sea regime. It is therefore important to compare their values computed for $B(0)^{exp}$ and $B(0)^{cal}$ and presented in Table 2 (upper and lower lines respectively). Here Γ--parameter of deep-sea regime, μ--average cosine, $1/\bar{\mu}$--coefficient of angular distribution of descending radiation, R--coefficient of diffuse reflection, θ and $\bar{\theta}^2$--average angle of square of the angle of brightness distribution body. As we see, Γ, μ and $1/\bar{\mu}$ are very close to each other all the way to small λ. In this case the relative deviations for the milky medium for Γ are no more than 2%, while for μ--no more than 1%, and for μ^{-1}, no more than 3%. For the latex medium they are no more than 4%, 8% and 6% respectively.

TABLE 2.

λ	Integrated Parameters of Light Field					
	Γ	μ	$1/\bar{\mu}$	R	θ, rad	$\bar{\theta}^2$ rad
			Black Sea water			
0,82	0,23	0,79	1,21	0,017	0,579	0,491
		0,79	1,23	0,014	0,572	0,79
			Milky medium			
0,90	0,19	0,53	1,46	0,078	0,883	1,09
	0,19	0,54	1,49	0,081	0,920	1,16

[Table continued on next page]

TABLE 2. (continued)

0,80	0,30	0,66	1,35	0,032	0,745	0,79
0,80	0,30	0,66	1,36	0,033	0,760	0,802
0,70	0,40	0,74	1,28	0,017	0,660	0,610
	0,41	0,74	1,28	0,018	0,640	0,606
0,60	0,50	0,80	1,24	0,012	0,622	0,540
	0,51	0,79	1,22	0,010	0,554	0,471
0,50	0,60	0,84	1,19	0,008	0,600	0,520
	0,60	0,82	1,17	0,006	0,479	0,369
0,40	0,68	0,86	1,16	0,005	—	—
	0,69	0,87	1,13	0,004	0,407	0,284
0,30	0,77	0,91	1,13	0 003	—	—
	0,78	0,90	1,10	0,002	0,332	0,208

Latex medium

0,90	0,35	0,29	1,73	0,310	1,19	1,87
	0,37	0,27	1,72	0,330	1,25	2,00
0,80	0,52	0,38	1,61	0,160	1,02	1,50
	0,52	0,39	1,60	0,200	1,01	1,64
0,70	0,64	0,45	1,55	0,120	0,940	1,27
	0,63	0,47	1,51	0,100	0,990	1,27
0,60	0,75	0,52	1,50	0,090	0,890	1,10
	0,72	0,55	1,43	0,089	0,890	1,14
0,50	0,83	0,59	1,44	0,065	0,850	1,00
	0,80	0,62	1,36	0,060	0,790	0,940
0,40	0,89	0,67	1,36	0,050	0,800	0,920
	0,87	0,69	1,29	0,039	0,680	0,750
0,30	0,95	0,74	1,28	—	—	—
	0,92	0,77	1,22	0,024	0,570	0,560

3—45[4]

As for R, $\bar{\sigma}$ and σ^2, their relative deviations are considerably higher with small Λ. Thus, with $\Lambda = 0.5$ for a milky medium they are equal to: for R--17%, for σ-- /32
20%, and for $\bar{\sigma}^2$--29%, while for a latex medium, 8%, 7%, and 6% respectively.

Thus, this analysis shows that this method of mathematical modeling of the light field in a deep-sea regime applied to real turbid media, yields quite satisfactory results.

Since $\chi(\gamma)$ and Λ of sea and ocean waters lie practically within the examined range of changes of these optical characteristics, one can hypothesize that the suggested method will be suitable for modeling light fields in natural waters as well.

BIBLIOGRAPHY /34

1. Ambartsumyan, V. A. "New Method of Calculating Light Scattering in a Turbid Medium," Izv. AN SSSR, Ser. Geogr. geofiz., No 3, 1942.

2. Sobolev, V. V. "Light Regime in Deep Layers of a Turbid Medium," Izv. AN SSSR, Ser. Geogr. geofiz, 8, No 5, 1944.

3. Loskutov, V. N. "Light Regime in Deep Layers of a Turbid Medium with Very Extended Scattering Indicatrixes," Vestnik LGU, ser. matem. mekh. astr. No 3, issue 3, 1969.

4. Zege, E. P. "Light Field in the Depth of a Scattering and Absorbing Medium," Izv. AN SSSR, FAO, 7, NO 2, 1971.

5. Sobolev, V. V. Rasseyaniye sveta v atmosferakh zvezd i planet ["Light Scattering in Atmospheres of Stars and Planets"], Moscow, Nauka, 1972.

6. Solov'yev, M. V.; and Shemshura, V. Ye. "Approximating the Light Scattering Indicatrix by Sea Water by Haney -Greenstein Indicatrixes," Morskiye gidrofizicheskiye issledovaniya, No 2(72), 1976, Sevastopol', Izd. MGI AN UkSSR,.

7. Solov'yev, M. V.; and Shemshura, V. Ye., "Effect of the Shape of the Scattering Indicatrix on the Light Field in a Deep-Sea Regime," Morskiye gidrofizicheskiye issledovaniya, No 1 (75), 1978, Sevastopol', Izd. MGI AN UkSSR, 1978.

9. Timofeyeva, V. A.; and Koveshnikova, L. A. "Experimental Determination of the Coefficient of Extinction of Turbid Media," Izv. AN SSSR, FAO, 2, No 3, 1966.

10. Man'kovskiy, V. I.; Semenikhin, V. M.; Neuymin, G. G. "Marine Submergible Nephelometer," Morskiye gidrofizicheskiye issledovaniya, No 2 (48), 1970, Sevastopol', Izv. MGI AN UkSSR.

11. Timofeyeva, V. A.; and Solomc , V. K. "Shape of the Stationary Distribution Diagram of Brightness in Tur' Media of the Sea Water Type," Izv. AN SSSR, FAO, 6, No 6, 1970.

12. Prokudina, T. M.; and Pelevin, V. M. "Determination of the Size of the Survival Parameter of the Light Quantum According to Characteristics of Light Fields in the Sea", in Optika okeana i atmosfery ["Optics of the Ocean and Atmosphere"], Leningrad, Nauka, 1972.

13. Man'kovskiy, V. I. "Experimental Scattering Indicatrixes of Light by Sea Water", Morskiye gidrofizicheskiye issledovaniya, No 3 (62), 1973, Sevastopol', Izd. MGI AN UkSSR, 1973.

13. Schellenberger, V. G. 1964. "Asymptotic Radiation Field in Water Areas for Scattering Conditions", Pure and appl. geophys., 58, N 3.

DEPENDENCE OF PARAMETERS OF DEEP-SEA BRIGHTNESS BODY ON "P" CRITERION

PELEVIN, V. N. AND PROKUDINA, T. M.

Based on model experiments and full-scale measurements in the sea, an empirical dependence is established for a number of parameters of a deep-sea light regime on the values $P = \sigma\gamma^{-2}/\chi$ which are the ratio of the second moment of the volumetric scattering functior to the absorption index.

The link between light field parameters in a deep-sea regime and primary hydro-optical characteristics (PHC) has been studied by many authors [1-7, et al]. However, as yet there are no simple relationships which make it possible to graphically analyze field structure changes during fluctuations in the medium PHC.

This study searched for approximate relationships suitable for this analysis and engineering estimates of parameters of a deep-sea light field using given sea water characteristics.

The studies were made on models and directly in the sea. The laboratory unit for modeling the light field on artificial media was designed from experimental basins developed in the BSSR Academy of Sciences Institute of Physics [7]. The modeling method was similar to that of V. A. Timofeyeva [6]. The main difference in the unit (designed b y V. G. Yepishin) was flexible light guides connecting miniature photometric sensors in the medium, and photodetectors (or light sources) outside the basin. This drastically reduced the shading of the medium by

the design components. This is very important with high coefficients of similarity, and at the same time reduces errors in the model measurements.

Modeling was done using milky and alcohol-rosin suspensions in water and a solution of nigrosine as the light-absorbing agent.

The measurements of spatial-angular distributions of brightness in the sea used instruments previously described [8 - 9].

The parameters which characterize the shape of the scattering indicatrix $\chi(\gamma)$ in the media where the deep-sea regime was studied are given in the table.

TABLE. PARAMETERS CHARACTERIZING THE SHAPE OF THE SCATTERING INDICATRIX

Number of station	Depth, m	Region	$\bar{\gamma}$	$\bar{\gamma}^2$	$\gamma_{0,9}$	$\beta \cdot 100\%$	Δ	K
100	100	Black Sea	0,062	0,037	7°	0,41	6,5	322
367	30	Pacific Ocean	0,152	0,098	18°	0,98	5,0	100
397	100	Pacific Ocean	0,230	0,214	30°	2,54	4,6	39
367	150	Pacific Ocean	0,300	0,320	45°	4,12	4,2	23
347	300	Southern part of Sargasso	0,427	0,600	70°	7,25	4,2	10,5
		Rosin medium	0,211	0,189	30°	2,05	5,0	19
			0,412	0,436	60°	4,48	4,5	21

Here $\bar{\gamma} = \int_{(4\pi)} \gamma \, x(\gamma) d\omega$; $\bar{\gamma}^2 = \int_{(4\pi)} \gamma^2 \cdot x(\gamma) d\omega$ ---average angle and average square of the angle of single scattering; $\gamma_{0,9}$--angle within whose limits there is 90% light, scattered during single scattering. $\Delta = \lg \frac{\chi_{max}}{\chi_{min}}$ --degree of extension of the indicatrix. $K = \frac{\sigma - \beta}{\beta}$ --coefficient of asymmetry (σ and β--indices of scattering and back-scattering, respectively, [10]. /36

It is apparent from the table that the difference in the indicatrixes of milky and rosin suspensions is significant between them, although it is smaller than the

differences in the indicatrixes of different water areas in the ocean. The milky indicatrix seemingly corresponds to the "average" ocean, while the rosin is close to that for clean waters of the Sargasso Sea.

The parameter of photon survival $\Lambda = \frac{\sigma}{\sigma + \chi}$, where χ --absorption index, changed in the model media in limits of $0.3 < \Lambda < 0.99$ by creating different concentrations of nigrosine. The quantity Λ in artificial media and in the sea was determined by the technique described in (11).

The angular distributions of brightness $b(\omega)$ were measured in a deep-sea light field. The average distribution cone was computed from the values $B(\omega)$

$$\mu = \int_{(\omega)} \cos\Theta \cdot B(\Theta)\, d\omega \Big/ \int_{(\omega)} B(\Theta)\, d\omega,$$

The coefficient of diffuse reflection

$$R = \int_{\Theta_1}^{\pi} B(\Theta) \cos\Theta \sin\Theta d\Theta \Big/ \int_{0}^{\pi} B(\Theta) \cos\Theta \sin\Theta d\Theta,$$

The average angle of distribution

$$\bar{\Theta} = \int_{0}^{\pi} \Theta \cdot B(\Theta) \sin\Theta d\Theta \Big/ \int_{0}^{\pi} B(\Theta) \sin\Theta d\Theta.$$

The index of vertical attenuation $\alpha(12)$ was measured indirectly.

Analysis of the findings demonstrated that no unequivocal dependence is observed of the dimensionless field parameters on the value Λ, or on the parameter $\varepsilon = \chi + \sigma$, (12), where $\varepsilon = \varepsilon(12)$, in the given interval of change in Λ and $\chi(\gamma)$. At the same time, the angular brightness distributions which were normed for one, with the most diverse scattering indicatrix of the medium and different Λ, look as if they represent a certain unified family which depends on one, yet unknown parameter. This parameter must include all three primary characteristics of the medium: χ, σ and $\chi(\gamma)$.

In order to search for this parameter, one should take into consideration that the dimensionless brightness body essentially depends on two dimension characteristics of the medium: volumetric scattering function $\sigma \times \chi(\gamma)$ m^{-1} (10) and absorption index $\varkappa$ M^{-1}. It is clear from the similarity theory, that the dimensionless parameters of the SP (light-signal instrument) may depend only on the dimensionless characteristics of the medium. Only a dimensionless volumetric scattering function $\overset{\times}{(\lambda)\chi\cdot\sigma}$ can serve as the latter. Assigning this function is equivalent to assigning its moment, and only the first moments have definitive importance. /37

Under conditions of multiple light scattering, when a deep-sea regime is formed, it is natural to hypothesize that the second moment of the dimensionless volumetric scattering function has the greatest value, i.e., the quantity

$$\int_{(4\pi)} \gamma^2 \frac{\sigma\cdot\chi(\gamma)}{\varkappa} d\omega = \frac{\sigma}{\varkappa} \int_{(4\pi)} \gamma^2 \cdot \chi(\gamma)\, d\omega = \frac{\sigma\bar{\gamma}^2}{\varkappa}.$$

Analysis of the experimental data confirmed this hypothesis. The family of brightness bodies in the deep-sea regime obtained with different Λ and indicatrixes, was dependent on the quantity $P = \frac{\sigma\bar{\gamma}^2}{\varkappa}$; and on the parameter. The dependences of the average cosine of the brightness body μ, the coefficient of diffuse reflection R, the average angle of brightness θ on the quantity P were the same both for media with "milky" and "rosin" indicatrixes, and for all sea water in which measurements were made, in the following ranges of P, μ, R and θ: $0.2 \leq P \leq 9$; $0.008 \leq R \leq 0.3$; $0.3 \leq \mu \leq 0.83$; $0.55 \leq \theta \leq 1.2$ (the θ angle in radians).

In the region $0.2 \leq P \leq 1$, especially important for sea water, the relationships $\mu(P)$ and $R(P)$ are described by the empirical formulas:

$$\mu = (1 - 0{,}37\, P)^{+0{,}01}_{-0{,}0} \quad (1)$$

$$R = 0{,}04 \cdot P^{1\pm 0{,}008} \quad (2)$$

here the greatest deviations of available experimental data from the relationship (1) are given for μ. For R, the standard value of the deviation is presented from the available data for the sea and model media.

Calculation of the index for vertical attenuation in the deep-sea regime was made according to the known formula:

$$\alpha_\infty = \varkappa \cdot \mu^{-1}. \qquad (3)$$

We now may hypothesize the following engineering technique for computing the parameters of deep-sea light regime in the sea.

According to the PHC of the medium, $P = \frac{\sigma\bar{\gamma}^2}{\varkappa}$ is computed. The spectral distribution P_λ is obtained when spectral values σ, $\varkappa$, $x(\gamma)$ are used.

2. The parameters μ and R_λ are determined from formulas (1, 2). /38

3. According to (3), the deep-sea indicator of attenuation α_∞ and its spectral distribution are computed.

The error in this calculation is formed from a) inaccurate value of PHC of the medium; b) error in the empirical formulas (1, 2).

Assume that the values $\varkappa$, σ, $\bar{\gamma}^2$ are known with standard deviation of 5% each. Taking into consideration the structures of the formula for P, and assuming statistical independence of deviations $\varkappa$, σ and γ^2 on the true values, we will assess the coefficient for variation in P as $0{,}05\sqrt{3} \approx 0.085$. It follows from (1) that $\left|\frac{d\mu}{dP}\right| = 0.185 \cdot P^{-1/2}$. For the values P = 0.25 and 1.0 which correspond to the interval of the most widespread values P in the ocean water (in the region of the spectral "window of transparency," (close to 500 nm) the corresponding values are $\left|\frac{d\mu}{dP}\right| = 0.37$ and 0.185. From here the standard deviation for μ equals 0.37 x 0.085 x 0.25 = 0.008

and 0.016 respectively. The quantities are smaller than the limiting deviation μ, indicated in formula (1). Therefore in evaluating the errors in α_∞ we will take the latter into consideration. For the boundaries of the mentioned segments $0.25 \leq P \leq 1$ (on these boundaries the values $\mu = 0.81$ and 0.63), the amount of limiting error in α_∞ is 7% and 8.4% respectively.

We introduced the parameter $P = \frac{\sigma\bar{\gamma}^2}{\chi}$ previously (13) in analyzing the light fields of isotropic light source in the sea. One should note, however, that a close parameter compiled from the PHC of the medium, was introduced even earlier by G. V. Rozenberg (3). L. S. Dolin also obtained an expression corresponding to his parameter in analyzing the field structure in a small-angular approximation (14).

The measurement results described here demonstrated the usefulness of using this parameter to evaluate the link between all the main characteristics of the light field and the PHC of the medium in a deep-sea regime, where the field is formed by multiple-scattered light. At the same time, the new empirical relationships were obtained which make it possible to plan a simple technique for evaluating the parameters of the light field in a deep-sea regime according to the given characteristics of the marine medium.

BIBLIOGRAPHY

1. Ambartsumyan, V. A. "New Method of Calculating Light Scattering in a Turbid Medium," Izv. AN SSSR, Ser. Geogr. i geof., No 3, 1942.

2. Sobolev, V. V. "Light Regime in Deep Layers of Turbid Medium," Izv. AN SSSR, Ser. Geogr. i geof., vol 8, No 5, 1944.

3. Rozenberg, G. V. "Light Regime in Depth of Scattering Medium and Spectroscopy of Dispersed Substances," Dokl. AN SSSR, 122, No 2, 1958, p 211.

4. Loskutov, V. M. "Light Regime in Deep-Sea Layers of Turbid Medium with Very Extended Scattering Indicatrix," Vestnik LGU, Ser. Matem. nekh, astr, No 3, issue 3, 1969. /39

5. Zege, E. P. "Light Field in Depth of Scattering and Absorbing Media," Izv. AN SSSR, FAO, vol 7, No 2, 1971.

6. Timofeyeva, V. A. "Experimental Study of Light Field in Turbid Media," in Voprosy fiziki morya. Tr. MGI AN UkSSR ["Questions of Physics of the Sea, Proceedings of Marine Hydrophysical Institute of the Ukrainian SSR Academy of Sciences"], Izv. Naukova dumka, vol 37, 1966.

7. Ivanov, A. P. Optika rasseivayushchikh sred ["Optics of Scattering Media"], Izd-vo Nauka i tekhnika, Minsk, 1969.

8. Ochakovskiy, Yu. Ye.; Pelevin, V. N.; and Yefimenko, I. D.; Karlsen, G. G., and Shifrin, K. S. "Spread of Natural Radiation in the Ocean," in Gidrofizicheskiye i gidrooptricheskiye issledovaniya v Atlanticheskom i Tikhom okeanakh ["Hydrophysical and Hydrooptical Studies in the Atlantic and Pacific Oceans"], ed. by A. S. Monin and K. S. Shifrin, Izd-vo Nauka, Moscow, 1974, 166 - 190.

9. Yefimenko, I. D., and Pelevin, V. N. "Angular Distribution of Brightness of Solar Radiation in Water of Indian Ocean," in Gidrofizicheskiye i opticheskiye issledovaniya v indiyskom okeane ["Hydrophysical and Optical Studies in the Indian Ocean"], ed. by L. M. Brekhovskiye and K. S. Shifrin, Izd-vo Nauka, Moscow, 1975.

10. GOST 19210-73, 1974 Gidrooptricheskiye kharakteristiki, terminy i opredeleniya ["State Standard. Hydrooptical Characteristics, Terms and Definitions"], Moscow.

11. Pelevin, V. N.; Prokudina, T. M. "Determination of Absorption Indices and Parameters of Photon Survival According to Characteristics of a Light Field in the Sea," Gidrofizicheskiye i gidrooptricheskiye issledovaniya v Atlanticheskom i Tikhom okeanakh, Izd-vo Nauka, Moscow, 1974.

12. GOST 19209-73, 1974. Svetovoye pole v vodnoy srede; terminy i opredeleniya ["State Standard. Light Field in an Aquatic Medium, Terms and Definitions"], Moscow.

13. Pelevin, V. N.; and Prokudina, T. M. "Light Field in the Sea Created by Localized Isotropic Radiation Source," in Gidrofizicheskiye i gidrooptricheskiye issledovaniya v Atlanticheskom i Tikhom okeanakh, Izd-vo Nauka, Moscow, 1974.

14. Dolin, L. S. "Spread of a Narrow Light Beam in a Medium with Strongly Anisotropic Scattering," Izv. vyssh. uchebn. zaved, Radiofizika, 9, No 1, 1966.

MEASUREMENT OF PHOTOSYNTHETIC RADIANT ENERGY IN THE OCEAN

B. A. VAYNEMAN

Requirements for the measurements and calculations of photosynethetic radiant energy (PRE) in the ocean are examined. Different methods and instruments are compared for measuring and computing the PRE. A conclusion is drawn regarding the expediency of using methods based on measurements by simple instruments with subsequent calculation of the total (in the PRE range) irradiance for standard mass measurement of PRE. It is noted that it is necessary to further study the spectral distribution of underwater energy to pinpoint the optical classification of waters and to improve the methods of PRE computation. Certain results are presented of computing the PRE in the Black Sea.

Solid energy necessary for photosynethetic processes in the World oceans. Penetrating the water, solar radiation creates in its upper layer an illuminated (photic) zone whose lower boundary is usually determined by the depth at which the irradiance is 1% of the subsurface. Photosynthesis occurs in the photic zone which governs primary production of the ocean.

In studying primary production, one of the main problems is to determine its dependence on the irradiance conditions since it is the radiation energy absorbed /40 by the photosynthetically active pigments which is used to transform inorganic material into organic.

There are difficulties, however, in determining the photosensitivity of phytoplankton populations of a mixed type. Their adaptations to the radiation flux can be very diverse, especially the spectral composition of this flux. The flux spectral composition changes differently with depth, depending on optical properties of the water.

The importance of unifying techniques to measure and calculate radiant energy in all the oceans led to the creation of Working Group No. 15 (WG 15) on photosynthetic radiation energy [27] through the efforts of UNESCO, the scientific committee on oceanographic research (SCOR) and the international association of physical

oceanography (IAPO).

WG 15 made a decision to consider photosynthetic radiant energy (PRE) in the ocean a limited region of wavelengths from 350 to 700 nm as a consequence of the fact that energy with wavelength shorter than 350 nm can be harmful, while wavelengths over 700 nm have little value for photosynthesis in the ocean.

The method of collecting radiation energy in light fields in an aquatic medium must correspond to the physical concepts of irradiance (from above or from below) or spatial irradiance.

Irradiance (above or from below):

$$E = \int_{(2\pi)} B \cos\theta \, d\Omega, \tag{1}$$

Spatial irradiance:

$$E^0 = \int_{(4\pi)} B \, d\Omega, \tag{2}$$

where: B--energy brightness, θ--vertical angle, Ω --solid angle.

Integration presented in (1) and (2) can be done in practice with good accuracy by means of optical integrals (collectors), and thus, simple instruments can be designed for the measurements.

Are the aforementioned physical concepts sufficiently representative for the method of collecting radiant energy used by the phytoplankton? This question cannot be accurately answered, but heuristic arguments demonstrate that the correspondence must be high.

Irradiance measurements should be made in a quantum unit, since it is precisely the number of quanta which determines the intensity of photosynthesis.

One quantum, regardless of the energy it contains, can excite only one molecule. At the same time, the energy contained in one quantum is inversely proportional to

the radiation wavelength, i.e., the radiation quanta with shorter wavelength contain more energy than the radiation quanta with greater wavelength, or what is the same, with equality of energy, the longer wavelength radiation contains a larger number of quanta. In the comparison of equal quantities of energy equal narrow spectral intervals with λ_{eff} = 350 nm and λ_{eff} = 700 nm, it is apparent that radiation with λ_{eff} = 700 nm contains double the number of quanta. This red radiation is thus capable of exciting double the number of molecules than blue radiation with the same energy. /41

What has been said makes it possible to conclude that in photobiological studies during irradiation of characteristics of pigmented systems, one should use quantum units. If energy units are used, the effect of red radiation will be underestimated.

However, in measuring the total PRE in the entire range 350 - 700 nm, one can also use energy units, since experimental studies have established that the ratio of total quantum irradiance to total energy irradiance Q_Σ/E_Σ in a broad range of water types remains approximately constant [11, 12].

It should be stressed that use of light terms and units such as degree of illumination, lumen, lux, etc., which hydrobiologists at times permit, is inapplicable. All the light concepts and units are based on the physiological action of light on the human eye, and therefore have a subjective nature which does not permit them to be correctly employed in any other areas except the areas associated with human vision.

WG 15 acknowledged that knowledge of the total quantum or energy irradiance (in the entire PRE range) is not sufficiently informative, because the reaction of ocean photosynthetic organisms depends on wave distribution of the radiant energy. It recommended that spectral measurements of underwater irradiance be made. It was noted at the same time, that the detailed measurements of spectral energy distribution

in situ, and in devices which simulate conditions in situ are not feasible as a simple standard method in studying primary production, in light of the fact that these measurements require complicated and expensive equipment, while the measurements themselves are complicated and require a lot of time. Radiation energy which is suitable for underwater photosynthesis can be assessed through measurements by a simple instrument with subsequent determination of the water type according to the optical classification of waters of N. Yerlov [18], and from here, the probable spectral distribution of energy. One can thus determine the total energy. The WG 15 evaluated the possibility of using these methods through mathematical calculations [28] and experiments in the ocean [29]. It recommended the creation of simple equipment for these methods.

We will examine the existing methods and instruments for measuring PRE in the ocean.

The most complete information about underwater radiant energy is provided by /42 the methods of detailed measurements of spectral distribution of this energy. There are different instruments which realize these methods.

The spectroradiometer which was developed in the laboratory of visibility of the Scripps Institute of Oceanography [26] is a double monochromator with diffraction arrays. A digital volt meter and automatic self-recorder are attached at the instrument outlet. The spectroradiometer is characterized by high resolution for the spectrum ($\Delta\lambda$ = 5 nm), good angular characteristics of the irradiance collector and absolute calibration in energy units. However, this instrument has inherent significant shortcomings: production of the entire spectrum (350 - 750 nm) at one level takes more than 20 minutes, while the maximum depth of recording radiance in clean water does not exceed 35 m.

The autonomous spectral radiometer developed in the laboratory of physical oceanography of the Paris University [13] has a considerably greater fast response. The instrument is made based on a monochromator with diffraction array. Distribution of irradiance for the spectrum in the range 375 - 850 nm is recorded on a roll of photopaper. The diffraction array scans in less than 3 seconds. This makes it possible to obtain about 30 recordings in 30 minutes from the surface to depth 100 m. However, the lengthy time for developing the photo paper and complex processing of the recordings significantly reduce the advantages of the fast operation of the instrument itself.

The colleagues of the New England Aquarium in Boston used another possibility. Scanning of the spectrum in the LSDS instrument [23] was done by turning a round interference filter with continually variable wavelength. The instrument output was made in the form of an analog signal which could be viewed on an oscillograph screen or recorded on magnetic tape.

Spectral scanning in the Japanese instrument [25] is done by rotation of a diffraction array and synchronous movement of a wedge-shaped interference filter at continuously variable wavelength. Scanning in the range 400 - 700 nm (at one level) takes 60 seconds. Recording is done on a two-coordinate self-recorder on board the ship. The instrument is connected to the ship by a multiple-strand cable.

All the instruments described above are complicated, expensive, and working with them requires a high degree of skill.

There are instruments which measure radiant energy in several narrow or relatively narrow spectral regions which are isolated either with the help of a certain number of selective receivers [21], or with the help of changeable light filters [4, 5, 7, 17]. However, construction of the spectral distribution of energy by

interpolating the measurement results in individual sections of the spectrum, or calculation of the total PRE by integrating these results is accompanied by large /43 errors because of the fairly large discreteness of the measurements and the complicated structure of the underwater energy spectrum.

In order to determine the total energy from the entire PRE range, one can use nonselective thermoelectric receivers, pyranometers which are banks of thermal elements [14]. However, the low sensitivity of these instruments does not make it possible to use them at distance over 40 m without special amplifiers. In addition, difficulties arise in considering the percentages of energy with wavelengths over 700 nm which are introduced into the instrument readings. This will significantly distort the readings, especially at low depths.

The VARIPO is an instrument which uses the variospectrometric method of measuring irradiance [3]. This instrument contains a direct-vision prism (Amici prism) jointly with a norming diaphragm which makes it possible to create the necessary shape of the spectral characteristics. The instrument can be nonselective in the range 350 - 700 nm, or its sensitivity can be made proportional to the wavelength. The high sensitivity of the VARIPO which is achieved because a photomultiplier (PM) is used permits the instrument to operate to depths 200 - 250 m.

The instrument named quantometer was made by N. Yerlov and K. Nyugard [20]. Its radiation receiver is selenium photoelement whose various sections of the active surface are covered with different colored filters. By selecting the combinations of filters one can form the required spectral characteristics of the instrument. The instrument can be nonselective, or its sensitivity can be proportional to wavelength in the PRL range. It will then be an energy meter or quantometer respectively. The quantometer is very simple and inexpensive.

The instrument of L. Prier is another solution to the problem of creating a quantometer [24]. A corrector is located between the collector of the instrument and the detector which is a PM. The corrector consists of an interference filter with continuously variable wavelength and diaphragm. It has selectivity which compensates for the selectivity of the detector such that the resulting spectral sensitivity of the instrument becomes proportional to the wavelength, i.e., the output of the instrument is proportional to the sum of the quanta in the PRE range. Because a PM is used, this instrument is more sensitive than the quantometer of N. Yerlov, however it is more complicated and more expensive.

The use of quantometers, in the same way as instruments which employ thermal elements, causes certain difficulties. Because the long wavelength section of the spectrum is strongly absorbed by the surface layer of water, wave action causes great fluctuations in the recording instrument. Measurement of the subsurface irradiance often cannot be done with sufficient accuracy without the use of an integrating self-recording.

The methods based on irradiance measurement in one relatively narrow spectral /44
region which corresponds to the maximum transmission of ocean water, i.e., in the blue region (λ_{eff} = 460 - 490 nm) with subsequent calculation of the PRE based on the optical classification of waters, do not have the majority of shortcomings mentioned above. In contrast to the spectroradiometers, energy meters and quantometers, an irradiance gage which is designed to operate in the blue spectral region, is a simple and inexpensive instrument. It can be equipped with a selenium photo element in combination with a blue filter and with neutral attenuator. This gage does not have the significant inconveniences which develop when energy meters and quantometers are used, since it can operate well in the surface layer of the ocean because of the high transmission by water of radiation in the blue spectral region.

The sea tests done by WG 15 in the Gulf of California demonstrated that relatively narrow-band filters with maximum transmission corresponding to the maximum transmission of ocean water, may be used to estimate the underwater PRE in waters of all types with satisfactory accuracy [29].

Publication [19] has suggested a simple method for measuring the quantum PRE ($Q_{(350 - 700\ nm)}$) in the ocean, based on the use of a simple irradiance gage in the blue spectral region ($E_{(\lambda\ eff=465\ nm)}$):

$$Q_{(350-700)} = E_{(465)} \left(0{,}23 + \frac{5{,}6}{3 + z}\right), \tag{3}$$

where: z--depth in meters, Q and E--assigned in percentages of subsurface values.

The essence of this method is that only the relative quantities are measured underwater. The instrument therefore does not need graduation. Part of the problem is estimating the subsurface quantities in absolute units. This can be done by two methods.

Measurement in the blue spectral region can serve to determine the quantum irradiance above the ocean under all conditions, except low position of the sun ($h_0 < 15°$), because spectral distribution of total (from the sun and the sky) in the range 350 - 70 nm does not depend very much on turbidity of the air, cloud cover, and altitude of the sun [8]. Calibration in this case is done by simple comparison of the irradiance gage with a quantometer in daylight.

Another method for evaluating quantum irradiance above the ocean is to use the readings of a shipboard pyranometer ($E_{(350-3000\ nm)}$). The theoretical studies of K. S. Shifrin et al. [1] for a standard atmospheric model demonstrated that

$$E_{(350-700)} = k \cdot E_{(350-\ldots)} \tag{4}$$
$$k = 0{,}44 \pm 0{,}03$$

With the help of the transform: /45

$$\frac{Q_{(350\ 700)}\,\text{Quanta}_M \cdot S^{-1}}{E_{(350\ 3000)}\,[W \cdot M^{-2}]} = 2{,}75 \cdot 10^{18} \qquad (5)$$

A correlation is obtained which makes it possible to evaluate the quantum irradiance above the ocean from the pyranometer readings:

$$Q_{(350-700)} = 1{,}2 \cdot 10^{18} E_{(350-3000)}. \qquad (6)$$

It remains to examine the reflection from the ocean surface which reduces the quantity of quantum irradiance to subsurface.

Publication [6] has described a method for calculating underwater irradiance from above in any section of the spectrum in the PRE range based on simple measurements of irradiance in the blue spectral region (λ_{eff} = 490 nm) using the optical classification of waters. The method consists of the following: the distribution of irradiance according to depth is measured, these measurements are used to calculate the coefficient of underwater irradiance η and the indicator of vertical attenuation of irradiance from above α_E (λ_{eff} = 490 nm). The water type is determined from the found quantity α_E (λ_{eff} = 490 nm), while the quantities $\alpha(\lambda)$ for other wavelengths are found from the water type. The found values $\alpha(\lambda)$ are used to compute the quantities $\eta\downarrow$. By using spectral distribution of energy which falls on the ocean surface $J(\lambda)$ [8], and the quantity of albedo A [10], one can compute the value of irradiance from above in relative units in the necessary spectral region at different depths:

$$E_{\downarrow}(z) = \int_{\lambda_1}^{\lambda_2} (1-A)\, J(\lambda)\, \eta_{\downarrow}(\lambda, z)\, d\lambda, \qquad (7)$$

where z--depth.

The transition to absolute values of irradiance underwater $E\downarrow(z)$ is made from the absolute values of energies falling on the ocean surface measured by the shipboard pyranometer.

The methods described above for computing PRE based on measurements by simple instruments use the optical classification of water of N. Yerlov [18]. This classification has certain shortcomings however. In particular, typification of the water is done with great discreteness. The one-parameteric optical classification of water according to the value $\alpha(\lambda = 500\ nm)$ suggested by V. N. Pelevin and V. A. Rutkovskaya [9] has important advantages. The nomogram presented in the work for the spectral course $\alpha(\lambda)$ provides a more detailed division into water types. The classification makes it possible to isolate water types without losing information about the measured value α, and to estimate the water types with tolerance reflecting the accuracy of some measurements, and to pinpoint the water types by measurements of $\alpha(\lambda)$ at the required wavelength λ. /47

The use of the water classification of V. N. Pelevin and V. A. Rutkovskaya in methods of PRE computation will increase the accuracy of these methods.

There are different designs of more or less simple irradiance gages in one spectral region which are suitable for the aforementioned methods of PRE computation.

Instrument [15] is separated from the ship with the help of a buoy at a distance of 50 m in order to reduce the shading by the ship and to make a freefall in the water with a velocity of about 1 m x s^{-1}. Its energy receiver is a selenium photo element covered with a narrow-band filter. The instrument is connected by a communications cable to the ship. The recording is done on the ship on a two-coordinate self-recorder.

The autonomous instrument [12] can be lowered on any cable since it does not require connection by any cable to the ship. Recording of the $E_{\downarrow}(z)$ is done on Polaroid film placed inside the instrument. Its energy receiver is a PM covered with narrow-band filter.

In cases where it is necessary to measure the quantity of irradiation in a certain time interval, one can use a time-integrating electronic circuit on an electrochemical tetrode [16].

The instrument of the Marine Geophysical Institute of the Ukrainian SSR Academy of Sciences [2] was developed with regard for requirements for the gage of underwater irradiance in one relatively narrow spectral region as applied to methods of PRE computation described above. It has a cosine collector, color filter, selenium photo element and depth gage. When the instrument is running, it is suspended from a three-strand cable or any other cable. In the latter case, a three-strand communications cable is required. The function $E\downarrow(z)$ is recorded on board the ship on a two-coordinate self-recorder. This gage is simple, reliable and inexpensive. It requires no more than 2 minutes to probe from the surface of the ocean to a depth of 100 m. This significantly diminishes the effect on the measurements of ship drift and variations in the total incident radiation caused by changes in the sun's altitude and the condition of the atmosphere.

As an example of using this instrument to determine the underwater PRE according to the technique stated in the aforementioned publication [19], Table 1 presents the results of computing $Q_{(350-700\ nm)}$ and $\alpha_{\downarrow}(\lambda_{eff} = 480\ nm, \Delta z = 5\ m)$. The calculation was made based on measurements of $E\downarrow(z)$ and total incident radiation $E_{(350-3000\ nm)}$ made in the spring and fall of 1977 in the Kerchenskiy Strait and the northeast section of the Black Sea adjacent to it. The location of the stations is illustrated in Figure 1.

It is apparent from all that has been examined above that the problem of unifying /48
the technique of measuring and computing the PRE in scales of the entire ocean is being solved very successfully both in our country, and abroad. The majority of data

TABLE 1. DATES, TIME OF MEASUREMENTS, INDEX OF VERTICAL ATTENUATION OF IRRADIANCE FROM ABOVE $\alpha_{E\downarrow}(\lambda_{eff} = 480$ nm, $\Delta z = 5$ m), TOTAL INCIDENT ENERGY $E_{(350-3000\ nm)}$ AND QUANTUM IRRADIANCE UNDERWATER $Q_{(350-700\ nm)}$

Number of Station	Date (1977)	Time, ms	$\alpha_{E\downarrow}(\lambda_{eff} = 480$ nm, $\Delta z = 5$ m) Layer Δz, m					$E_{(350-3000\ nm)}$, W x m^{-2}	$Q_{(350-700\ nm)}$, Quanta x m^{-2} x s^{-1} x 10^{18} Depth z, m					
			0–5	5–10	10–15	15–20	20–25		0	5	10	15	20	25
		3	4	5	6	7	8	9	10	11	12	13	14	15
1	6 June	11–00	0,02	0,05	0,02	0,02	—	327,6	377	205	93	64	46	—
2	6 June	14–00	0,03	0,05	0,03	0,04	0,03	—	—	—	—	—	—	—
7	7 June	12–15	0,15	0,11	—	—	—	759,8	876	107	24	—	—	—
8	7 June	14–00	0,07	0,11	0,04	—	—	731,9	843	278	59	32	—	—
9	7 June	16–20	0,05	0,06	0,06	0,04	0,05	494,9	564	217	88	38	22	11
10	7 June	18–05	0,05	0,04	0,04	0,05	0,04	174,3	190	73	37	20	10	6
3a	8 June	11–25	0,06	0,07	0,05	—	—	641,2	738	253	92	45	—	—
4a	8 June	12–50	0,08	0,06	—	—	—	724,9	835	228	92	—	—	—
8a	8 June	18–05	0,06	0,0	0,02	0,05	0,04	167,9	183	64	36	25	13	8
11a	9 June	12–30	0,05	0,04	0,03	0,05	0,05	780,6	900	346	177	109	55	29
12a	9 June	14–30	0,06	0,06	—	—	—	641,2	738	253	103	—	—	—
14a	9 June	18–00	0,02	0,03	0,03	0,03	0,04	167,9	183	100	57	35	22	13
2b	7 Sept.	13–35	0,06	0,03	0,06	0,14	—	529,7	610	209	120	52	10	—
10b	8 Sept.	11–18	0,05			—	—	494,9	564	217	—	—	—	—
11b	8 Sept.	16–10	0,2	—			—	167,9	183	73	—	—	—	—
12b	8 Sept.	14–35	0,07	0,08	—	—		425,2	490	150	48	—	—	—
13b	8 Sept.	13–45	0,07	0,0	—			571,5	658	201	73	—	—	—

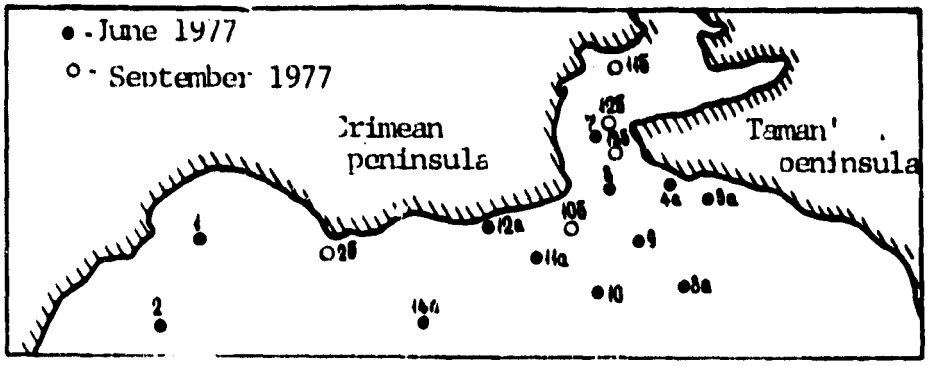

Figure 1. Location of Stations to Measure $E_{(350-3000\ nm)}$ and $E(\lambda_{eff} = 480\ nm, z)$

indicate that methods based on measurements with simple instruments with subsequent calculation of the total irradiance are the most applicable for standard mass measurements of PRE.

One should note the need for further study of the spectral distribution of underwater energy, especially in the coastal waters in order to perfect the optical classification of waters and the methods of PRE computation.

In conclusion, the author expresses gratitude to V. N. Pelevin for reading the manuscript and valuable remarks.

BIBLIOGRAPHY

1. Avaste, O., Moldau, Kn.; and Shifrin, K. S. "Spectral Distribution of Direct and Scattered Radiation," Tr. Instituta fiziki i astronomii AN ESSR. Issledovaniye po fizike atmosfery, No 3, 1962.

2. Vaynerman, B. A.; Neuyman, G. G. "Instrument for Measuring Underwater Irradiance," Eksperimental'nyye metodi issledovaniya okeana ["Experimental Methods of Studying the Ocean"], Izd. MGI AN UkSSR, Sevastopol', 1978.

3. Variospektrometricheskiy izmeritel' podvodnoy obluchennosti VARIPO ["Variospectrometric Gage of Underwater Irradiance VARIPO"], VDNKh SSSR, Moscow, 1972.

4. Zhukov, S. F.; Kaygorodov, M. N.; and Neuymin, G. G. "Photoelectron Gage of Underwater Radiance," Tr. MGI AN USSR, 41, 1961.

5. Karabyshev,G. S. "Photometer to Study Spectral Functions of Attenuation of Irradiance in the Sea," Okeanologiya, vol 6, No 5, 1966.

6. Karabysheva, E. I.; Ochakovskiy, Yu. Ye.; and Rutkovskaya, V. A. "Certain Results of Comparing Different Methods of Measurement and Calculation of Radiant Energy in the Sea," Okeanologiya, vol 8, No 2, 1968.

7. Karelin, A. K.; and Pelevin, V. N. "Marine Gage of Underwater Irradiance FMPO-64 and its Application in Hydro-Optical Studies," Okeanologiya, vol 10, No 2, 1970.

8. Kondrat'yev, K. Ya. Aktinometriya ["Actinometry"], Leningrad, Gidrometeoizdat, 1965.

9. Pelevin, V. N.; Rutkovskaya, V. A. "Optical Classification of Ocean Water According to Spectral Attenuation of Solar Radiation," Okeanologiya, vol 17, No 1, 1977. /49

10. Pivovarov, A. A.; and Lavorko, V. S. "Diurnal Course of Components of Solar Radiation and Albedo of the Sea," Meteorologiya i gidrologiya, No 1, 1961.

11. AASE, 1971. "The Natural History of the Hardangerfjord."'Irradianct in Hardangerfjorden, 9, 1967, Sarsia, 46.

12. Bauer, D.; and Ivanoff, A. 1970. Bathy-irradiance Meter. Cah. océanogr. XXII, N 5.

13. Bauer, D.; and Ivanoff, A. 1970. Spectro-irradiance Meter. Cah. océanogr. XXII, N. 5.

14. Bethoux, I. P.; and Ivanoff, A. 1970. Measurement of Submarine Energy Illumination. Cah. océanogr. XXII, N 5.

15. Carpenter, D. I., and Jitts, H. R. "A Remote Operating Submarine Irradiance Meter," Deep Sea Res., vol 20, No 9, 1973.

16. Dera, J.; Olszewski, J.; and Legovski, S. T. "Method of the Irradiation Measurements in the Sea by Means of an Irradiance Integration with 'Solion' Tetrode," Acta Geoph. Pol, XV, No 1, 1967.

17. Hojerslev, N. K. "Inherent and Apparent Optical Properties of the Western Mediterranean and the Hardangerfjord," Rep. Inst. Fys. Oceanogr. Kbennhavns Univ., No 21, 1973.

18. Jerlov, N. G. Marine Optics, Elsevier Ocean. Series, Amsterdam, 1976.

19. Jerlov, N. G. "A Simple Method for Measuring Quanta Irradiance in the Ocean", Rep. Inst. Fys. Oceanogr. Kbenhavns Univ., No 24, 1974.

20. Jerlov, N. G.; and Nugrd, K. "A Quanta and Energy Meter for Photosynthetic Studies", Rep. Inst. Fys. Oceanogr. Kbenhavns Univ., No 10, 1969.

21. Kehlibarov, T. I.; Mladenov, A. L.; and Minev, D. M. "Submersible Spectroradiometer", Doklady Bolgarskoy akademii nauk, 24, No 11, 1971.

22. Morel, A.; and Smithe, R. C. "Relation between Total Quanta and Total Energy for Aquatic Photosynthesis", Limn. and Oceanogr., vol 9, No. 4, 1974.

23. Neefus, C.; and McLeod, G. C. "A Subsurface Light Data Sphere for Irradiance Measurements", Naval Research, vol 27, No 10, 1974

24. Prioer, L. 1970 "Marine Photometer to Measure Proton Flux (quanta meter)". Cah. oceanogr. XXII, N 5.

25. Sugihara, S.; and Inoue, N. "Measurements of Spectra of Physical and Chemical Research, vol 70, No. 1, 1976.

26. Tyler, J. and Smith, R. C. Measurements of Spectral Irradiance Underwater, Gordon and Breach Science Publ., New York, London, Paris, 1970.

27. Report of the First Meeting of the Joint Group of Experts on Photosynthetic Radiant Energy, UNESCO Technical Papers on Marine Science No 2, 1965.

28. Report of Second Meeting of the Joint Group of Experts on Photosynthetic Radiant Energy, UNESCO Technical Papers on Marine Science, No 5, 1966.

29. Technical Report of Sea Trials Conducted by the WORKING GROUP on Photosynthetic Radiant Energy, UNESCO Technical Papers on Marine Science, No 13, 1969

DEPENDENCE OF SPECTRAL BRIGHTNESS COEFFICIENT OF THE SEA ON ILLUMINATION CONDITIONS OF WATER SURFACE

E. N. KHALEMSKIY

/50

This article examines the dependence of the brightness coefficient $\rho\lambda$ on different conditions of illumination of the sea surface. The question is very urgent because of the possibility of noncontact (long-range) analysis of $\rho\lambda$ and its use as the optical water indicator. The results of the studies are used to show that the absolute quantity of $\rho\lambda$ depends on the sun's altitude $h_\odot$ at $h < 25^\circ$, and is also associated with the geometric structure of surface radiation. With mixed incident radiation, $\rho\lambda$ is always greater than with scattered. All of this should be taken into consideration when the quantity $\rho\lambda$ is used as the optical water indicator. A conclusion is drawn that analogous use of the $\rho = f(\lambda)$ curve is more universal. Its shape does not depend on the illumination conditions of the sea surface.

An important problem of marine optics is development of methods of optical recording of water, i.e., separation of waters whose optical properties differ. It is more reliable to separate waters based on primary optical characteristics directly associated with natural optical properties of the water. Waters can also be separated based on characteristics of light fields in the sea, although this is less reliable. One example is the optical classification of waters of N. Yerlov [1].

Because of the development of noncontact methods for studying the ocean, including, from an AES, it is currently important to examine the possibility and the conditions for using the spectral brightness coefficient of the sea $\rho\lambda$ for purposes of optical indication of water. It is common knowledge that this coefficient characterizes the natural radiation of the water mass in the visible spectral region which emerges through the water surface into the

atmosphere. It, therefore, carries definite information regarding the natural optical properties of the water which form the outgoing radiation. The quantity of the brightness coefficient is influenced by the features of the light flux falling on the sea surface. It is clear from here that in order to use the brightness coefficient of the sea as an optical indicator of water, it is first of all necessary to evaluate those factors of variability in superficial radiation which have the greatest influence on the quantity of the brightness coefficient.

This work covers an evaluation of these factors and analysis of the possible use of the spectral brightness coefficient of the sea as an optical indicator of waters.

Values of the brightness coefficient $\rho\lambda$ obtained in studies conducted by the Institute of Oceanology in different regions of the World Ocean were used to solve these problems. Measurements of $\rho\lambda$ were made with the help of the FM-46 instrument described in [2]. This is a visual hydrophotometer. During the measurements, the brightness of two fields is equalized. One of the fields is created by the natural radiation of the sea, the other by the natural light of the sun and the sky illuminating a plate made of diffusing opaque glass. The instrument makes it possible to measure $\rho\lambda$ in six sections of the visible spectral region with relative error of 5-10%. During observations, the values of $\rho\lambda$ are determined with different angles of inclination to the vertical and different azimuths in relation to the sun, however, for optical indication of water it is most convenient to use the values of the

brightness coefficient which are measured at the nadir, therefore all further conclusions refer precisely to this quantity ρ_λ. /51

As a result of studies it was established that change in two factors has the greatest effect on the ρ_λ quantity: altitude of the sun and geometric structure of the incident radiation.

Figure 1 presents the ρ_λ values with different altitude of the sun $h_\odot$ measured in two different sea regions: in waters of high transparency (A) and in more turbid waters (B). Although there are no measurements of ρ_λ with the smallest values of the sun's altitude in the group of curves A, the general nature of the studied link is fairly evident: with a change in the altitude of the sun from 0° to 20° - 25°, the quantity ρ_λ rapidly rises,* but further, with $h° > 25°$, the coefficient of brightness remains constant.** The data in Figure 1 refer to two wavelengths λ = 482 nm and λ = 569 nm, but this relationship is manifest similarly in other sections of the visible spectral region.

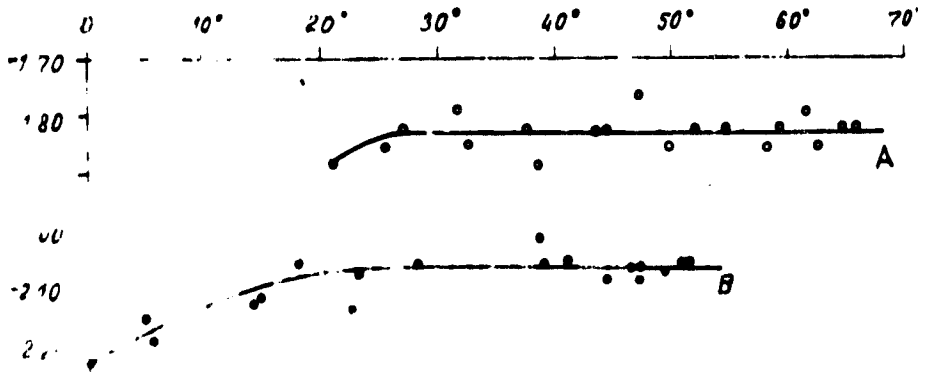

Figure 1. Dependence of the Brightness Coefficient of the Sea ρ_λ on the Solar Altitude $h_\odot$. 1--for λ = 480 nm.

*With $h_\odot = 0°$, $\rho_\lambda \neq 0$, since in a certain time before rising of the sun there is natural radiation of the sea formed as a consequence of illumination of the sea surface by scattered radiation of the sky illuminated by the solar rays which are behind the horizon. The same occurs during the setting of the sun.

**The spread of values ρ_λ observed in Figure 1 is associated with the fact that data obtained from one point of the sea are presented here, but on different days, as a consequence of which the quantity is influenced by the small-scale variability in optical properties of the water.

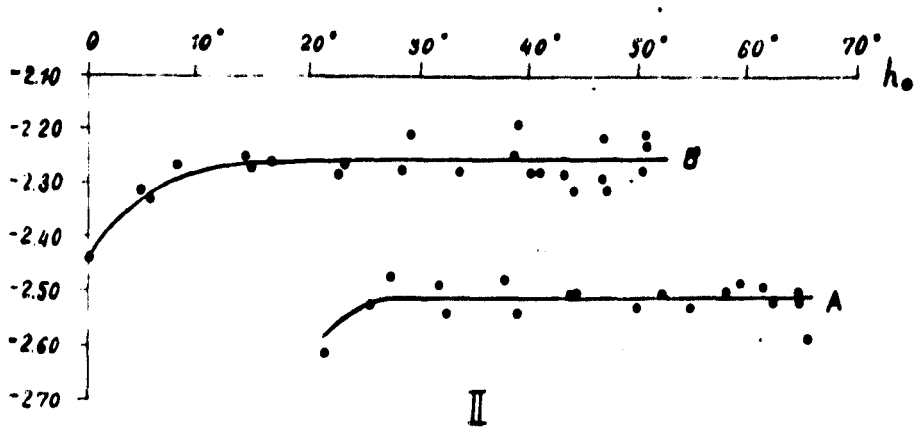

/52

Figure 1. II. For λ = 569 nm.

One can hypothesize that this nature of the dependence of λ_0 on h_0 is associated with a change in the total quantity of light which penetrates into the water and rapidly rises the first time after the ascent of the sun, but changes relatively little with $h_0 > 25° - 30°$.

In fact, the subsurface brightness of natural radiation of the sea, and correspondingly, the brightness coefficient ρ_λ, significantly depend on the coefficient of transmission of the water surface for light traveling from the air into the water T'. It in turn depends on the angle of incidence of radiation 0 (or altitude of the sun h_0). From here, the change in brightness coefficient of the sea with altitude of the sun must be analogous to the corresponding change in the quantity of the transmission coefficient T'. This is confirmed by the graph in Figure 2, where curves 2 and 3 which illustrate the dependence of $\rho_\lambda/\rho_{\lambda\,max}$ on h_0 are presented together with curve 1 which corresponds to $T' = f(h_0)$. It is apparent from the figure that the quantity T' ceases to change significantly $h_0 > 30°$, i.e., roughly in the same place as ρ_λ.

/53

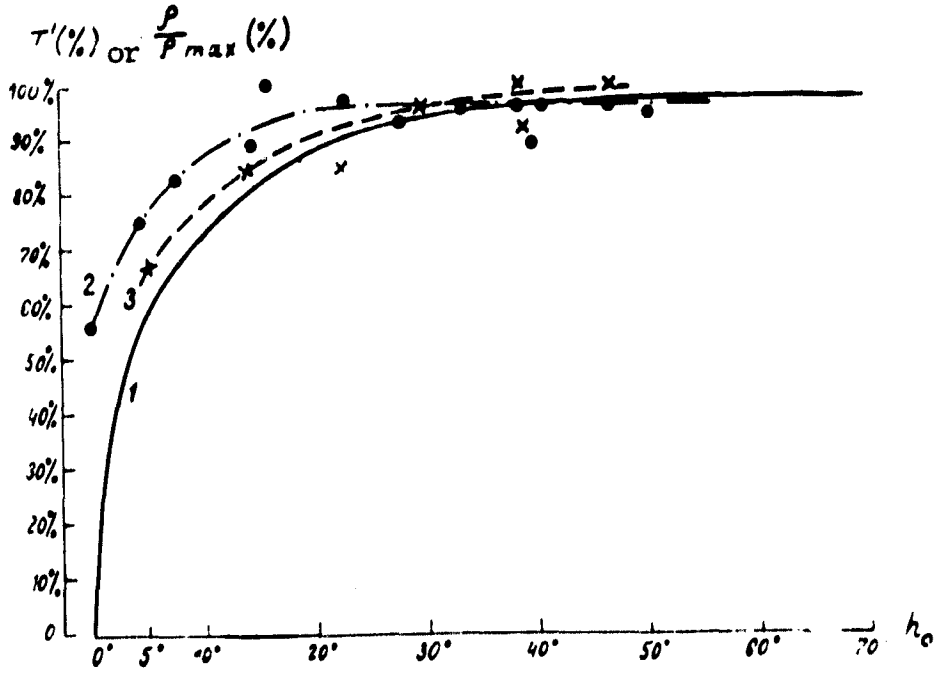

Figure 2. Change with Altitude of Sun h_o in Transmission Coefficient of Light T' (curve 1) and Brightness Coefficient of the Sea $\rho(\lambda = 517$ nm) Normed for its Maximum Value $\rho_{\lambda\ max}$ in Each Series of Measurements (curves 2 and 3) (region of transparent waters).

A conclusion which is important for practice follows from here. It states that comparison of the absolute values of ρ_λ which refer to different waters is lawful only in the case where they are measured with $h_o > 25°$. With smaller values of the solar altitude, only the quantities ρ_λ obtained with the same or close values of h_o can be compared.

At the same time, as shown by the measurement results in the regions A and B indicated above (Figure 3), the shape of the curves for spectral distribution of brightness coefficient remains practically unchanged with any values of solar altitude. An analogous phenomenon is observed in other regions of the ocean.

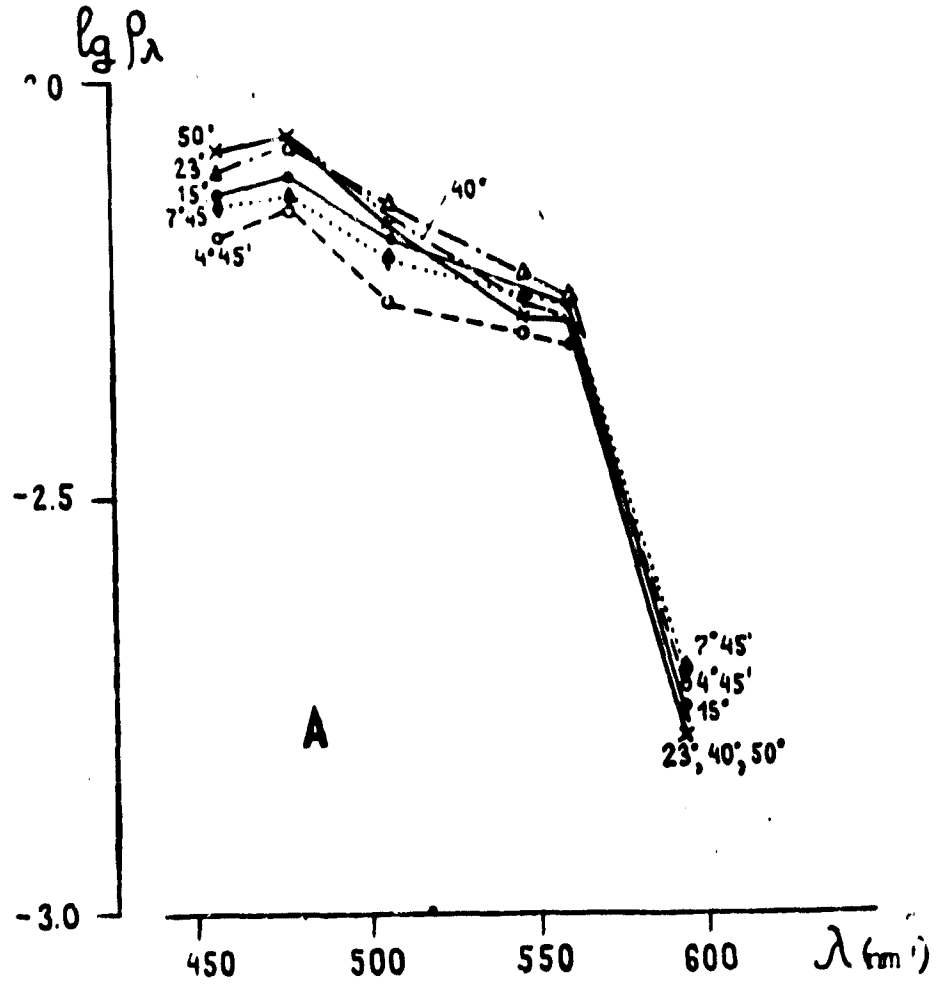

Figure 3. Spectral Distribution of Brightness Coefficient of the Sea ρ with Different Values of Solar Altitude h in Region of Transparent (A) and Relatively Turbid Waters (B).

All that has been said above refers to the case of mixed radiation on the sea surface, but the brightness coefficient of the sea also perceptibly depends on the geometric structure of the incident radiation. Comparison of the ρ_λ values measured with mixed and completely scattered superficial light in different sea regions demonstrates that the absolute quantity ρ_λ with completely scattered radiation is always smaller than the mixed superficial radiation (Figure 4). This correlation is manifest in the most diverse waters, regardless of their optical properties, and is also associated with the total quantity of incoming light which is greater in sunny weather than in overcast, with other conditions equal.

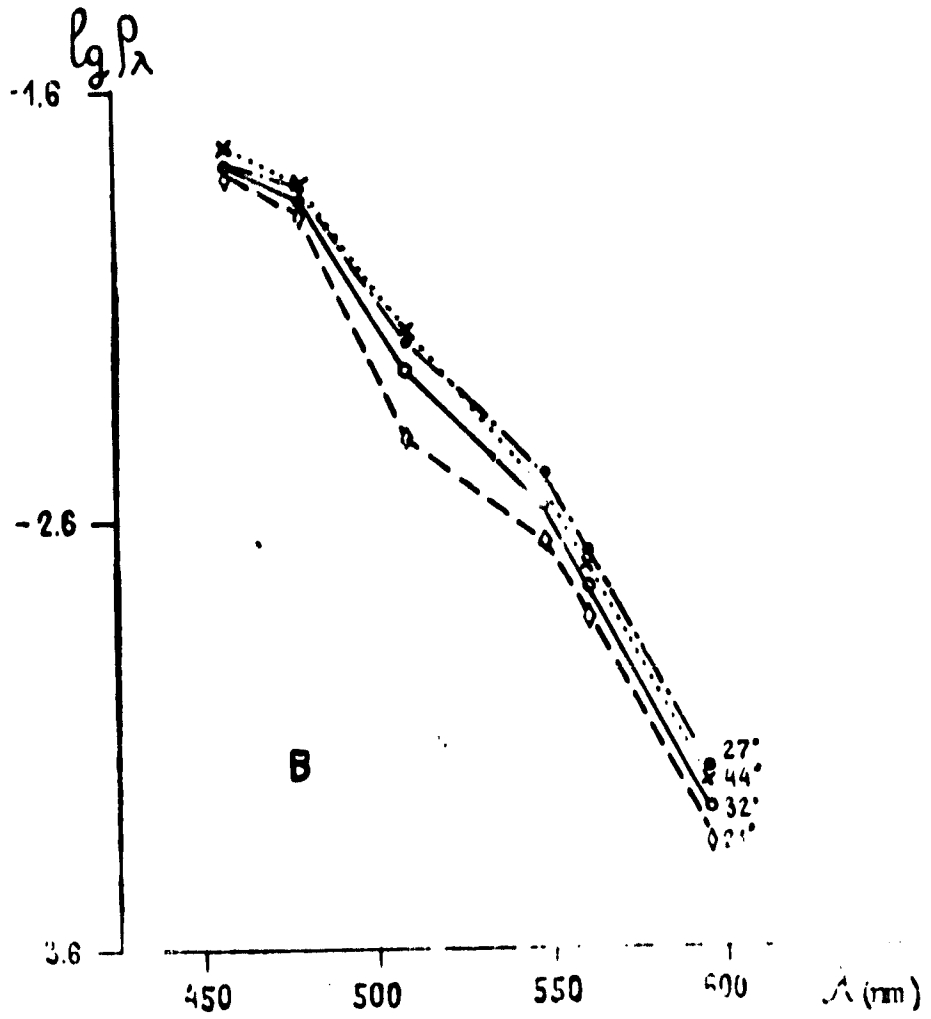

Figure 3. B

This allows us to draw a second important conclusion that it is correct to compare only those values of ρ_λ which were obtained with the same type (geometric structure) of incoming superficial radiation. At the same time, the shape of the ρ_λ curves, as with a change in solar altitude, remains practically constant regardless of the change in the type of superficial radiation.

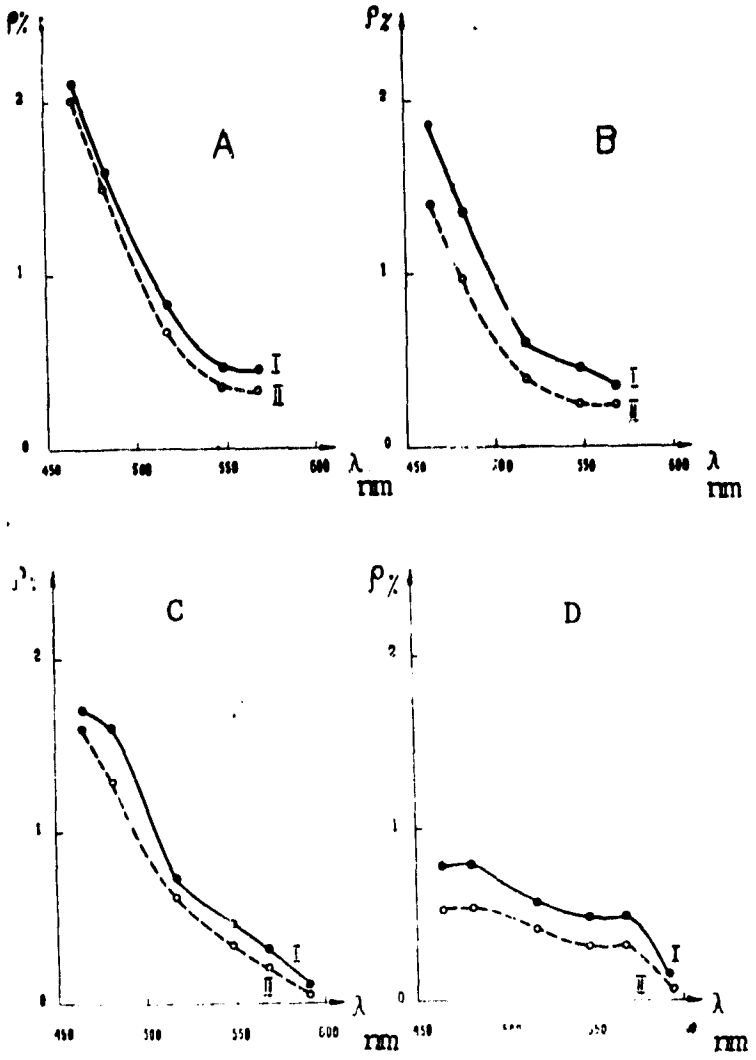

Figure 4. Spectral Distribution of Brightness Coefficient of Sea ρ with Different Types of Surface Radiation of Mixed Radiation (curve 1) and Completely Scattered Radiation (curves II). A, B--region of waters of high transparency, C--region of transparent waters, D--region of relatively turbid waters.

The shape of the ρ_λ curves, i.e., the relative spectral distribution of the brightness coefficient of the sea characterizes the true color of sea water. It is determined only by the natural optical properties of the water, and does not depend either on the quantity or on the structure of the incident superficial

radiation. This distinguishes the true color of the sea from its visible color, formed by light from the sea and light reflected from the sea surface. Thus, the sea visible color greatly depends on the illumination condition surface.

This leads to the conclusion that the use of relative spectral distribution of sea brightness coefficient as a parameter, depending on the natural optical properties of the water, and not the absolute values of $\rho\lambda$ (which can only be compared if they are obtained under similar illumination conditions of the sea water) is more universal for optical recording of water.

BIBILIOGRAPHY

1. Yerlov, N. G. Opticheskaya okeanografiya ("Optical Oceanography"), Moscow, Izdvo, Mir, 1970.
2. Kozlyaninov, M. V. "Manual on Hydro-Optical Measurements in the Sea", TRUD IOAN, vol 47, Moscow, 1961.

EFFECT OF FLUCTUATIONS IN RADIATION BRIGHTNESS REFLECTED BY A DISTURBED SEA SURFACE ON THE ACCURACY OF DETERMINING THE BRIGHTNESS COEFFICIENT OF THE SEA

V. I. BURENKOV, A. P. VISIL'KOV,
B. F. KEL'BALIKHANOV, L. A. STEFANTSEV

This work evaluates the effect of fluctuations in brightness of radiation reflected by the sea surface on the accuracy of determining the brightness coefficient of the sea. It is demonstrated that in certain cases, the examined effect introduces a significant systematic error into the determination of the brightness coefficient values.

Existing techniques for long-range analysis of the sea chlorophyll concentration require higher measurement accuracy of the spectral brightness coeffi- of the sea $\rho(\lambda)$. The sea brightness coefficient of the sea is expressed by the formula

$$\rho = \frac{n^2}{T_1 T_2} \cdot \frac{B_M - RB_H}{E_0} \qquad (1)$$

The designations in (1) correspond to the designations in [1]. Measurement error of B_m, B_H and E_o which include random errors and systematic

errors of instrument graduation, depend on the characteristics of the specific instrument, thus, for example, random error in determining B_m, B_H and E_0 of the spectrophotometer used in publication [1] is 2% in the wavelength range 450 - 650 nm. However, the error in determining $\rho(\lambda)$ according to (1) significantly depends on the ratios of B_m and RB_h. For waters with high content of absorbing substances, the contribution to B_m of radiation RB_H reflected from the sea surface can even exceed the contribution of radiation which is diffusely reflected by the sea mass $B_g = B_m - RB_H$. For these conditions it is important to have correct analysis of the quantity RB_H. This article evaluates the effects of fluctuations in radiation brightness reflected by the sea surface.

Measurements of ascending radiation B_m, even in the absence of sun glints reveal brightness fluctuations which are governed by glints in the sky, i.e., reflection vertically upwards from the disturbed sea surface of sections of the sky with differences in brightness. In this case, the value of brightness of the reflected radiation which is averaged for distribution of inclinations of the disturbed sea surface generally speaking will differ from the corresponding value of brightness in the zenith. This results in an error in the quantity RB_H in formula (1). For our estimate we will assume in the first approximation that the brightness of the sky does not depend on the azimuth φ, i.e.,

$$B_n = B_n(\Theta, \varphi) \tag{2}$$

where Θ --zenith angle, ϕ --zenith angle of the sun. Hypothesis (2) is not basic. It is assumed because in practice there mainly is information regarding the brightness indicatrix of the sky only for the plane of the solar vertical. For the distribution of inclinations of areas of a disturbed sea surface, we will adopt the distribution /58 function of Cox and Munk [2] in a simplified form

$$p = \frac{1}{2\pi\sigma_x\sigma_y}\exp\left(-\frac{\xi^2+\eta^2}{2}\right)$$
$$\xi = Z_x'/\sigma_x,\ \eta = Z_y'/\sigma_y,\ Z_x' = \sin\varepsilon\,\mathrm{tg}\,\Theta,\ Z_y' = \cos\varepsilon\,\mathrm{tg}\,\Theta \qquad (3)$$
$$\sigma_x^2 = 0.003 + 1.92\cdot10^{-3}v,\ \sigma_y^2 = 3.16\cdot10^{-3}v,$$

where v --wind velocity in m/s. The distribution function (3) can be integrated for the azimuth [3]. As a result we obtain an approximately Gaussian distribution

$$p(\Theta) \approx C\exp\left[-\frac{\mathrm{tg}^2\Theta}{4}\left(\frac{1}{\sigma_x^2}+\frac{1}{\sigma_y^2}\right)\right] \qquad (4)$$

The constant C in (4) is defined from the condition of norming. The average value of radiation brightness of the sky reflected by the sea surface at the zenith is expressed by the integral

$$\langle B_H\rangle = \int_0^{\pi/2} R(\Theta)B_H(2\Theta)\,p(\Theta)\,d\Theta \qquad (5)$$

Taking into consideration that $p(\Theta)$ rapidly diminishes with large Θ, in (5) one can assume that $R(\Theta) \approx 0.02$---value of Fresnel's coefficient of reflection with normal incidence. Integral (5) was computed numerically. The brightness indicatrix of the sky was taken from [4]. In this case the brightness values for the solar corona were determined by extrapolation.

The most important feature of the findings was the fact that $\langle B_H\rangle$ can noticeably differ from RB(0). Figure 1 presents the values $\Delta B = \langle B_H\rangle - RB(0)$ referring to $\langle B_H\rangle$, depending on the wind velocity for several values of the zenith solar angle ϕ (λ = 445 nm). Attention is drawn to the nonmonotonic dependence of $\Delta B/\langle B_H\rangle$ on ϕ (Figure 2). We also note that $\Delta B/\langle B_H\rangle$ with λ = 635 nm is greater than the corresponding value with λ = 445 nm, because of the greater extension of the brightness indicatrix of the sky with λ = 635 nm.

The relative error in determining $\rho(\lambda)$ associated with fluctuations in brightness of the reflected radiation is expressed by the formula

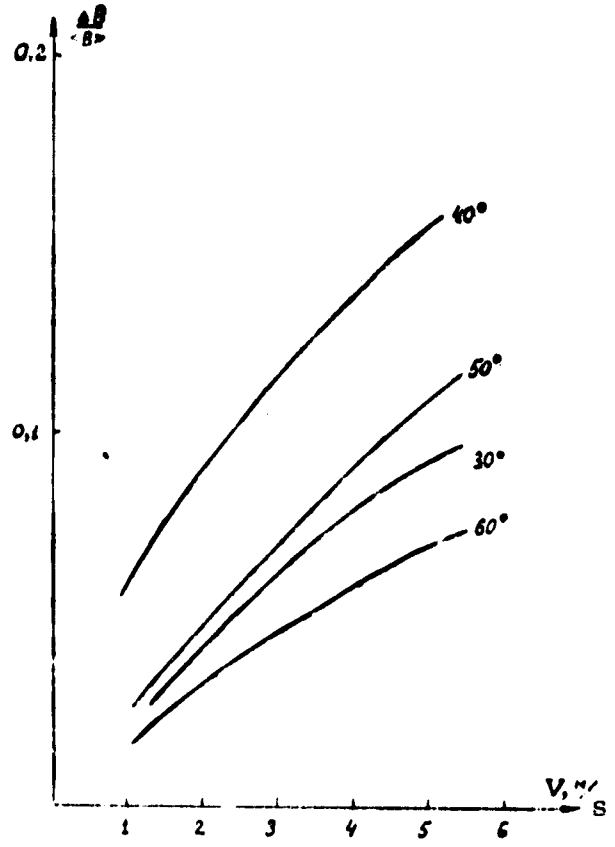

Figure 1. Dependence of $\Delta B/\langle B \rangle$ on Wind Velocity on λ = 445 nm with Different Zenith Angles on the Sun.

$$\frac{\delta\rho}{\rho} \quad \frac{\Delta B}{\langle B_H \rangle} \quad \frac{\langle B_H \rangle}{B_g} \tag{6}$$

where $B_g = B_m - RB_H$--brightness of radiation diffusely reflected by sea mass at the zenith. We note that for waters with high content of absorbing substances in the blue spectral region, the ratio $\langle B_H \rangle / B_g$ can even exceed one. Therefore, for these waters consideration of brightness fluctuations of reflected radiation is basically important. As one can see from (6), difference in $\langle B_H \rangle$ from $B_H(0)$ can result not /59 only in errors in determining ρ, but also, what is more important, in the spectral dependence of this error.

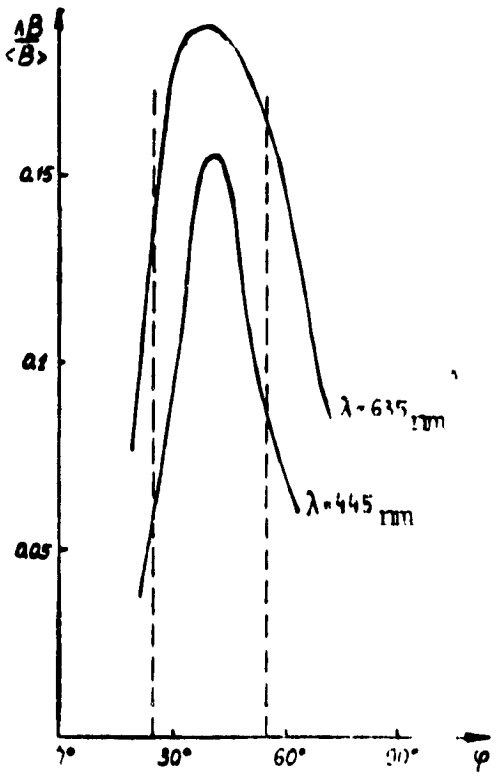

Figure 2. Dependence of $\Delta B/\langle B\rangle$ on Zenith Angle of Sun.

In order to evaluate the quantity of fluctuations in brightness of the ascending radiation B_m, the second moment was also included

$$\langle B_m^2 \rangle = \int_{-\pi/2}^{\pi/2} R(\Theta)\,(B_m(2\Theta) - \langle B_m\rangle)^2\, p(\Theta)\, d\Theta \qquad (7)$$

Then the relative dispersion B_m will be expressed by the formula

$$\frac{\sigma_m}{\langle B_m\rangle} = \frac{\sqrt{\langle B_m^2\rangle}}{(1+\mu)\langle B_m\rangle} \qquad (8)$$

where $\mu = B_g/\langle B_h\rangle$. For the Gulf of Odessa, based on experimental data, it was assumed

λ	445	555	635
μ	0.3	1.5	0.7

Figure 3 illustrates the dependence of relative dispersion on the wind velocity. The considerably smaller values of $\sigma_B/\langle B_m\rangle$ with λ = 565 nm are explained by the

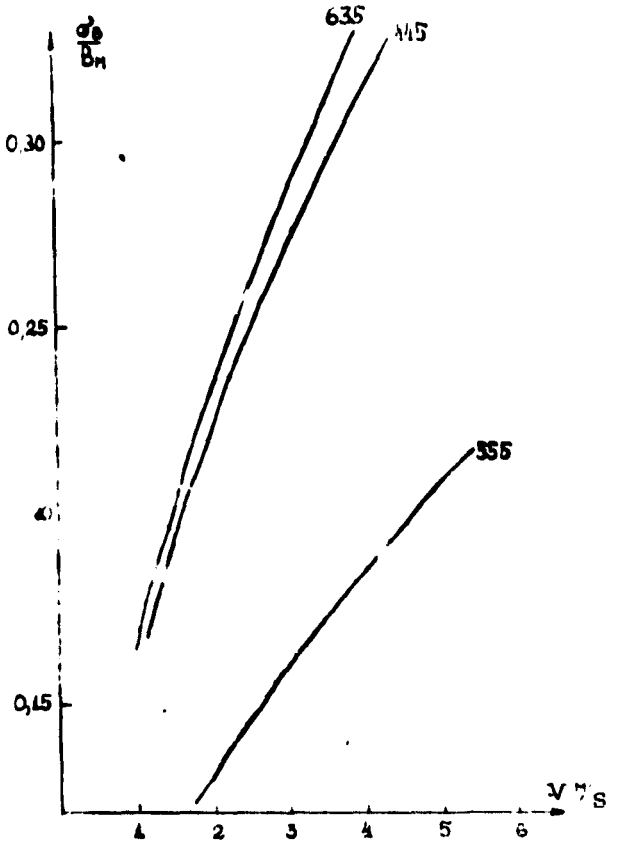

Figure 3. Dependence of Relative Dispersion of brightness Fluctuations in the Sea on Wind Velocity for Zenith Angle of the Sun $\phi = 40°$. The numbers on the curves are the wavelengths in nm.

fact that the maximum of diffusely scattered radiation corresponds to this spectral /60
region. We note that the data in Figure 3 to a certain extent represents the upper estimate, since the calculation adopted extreme values of μ, and in addition, the zenith angle $\phi = 40°$ also corresponds to the maximum brightness fluctuations.

It should be stressed that because of the adopted assumptions, the presented data have an estimated nature. Thus, the calculations show that in certain cases the examined effect will introduce a significant systematic error into the determina- /61
tion of the $\rho(\lambda)$ values. At the same time, the deviation in $\langle B_\lambda \rangle$ from brightness of the sky at the zenith is apparently more basic. It is obviously difficult to

consider the error in each case, since this requires additional measurements. One can comapute the deviation in $\Delta B/< B_H >$ for averages brightness indicatrixes above the sea at different wind velocities. Thus (6) can be used to estimate the relative error $\delta\rho/\rho$. Since variability in brightness indicatrixes is usually low, measurements of wind velocity and solar altitude can be used for the corresponding correction, thus reducing measurement error. However, there is currently not sufficient statistical material on the brightness indicatrixes above the sea.

BIBLIOGRAPHY

1. Burnkov, V. I.; Vasil'kov, A. P.; Kel'balikhanov, B. F.; and Stefantsev, L. A. "Evaluation of the Chlorophyll Concentration in the Sea from the Spectrum of Ascending Radiation for Waters with High Content of Dissolved Organic Substances", this collection.
2. Cox, C.; and Munk, W. "Slopes of the Sea Surface Deduced from Photographs of Sun Glitter", Bull. Scripps Inst. Oceanogr., vol 6, No 9, 1956.
3. Schau, H. C. "Measurement of Capillary Wave Slopes on the Ocean", Appl. Opt. vol 17, No 1, 1978.
4. Sandomirskiy, A. B.; Al'tovskaya, N. P.; and Trifoneva, G. I. "Brightness Indicatrixes at Altitudes 8-17 km", Izv. AN SSSR, Ser. Geofiz, No 6, 1964.

MEASUREMENTS OF NATURAL UNDERWATER IRRADIANCE IN THE INDIAN OCEAN

V. I. YEREMIN, G. G. KARLSEN, O. I. ABRAMOV and L. I. LOBOV

This article presents the results of deep-sea (to a depth of 450 m) measurements of natural underwater irradiance in the blue-green and UF-regions of the spectrum that were made at 10 stations of the Indian Ocean on the 10th trip of the scientific research vessel "Dm. Mendeleyev". Plans and a description are given for an irradiance recorder which guarantees a dynamic range of measurements of eight orders with continuous recording of the results on a self-recorder tape.

A technique is described for graduating the photorecorder and making measurements with it. A concise analysis of the findings is made.

On the 10th trip of the scientific research vessel "Dm. Mendeleyev" in the Indian Ocean, deep-sea (to a depth of 450 m) measurements of natural underwater irradiance were made. As on the 5th trip where similar measurements were made[1]

[1] See the monograph Gidrofizicheskiye i gidrooptricheskiye issledovaniya v Atlanticheskom i Tikhom okeanakh ("Hydrophysical and Hydrooptical Studies in the Atlantic and Pacific Oceans"), Izd. Nauka, 1974, pp 170, 183.

the submergible photoreceiver was a PM installed in a hermetically-sealed box with wide flat illuminator. No collectors were used to correct the beam pattern of the receiver. Hermetically sealed glass colored filters with relatively wide band of transmission were installed on top of the illuminator on the receiver. In order to measure irradiance changing in broad limits, the power voltage of the PM was regulated. As a result, because of the simplifications adopted in the receiver and the use of a highly-sensitive PM, threshold sensitivity on the order of 10^{-8} of the quantity of above-water irradiance was obtained.

In preparing the measurement equipment, primary attention was focused on expanding the dynamic range of the receiver and guaranteeing automatic recording. When the instrument was submerged, it would permit obtaining of a vertical course of irradiance at the greatest possible water masses with a constant rate without switching the regimes.

The receiver was equipped with a cable with current-collector. The PM was powered from an automatic device with output to the self-recorder.

The structural plan and schematics of the receiver are shown in Figures 1 and 2. Voltage is fed to the PFM separator from a transformer on the toroidal transformer Tr2 and transistors T4, T5 operating in a key regime with switching frequency of 2 kHz. The voltage coming to the transformer is regulated by transistor T3 and by direct current amplifier on T1 and T2. At its inlet, the current of the PCM and the reference direct current i_{stab} is compared. In this case, because of feedback, a regime of approximate equality of these currents is established in the receiver regardless of the irradiance of the PM cathode.

Voltage is fed from the transformer outlet to the self-recorder. It serves to measure the radiation falling on the PCM cathode.

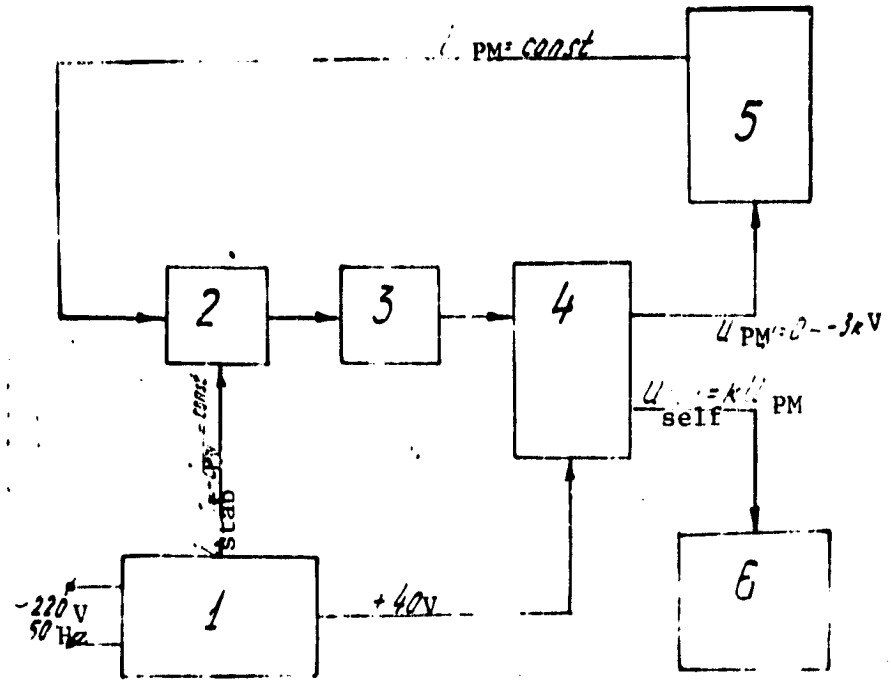

Figure 1. Structural Plan of Radiance Recorder

Key:

1. rectifier
2. comparison circuit
3. amplifier
4. LV/HV transformer
5. PM
6. self-recorder

Dependence of irradiance on deviation of the self-recorder in the receiver with PCM-53 is shown in Figure 3. In order to obtain a graduated curve, a tube is used with a set of diaphragms with diameters from 100 mm to 0.01 mm (Figure 4). When graduation is done with a direct radiation source, this guarantees range of fixed values of irradiance of eight orders with spacing of 0.5 orders. Large-diameter /64 diaphragms were cut into the machine, average diameters (Ø 5.6 - 0.32 mm) were drilled, while diaphragms with Ø 0.18 mm and less were punched in foil 0.01 mm thick and measured under a microscope.

Usually solar radiation at the noon hour was used for graduation. The receiver with the tube installed on its illuminator was oriented with its axis towards the sun.

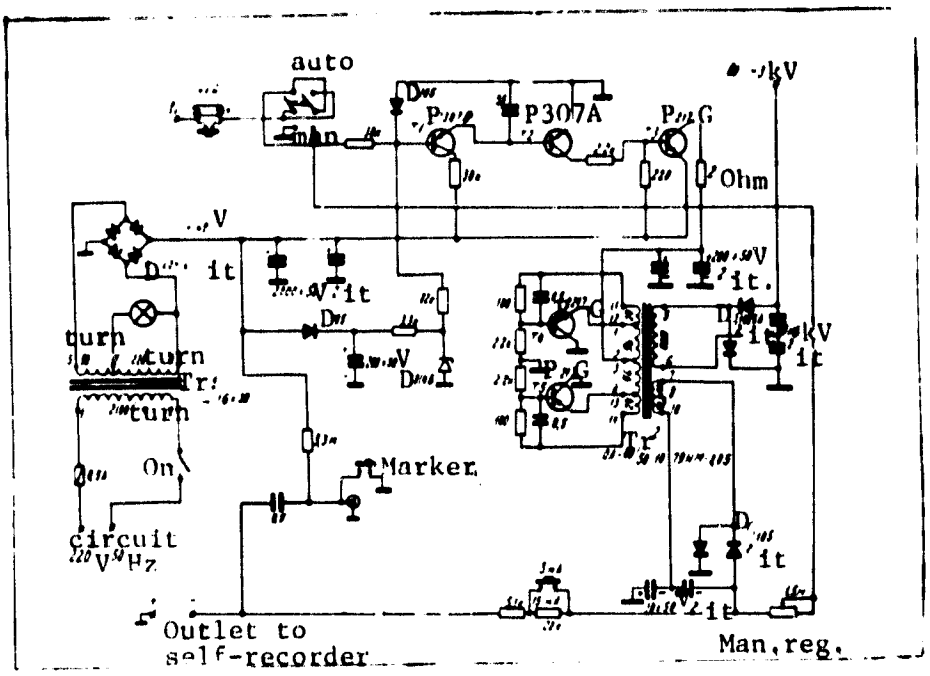

Figure 2. Schematics of Power Block for PM with Automatic Amplification Regulation

The power block in the self-recorder was turned on, the diaphragm was changed from the maximum to the minimum. A graduated curve was plotted from the obtained graduated recording.

The technique for measuring underwater radiance from a drifting ship was reduced to submerging the receiver on a cable with unchanged above-water illumination, and obtaining a recording of the output signal on the self-recorder tape with depth markings. An example of the recording obtained on one of the stations is shown in Figure 5. Dependences of underwater irradiance on depth were constructed from the recording with the help of a graduated curve.

One should note that despite the need for converting the obtained data, the /65 undoubted advantages of continuous recording are preserved. The self-recording tape successfully traces important sections of the course of the irradiance with depth,

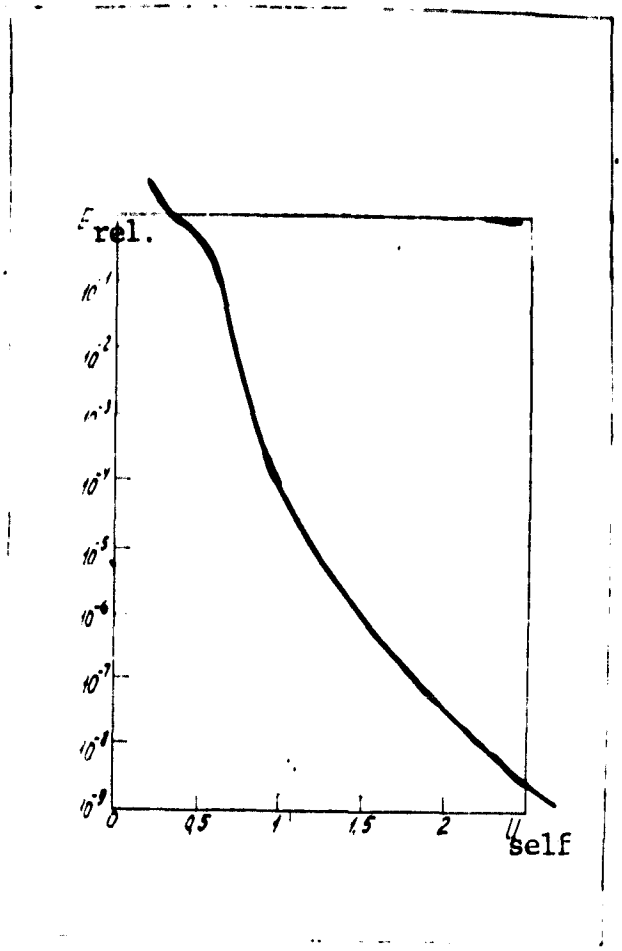

Figure 3. Graduated Curve of Irradiance Recorder (stabilization current 100 μA)

the effect of the ship's shadow during operation from the shaded side, etc., factors which were usually lost during measurements by points.

The equipment used in these measurements has the following specifications:

Covered range of change in radiance	Up to 8 orders
Error in measurements	Not more than 0.2 orders
Spectral ranges of measurements	1. λ_{max} = 0.52 μm; $\Delta\lambda$ = 0.06 μm (green filter); /37 2. UV-range; attenuation at $\lambda \geq$ 0.4 m no less than 5 orders (UFS-6 filter)
Recording of irradiance	Automatic with conversion for graduated curve
Indication of depth	On block-counter of cable with markers on self-recording tape by pressing knob
Rate of stratification	1 - 2 m/s

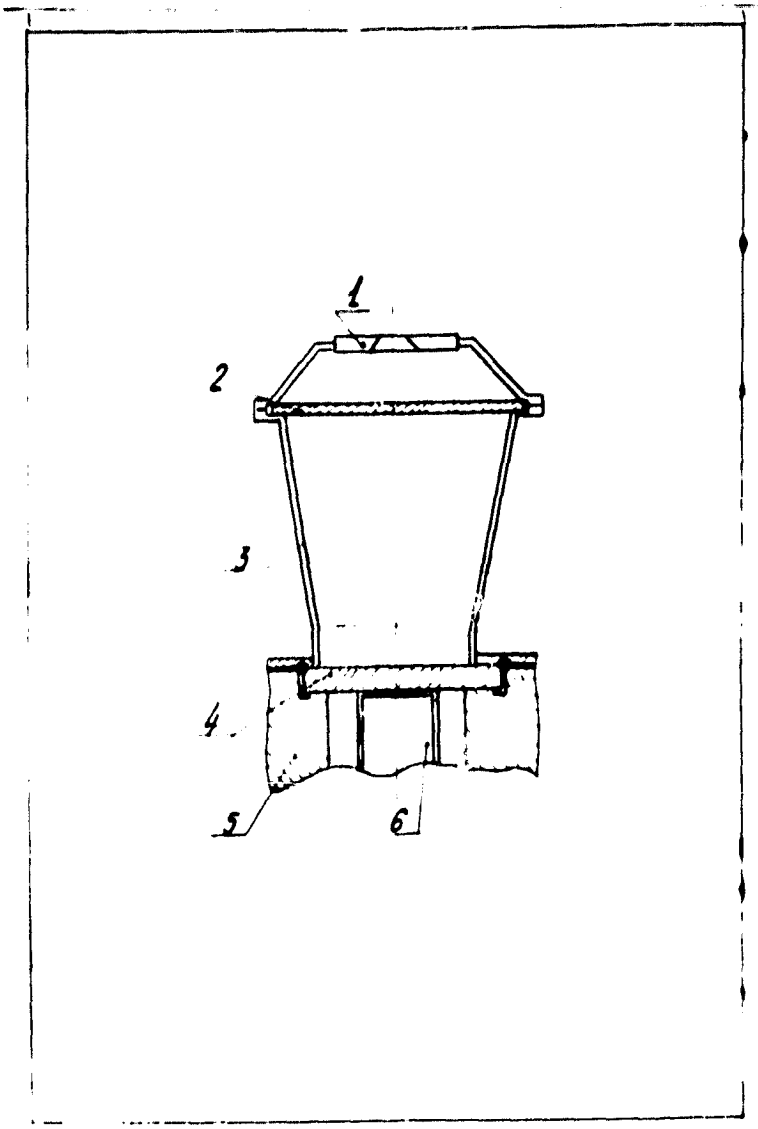

/66

Figure 4. Graduating Device

Key:

1. diaphragm
2. frosted glass with two-sided frosting
3. tube
4. illuminator
5. photoreceiver housing
6. PM

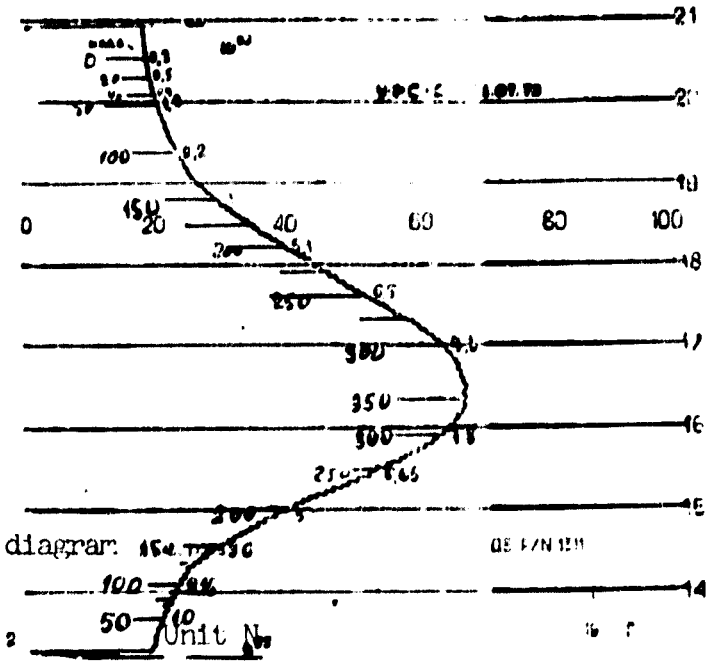

Figure 5. Example of Recording on Self-Recording Tape with Measurements of Irradiance. UV spectral region, depth to 350 m.

The measurements were made at the following stations in the Indian Ocean:

Station 739, 740--in the central region of the Indian Ocean, at 20° southern latitude;

Station 741--200 miles to the east of Rodrigues Island;

Station 757--in the northern section of the Gulf of Mozambique, northwest of the Aldabra Island;

Station 765--200 miles to the west of the Amirante Isles,

Station 769--100 miles to the east of Chagos Islands;

Station 779, 780--in the eastern section of the Gulf of Bengal; /68

Station 790--in the Andaman Sea near the Andaman Island.

The obtained results, the course with depth of natural underwater irradiance in the blue-green and UV spectral region, as well as the data from computing the indicators of vertical attenuation of irradiance (with a decimal base) are given in Figures 6 - 8.

The findings were used to solve a number of applied problems. Detailed analysis of the results, their comparison with geographical, hydro-optical characteristics of the stations, the weather situation, wave action, etc. is beyond the framework of this article. One can only note certain of the observed laws.

Stations 739, 740 and 741 were characterized by high transparency of the water in the UV-region, and constancy of the indicators of vertical attenuation by depth, starting with the upper levels. At Station 745 in Madagascar, the deep layers of the water(deeperthan 100 m) were more transparent in the blue-green region than the upper layer, while in the UV-range, the transparency was reduced in the entire mass at depth of 250 m (maximum for the UV-filter at this station) At the subsequent stations, because of the currents and proximity of the shore and islands, the water was more nonuniform in depth and its transparency in the UV-region was reduced, especially in the waters of the Gulf of Bengal (Stations 779 and 780). At Station 779 one can note a change in the course of curves at two depths: 50 and 80 m. The more turbid layer at depth from 50 to 80 m was traced both in the blue-green and in the UV-regions of the spectrum. Attenuation was apparently caused here by suspensions of mineral origin whose characteristics are not very selective for the spectrum.

A general law governing the obtained curves is stability in the indicators of the vertical attenuation at depths greater than 150 - 170 m. Whether this means that in measurements of natural underwater irradiation it is sufficient to be limited to depths to 200 m must be shown by mass measurements in waters of different type and comparison of the data of these measurements with primary and other hydro-optical characteristics whose heterogeneity is generally observed to much greater depths.

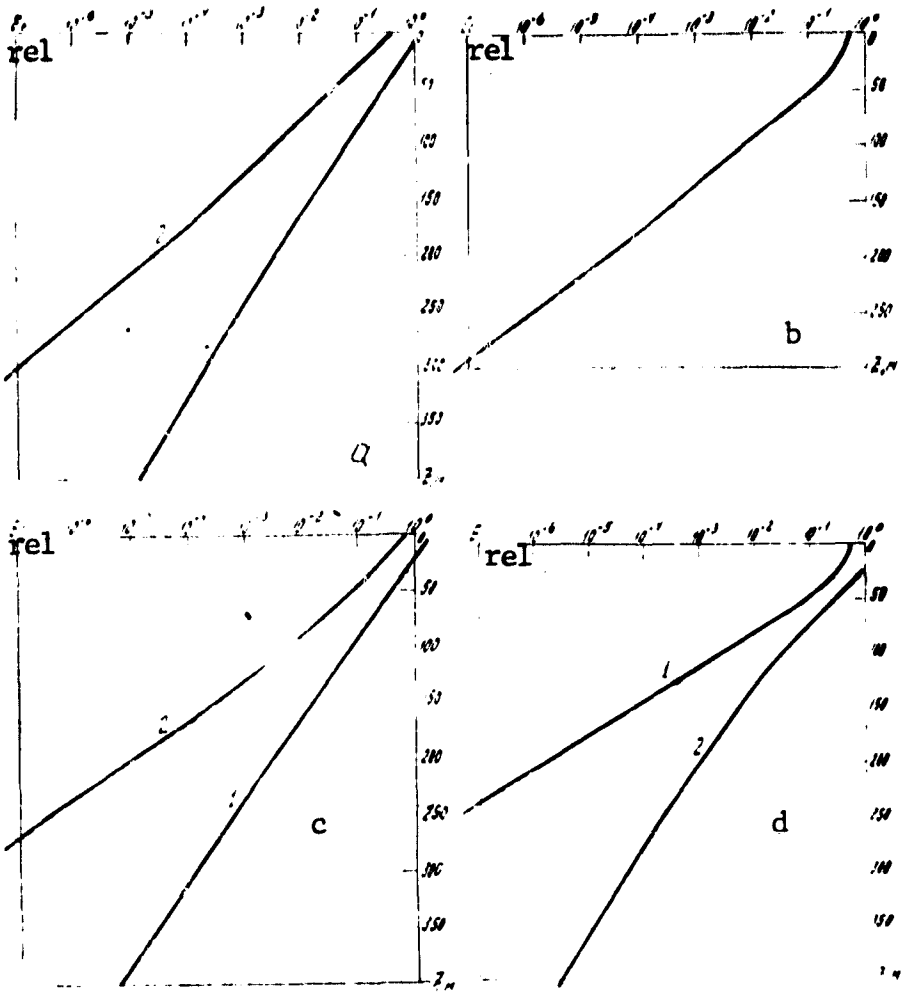

Figure 6. a. Station No 739. 27 July 1973. Sun through naze, clouds. 1. green filter 11:20 α_{cp} (50 - 400 m) = 0.013 1/m 2. UFS-6 filter, 13:20, α_{cp} (50 - 300 m) = 0.024 1/m.
b. Station No 740, 29 July 1973, clouds, sun through haze; 11:30; UFS-6 filter α_{cp} (50 - 300 m) = 0.025 1/m.
c. Station No 741, 31 July 1973, overcast; 1. green filter 9:35, α_{cp} (50 - 400 m) = 0.014 1/m, UFS-6 filter, 9:55, α_{cp} (50 - 300 m) = 0.027 1/m.
d. Station No 745, 6 August 1973, cloud cover 3 - 5 points; 1. UFS-6 filter, 10:45, α_{cp} (50 - 250 m) = 0.0321/m 2. green filter, 11:25, α_{cp} (50 - 100 m) = 0.02. 1/m α_{cp} (100 - 400 m) = 0.014 1/m.

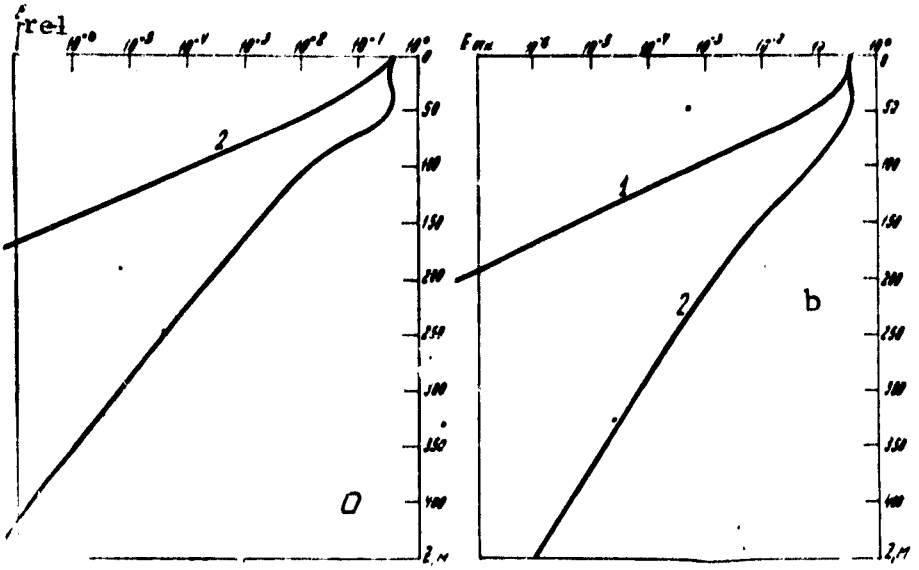

Figure 7. Station No 757, 11 August 1973, cloud cover 1 - 3 points, shady side 1. UFS-6 filter 12:30 α_{cp} (50 - 200 m) = 0.041 1/m 2. green filter 13:18, α_{cp} (50 - 400 m) = 0.014 1/m
b. Station No 765, 18 August 1973, clear, shady side; 1. green filter, 12:10, α_{cp} (200 - 450 m) = 0.015 1/m 2. UFS-6 filter 12:20 α_{cp} (100 - 150 m) = 0.046 1/m

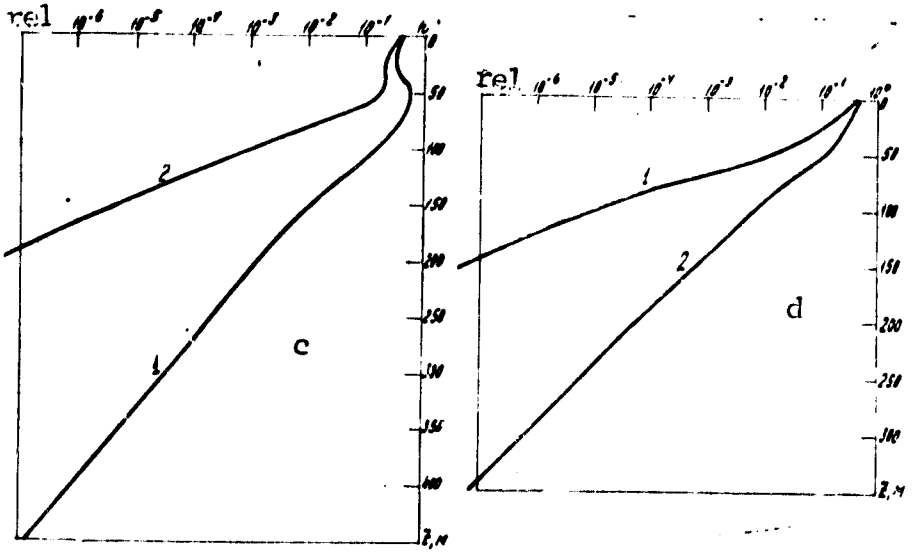

c. Station No 769, 31 August 1973, clear, shady side 1. green filter, 13:10, α_{cp} (200 - 450 m) = 0.016 1/m 2. UFS-6 filter, 13:20, α_{cp} (150 - 200 m) = 0.041/m
d. Station No 779, 15 September 1973, cloudy, sun through haze, sunny side 1. UFS-6 filter, 15:55, α_{cp} (0 - 50 m) = 0.029, α_{cp} (50 - 150 m) = 0.055 1/m 2. green filter, 16:10, α_{cp} (0 - 30 m) = 0.012, α_{cp} (50 - 350 m) = 0.021 1/m

Because of shortcomings of the equipment and measurement techniques, the measurements have low selectivity for the spectrum, and the dynamic range is inadequate at large irradiance, despite measures to expand it. Stratification could not be done in certain cases, starting with above-water irradiance. These shortcomings were partially removed in later studies of natural underwater and under-ice irradiance. Measures have been taken to linearize (in a logarithmic scale) the receiver graduated curve. However, these measures cannot result in increased accuracy and constriction of their dynamic measurement range since extreme (in the region of greatest and least irradiance) sections of the receiver characteristics are excluded. These sections are the most difficult to linearize. /73

In conclusion, the authors are grateful to the hydrooptics department of the P. P. Shirshov Institute of Oceanology for great help in preparing and conducting the studies.

ATTENUATION OF SOLAR ENERGY FLUX WITH DEPTH IN WATERS OF THE INDIAN OCEAN

PELEVIN, V. N. and RUTKOVSKAYA, V. A.

Extensive experimental material shows a close correlation between the vertical light attenuation indices in the ocean $\alpha\downarrow\lambda$ in the range $380 \leq \lambda \leq 600$ nm. Coefficients are obtained for a linear regression relationship between $\alpha\downarrow_{500}$ and $\alpha\downarrow\lambda$ for this spectral interval. A map is given for the distribution of the optical water type indices $m=100\ \alpha\downarrow_{500}$ in the Indian Ocean. The link between the distribution and the basin hydrology is explained. The attenuation of photosynthetic radiant energy (PRE) with depth corresponding to an optical classification of waters is computed. A simple technique is presented for evaluating the level of underwater PRE irradiance and spectral light composition to 100 m in different regions of the ocean. The optical water type index m and the level of primary production are given.

Data on the spectral attenuation of light based on the classification of ocean waters of Yerlov [2] were used [1] to calculate attenuation of the solar energy flux in the Indian Ocean. Study [3] has suggested a new optical classification of ocean waters based on spectral attenuation of solar radiation in the near-surface layers of water which is a development of Yerlov's classification and is based on measurement data from instruments with high spectral resolution. In [4] the new

classification calculates attenuation of solar radiation flux of the Pacific Ocean. The expected levels of irradiance created by photosynthetic radiant energy (PRE) $380 \leq \lambda \leq 710$ nm are computed at depths to 100 m in different water areas of the Pacific Ocean. The width of the spectral interval of the solar radiation flux is estimated at different levels and the values of the index of the optical type of water are compared with the level of primary production.

In this work we continue this trend, examining the question of attenuation of solar energy in the waters of the Indian Ocean. We will examine the degree to which the pinpointed data for typical spectral courses $\alpha\downarrow\lambda$ change the estimates of attenuation in solar radiation.

We will first dwell on certain questions associated with verifying and selecting /74
the most convenient presentation of classifications suggested in [3]. Additional experimental material [4] was used for these purposes: 129 stations in the water area of the Pacific Ocean, 76 stations in the Indian Ocean made by different authors, and data of measurements of Morel and Prieur [5] in the Atlantic and eastern section of the Pacific Ocean. We examined the question of how well the values $\alpha\downarrow\lambda$ correlate in different regions of the visible spectral area with values $\alpha\downarrow_{560}$ which comprise the basis of the one-parametric classification of ocean waters. All the data employed for $\alpha\downarrow\lambda$ were obtained with high sun ($h_o \geq 45°$) and were averaged for the layer up to 100 meters thick. At certain stations, the measurements were made to depths less than 100 meters. In these cases, $\alpha\downarrow\lambda$ were averaged for the layer of water of less thickness, but no less than 40 m.

The results of processing the measurements in the Pacific and Indian Oceans which were used to plot maps in [1, 4] are presented in Figure 1. The values $\alpha\downarrow\lambda$ are plotted on the y-axis for wavelengths 432 - 445 nm (a) and 465 - 480 nm (b). The corresponding values of the water type index m according to classification 3 are

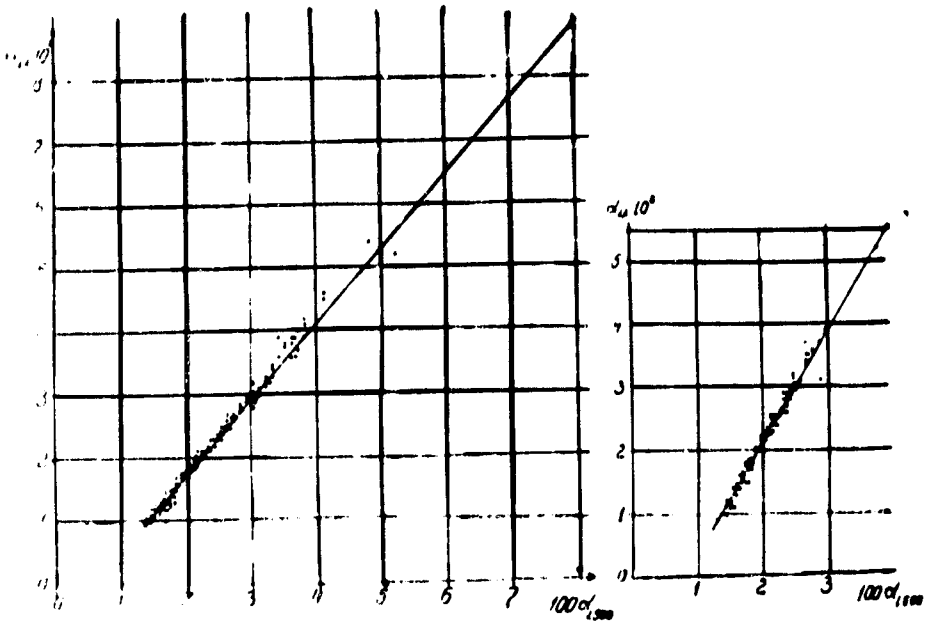

Figure 1. Dependences of $\alpha\downarrow_{432-445,\ 465-475}$ on Value of Water Type Index $m = 100\ \alpha\downarrow_{500}$.

plotted on the x-axis ($m = 100\ \alpha\downarrow_{590}$). In Figure 2, $\alpha\downarrow_{400}$ (a), $\alpha\downarrow_{530}$ (b) and $\alpha\downarrow_{580}$ (c) are plotted on the y-axis according to [5], while the corresponding $\alpha\downarrow_{500}$ are plotted on the x-axis. All the values of $\alpha\downarrow\lambda$ were taken with a decimal base.

It follows from these figures then: 1) there is a correlation between $\alpha\downarrow\lambda$ and /75 $\alpha\downarrow_{500}$ in the range of wavelengths $400 \leq \lambda \leq 580$ nm. The correlation is especially high for the interval $432 \leqslant \lambda \leqslant 530$ nm; 2) the relationship between $\alpha\downarrow\lambda$ and $\alpha\downarrow_{500}$ for all the examined waters from extremely transparent with index type approaching one, to very turbid water of the near-continental upwellings characterized by index 8 and higher, is described well by the linear regression equation.

The regression equations and the sampling standard deviation are given in Table 1.

TABLE 1. DEPENDENCE OF $\alpha\downarrow\lambda$ ON $\alpha\downarrow 500$

α, M^{-1}	Standard Deviations	
	$m \leq 5$	$m > 5$
$\alpha\downarrow_{400} = -0{,}008 + 1{,}6\,\alpha\downarrow_{500}$	0,007	0,012
$\alpha\downarrow_{432-445} = -0{,}014 + 1{,}75\,\alpha\downarrow_{500}$	0,0015	
$\alpha\downarrow_{445-480} = 0{,}006 + 1{,}2\,\alpha\downarrow_{500}$	0,001	0,004
$\alpha\downarrow_{530} = 0{,}012 + 0{,}8\,\alpha\downarrow_{500}$	0,001	0,004
$\alpha\downarrow_{580} = 0{,}03 + 0{,}7\,\alpha\downarrow_{500}$	0,006	0,010

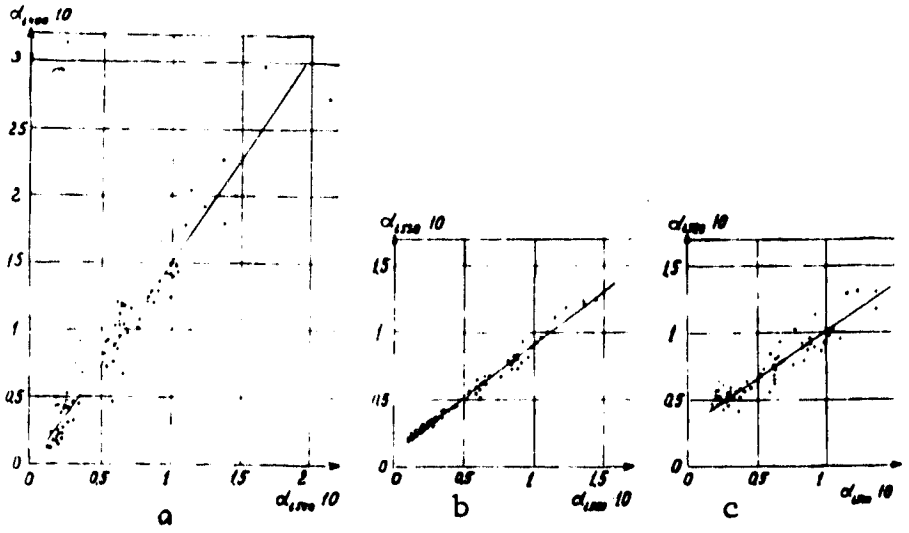

Figure 2. Dependences of $\alpha\downarrow_{400}$, $\alpha\downarrow_{530}$ and $\alpha\downarrow_{580}$ on $\alpha\downarrow_{500}$

It is apparent from the table that the standard deviations of the measured values $\alpha\downarrow$ from those predicted by the regression equations are very small. The case $m \leq 5$ encompasses an overwhelming part of the water area of the World Ocean. This means that for example, with probability of 95%, the prediction for $\alpha\downarrow_{432-445}$ according to the optical index of water type differs from the measured by no more than 0.003 m^{-1} to a certain side. The latter quantity yields, for example, for clean waters

(m = 2.0) relative error equal to 15%. The main error in evaluating $\alpha\downarrow\lambda$ is not caused by error in the regression equation, but insufficiently accurate knowledge of the water type index m. Thus, publication [6] notes that with direct measurements of $\alpha\downarrow\lambda$, accuracy of 8% is guaranteed (standard error). In this case, the confidence interval of 95% for m is $\pm$ 16%. For example, water with index m = 2, this means that the true quantity $\alpha\downarrow_{432-445}$ with probability of 0.95 differs from the predicted by no more than 28%. This confidence interval significantly exceeds that determined by the regression equation, therefore accuracy of the prediction under real conditions is determined by the accurate knowledge of the water index. With additional measures for increasing accuracy of knowledge of m, the error of prediction will be determined by the quantity of the standard deviation (Table 1). /76

Since a good linear relationship has been found between $\alpha\downarrow\lambda$ and m, the system of curves of optical classification presented in graphic form in [3] or in tabular form in [4], can be represented in the form of the following equation:

$$\alpha_{\lambda} = a_{\lambda} + b_{\lambda} \cdot m, \qquad (1)$$

where a_λ and b_λ--coefficients computed for five spectral regions from data presented in Figures 1 and 2, and for the remaining λ obtained analogously. The values of the coefficients a_λ and b_λ are presented in Table 2.

The right side of the table presents the standard deviations σ for $\alpha\downarrow\lambda$ from the quantities computed according to (1) with known m. For waters with $m \leq 5$ (this gradation includes almost all waters of the World Ocean) σ_α is small, but in turbid waters where $m > 5$, the standard deviation drastically rises.

If measurements of $\alpha\downarrow\lambda$ are made in some waters with wavelength $\lambda^* \neq 500$ nm (with narrow-band light filter of width no more than 8 - 10 nm), then the water type index can be estimated as $m = \frac{\alpha_{\lambda^*} - a_\lambda}{b_\lambda}$.

TABLE 2. VALUES OF COEFFICIENTS IN EQUATION (1)

λ, nm	$a_\lambda \cdot 10^2$, м$^{-1}$	$b_\lambda \cdot 10^2$, м$^{-1}$	$\sigma_a \cdot 10^2$	
			$m \leq 5$	$m > 5$
380	−1,0	1,7		
400	−1,2	1,8	0,6	1.2
410	−1,7	2,2		
420	−1,6	1.84		
440	−1,4	1,75	0,15	
460	−0,8	1.35		
480	−0,5	1,2	0.10	0.4
500	0	1	0	0
520	1,0	0,83		
530	1,2	0,80	0.10	0.3
540	1,5	0.76		
560	2,4	0,70		
580	3,0	0,64	0.6	1,0
600	6 2	0,60		

The error in determining $\alpha\downarrow\lambda$* (i.e., $\Delta\alpha\downarrow\lambda$ *) is the main reason for the error /77
in Δm in the value of the water type index which in the majority of cases exceeds the error of the regression equation. These errors are associated by the correlation $b_\lambda \Delta m = \Delta\alpha\downarrow\lambda$*.

In evaluating the water type index, it is recommended that measurements of α_λ be used with $432 \leq \lambda \leq 530$ nm, because of the strong increase in the errors beyond the limits of this region (compare the values of standard deviations in Table 2).

The values of the water type index for the Indian Ocean were evaluated according to (1).

We will now return to the question of attenuation in the solar radiation flux in the waters of the Indian Ocean. It is first of all necessary to examine the distribution of water type over the water area of the Indian Ocean.

The map of geographical distribution of optical index of water types of the new classification in the Indian Ocean is given in Figure 3. Its plotting used the same experimental data as in [1]. Stations were selected which refer to the winter /78
period in the Northern Hemisphere. To the south of the equator, all the available data were left, regardless of the season, since the hydrometeorological situation here is more stable than in the Northern Hemisphere where the direction of the monsoon winds changes during the year. At the points designating the stations in Figure 3, we did not put the number of water types according to Yerlov, i.e., I, IA, IB, II,III, but the optical index of the water type $m = 100\ \alpha\downarrow_{500}$. If measurements of $\alpha\downarrow\lambda$ * were made at this station with $\lambda^* \neq 500$ nm, the estimate of m used ratio (1). This technique actually does not differ from that described in [4].

In the case where measurements were made at one station in several light filters, the estimate of m was made according to $\alpha\downarrow\lambda$ in several spectral regions within the range $432 \leq \lambda \leq 530$ nm, and then the obtained values of m were averaged. In those cases where measurement results were processed which were obtained in broad-band light filters (with transmission band exceeding 8 - 10 nm) the change in effective /79
wavelength transmission with depth was taken into consideration, as described in [4]. It is also indicated there that the standard error σ_m in evaluating the value of the m index with averaging of the data in the 100-meter layer of water does not exceed 10% of the index value when measurements are used made with solar altitudes $h_\odot \geq 45°$, with light filters that do not go beyond the limits of the stipulated spectral interval.

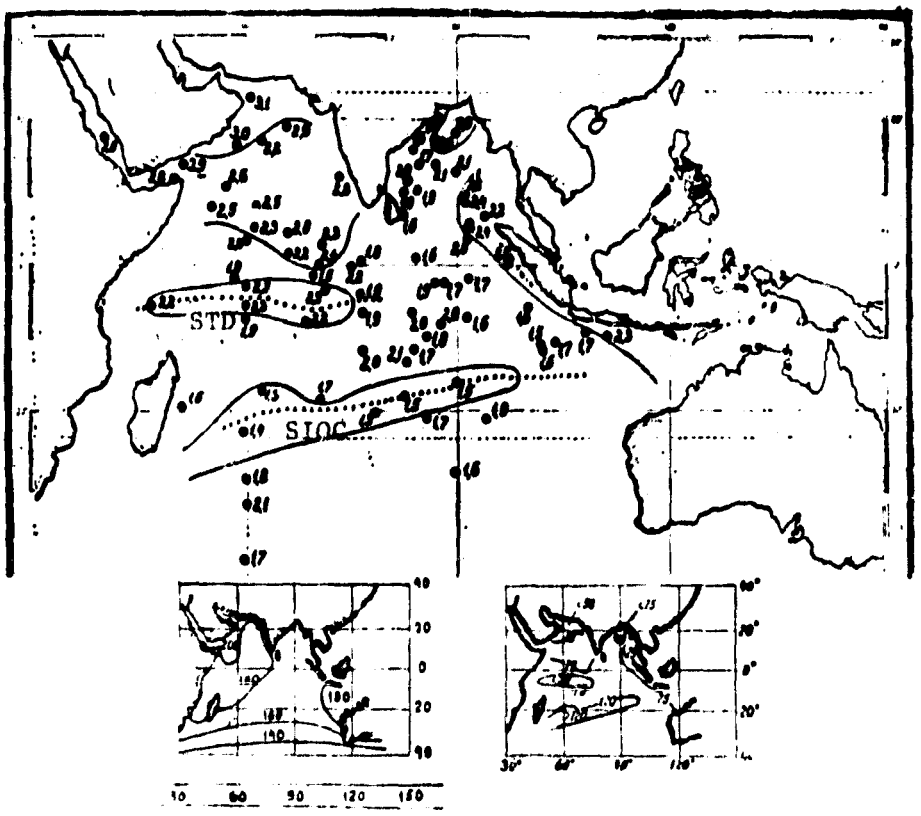

Figure 3. Distribution of Values for Water Type Index m Over Water Area of Indian Ocean. Left insert--level of annual influx of solar energy; right insert--depths at which PRE level was attenuated 100-fold.

The isolines on the map were made according to division of the values m into the same groups as for waters of the Pacific Ocean [4]: $m \leq 1.5$; $1.5 < m \leq 2.1$, $2.1 < m \leq 2.9$; $2.9 < m \leq 4.1$; $m > 4.1$. Thus, the distance from the middle of the interval to the boundaries was about $2\sigma_m$. Greater detail in the division for making the isolines would be unjustified with the available accuracy of the measurement data.

One can see the following pattern for distribution of optical water types in the Indian Ocean in Figure 3: the greater part of the ocean (> 60%) from the Asian continent in the north to ~ 30° s.l. in the south (in the more southern regions, there are insufficient optical data or there are none at all) is occupied by typical clean

ocean waters with $1.5 < m \leq 2.1$. This also includes waters of the equatorial counter current which follows to the east along the equator, and the trade wind current which is observed in this season in the south and southeast of the Hindustan Peninsula [7], as well as the greater part of waters of the Bengal Gulf in the zone of the anticyclone circulation.

Within this enormous mass of typical clean ocean waters, to the south of the equator there are two "enclaves" which are significant in dimensions and have extremely different optical characteristics. These are the zones of the south-Indian Ocean convergence (SIOC) and the south-tropical divergence (STD). The axis of the convergence in Figure 3 is shown by crosses, and the axis of divergence is shown by dots. The SIOC is formed on the boundary of the trade wind current which follows to the west and the south-Indian Ocean current which is directed to the east and northeast [7]. In this zone, which does not have an influx of nutrient substances from below and which is far from the coasts, conditions for development of phytoplankton are difficult. This determines the high cleanliness of the waters ($m \leq 1.5$).

The STD is located in the western section of the ocean, somewhat to the south of the equator. It is formed by cyclone circulation on the boundary of the trade wind current and the equatorial counter current [7]. Elevation of biogenic substances from deeper layers causes intensive development of phytoplankton in the superficial waters, and correspondingly, increase in their turbidity ($2.1 < m \leq 2.9$).

In the Arabian Sea, in the winter period, a closed current of cyclone nature is observed which creates a zone of divergence that encompasses the entire sea [7]. This causes active reproduction of phytoplankton. In addition, the aeolian sources /80 of suspension from the Arabian deserts can be influential here. Both of these factors determine the increased optical index $2.1 < m \leq 2.9$ (analogous to the STD index)

which is clearly traced on the map. Waters of the northwest periphery of the Arabian Sea with index $2.9 < m \leq 4.1$ are classified as very turbid ocean waters. In addition to the indicated factors, the influx of water from the Gulf of Persia and the Gulf of Oman which are rich in suspended matter and nutrient substances can also play an additional role here.

In the Gulf of Bengal, on the contrary, an anticyclone circulation of water is observed [7]. It results in the development of convergence, and despite the proximity of the coasts with high water run-off carrying suspended and nutrient substances, clean waters are observed in the greater part of the gulf ($1.5 < m \leq 2.1$) which are washed off with the main mass of typical clean waters of the Indian Ocean. A tendency towards increase in the optical index of the water type is only noted in the region of the Ganges delta. In the eastern part of the Gulf of Bengal, on the shores of Sumatra and in the region of Nicobar Islands waters of increased turbidity are noted: $2.1 < m \leq 2.9$ which stretch to the meridian 90° e.l. Further to the west, to the coast of the Island of Ceylon and the northeast coast of the Hindustan Peninsula, typical clean waters are observed $1.5 < m \leq 2.1$.

The optical characteristics of water in the Indian Ocean in direct proximity to the shores of Africa and Australia have not been studied. On the map in Figure 3, these regions are the "white spots", and to the south of 30° s.l.

The discussion above of the map results in the hypothesis that on the water area of the Indian Ocean the main factor which determines the optical properties of the waters (mediated through hydrodynamic processes, the phenomena of convergences and divergences) is the vital activity of biocenoses, and primarily, phytoplankton. It is therefore important to compare the map in Figure 3 with the maps for distribution of phytoplankton concentration or level of primary production (PP). A detailed map

of primary production in the near-surface water layer was used [8]. This publication isolated four gradations of PP level in open waters: up to 1.0, from 1.0 to 5.0, from 5.0 to 10.0, from 10.0 to 50 mgC/m^3 x day. In Figure 4, the centers of these gradations of PP level are plotted on the x-axis in a logarithmic scale, while the corresponding values of the water type index at the stations are plotted on the y-axis. The standard deviations of these values are presented. The field of the figure indicates the number of stations in the corresponding samplings referring to each of the PP level gradations. Regression close to linear is observed with a considerable spread of the data in Figure 4.

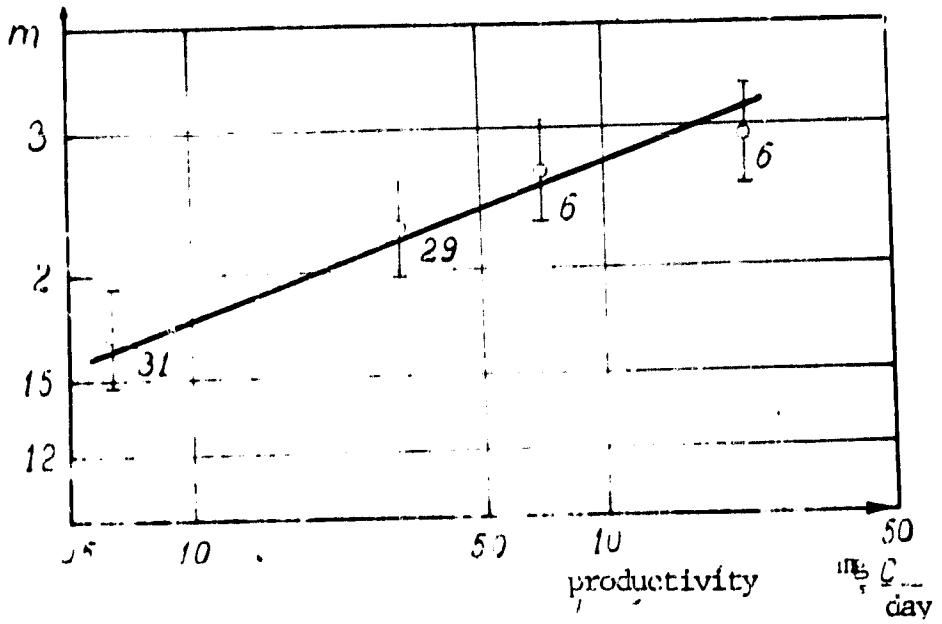

Figure 4. Comparison of the Level of Primary Production in the Near-Surface Layer of the Indian Ocean [8] and Value of Typical Water Type Index m. The centers of four gradations in level of productivity are plotted on the x-axis, the average value m in the corresponding regions and standard deviations are plotted on the y-axis. The numbers on the figure field are the number of stations in the sampling.

Calculation of the quantity of radiant solar energy which reaches a definite depth in the Indian Ocean was made in the same way as for the Pacific Ocean [4], from the value of the water type index and the level of irradiance of the surface. The basis for this is the fact that when the system of optical classification of water for spectral attenuation of solar light with depth was developed, experimental data were used obtained in waters of three oceans, Pacific, Indian and Atlantic [3], and no difference was noted in the central courses of $\alpha\downarrow\lambda$. /81

The order of the computation of attenuation in solar energy is described in [4]. Because of the completeness of the presentation, a figure is reproduced from this publication. The level of integral irradiance by light in the range $380 \leq\lambda\leq 710$ nm in percentages of the level of surface irradiance in the same spectral range is plotted on the y-axis (Figure 5). The values of the water type index are plotted on the x-axis. The curves refer to depths from 5 to 100 m. Calculation of the nomogram in Figure 5 used data regarding the spectral distribution of solar radiation at the level of the sea surface for a high sun, taken from [9, 10].

By knowing the integral irradiance of the ocean surface in the interval 380 - 710 nm (i.e., the PRE at the surface), it is sufficient to multiply it by the coefficient taken from Figure 5 in order to obtain the PRE at the given level. For example, in order to determine the annual influx of PRE (close to the general level of influx /82 of solar energy, starting from depths of several meters) at a definite level in a given water area, it is necessary to fulfill the following operations. First of all, we used the data [11] presented on the left insert of Figure 3 which give the annual influx of solar radiation to the surface of the Indian Ocean. Secondly, the value taken from the map should be multiplied by the coefficient which estimates the percentage of PRE in the general solar energy flux at the level of the sea surface. According to the data of measurements in the Indian Ocean, this coefficient averages

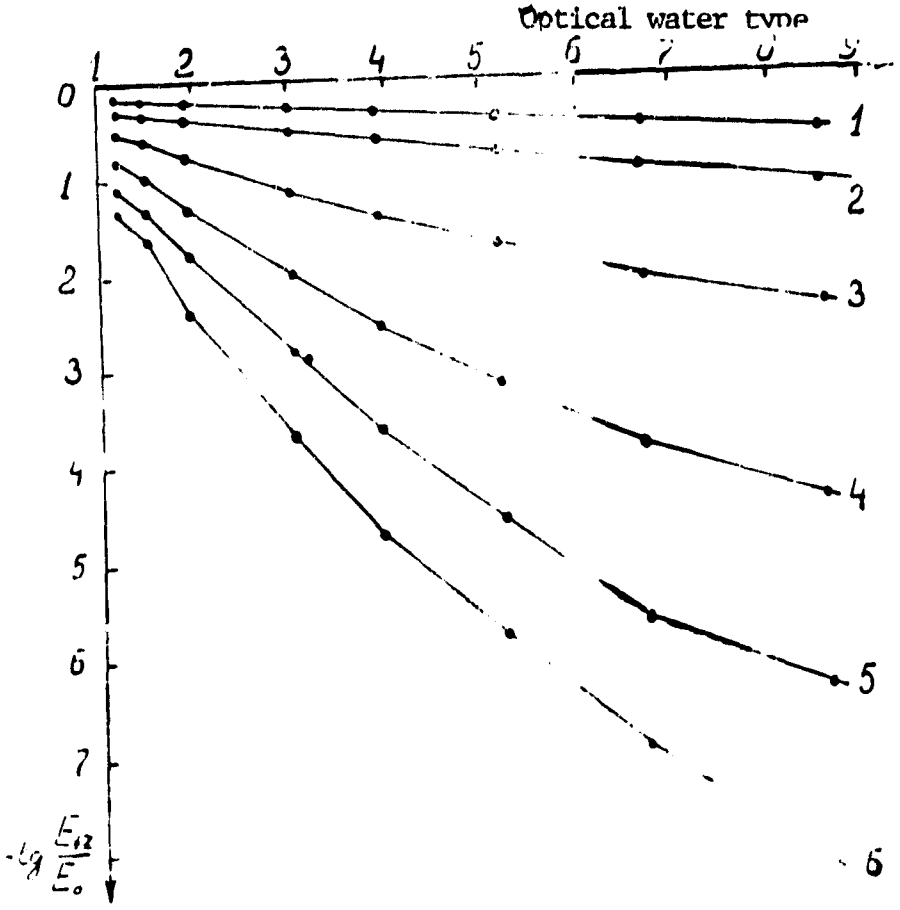

Figure 5. Transmission Coefficient of Photosynthetic Radiant Energy ($360 \leq \lambda \leq 710$ nm) of the Upper Ocean Mass Depending on the Water Type Index m. E_0 and E_z--surface irradiance and irradiance from above at depth z respectively. 1--z = 5 m, 2--10, 3--25, 4--50, 5--75 and 6--100 m.

0.44 [12]. Thirdly, the obtained value should be multiplied by the coefficient which is determined from the index m from the graph in Figure 5.

Publication [4] has shown that the main error in this calculation develops be- /83
cause of inaccurate knowledge of the water type index. It increases with depth as $2.3 \times z \times \Delta\alpha\downarrow \approx 2.3 \times 10^{-2} z \times \Delta m$, where Δm is the error in the value of the water type index. With relative error in estimating the index m in constructing the map (Figure 3) corresponding to 0.1, i.e., 10%, the relative error in calculating the

underwater irradiance equalled $2.3 \times 10^{-3}\ z \times m$ (z in meters). For example, for water type 2.0 ± 0.2, the relative error in computing the PRE for depths 10 m and 100 m equalled respectively 0.046 and 0.46, i.e., 4.6% and 46%. These estimates make it possible to compute the error in $E\downarrow$ for each specific region and level.

One can use the same Figure 5 to examine the question of at which depths the PRE level attenuates a certain number of times. The depth at which the PRE level diminishes 10^2 times, is sometimes adopted as the conditional local boundary for the layer of active photosynthesis. The corresponding levels for the water area of the Indian Ocean are given on the right insert of Figure 3.

The spectral composition of light underwater is also associated with the optical index of water type. Publication [4] gives estimates of the width of the spectral intervals which include solar radiation at different depths (for level e^{-1} from the maximum $E\downarrow\lambda(z)$). Whereas at depth 10 m, the width of this interval is 240 - 210 nm (with change in the index m, respectively, from 1.2 to 5), at depth 50 m, the interval diminishes to 125 - 100 nm, at depth 100 m--to 100 - 75 nm (with indices 1.2 and 5 respectively). In this case the wavelength of the greatest spectral density of underwater irradiance λ_{max} does not change with submersion for clean ocean waters $1.2 < m \leq 2.1$, and corresponds to $\lambda_{max} = 480 \pm 10$ nm. With an increase in the water type index 2.1 to 9, λ_{max} increases with submersion, reaching the asymptotic value 570 ± 10 nm for $m = 9$. The asymptotic values λ_{max} are reached with submersion very quickly and are actually determined only by the water type index.

We will compare the results obtained in this work and in [1]. Comparison of the map in Figure 3 with the map from [1] makes it possible to see both their common features, for example, the existence of two "enclaves" to the south of the equator, and their differences. In [1], the authors note the high turbidity of the waters in

the trade wind current to the south of the Hindustan Peninsula and the Island of Sri Lanka, classifying them as the same type of water as the Arabian Sea. In the map of Figure 3 of this work, on the contrary, the trade wind current does not differ in optical water indices from the equatorial counter current and the main mass of water in the central part of the ocean. This discrepancy is apparently explained by the use in this work of an optical water index which changes more smoothly.

We will now compare the data from computing $E^{\downarrow}(z)$ according to the technique presented here, with the results obtained in [1] with the use of the Yerlov water classification and the table for attenuation of solar radiation flux in waters of different type [2] given by him. The comparison results are presented in Table 3 /84 for several regions. Comparison of the left and right halves of the table make it possible to note that: 1) discrepancy in the estimates of the E (z) level by two methods is in limits of the stipulated calculation errors, 2) a systematic difference is observed in the levels E(z), rising with depth, and this work has obtained an average of somewhat larger values than in [1], 3) error in the calculations according to the technique of this work is smaller than in [1], compare columns 5 and 9 with 6 and 10 of Table 3.

The authors are grateful to O. V. Kopelevich for useful discussion of the work and remarks made.

TABLE 3. COMPARISON OF RESULTS OF EVALUATING THE LEVEL OF ANNUAL INFLUX OF SOLAR ENERGY AT DIFFERENT DEPTHS

Region	Estimates According to [1] z, m	Type by Yerlov	E↓(z) Kcal. cm² Year	Error [1] (rel.)	Error Kcal. cm² Yr.	Water Type Index m	Estimates According to the data of this publication E↓(z) Kcal. cm² Yr.	Rel. Error	Standard Error Kcal. cm² Yr.
Trade wind current	Above sur.	IB	150–160			1,75	170		
	10	IB	25–27	0,18	4,7	(Average for region)	31	0,01	1,2
	20		12–13	0,36	4,5		14	0,1	1,4
	50		2,7–2,9	0,9	2,5		4	0,2	0,8
	100		0 2	1,8	0,46		0,5	0,4	0,2
Arabian Sea	Above sur.	II	[illegible]00			2,55	00		
	10		24–28	0,11	10	/ . /	23	0,06	2,0
	20		7–8	0,82	6		8,8	0,15	1,3
	50		1,2–1,4	3,05	2,6		1,7	0,3	0,5
	100		<0,1	4,1	0,4		0,04	0,5	0,02
SIOC axis	Above sur.		150–160				160		
	10		31–33	0,07	2,3	1,3	34	0,03	1,0
	20		20–22	0,14	3,0	/ /	20	0,075	1,5
	50		8–8,5	0,35	2,9		8,4	0,15	1,5
	100		0,9	0,7	0,6		1,6	0,3	0,75

BIBLIOGRAPHY /85

1. Rutkovskaya, V. A.; Khalemskiy, E. N. "Calculation of Solar Energy Penetrating the Water Mass of the Indian Ocean," Okeanologiya, vol 17, No 2, 1977.

2. Yerlov, N. Opticheskaya okeanografiya ["Optical Oceanography"], Moscow, Mir, 1970.

3. Pelevin, V. N.; and Rutkovskaya, V. A. "Optical Classification of Ocean Water According to Spectral Attenuation of Solar Radiation," Okeanologiya, vol 17, No 1, 1977.

4. Pelevin, V. N.; and Rutkovskaya, V. A. "Attenuation of Photosynthetic Radiation in Waters of the Pacific Ocean," Okeanologiya, vol 18, No 4, 1978.

5. Morel, A.; and Prieur, L. Spectral analysis of diffuse attenuation coefficients of diffuse reflection, absorption, and retrodiffusion for different marine regions. Report No. 17, July, Villfranch-sur-Mer.

6. Degtyarev, V. I.; Ochakovskiy, Yu. Ye.; and Pelevin, V. N. "Errors in Measuring Underwater Irradiance in the Sea," in Optika okeana i atmosfery ["Optics of the Ocean and the Atmosphere"], Moscow-Leningrad, Nauka, 1972.

7. Kanayev, V. F.; Neyman, V. G.; Parin, N. V. Indiyskiy okean ["Indian Ocean"], Moscow, Mysl', 1975.

8. Kabanova, Yu. G. "Primary Production of Northern Part of the Indian Ocean," Okeanologiya, vol 8, No 2, 1968.

9. Avaste, O. A. "Influx of Heat of Solar Radiation in Atmosphere and Total Radiation Flux on the Sea Surface," in Issledovaniya radiatsionnogo reznima atmosfery ["Studies of the Radiation Regime of the Atmosphere"], ESSR Academy of Sciences, No 8, Institute of Physics and Astronomy, Tartu, 1967.

10. Vysotskiy, A. V.; Garadzha, M. P.; and Nezval', Ye. I. "Certain Results of Measuring Spectral Composition of Solar Radiation in the Spectral Region 400 - 700 nm in Moscow," Meteorologiya i gidrologiya, No 1, 1977.

11. Atlas okeanov. Atlanticheskiy i Indiyskiy okean ["Atlas of Oceans. Atlantic and Indian Ocean"], Izd. Ministerstva oborony SSSR, VMF, 1977.

12. Rutkovskaya, V. A.; and Pelevin, V. N. "Total and Photosynthetic Radiant Energy Above the Ocean," Gidrofizicheskiye i opticheskiye issledovaniye v Indiyskom okeane ["Hydrophysical and Optical Studies in the Indian Ocean"], Moscow, Nauka, 1975.

RESULTS OF SIMULTANEOUS MEASUREMENTS OF A NUMBER OF HYDRO-OPTICAL CHARACTERISTICS IN THE BALTIC SEA

PELEVIN, V.N., SUD'BIN, A.I., MOZGOVOY, V.I.

Simultaneous measurements of the spectral index of vertical attenuation $\alpha\downarrow\lambda$, coeficient of diffuse reflection $R\lambda$ and brightness coefficient of the sea $\rho\lambda$ are made in the Baltic Sea. Analysis of the data permits the hypothesis to be advanced that optical classification of the ocean waters of V. M. Pelevin and V. A. Rutkovskaya can apparently be applied to the case of very turbid waters of the Gulfs of Finland and Riga where values of the optical water type index m reach a level of 15 and 20 respectively.

In the Baltic 1977 flight and sea expedition, measurements were made of the vertical attenuation index $\alpha\downarrow\lambda$, the diffuse reflection coefficient $R\lambda$ from a boat and the sea spectral brightness coefficient at the nadir $\rho\lambda$ from the helicopter KA-26. Measurements "in situ" were made with the combined radiation receiver of A. S. Suslyayev [1]. It has interference filters with maximum transmission at wavelengths: 382 nm, 402 nm, 443 nm, 493 nm, 545 nm, 583 nm and 680 nm with transmission width for half altitude ~10 nm. The receiver was lowered from the cutter, and the average irradiance from above was determined at levels 0, 2, 5, 10, 20 m. The receiver

was then turned over, and the average values of irradiance from below was determined at level 2m. At the same time a ship-board photometer was used to control the external illumination whose changes were taken into consideration in the calculations. The condition of the sea surface was defined individually. The coordinates of the measurement points and the characteristics of the external conditions are presented in Table 1.

TABLE 1. COORDINATES AND CONDITIONS FOR CONDUCTING MEASUREMENTS

Number of Series	Date	Time	Coordinates	Condition of Sea Surface	Cloud Cover	Remarks
1	4.10.77	11:30	Southeast of Muhu Island, at the outlet into the Virt-su-Vyayn Gulf	3 points	Solid; sun O	
2	15.10.77	12:00	59°31'N 24°43'E	3 points	9 points; sometimes sun O	
3	15.10.77	14:00	59°34'N 24°35'E	3 points	9 points; sometimes sun O	Z = 6m
4	3.10.77	15:00	58°17'N 23°37'E	2 points wind-driven and swells	5 - 7 points, cumulus	Drastic changes in illumination of surface

The results of measuring $\alpha\downarrow\lambda$ are presented in Figure 1. The measurement error is no more than 15% in the short-wave spectral region, and no more than 10% in the long-wave, except for series 4 in which drastic changes in external illumination during the measurements resulted in errors, sometimes exceeding 25%. Values of $\alpha\downarrow$ were not successfully obtained at λ = 680 nm because of too few regions at great depths.

Attention is drawn to the clearly pronounced stable maximum $\alpha\downarrow\lambda$ in the region ~400 nm. Our measurements were made at discrete points corresponding to transmission of the interference filters. With measurements with a monochromator, the maximum is possibly somewhat shifted into the long-wave region of the spectrum (by

10 - 15 m). The presence of this maximum indicates that in these waters the correlation between the concentration of chlorophyll and yellow substance is apparently such that absorption by chlorophyll together with its accompanying pigments (carotinoids) and pheophytins determines the course of the indicator $\varkappa$ in this spectral region, and not the absorption by yellow substance.

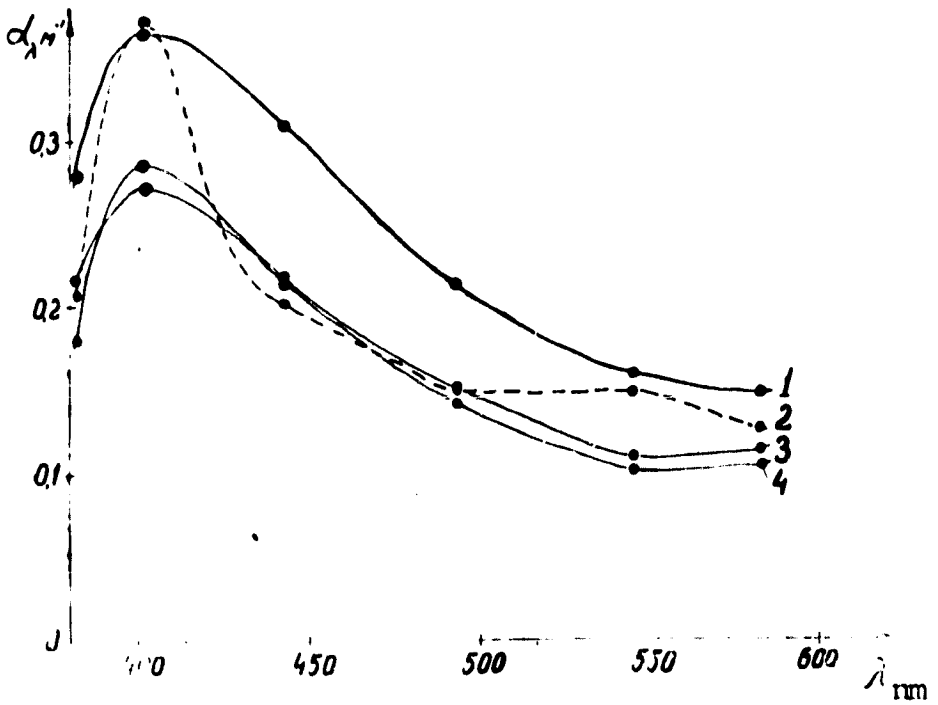

Figure 1. Results of Measuring Spectral Indicator of Vertical Attenuation $\alpha\lambda$ at Stations Whose Coordinates are Indicated in Table 1 (numbers at curves correspond to numbers from table)

The results of measuring the coefficient of diffuse reflection R_λ which correspond to series 2 from Table 1, are presented in Table 2. The minimum is observed here in the region of absorption by chlorophyll with accompanying pigments. /87

Measurement of the spectral brightness coefficient of the sea $\rho\lambda$ at the nadir was made from the helicopter flying at an altitude of 100 m with low velocity above

TABLE 2. VALUES OF R_λ, %

λ, nm.	382	402	443	493	545	583
R, %	0,5	0,4	0,56	1,25	1,9	1,56

the cutter. The technique of measuring ρ_λ is described in [2]. The observed brightness of the sea surface was used to compute the contribution created by the Fresnel reflection of brightness of the sky by the surface of the sea. This quantity was classified as the brightness of a horizontal white scatterer illuminated by the same light as the surface of the sea. The obtained values of ρ_λ are given /88 in Table 3.

TABLE 3. VALUES OF ρ_λ, %

λ, nm	369	383	426	457	558	590
ρ_λ, %	0,83	0,70	0,43	0,11	0,63	0,50

Comparison of Tables 3 and 2 shows that the spectral course of ρ in general features repeats the course of $R\lambda$, but the value ρ_λ is lower on the average. The minimum ρ_λ in the region of absorption by chlorophyll with accompanying pigments and pheophytins is more pronounced than the minimum R_λ which corresponds to the estimates given in [2].

Simultaneous measurements of $\alpha\downarrow\lambda$, R_λ and ρ_λ in the same water are of great importance and are very rare, therefore, despite the few data, we will compare them with the materials and recommendations presented in [2 - 5].

A deep decrease in the values $\alpha\downarrow\lambda$ in the near ultraviolet with $\lambda < 400$ nm observed in Figure 1 is in complete correspondence with the pattern of spectral

courses of $\alpha\downarrow\lambda$ in the turbid waters given in the classification of ocean waters [3] (see the nomogram of Figure 3 from [3]). The minimum value of $\alpha\downarrow\lambda$ is in the region 550 - 580 nm. This also corresponds to the nomogram. In this case, the water index $m = 100\,\alpha\downarrow_{500}$ for curves 2 - 4 (Gulf of Finland) is close to 15, while for curve 1 (northern shallow region of the Gulf of Riga) is even close to 20. This is far beyond the limits of m = 1.1 - 9.0 studied in the classification [3].

Nevertheless, we will verify the possibility of evaluating the water type index m from measurements in different spectral sections, as is recommended in [4], according to the formula:

$$m = \frac{\alpha\downarrow\lambda^* - a_\lambda}{b_\lambda}, \qquad (1)$$

where λ^* corresponds to the wavelengths of the employed interference light filters, and the values a_λ and b_λ are given in [4]. Evaluation of the water type index for six values of λ^* for which measurements of $\alpha\downarrow\lambda$ ($382 \leq \lambda \leq 583$ nm) were made, yielded values in Table 4.

TABLE 4.

Wavelength λ, from which m was Estimated	Estimation of m for Curves $\alpha\downarrow\lambda$ from Figure 1			
	1	2	3	4
382	17	11	13.5	13.5
402	20	16	15.5	20
443	20	15	15	14
493	21	13	13.5	15
545	19	13,3	12	17
583	19	13.5	12	16
Average $\bar{m}$	19.5	14.0	13,6	16
Variation δ	0,1	0.16	0.13	0.11

Evaluation of m was made for a broad interval of λ. Nevertheless, we see that the spread of obtained values is small. If, according to the recommendations in [4],

we evaluate m for not exceeding the interval 432 $\leq \lambda \leq$ 540, then the standard deviation of values does not go beyond the limits of 10% of the average $\bar{m}$ for all the series, even for the fourth, which as noted above, was measured under poor hydrometeorological conditions. The difference between $\bar{m}$ for series 2 - 3 is statis- /89
tically unreliable. This corresponds to the measurement at not very distant stations (see the coordinates in Table 1). The difference between m and $100\,\alpha_{493}$ for all series is also small and does not exceed the measurement error α_λ. The latter circumstance indicates that evaluation of m can be made both for one measurement of α_λ with λ = 500 nm, and for a set of measurements in several spectral regions with the use of (1). The fact that the estimates made with the help of (1) for the optical index of water type from experimental α_λ were close to those for different 382 $\leq \lambda \leq$ 583 provides the grounds to hypothesize the classification [3, 4] can be applied to more turbid sea water than those which were examined in [3, 4]. In order to verify this hypothesis, it is required that additional experimental material be obtained on the spectral α_λ in turbid sea water.

We will now pass to an analysis of the spectral course of R_λ given in Table 1. These R_λ values were measured in turbid waters whose index type we have estimated well. This index goes far beyond the limits of the range studied in [5]. It was therefore of great importance to compare the measured R_λ with the data presented in [5]. We recall that in [5] a good correlation was found and illustrated between the values and the spectral courses of the coefficient R_λ in ocean waters with value of the index $m = 100\,\alpha_{500}$.

Figure 2 presents in one scale a number of curves of Figure 2 from publica- /90
tion [5] which describe the average course of R_λ for samplings which have an average value of m equal to 2.1, 3.3, 6.0 and 9.5, and the experimental curve R_λ in the Baltic Sea referring to series 2 (m = 14) from Table 2. It is apparent that the

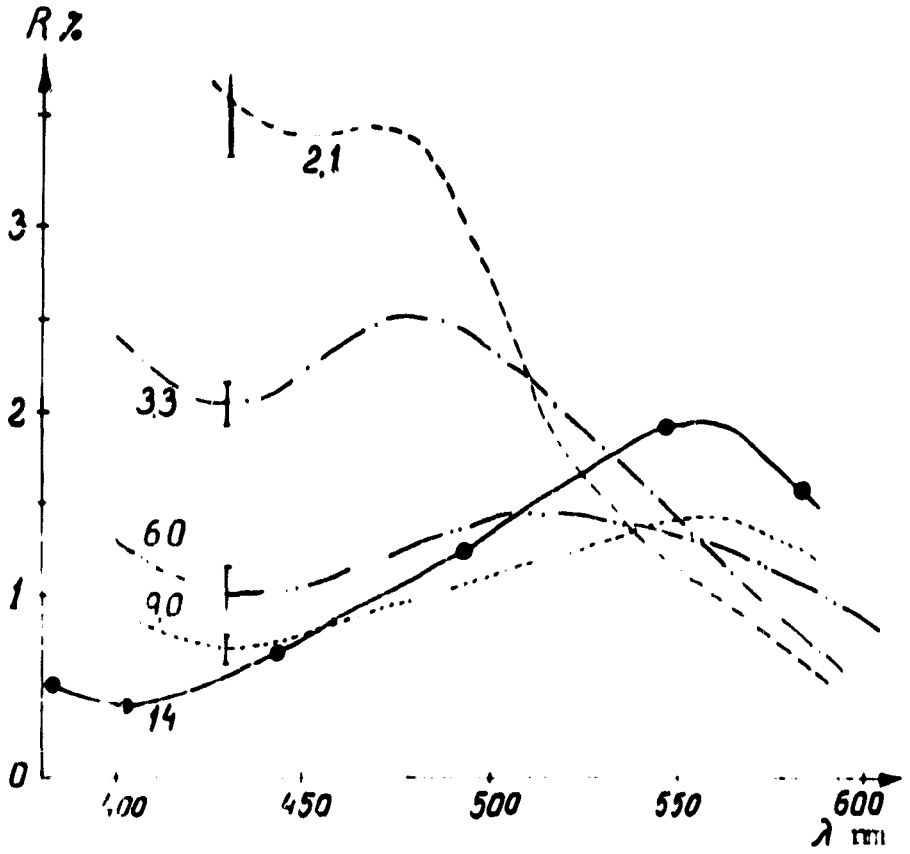

Figure 2. Comparison of Spectral Course R Measured in the Sea with m = 14 with Spectral Courses R_λ with m = 2.1 - 9.0 (the latter taken from [5]).

single experimental curve continues the trend traced in the series of average curves with a rise in the index m. In a similar manner, Figure 3 gives a number of average values of ρ_λ from Figure 3 of publication [5] and the experimental curve ρ_λ for measurements from a helicopter from Table 3. A general trend for change in the type of curves with an increase in m is also traced.

These data indicate the promising nature of expanding the area of natural links /91 found in [5, 3] between different spectral characteristics of the light field in open and sea waters.

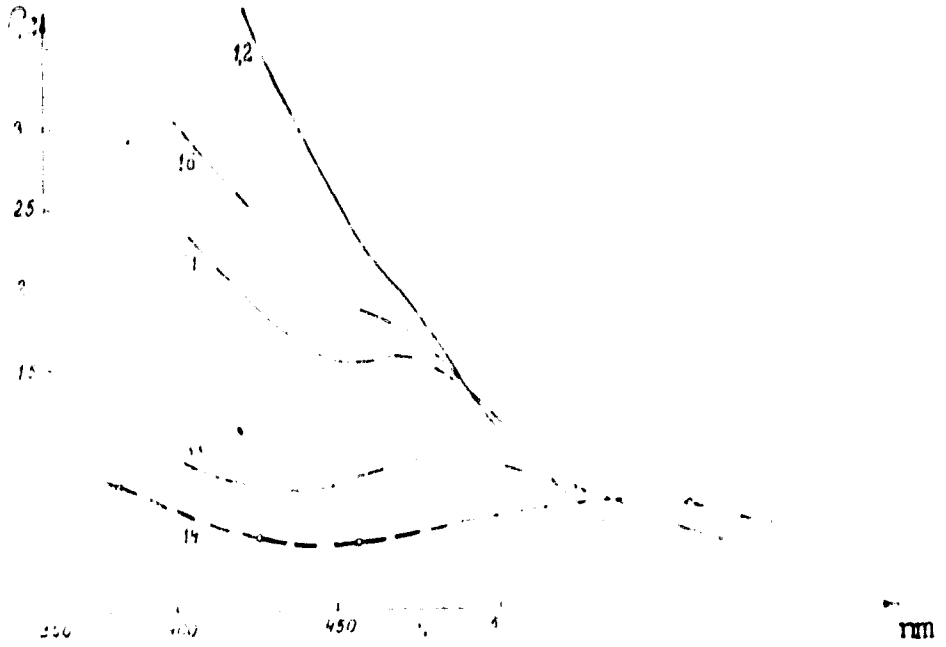

Figure 3. Comparison of Measured Spectral Values $\rho\lambda$ with m = 1.4 (Gulf of Finland) with Spectral Courses $\rho\lambda$ with m = 1.2 - 3.3 taken from [5].

BIBLIOGRAPHY

1. Shifrin, K. S.; Pelevin, V. N.; and Sud'bin, A. I. "Stuay of Fluctuations in Underwater Irradiance," in Optika okeana i atmosfery ["Optics of the Ocean and Atmosphere"], Izd-vo Nauka, Leningrad, 1972.

2. Pelevin, V. N. "Evaluation of the Concentrations of Suspended Matter and Chlorophyll in the Sea from Spectrum of Outgoing Radiation Measured from a Helicopter," Okeanologiya, vol 18, No 3, 1978.

3. Pelevin, V. N., Rutkovskaya, V. A. "Optical Classification of Ocean Water According to Spectral Attenuation of Solar Radiation," Okeanologiya, vol 17, No 1, 1977.

4. Pelevin, V. N.; and Rutkovskaya, V. A. "Attenuation of Solar Energy Flux with Depth in Waters of the Indian Ocean," in this collection, 1978.

5. Pelevin, V. N. "Spectral Characteristics of the Field of Solar Radiation in the Sea and Above its Surface," in this collection, 1978.

TECHNIQUE AND RESULTS OF MEASURING SPECTRAL ABSORPTION OF LIGHT BY DISSOLVED ORGANIC "YELLOW" SUBSTANCE IN WATERS OF THE BALTIC SEA

PELEVINA, M. A.

A technique is presented for measuring the spectral absorption of light by yellow substance which was used in the Baltic summer sea expeditions of the Institute of Oceanography of the USSR Academy of Sciences. Results are given from measuring the exponent of spectral relationship of absorption by yellow substance in the waters of the Gulfs of Pyarnu and Riga and the mouths of the Pyarnu and Daugava Rivers.

It is known that products or organic substance breakdown dissolved in sea water intensively absorb short-wave radiation and with high concentrations stain the water a yellow color, from which they have obtained the name "yellow substance". Study [1] gives data unsubstantiated by experiment that the dependence of light absorption by the yellow substance on wavelength is exponential.

This component of sea water which strongly absorbs light must influence the spectral brightness coefficient of the sea in the blue and UV spectral.

The Baltic summer expeditions of 1975-1977 using long-range methods of analyzing optical properties of sea water from a low-flying aircraft measured the spectral light absorption by yellow substance $x_{y.s.}$ in water samples taken from the sea.

The technique was developed to measure the concentration of yellow substance in relative optical units and the spectral index of light absorption by the yellow substance $x_{y.s.}$ was measured. The technique is as follows:

The sea water taken from the helicopter was filtered through SYNPOR membrane filters with pore diameter 0.6-0.7 μm. The suspension extracted from the water was analyzed for the quantity of chlorophyll and carotinoids, and was also used to evaluate the total concentration of suspended substance. 10 ml of sea water purified of suspension (filtrate) was used to measure the $x_{y.x}$. Initially, the optical density of the filtrate was increased by evaporating

it several times in a vacuum in a rotary evaporator at temperature not exceeding 40°C. After the specific optical density of the filtrate was increased k-fold, the latter could be recorded on a SPECORD spectrophotometer not only in the UV-range, but also in the visible spectral range. The remaining bidistillate was in a comparison vessel.

In order to use this technique, it was first of all necessary to establish the maximum permissible quantity of $k = V_f/V_{ae}$, where V_f--initial volume of filtrate, V_{ae}--volume remaining after evaporation. With a definite degree of evaporation, the sediment is precipitated out, the intensity of condensation of yellow substance on the walls of the test tubes or at the centers of condensation within the sample increases, etc. As a result, serious errors develop in the measured quantity $\varkappa_{y.s.}$.

Experiments were done with filtrates of two samples, taken from the mouth of the Pyarnu River which contains a record quantity of yellow substance (there are many peat bogs and swamps in the vicinity of the river), and one taken in the open section of the Gulf. The same quantities of filtrates of one sample were evaporated to a varying degree. The attained solutions were measured by the SPECORD. It was found that initially the optical density of the solutions with $\lambda = 360$ nm increases strictly proportionally to the degree of evaporation k: $D_{360} \sim k$. In this case one should stress that the spectral curves D_λ for samples with different k remained similar to each other. However, starting with the value $k \sim 7 - 8$ for the sea sample, the dependence of $D_{360}(k)$ smoothly deviates from the straight line, and the proportionality of these quantities was disrupted. For the river sample, this deviation was observed starting with k = 4. From here follows the conclusion that when the technique of evaporating the sample in order to increase its optical density is used, one should be restricted to the degree of evaporation k = 8 for sea water of this water area and k = 4 for the river water. Practice has shown that evaporation this number of

times is sufficient to record the optical density D_λ of solutions in the visible spectral region and subsequent calculation of the index of absorption of yellow substance $\varkappa_{y.s.}$ in the sea.

We will now pass to a presentation of the results. An example of recording D_λ of yellow substance is presented in Figure 1. It is apparent from the figure that the spectral courses of D_λ of yellow substance in different samples are practically /94
the same. This was confirmed for the entire water area of the Gulf of Riga and the Pyarnu Gulf, as well as in the samples taken at the mouths of the rivers Pyarnu and Daugava.

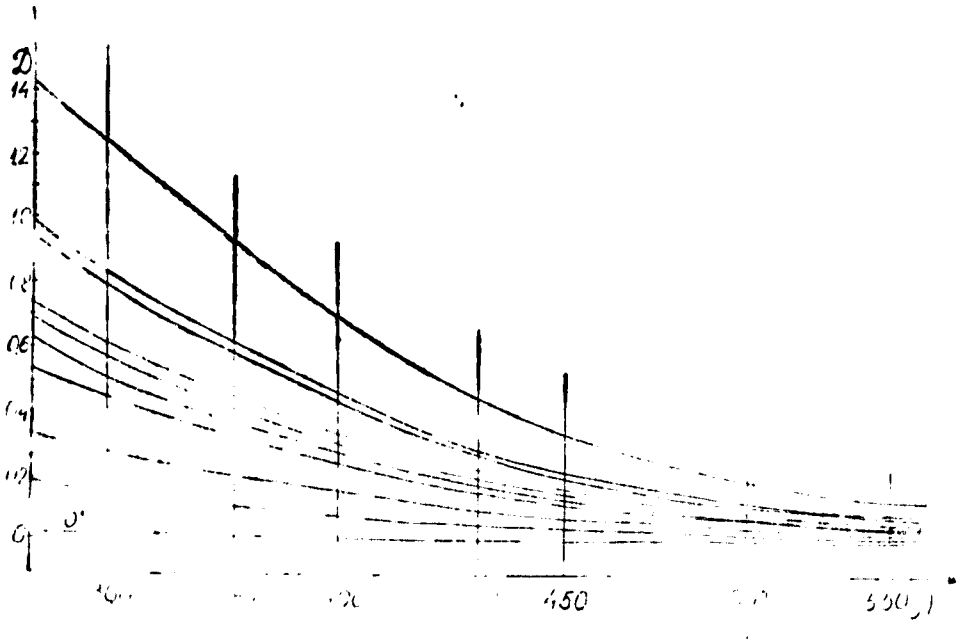

Figure 1. Examples of Recordings on SPECORD of Absorption Spectra of Yellow Substance (filtrates of sea water evaporated 4 - 8 times).

Examples of recording the absorption spectra of the evaporated filtrates in a broader spectral range are presented in Figure 2.

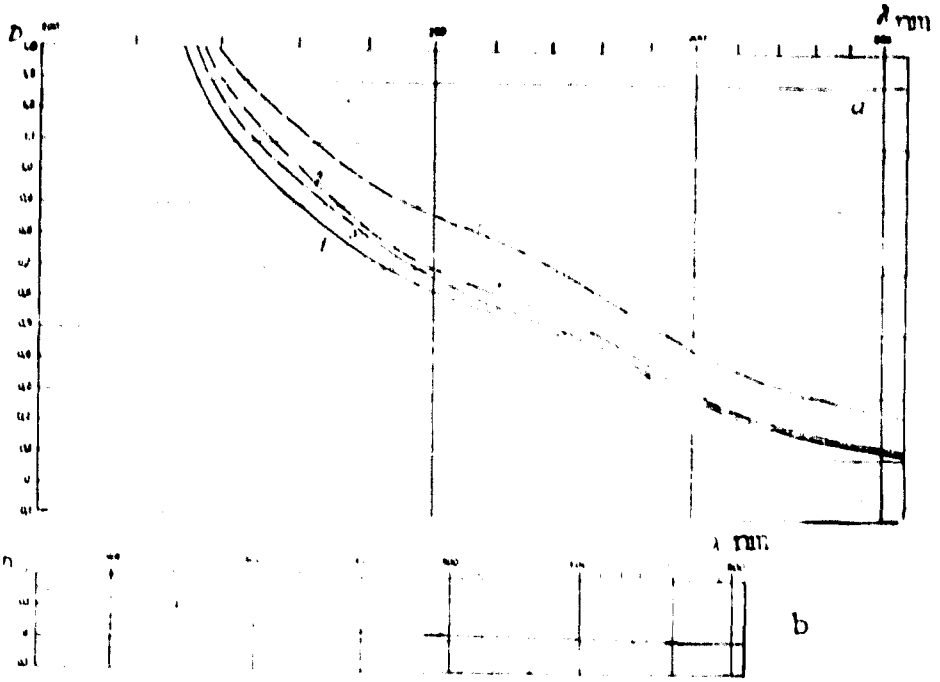

Figure 2. Examples of Recording Absorption Spectra of Evaporated Filtrates of Sea Water in Broader Spectral Region (1 – 4-fold samples).

Figure 3 presents curves of light absorption by pigments of phytoplankton in acetone extract obtained from the same water samples for comparison.

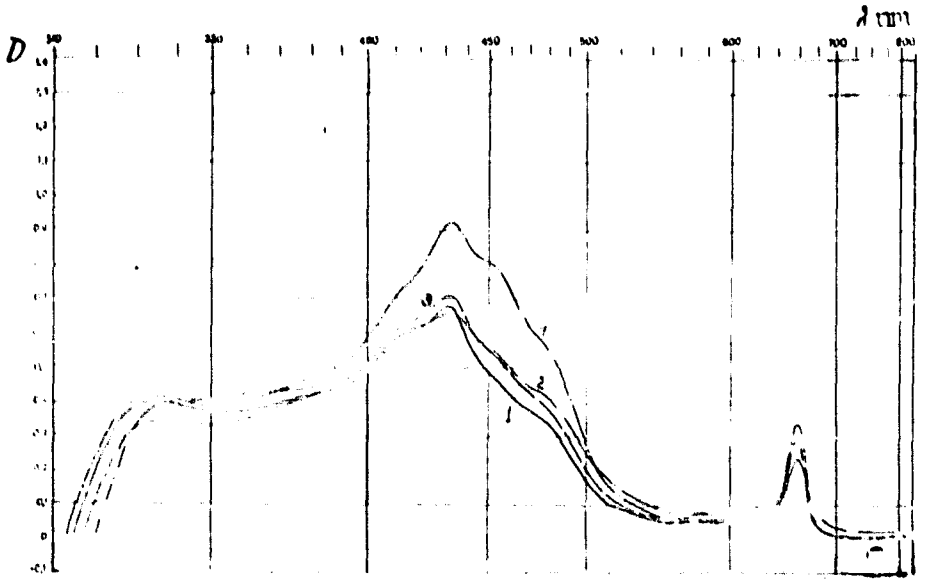

Figure 3. Absorption Curves of Phytoplankton igments Extracted from the same Samples of Sea Water

In order to clarify the law governing the change in $\varkappa_{y.s.}$ according to the spectrum, the graphs obtained on SPECORD are presented in the form of dependences of $\lg \varkappa_{y.s.}$ on λ, and the λ- axis is constructed in a linear scale as is shown in Figure 4. The points on the figure correspond to the carefully transferred values of $\lg \varkappa_{y.s.}$ from continuous realizations of the type presented in Figure 1.

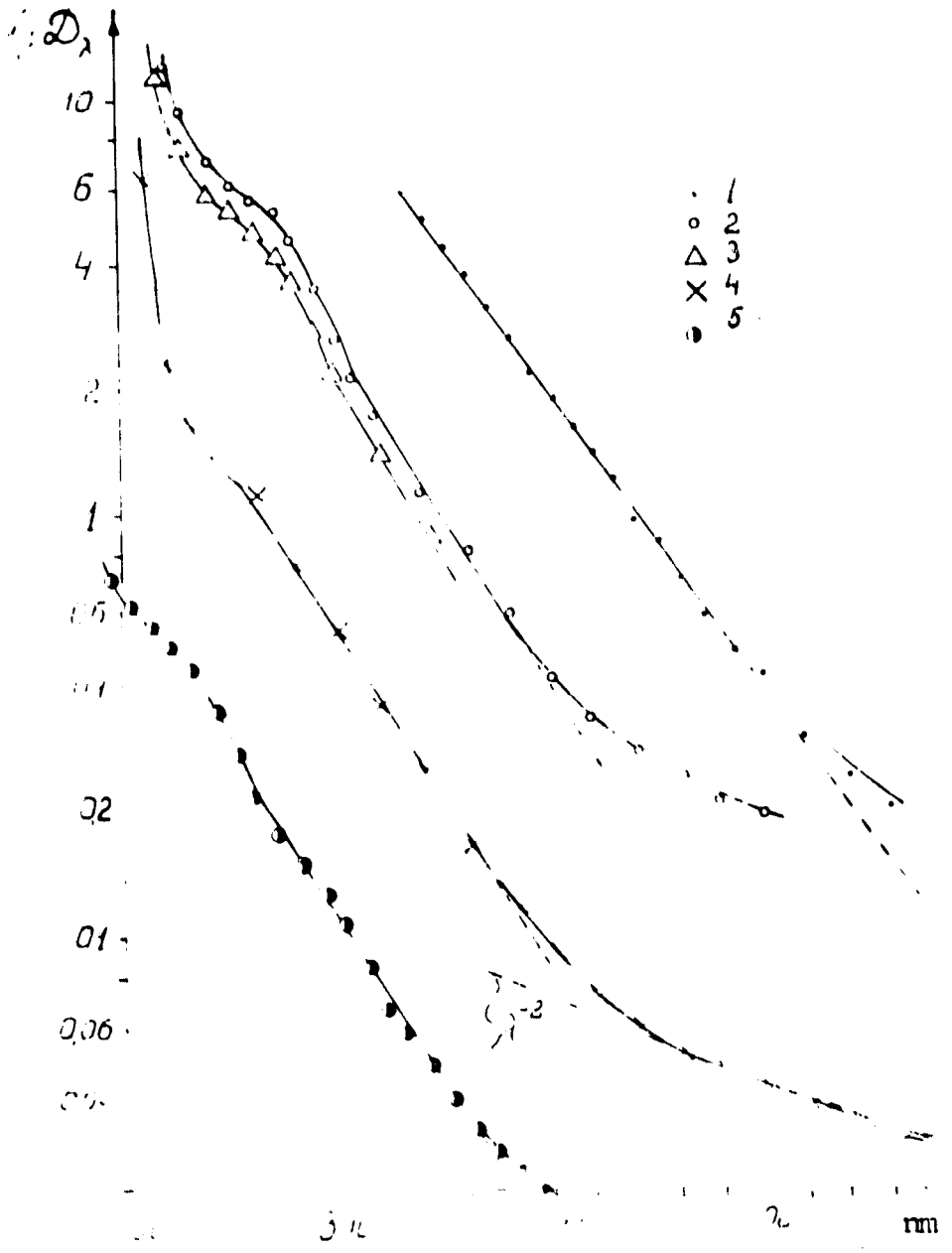

Figure 4. Specteral Dependence of Light Absorption by Evaporated Filtrates of Sea Water (in relative units) for Different Samples [key on next page]

Figure 4. (continued)
Key:
1. mouth of Pyarnu River
2-4. Gulf of Pyarnu
5. open water area of the Gulf of Riga

/96

In the interval λ > 300 nm the course of the curves is determined by light absorption by yellow substance $\varkappa_{y.s.}$. Deviation of the curves from the linear relationship in the region of large λ (i.e., with small D) is explained by the influence of insufficiently completely filtered fine suspended matter in the filtrate.

A strict linear dependence on $\lg \varkappa_{y.s.}$ on λ is visible in Figure 4, i.e., the exponential dependence of $\varkappa_{y.s.}$ on λ with λ >300 nm. This confirms the data of publication [1]. Only in the long wavelength section of the spectrum with very small values of $\varkappa_{y.s.\,\lambda}$ does the experimental curve divert from the exponent. In order to clarify the reason for this deviation, measurements were made of the filtrates obtained through filters with different pore diameters, all the way to size 0.2 μ. It was found that /95 the smaller the pore size of the filter, the larger the values of λ, i.e., smaller levels of $\varkappa_{y.s.}(\lambda)$ at which a deviation in the experimental dependence of $\varkappa_{y.s.}(\lambda)$ on the exponent is observed. This is proof that deviation from the exponent is caused by scattering and absorption of the beam of the spectral photometer on particles of suspended matter which remain in the sample after filtering. There are no grounds to hypothesize that dependence $\varkappa_{y.s.}(\lambda)$ directly differs from the exponential in the long wavelength region of the spectrum of visible radiation. The value of the indicator a depending on $\varkappa_{y.s.} \sim 10^{-a\lambda}$ according to our measurements $\lambda \geq$ 360 nm in the waters of the Gulfs of Riga and Pyarnu equals a = 7.2 - 8.1 μm^{-1}. This quantity somewhat exceeds the quantity a = 6.5 μm^{-1} which was computed according to the data presented in [1] "for waters of the Baltic Sea."

We will now pass to the question of relative distribution of the concentration of yellow substance in samples taken at different points of the studied water area. Since the spectral courses $\varkappa_{y.s.}(\lambda)$ for all samples are close to each other, the

relative content of yellow substance can be estimated from the value $\varkappa_{y.s.}$ with any selected wavelength λ^*. It is convenient to select λ^* in the short wavelength spectrum, close to λ = 360 nm, in light of the large values of $\varkappa_{y.s.}$, and consequently, the smaller errors in this area. In this region the salts contained in the sea water do not yet absorb light.

On the other hand, a shorter wavelength light filter during photo metering of /97
the sea from a helicopter had λ_{max} = 369 nm. Therefore we selected the values $\varkappa_{y.s.369}$ m^{-1} in the sea for comparative estimates of the $\varkappa_{y.s.}$ content over the water area.

The values of $\varkappa_{y.s.369}$ from 0.4 to 1.5 m^{-1} were adopted for the water area of the Gulfs of Riga and Pyarnu (with decimal base), while in the mouths of the Daugava and Pyarnu Rivers they reached values of 3.6 - 6 m^{-1}. Geographical distribution of this quantity over the indicated basin can be seen in publication [2], which compares $\varkappa_{y.s.369}$ with the spectral features of the outgoing radiation.

The author is grateful to D. Yankovskiy, M. I. Vortman, V. I. Mozgoviy and A. I. Sud'bin for help in conducting the experiment.

BIBLIOGRAPHY

1. Yerlov, N. Opticheskaya okeanografiya ["Optical Oceanography"], 1970, Izd-vo Mir.

2. Pelevin, V. N.; Gruzevich, A. K.; and Lokk, Ya. F. "Possibility of Evaluating the Distribution of Yellow Substance Concentration in Sea Water from Spectra of Outgoing Radiation," this collection, 1978.

II. STUDY OF STATIONARY AND NONSTATIONARY LIGHT FIELDS CREATED IN THE SEA BY ARTIFICIAL SOURCES

/98

SOLUTION OF THE INTEGRAL TRANSPORT EQUATION AS APPLIED TO LIGHT FIELDS IN WATER MEDIA CREATED BY ARTIFICIAL SOURCES

V. I. SAVENKOV, G. A. MEL'NIKOV

An integral transport equation is derived for the case of a point collimated monochromatic light source and its solution is given. A solution is suggested for this equation as applied to aquatic media for the case of a point isotropic monochromatic light source. The calculated and experimental results are compared.

Recently, because of great demand, the theory of stationary radiation fields (light fields) of artificial light sources in water has been intensively developed. Studies of the formation of these fields are not only of great scientific importance, but are also necessary to solve important practical problems associated: with underwater illumination; visibility underwater with artificial illumination; underwater photography, movies and television, light location, navigation and communications, etc.

To construct effective and economically advantageous light engineering units, it is necessary to develop engineering methods for computing artificial light fields from sources submerged in water with random light distribution.

It is noted in [1] that to solve this problem it is most optimal to study the AEF (artificial light field) structure created by sources with simple light distribution, i.e., such as localized: collimated, isotropic and Lambertian. Based on data obtained, using the principle of elementary solution superposition and using the detected characteristics of the ALF as Green functions in the Stieltjes convolution (method of Green functions), one can compute analogous parameters of the ALF created by sources with complicated curves of the light force.

Theoretical studies of laws on radiation propogation and formation of the ALF in water media were made by solving the equation (integrodifferential) transport of radiant energy with corresponding boundary conditions.

There is currently no complete solution to the transport equation as applied to aquatic media, media with the presence of true absorption and strongly anisotropic scattering of radiation. This is associated with the fact that its analytical solution is possible either for the simplest idealized situation (flat symmetry, isotropic scattering, absence of absorption, simple boundary conditions), or for ranges of change in arguments in which separation of the variables is possible (asymptotic solutions) [2]. At the same time, the solutions obtained even with very significant simplified hypotheses, are insufficiently accurate, cumbersome and far from an appearance suitable for engineering hydrological, light and technical calculations. In addition, the classic form of the transport equation in the most general form does not take into consideration the possible presence in the medium of a radiation receiver.

The purpose of this article was to supplement the information available in the theoretical hydro-optics concerning the ALF in aquatic media. It derives a linear integral transport equation of radiant energy which is general for localized sources of optical radiation in the example of a localized collimated light source (δ-source). It suggests a particular solution for the case of localized isotropic monochromatic light source suitable for engineering calculations as applied to aquatic media.

1. INTEGRAL TRANSPORT EQUATION OF RADIANT ENERGY (CASE OF LOCALIZED COLLIMATED LIGHT SOURCE)

We will introduce the Cartesian system of coordinates $\vec{XYZ}$ with center at point of location of the δ-source, and with orientation of the unit vector $\vec{z}$ in direction of the source radiation. We will write the classic transport equation of radiant energy for the case of homogeneous turbid medium (Figure 1):

$$(\dot{l}_0, \operatorname{grad} L(r, \dot{l}_0)) + c L(r, \dot{l}_0) = \frac{\lambda_c}{4\pi} \int_{(4\pi)} \varkappa(\gamma) L(r, \dot{l}_0') \, d\omega(\dot{l}_0'), \tag{1}$$

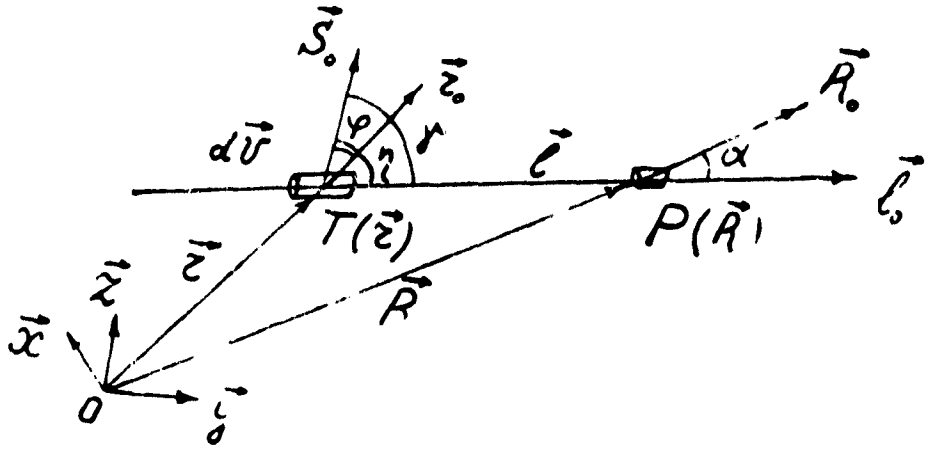

Figure 1. Plan of Numerical Experiment to Derive Integral Equation for Transport of Radiant Energy in Computation of Brightness of Primary Scattering

where $L(\vec{r}; \vec{l}_0)$ and $L(\vec{r}; \vec{l}_0')$--brightness of elementary volume of medium in environs /100 of point $\vec{r} = \vec{r}(x, y, z)$ in directions of single vectors $\vec{l}_0(\alpha; \beta)$ and $\vec{l}_0'(\phi; \theta)$, Λ and $\chi(\gamma)$--respectively the indicator of attenuation, albedo of single scattering and scattering indicatrix of medium which takes into consideration the molecular scattering and the scattering on the suspension (particles), and is normed by the condition $0{,}5\int_{-1}^{1}\chi(\gamma)\,d\cos\gamma = 1$, where γ--angle of scattering which is determined from the main correlation of spherical trigonometry $\cos\gamma = \cos\alpha\cos\varphi + \sin\alpha\sin\varphi\cos(\beta - \theta)$; $d\omega(\vec{l}_0')$ — element of solid angle with optical axis l_0'.

The boundary conditions placed on (1, are the following:

$$L(\vec{r}; \vec{l}_0)|_{r\to\infty} \to 0 \qquad (2)$$
$$L(\vec{r}; \vec{l}_0)|_{r\to 0} \to L_\sigma = \frac{1}{2\pi}\Phi_\sigma\,\delta(x)\,\delta(y)\,\delta[1 - (\vec{z}, \vec{l}_0)],$$

where Φ_σ and L_σ--light flux and brightness of δ-source. The condition for norming L_σ is the identity

$$\int_{4\pi}\int_{\Phi}(d\vec{\omega}, d\vec{A}) = 1$$

where $(d\omega, dA)$--scalar product of vectors of elements of the area and the solid angle of source radiation, equal to

$$(d\omega, dA) = 2\pi (z, l_0)\, d(z, l_0)\, dx\, dy$$

(z, l_0)--scalar product of single vectors z and l_0; $\delta(N)$--symbolic delta-function of Dirac of the corresponding argument N.

The adopted boundary conditions (2) correspond to the following physical problem: the localized collimated light source is located in the center of a sphere of infinite radius filled with a medium which anisotropically scatters and absorbs radiation. It is necessary to compute the light field of the source, i.e., to determine the spatial-angular distribution of brightness of the radiation of the δ-source scattered in the medium mass, and this is equivalent to solution of (1) on the condition of (2).

The integral is the most convenient for mathematical operation of the analytical form of (1) in the case of (2). It can be obtained as follows: we multiply each term in (1) by the quantity $\exp(\varepsilon l)$, and as a result of subsequent transforms we /101 obtain

$$\frac{d}{dl}[\exp(\varepsilon l)\, L(r; l_0)] = \frac{\Lambda \varepsilon}{4\pi} \int_{(4\pi)} \chi(\gamma)\, L(r; l_0')\exp(\varepsilon l)\, d\omega(l_0'). \tag{3}$$

By integrating (3) for the variable l in limits of the distance between points $T(\vec{r})$ and $P(\vec{R})$ (Figure 1), the last point fixes the position in the medium of the "radiation receiver," i.e., the calculated point of the light field (for simplification of the summary expressions we will assume at point $P(\vec{R})$ value l = 0, and as the positive direction of the vector $\vec{l}_0$--direction to the radiation receiver. Thus, integration is done from zero to l_{min}, which adopts the values

$$l_{min} = \begin{cases} -\infty, & \text{if } z \neq R_0 = l_0 \\ -R, & z = R_0 = l_0 \end{cases}$$

As a result of these computations, by making a replacement in this case of the variable of integration according to the formula $l = -l'$ (we will eliminate the hatching in the subsequent writings), we have

$$L(\dot{R};\dot{l}_0) = \begin{cases} \frac{\Lambda e}{4\pi}\int_0^{\infty}\exp(-e\,l)\int_{(4\pi)} x(\gamma)\,L(\dot{r};\dot{l}_0')\,d\omega(\dot{l}_0')\,dl, \\ \text{if } \dot{Z}\neq\dot{R}_0\neq\dot{l}_0 \\ L_*\exp(-e\,R) + \\ + \frac{4\pi}{\Lambda e}\int_0^{\infty}\exp(-e\,l)\int_{(4\pi)} x(\gamma)\,L(\dot{r};\dot{l}_0')\,d\omega(\dot{l}_0')\,dl. \\ \text{if } \dot{Z}=\dot{R}_0=\dot{l}_0 \end{cases} \tag{4}$$

Taking into consideration the nature of radiation of the δ-source, and specifically the equation of brightness of the δ-source, and by analyzing the system of equations (4) one can write a unified equation which will represent the linear integrated transport equation of radiant energy for the case of the δ-source as applied to homogeneous turbid media

$$L(\dot{R};\dot{l}_0) = L_*\exp(-e\,R) + \tag{5}$$
$$+ \frac{\Lambda e}{4\pi}\int_0^{\infty}\exp(-e\,l)\int_{(4\pi)} x(\gamma)\,L(\dot{r};\dot{l}_0')\,d\omega(\dot{l}_0')\,dl.$$

We will write equation (5) in an operational form /102

$$L = L_0' + \lambda K L', \tag{6}$$

where $L = L(\dot{R};\dot{l}_0)$; $L' = L_*\exp(-e\,R)$; λ --parameter of operational equation equal to $\lambda = (\Lambda e/4\pi)$; KL' --linear integrated operator

$$KL' = \int_0^{\infty}\exp(-e\,l)\int_{(4\pi)} x(\gamma)\,L(\dot{r};\dot{l}_0')\,d\omega(\dot{l}_0')\,dl. \tag{7}$$

In (7) we will replace the variable of integration l, using the law of sines for a triangle (Figure 1), according to formula

$$dl = R\frac{\sin\alpha}{\sin^2\eta}\,d\eta$$

and as a result we obtain

$$K L' = R \sin \alpha \int_{0}^{r} \exp\left[-\varepsilon R \frac{\sin(\eta - \alpha)}{\sin \eta} \right] \int_{(4\pi)} \chi(\gamma) L(r; l_0') \, d\omega(l_0') \frac{d\eta}{\sin^2 \eta} \tag{8}$$

It should be noted that equations of type (6) are subordinate to the principle of superposition. The physical realization of this principle in practice is the following: if we have a set of δ-sources distributed and oriented as we choose in the volume of the turbid medium, and for each of them we can write a similar expression $L_i = L_{0i} + \lambda K L_i$ and also if it is known that $L_{\Sigma} = \sum_{i=1}^{N} L_{0i}$, then evidently the general operational equation for computing the radiation brightness for a fixed direction at the calculated point of light field created by a set of sources will be $L_{\Sigma} = L'_{0\Sigma} + \lambda K L'_{\Sigma}$.

As is known, solution to the operational equation of type (6) is a Neumann series [3]. Consequently, solution to the integrated transport equation (5) in this case will look like

$$L = \sum_{n=0}^{\infty} \lambda^n K^n L_0 \tag{9}$$

where the operator $K^n L$ is described by the formula

$$K^n L_0 = R \sin \alpha \int_{0}^{r} \int_{(4\pi)} \frac{e^{-\varepsilon \eta(\gamma_0)} \chi(\gamma_1)}{\sin^2 \eta_1} \ldots$$

$$\ldots \int_{0}^{r} \int_{(4\pi)} \frac{e^{-\varepsilon \eta(\gamma_0)} \chi(\gamma_1)}{\sin^2 \eta_1} L_0 e^{-\varepsilon \eta(\gamma_0)} \, d\omega(l_0') \, d\eta_1 \ldots d\omega(l_0') \, d\eta \ldots$$

We note that this solution is applicable based on the principle of superposition /103 of elementary solutions, as applied to light fields created by sources with random light distribution, since any light source can be presented in the form of a set of δ-sources. Consequently, they have the most general nature, like (5).

As is apparent from (9), solution to the transport equation (5) is in the form of an infinite series by orders of the albedo of a single scattering of radiation in the medium A. In this case each term in the series, starting from the first, from a physical viewpoint is the radiation brightness of the corresponding multiplicity of scattering (the multiplicity of scattering corresponds to the ordinal number of the term in the series). These quantities are conventionally called brightness of the n-th (n = 1, 2,...) scattering [4]. The zero term in the series is the brightness of direct radiation of the source attenuated by the medium according to the Bouguer-Lambert law [5].

2. SOLUTION OF THE INTEGRATED TRANSPORT EQUATION OF RADIANT ENERGY AS APPLIED TO AQUATIC MEDIA (CASE OF POINT ISOTROPIC MONOCHROMATIC LIGHT SOURCE)

We will use the general solution (9) to the integrated transport equation (5). In order to obtain a solution which is suitable for engineering calculations, it is necessary to compute the sum of the Neumann series for a specific source of optical radiation, in particular for the case of a point isotropic monochromatic light source (PIMLS).

The brightness of PIMLS of a single light force is described by the formulas

$$L_0 = \frac{\delta[\omega(l_0)]}{R^2 \cdot} \cdot \frac{\delta(\alpha)}{2\pi R^2 \sin\alpha} \cdot \frac{\delta(\alpha)\, d\alpha}{R^2\, d\omega(l_0)}, \tag{10}$$

where $d\alpha$ and $d\omega(l_0)$--respectively the elements of linear and solid angles in the direction of radiation reception; R--distance between the source and the receiver of radiation.

The quantity L_0 can be obtained by integrating L for the complete solid angle (this determines the luminosity of the PIMLS), and after dividing the obtained result by 4π.

We will successively compute, starting from the first, the terms in the series (9). Their calculation is done by iteration method, which in the examined problem is reduced to the following: the brightness of direct radiation attenuated by the medium according to the Bouguer-Lambert law is substituted into the integrated oper- /104
ator (8), and then the inhomogeneous operational equation of the following type is solved

$$L_{n+1} - \lambda K L_n' = 0 \tag{11}$$

where $L_{n+1} = L_{n+1}(\dot{R}; \dot{l}_0)$; $L_n' = L_n(\dot{r}; \dot{l}_0')$, in relation to the quantity of brightness of the primary scattering $L_1(\vec{R}; \vec{l}_0)$. The solution obtained in this case (first iteration) is again substituted into (8), and the mathematical procedure described above is again repeated. Thus, the brightness of the secondary scattering was determined $L_2(\vec{R}; \vec{l}_0)$, and so forth. We note that $L_1(\vec{R}, \vec{l}_0)$ is computed precisely, while the brightnesses of the subsequent, starting with the secondary, scatterings are approximate with regard for the nature of radiation scattering in turbid media.

As a result, the unknown radiation brightness at the calculated point of the light field of the P.IMLS is in the form of a sum of the found iterations

$$L(\dot{R}; \dot{l}_0) = \sum_{n} L_n(\dot{R}; \dot{l}_0) \tag{12}$$

where $L_n(\vec{R}; \vec{l}_0)$ --brightness of the n ary scattering.

According to (11) and (8), $L_1(\vec{R}; \vec{l}_0)$ in the integrated form will look as follows

(13)

$$L_1(\dot{R}; \vec{l}_0) \quad \frac{\lambda \varepsilon R}{4\pi} \sin\alpha \int \exp\left| \quad \varepsilon R \frac{\sin(\eta - \alpha)}{\sin\eta} \right| \times$$

$$\times \int_{(4\pi)} \varkappa(\gamma) L_0(r; \dot{l}_0') \, d\omega(\dot{l}_0') \frac{d\eta}{\sin^2\eta}.$$

We will expand the value $L_0(\vec{r}; \vec{l}_0')$ which is included in the subintegral equation (13), by taking into consideration (10) and the Bouguer-Lambert law. In this

case, the current variable r is replaced through parameter R and the variable of integration η, by using the law of sines for a triangle (Figure 1). Thus

$$L_0(\vec{r}; \vec{l}_0') \quad \frac{1}{R^2} \quad \frac{\sin^2 \eta}{\sin^2 \alpha} \quad \frac{\delta(\eta)\, d\eta}{d\omega(\vec{l}_0')} \exp\left(- \varepsilon R \frac{\sin \alpha}{\sin \eta} \right) \tag{14}$$

We will substitute (14) into (13). As a result of subsequent integration, we /105 obtain the calculated equation of brightness of the primary scattering

$$I_1(\vec{R}, \vec{l}_0) = \frac{\lambda \varepsilon \exp(-\varepsilon R)}{4\pi R \sin \alpha} \times \tag{15}$$

$$\times \int_0^{\eta_0} \exp\left[-\varepsilon R \sin \alpha \left(\operatorname{tg} \frac{\eta_0}{2} - \operatorname{tg} \frac{\eta}{2} \right) \right] x(\eta)\, d\eta.$$

Solution (11) in relation to $L_2(\vec{R}, \vec{l}_0)$, by using (15) is made approximately, taking into consideration the feature of scattering of radiation in the mass of turbid media which is characteristic for the majority of turbid (in particular aquatic) media. Practically the entire scattered light flux (over 90%) is concentrated in the region of small angles (from 0 to 20°) in relation to the initial direction of spread of the radiation (this physical fact graphically illustrates the pencil-beam appearance of the scattering indicatrix). Thus, in solving (1) we assume the rightfulness of the following equality (Figure 2).

$$\int_{(\vec{s})} \frac{\lambda(\zeta)}{\sin \varphi} \int_{\eta}^{\eta_0} \exp\left[-\varepsilon (l_1(\eta_1) + r_1(\eta_1)) \right] x(\eta_1)\, d\eta_1\, d\omega(\vec{l}_0') \approx \tag{16}$$

$$\approx x(\eta) \exp(-\varepsilon r(\eta)) \int_{(\vec{l}_0)} \frac{\cos \varphi}{\sin \varphi} \int_{\eta}^{\eta_0} x(\eta_1)\, d\eta_1\, d\omega(\vec{l}_0')$$

Thus, as a result of the approximate computations, we obtain the calculated /106 brightness equation of secondary scattering

$$I_2(\vec{R}, \vec{l}_0) = \frac{\lambda \varepsilon \exp(-\varepsilon R)}{4\pi R \sin \alpha} \int_0^{\eta_0} \left(\sigma R \frac{\sin \alpha}{\sin \eta} \right) \exp\left[-\varepsilon R \sin \alpha \times \right. \tag{17}$$

$$\left. \times \left(\operatorname{tg} \frac{\eta_0}{2} - \operatorname{tg} \frac{\eta}{2} \right) \right] x(\eta)\, d\eta.$$

where σ --scattering index of radiation in the medium.

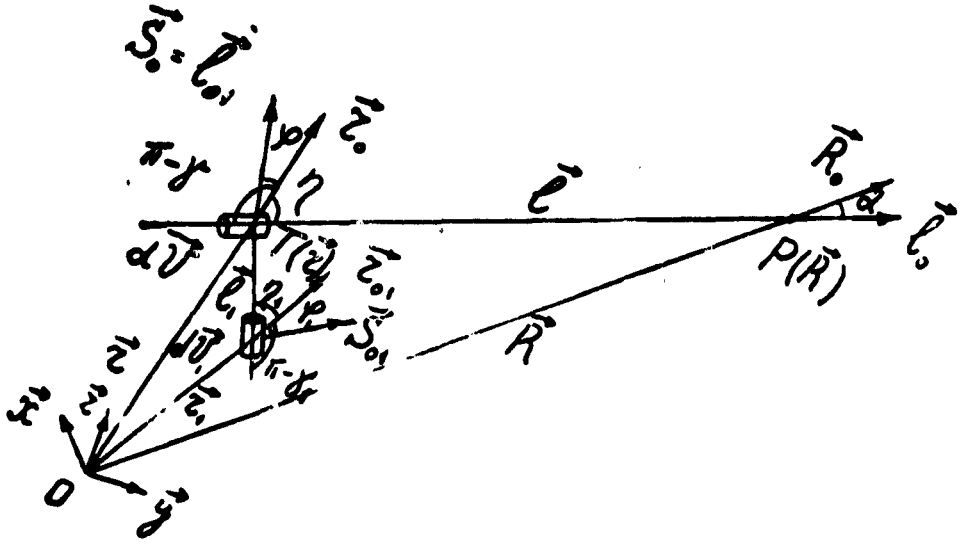

Figure 2. Plan of Numerical Experiment to Compute Brightness of Secondary Scattering

After revealing the law governing the result obtained in solution of (11) with regard for (16): the calculated expressions of brightnesses of the n-ary scattering, starting with the secondary and higher, differ from the analogous for brightness of the primary scattering only by the coefficients (conventionally called weight coefficients of the n-ary scattering [6]), included in the subintegral expression of the summary notations, we will write the calculated brightness equation of the n-ary scattering (n-th iteration):

$$I_n(\vec{R};\vec{l}_0) = \frac{\Lambda e^{\exp(-\varepsilon R)}}{4\pi R \sin\alpha} \int_0^{\infty} O_n(\vec{r}) \times \tag{18}$$

$$\times \exp\left\{ -\varepsilon R \sin\alpha \left(\operatorname{tg}\frac{\gamma_1}{2} - \operatorname{tg}\frac{\alpha}{2} \right) \right\} x(\eta)\, d\eta,$$

where $O_n(\vec{r}) \frac{\left(-\varepsilon \frac{\sin\alpha}{\sin\eta}\right)^{n-1}}{(n-1)!}$ -- weight coefficient of the n-ary scattering which shows from a physical viewpoint which weight the brightness of the corresponding multiplicity of scattering has as compared to the brightness of the primary scattering with summary action of multiple scattering governing the formation of brightness in veiling haze [6].

As previously indicated, the unknown radiation brightness at the calculated point of the light field of the PIMLS is computed according to the formula (12). As a result of summing the brightnesses of the n-ary without consideration for the brightness of direct radiation of the source, we obtain the calculated brightness equation of the veiling haze which develops because of multiple scattering in the mass of the radiation medium of PIMLS:

$$\beta(\dot{R}; \dot{l}_0) = \frac{\Lambda_0 \exp(-\varepsilon R)}{4\pi R \sin\alpha} \int_0^{\eta} H(\dot{r}) \exp\left[-\varepsilon R \sin\alpha \times \left(\operatorname{tg}\frac{\eta}{2} - \operatorname{tg}\frac{\alpha}{2}\right)\right] \varkappa(\eta)\, d\eta. \tag{19}$$

where $H(\dot{r}) = \exp\left(\varepsilon R \frac{\sin\alpha}{\sin\eta}\right)$ --weight function of multiple scattering which from a physical viewpoint determines the weight contribution of the total effect of multiple scattering of the source radiation as compared to single scattering in the formation of the veiling haze [6]. /107

Finally, the solution to the integral transport equation (5) for the case of PIMLS as applied to homogeneous turbid (including aquatic) media which is suitable for engineering calculation of spatial-angular distribution of radiation brightness in a medium, looks like

$$L(\dot{R}; \dot{l}_0) = L_{0e}(\dots) \frac{\Lambda_0 e^{-\varepsilon R}}{4\pi R \sin\alpha} \int_0^{\eta} \exp\left[\varepsilon R \frac{\sin\alpha}{\sin\eta} - \varepsilon R \sin\alpha \left(\operatorname{tg}\frac{\eta}{2} \operatorname{tg}\frac{\alpha}{2} - 1\right)\right] \varkappa(\eta)\, d\eta. \tag{20}$$

In making the hydrological-light-technical calculations of brightness of the veiling haze which is governed by multiple scattering in the aquatic medium of PIMLS radiation, it is suggested that the following formula be used

$$\beta(\dot{R}; \dot{l}_0) = \frac{\sigma k^2 (k a^{0.5} + 1)}{12\pi R \sin\alpha} \exp(-k a^{0.5} - \varkappa R), \tag{21}$$

where $\varkappa$--radiation absorption index in a medium which was obtained as a result of integrating (19) using an empirical equation for the form of the scattering indicatrix of the corresponding measurement plan in [7]

$$x(\gamma) = \frac{k^4}{\gamma} \exp(-k\gamma^{0.5}) \tag{22}$$

where k--steepness of the scattering indicatrix $(k = 5 - 15 \ln^{-0.5}_{\text{rad}})$.

We note in conclusion that the calculation results of the spatial-angular distribution of radiation brightness in the BIMILS light field according to the formulas (19) and (21) agree well with the data of full-scale measurements in the Black Sea presented in [8], at the interval of scattering angles from 0.5 to 20° with distances from the source to 115 m. It is common knowledge that the shape of the brightness body of scattered radiation in this range of angles is governed by the mechanism of radiation scattering on large suspended matter, to which the pencil-beam part of the real $x(\gamma)$ (Mie effect) correspond. In order to describe the shape of the brightness body in the region of medium and large scattering angles governed by the mechanisms of molecular scattering of radiation and on small suspended matter, the following formula is suggested /109

$$L(\vec{R}; \vec{l}_0) = \frac{\Lambda \varepsilon x(180°) \exp(-\varkappa R)}{4\pi R \sin\alpha} \int_0^{\infty} \exp\left[-\varkappa R \sin\alpha \times \left(tg\frac{\gamma}{2} - tg\frac{\gamma}{2}\right)\right] d\eta \tag{23}$$

obtained based on the results of this publication and [9], as well as on the assumption that the scattering indicatrix of these regions is spherical, and equal in size to the value of the real $x(\gamma)$ at 180° angle. In the examined example, formula (23) is real in the interval of scattering angles from 50 to 170°. In the intermediate interval of angles, i.e. from 20 to 50°, the shape of the brightness body of scattered radiation is computed jointly from formulas (21) and (23).

TABLE 1. BRIGHTNESS BODY AT RANDOM POINT OF LIGHT FIELD OF POINT ISOTROPIC MONOCHROMATIC LIGHT SOURCE (PIMLS)

$L \frac{L(R^*)}{\Phi}$, $\varepsilon = 0{,}4605$ (ln м$^{-1}$), $\Lambda = 0{,}8$; $F = 12$ (ln rad$^{-0.5}$), $x(\pi) = 0{,}015$; $\varkappa = 0{,}082$ (ln м$^{-1}$)

R м	10		15		20		40		60		78		92		115		Rм
γ deg	Э	Р	Э	Р	Э	Р	Э	Р	Э	Р	Э	Р	Э	Р	Э	Р	α deg
1	1,82	1,54	2,84	2,10	3,37	2,51	4,92	3,84	5,84	4,89	6,62	5,75	7,76	6,84	8,36	7,50	1
2	1,90	1,88	2,90	2,42	3,40	2,85	4,94	4,18	5,96	5,24	6,73	6,11	7,88	7,12	8,46	7,89	2
5	2,60	2,40	3,35	3,10	3,64	3,53	5,18	4,86	6,15	5,95	7,00	6,84	8,11	7,96	8,68	8,64	3
10	3,30	3,29	3,88	3,81	5,30	4,22	5,66	5,54	6,55	6,57	7,30	7,46	8,45	8,58	9,00	9,24	10
20	4,10	4,26	4,70	4,72	5,08	5,11	6,25	6,30	7,08	7,46	7,90	8,31	8,97	9,45	9,56	10,09	20
30	4,58	4,77	5,10	5,32	5,48	5,70	6,70	6,95	7,50	8,00	8,35	8,88	9,45	9,98	9,96	10,59	30
40	4,90	5,29	5,49	5,73	5,85	6,10	7,05	7,33	7,88	8,38	8,70	9,24	9,80	10,33	10,35	10,92	40
50	5,29	5,55	5,88	5,99	6,20	6,37	7,45	7,60	8,25	8,63	9,12	9,49	10,11	10,58	10,65	11,14	50
60	5,65	5,73	6,20	6,18	6,52	6,55	7,77	7,77	8,57	8,80	9,18	9,66	10,43	10,73	10,98	11,30	60
70	5,90	5,89	6,50	6,33	6,80	6,71	8,01	7,94	8,87	8,97	9,75	9,82	10,67	10,89	11,25	11,45	70
80	6,10	5,97	6,72	6,42	7,02	6,80	8,25	8,03	9,16	9,06	10,00	9,92	10,90	10,99	11,49	11,55	80
90	6,30	6,05	6,90	6,50	7,16	6,88	8,43	8,11	9,36	9,14	10,20	10,00	11,08	11,07	11,68	11,63	90
100	6,41	6,11	6,99	6,56	7,25	6,95	8,55	8,18	9,52	9,21	10,36	10,07	11,22	11,14	11,83	11,70	100
110	6,48	6,16	7,03	6,69	7,30	7,00	8,65	8,24	9,63	9,27	10,44	10,12	11,34	11,20	11,93	11,76	110
120	6,50	6,20	7,04	6,66	7,32	7,05	8,69	8,28	9,70	9,32	10,50	10,17	11,40	11,25	12,00	11,81	120
130	6,50	6,24	7,04	6,70	7,33	7,09	8,72	8,32	9,74	9,35	10,53	10,21	11,44	11,29	12,06	11,84	130
140	6,50	6,27	7,04	6,73	7,33	7,12	8,73	8,35	9,77	9,39	10,55	10,24	11,46	11,32	12,08	11,88	140
150	6,50	6,29	7,04	6,75	7,33	7,14	8,74	8,38	9,79	9,41	10,56	10,26	11,47	11,34	12,08	11,90	150
160	6,50	6,31	7,04	6,77	7,13	7,15	8,74	8,39	9,80	9,43	10,56	10,28	11,47	11,36	12,08	11,92	160
170	—	6,32	—	6,78	—	7,16	—	8,40		9,44	—	10,29	—	11,37	—	11,93	170

The results of computations described above are presented in the table (Table 1) and compared with similar measured quantities [9]. As is apparent from Table 1, discrepancy in the numerical values of $L(\vec{R}; \vec{l}_0)$ corresponds to 6% variation in the quantity of albedo of single scattering Λ. This does not exceed the errors of its measurement.

BIBLIOGRAPHY

1. Pelevin, V. N.; Prokudina, T. M. "Light Field in the Sea Created by Point Isotropic Radiation Source," in Gidrofizicheskiye i gidrooptricheskiye issledovaniya v Atlanticheskom i Tikhom okeanakh ["Hydrophysical and Hydro-Optical Studies in the Atlantic and Pacific Ocean"], Moscow, Nauka, 1974, pp 191-198.

2. Adzerikho, K. S. Lektsii po teorii perenosa luchistoy energii ["Lectures on the Transport Theory of Radiant Energy"], Minsk, Belorussian State University, 1975, 192 p.

3. Korn, G.; and Korn, T. Spravochnik po matematike (dlya nauchnykh rabotnikov i inzhenerov) ["Handbook on Mathematics (for Scientific Workers and Engineers)"], translated from English, ed. by I. G. Aramanovich, Moscow, Nauka, 1978, p 832.

4. Savenkov, V. I. "Haze of Direct Scattering," Svetotekhnika, No 6, 1978, pp 17-18.

5. Gutorov, M. M. Osnovy svetotekhniki i istochniki sveta ["Fundamentals of Light Engineering and Light Sources"], Moscow, Energiya, 1968, 392 p.

6. Savenkov, V. I.; and Gutorov, M. M. "Weight Function of Multiple Scattering," Tr. Mosk. energ. in-t, No 401, 1979, pp 9-17.

7. Savenkov, V. I. "Empirical Equation for the Shape of the Scattering Indicatrix of Waters in the World Ocean," Svetotekhnika, No 1, 1978, pp 20-21.

8. Prokudina, T. M.; Pelevin, V. N. "Determination of the Size of the Parameter of Light Quantum Survival and Characteristics of Light Fields in the Sea," Optika okeana i atmosfery ["Optics of the Ocean and Atmosphere"], Leningrad, Nauka, 1972, pp 157-168.

9. Savenkov, V. I.; Gutorov, M. M.; and Mel'nikov, G. A. "Light Vector from Point Isotropic Monochromatic Light Source in a Turbid Medium," in Svetovyye polya v okeane ["Light Fields in the Ocean"], Moscow.

LIGHT VECTOR FROM POINT ISOTROPIC MONOCHROMATIC LIGHT SOURCE IN A TURBID MEDIUM

M. M. GUTOROV and G. A. MEL'NIKOV

/110

A calculated equation of normal irradiance from a PIMLS is derived by solving the integral transport equation for a point isotropic monochromatic light source (PIMLS) as applied to turbid media when there is true absorption and very anisotropic scattering of radiation. A comparison is made of calculated quantities with data of full-scale measurements made by researchers in different parts of the World Ocean.

Publications of Soviet and foreign authors which cover experimental and theoretical studies of the formation of artificial light fields (ALF) in turbid (in particular, aquatic) media have appeared more often in recent years. The ALF of spot isotropic monochromatic light source (PIMLS) is currently the most well-studied experimentally. Many researchers have made full-scale measurements of integral characteristics (normal and spatial illuminations and light vector) of the ALF PIMLS in different parts of the World Ocean [1,2].

This work has attempted to obtain an equation of the light vector from the PIMLS located in a turbid medium which is suitable for engineering calculations.

We will use the solution obtained in [3] for the integral equation of radiant energy transport for PIMLS as applied to turbid media, media with true absorption and strongly anisotropic radiation scattering

$$L(\vec{R}; \vec{I}_0) = \frac{I(\alpha)\exp(-\varepsilon R)}{\varepsilon R^2 \sin\alpha} + \frac{I(\alpha)\exp(-\varepsilon R)}{\varepsilon R \sin\alpha} \int_{\tau}^{\infty} \varepsilon J(r)\exp \times$$

$$\times\left[-\varepsilon R \sin\alpha\left(tg\frac{\eta}{2} - tg\frac{\pi}{2}\right)\right] x(\eta)\, d\eta \qquad (1)$$

where $L(\vec{R}; \vec{I}_0)$--radiation brightness at the calculated point of the ALF $\vec{R}(x,y,z)$ in fixed direction of single vector $\vec{I}_0(\alpha;\beta)$;

I--light force of PIMLS;

ε, σ and $x(\eta)$--indices of attenuation and scattering and scattering index of radiation respectively;

$\delta(\alpha)$--symbolic delta-function of α angle characterizing the direction of reception of radiation at the calculated point ALF $\vec{R}$ in relation to direction of direct radiation of PIMLS;

$\Pi(\vec{r})$--weight function of multiple scattering, equal to [4] $\Pi(r) = \exp(\sigma r)$ /111

We note that the first term in the right part of (1) takes into consideration attenuation of brightness of direct radiation of the PIMLS because of processes of absorption and scattering of the latter in the medium mass (Bouguer-Lambert law). The second describes the brightness of the veiling haze which is governed by the total action of multiple scattering of radiation PIMLS in the medium.

It is common knowledge that the main function of the point in the light field is the light vector which determines the direction of transport of radiant energy and has the property that its projection in any direction is numerically equal to the difference of normal illumination of the two sides of an elementary area dA in the environs of the calculated point of the field which is placed perpendicularly to this direction. The calculated formula of the light vector in a general case is [5]

$$\vec{e}(\vec{R}) = \vec{R}_0 \int_{(\Omega)} L(\vec{R}_0; \vec{l}_0)\,(\vec{R}_0; \vec{l}_0)\,d\omega(\vec{l}_0), \tag{2}$$

where $(\vec{R}_0; \vec{l}_0)$--scalar product of single vectors, in this case equal to (Figure 1) $(\vec{R}_0; \vec{l}_0) = \cos\varphi$

We substitute in (2) the value $L(\vec{R}; \vec{l}_0)$ from (1), and by making the corresponding integration, we obtain the calculated equation $\vec{e}(\vec{R})$ as applied to turbid media. As a result of computations with the first term in (1), we determine the calculated formula for the component $\vec{e}_{pr}(\vec{R})$, governed by direct radiation of the PIMLS

$$\vec{e}_{pr}(\vec{R}) = \frac{I}{R^2}\exp(-\varepsilon R)\,\vec{R}_0. \tag{3}$$

By integrating the second term in (1) we have the following

$$\dot{e}_p(\dot{R}) = \frac{I_0}{2R} \dot{R}_0 \int_0^{\infty} \int_0^{\infty} r(\eta) \Pi(r) \exp[-\varepsilon(l(\eta) + r(\eta))] d\eta \cos\alpha d\alpha. \quad (4)$$

In order to simplify the subsequent computations, we will use the assumption: taking into consideration the strongly anisotropic scattering of radiation which is characteristic for the majority of turbid media (pencil-beam scattering indicatrix corresponds to this phenomenon), we assume that the main contribution to illumination dA is made by the radiation scattered at small angles (from 0 to 20°) in relation to the direction of the perpendicular to dA in the environs of the calculated point of the ALF FIMLS $P(\dot{R})$. It coincides with the direction of direct radiation of the source (Figure 1). Consequently, in the calculations one can assume the equality $l + r \approx R$, and thus, one can factor out beyond the integral sign in (4) the exponent which describes the Bouguer-Lambert law. /112

We will present the weight function $\Pi(\dot{r})$ in (4) in the form of a sum obtained when it is expanded into a Maclaurin series. In this case, the variable r which depends on the integration variable η, is expressed through the parameter R, by using the law of sines for a triangle Figure 1). /113

$$\Pi(\dot{r}) = \sum_{n=0}^{\infty} \frac{1}{n!} \left[R \frac{\sin\alpha}{\sin\eta} \right]^n \quad (5)$$

We substitute (5) into (4) and taking into consideration the assumption which has been made, we obtain

$$\dot{e}_p(\dot{R}) = \frac{I}{R^2} \exp(-\varepsilon R) \sum_{n=0}^{\infty} \frac{(\sigma R)^{n+1}}{(n+1)!} \dot{R}_0.$$

By using the inverse presentation of the obtained sum in the form of an exponent with positive degree, we determine the calculated formula of the component $\dot{e}_p(\dot{R})$ which is governed by luminescence of the mass of the turbid medium which develops

because of multiple scattering of the PIMLS radiation in it

$$\dot{E}_1(\dot{R}) = \frac{1}{R^2} \exp(-\varepsilon R)\,[\exp(\sigma R) - 1]\,\dot{R}_0. \qquad (6)$$

Finally, the calculated equation of the light vector from PIMLS in the mass of the turbid medium adopts the appearance

$$\dot{E}(\dot{R}) = \frac{1}{R^2} \exp(-\varkappa R)\,\dot{R}_0, \qquad (7)$$

where $\varkappa$--indicator of absorption of radiation in the medium.

As is apparent from formula (7), it does not take into consideration the influence on $\dot{E}(\dot{R})$ of the change in the shape of the brightness body of scattered radiation PIMLS with a rise in the distance from the source, i.e., formula (7) does not take into consideration the average cosine of the brightness body $\dot{\mu}(\dot{R})$. The degree of functional dependence of $\dot{E}(\dot{R})$ on $\dot{\mu}(\dot{R})$ can be established, for example, in computing the component $\dot{E}_D(\dot{R})$ according to formula (4) without any assumptions using a computer.

Comparison of the values calculated according to (7) of the light vector from the PIMLS with the results of natural measurements of it in different water areas of the World Ocean presented in [2] made it possible to reveal a good correspondence of the comparable quantities. Discrepancy in the calculated and experimental numerical values $\vec{e}(\vec{R})$ corresponds to less than 10% of the variations in $\varkappa$ for optical distances according to absorption in different waters $\tau = (\varkappa R) \leq 2.0 - 3.4$ (relative value of the rate of change $\varkappa$ equals the quantity $[1 - \bar{\mu}(R)]$, where $\bar{\mu}(R)$ is taken from [2]). /114

Since the calculated equation of the light vector from PIMLS in a turbid medium has the appearance as in the case of absolutely absorbing medium, then evidently, one can assume that it is also suitable for calculations of the normal $E_N(\vec{R})$ and spatial $E_O(\vec{R})$ illumination. This can be analytically confirmed for $E_O(\vec{R})$ by using the correlation $\operatorname{div}\vec{E}(R) = -\varkappa E_O(\vec{R})$ which is known in the literature [5], and for $E_N(\vec{R})$,

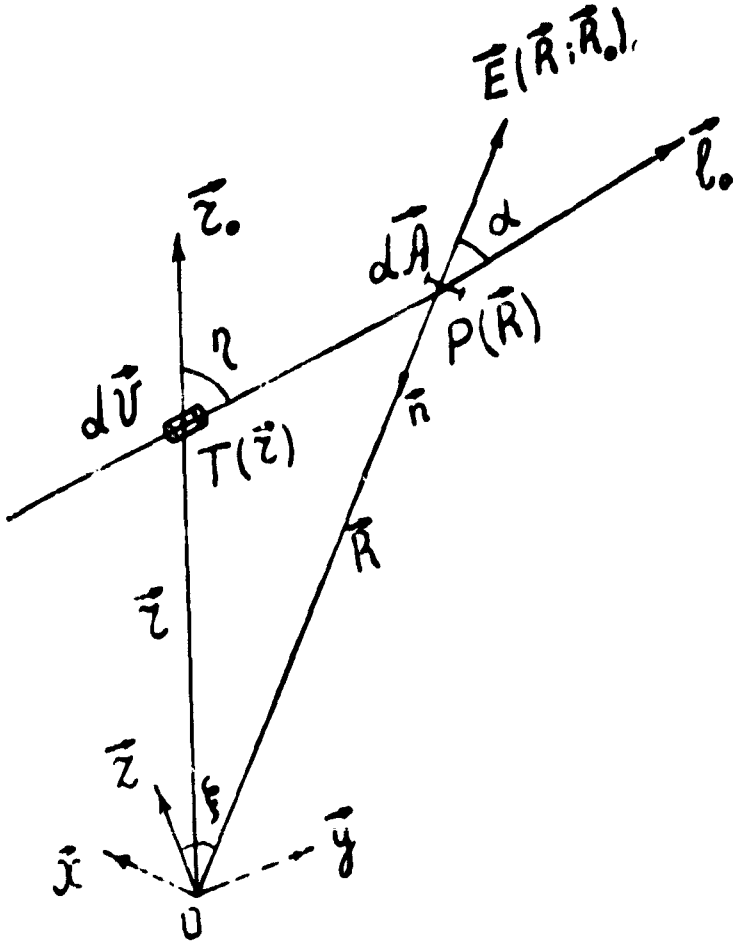

Figure 1. Geometry of Experiment

by using the correlation $E_N(R) = \frac{E(R)}{(1 - R_d)}$ and the experimental data for the coefficient of diffuse reflection presented for the case of aquatic media in [2] ($R_d \leq 0.01$ for $\tau_0 \geq 2.0 - 3.4$).

We note that the values $E_N(R)$ calculated according to formula (7) agree well with the data of measurements made by S. Duntley [1] (the discrepancy of the comparable quantities corresponds to 3% of the variation of $\varkappa$ for $\tau_0 \leq 10$). This fact was established previously in [6], but in this case the author obtained an identical calculated formula $E_N(R)$ empirically, by analyzing the experimental results of [1]. This result can be explained by studying the nature of scattering of radiation which is inherent to these waters: the scattering indicatrix of water in lake Pend Oreille

has a pencil-beam appearance (curvature of the indicatrix K = 12 ln rad$^{-0.5}$) (7). Consequently, essentially the entire scattered light flux (over 90%) is concentrated in the region of small scattering angles (from 0 to 10°), and therefore with small optical distances from the source, the losses of its light flux during the creation of illumination can be considered governed only by radiation absorption in the medium mass in the first approximation.

In conclusion we note the following: the larger the numerical value for steepness of the radiation scattering indicatrix in the studied media (in particular aquatic media), the higher the accuracy of the results of analytical calculations of integrated characteristics of the light field PIMLS according to formula (7) (average cosine of the brightness body $\pi(R)$ with a rise in k adopts values close to one).

BIBLIOGRAPHY

1. Duntley, S. Q."Light in the Sea," JOSA, vol 53, No 2, 1963, pp 214--233.

2. Pelevin, V. N., and Prokudina, T. M. "Light Field in the Sea Created by Spot Isotropic Radiation Source," in Gidrofizicheskiye i gidrooptricheskiye issledovaniya v Atlanticheskom i Tikhom okeanakn ["Hydrophysical and Hydrooptical Studies in the Atlantic and Pacific Oceans"], Moscow, Nauka, 1974, pp 191-198

3. Savenkov, V. I., Mel'nikov, G. A. "Solution of the Integral Equation of Transport as Applied to Light Fields in Aquatic Media Created by Artificial Sources," in this collection. /115

4. Savenkov, V. I.; and Guturov, N. M. "Weight Function of Multiple Scattering," Tr. Mosk. energ. in-t, No 401, 1979, pp 9--17.

5. Guturov, N. M. Osnovy svetotekhniki i istochniki sveta ["Fundamentals of Light Technology and Light Sources"], Moscow, Energiya, 1968, 392 p.

6. Libin, I. Sh. "Calculation of Illumination from Spot Source of Light in Water," Svetotekhnika, No 6, 1977, p 14.

7. Savenkov, V. I. "Empirical F tion for Shape of Scattering Indicatrix of Waters of World Ocean," Svetotekh No 1, 1978, pp 20-21.

CALCULATION OF THE TEMPORAL STRUCTURE OF SIGNAL REACHING A SMALL ANGULAR APERTURE DETECTOR LOCATED IN AN ARBITRARY POINT OF THE ENVIRONMENT. A. N. GURFINK

Results are presented from computing Green's functions in the δ-pulse system according to the time and dimensions of a cross section, a point receiver of small angular aperture placed at an arbitrary point of an aquatic medium.

One of the most urgent problems in the theory of transport of narrow light beams is the study of the temporal structure of a signal reaching a small angular aperture detector at an arbitrary point and oriented in a definite manner in space. Tasks of this type arise in developing systems of location, underwater television. etc.

Many authors have tried to solve this problem. L. M. Romanova [1,2] solved it analytically in a small-angular approximation, and then introduced corrections computed numerically. L. M. Romanova also developed a method for computing different characteristics of the light field from a narrow beam, based on computation of the planar moments. L. S. Delin in a small angular approximation studied the deformation of a direct-angular mono-directed light impulse [3]. I. L. Katsev, computing the light field in the deep layers of a turbid medium, used the nonstationary diffusion equation with initial and boundary conditions [4]. Its solution is a sum of an infinite series according to the Hanckel functions. G. A. Mikhaylov developed and introduced calculations of light fields by the Monte Carlo method [5]. Many problems to explain the dependence of light field intensity or density of light energy on different parameters under conditions of real problems were solved by S. D. Gutshabash [6], A. M. Gurfink [7], A. G. Luchinin [8] and others.

This work has computed the temporal structure of a signal reaching a spot small angular aperture detector located at a certain point and oriented in a definite manner in space.

Statement of the task. Assume that a δ-impulse falls under the boundary of /116
a uniform turbid medium by dimensions and time perpendicularly to the surface (Figure 1). The spot small angular aperture detector with semi-angle of taper arccosp is located at a point with polar coordinates R_c and θ (the azimuth is assumed to be equal to zero). Orientation of the detector in space is assigned by the zenith angle Ω and the azimuth angle Φ_{de}.

The optical properties of the medium are assigned by the scattering index σ [1n/m], the probability of photon survival in a single act of scattering Λ, and by the scattering indicatrix $x(\gamma)$ (Figure 16).

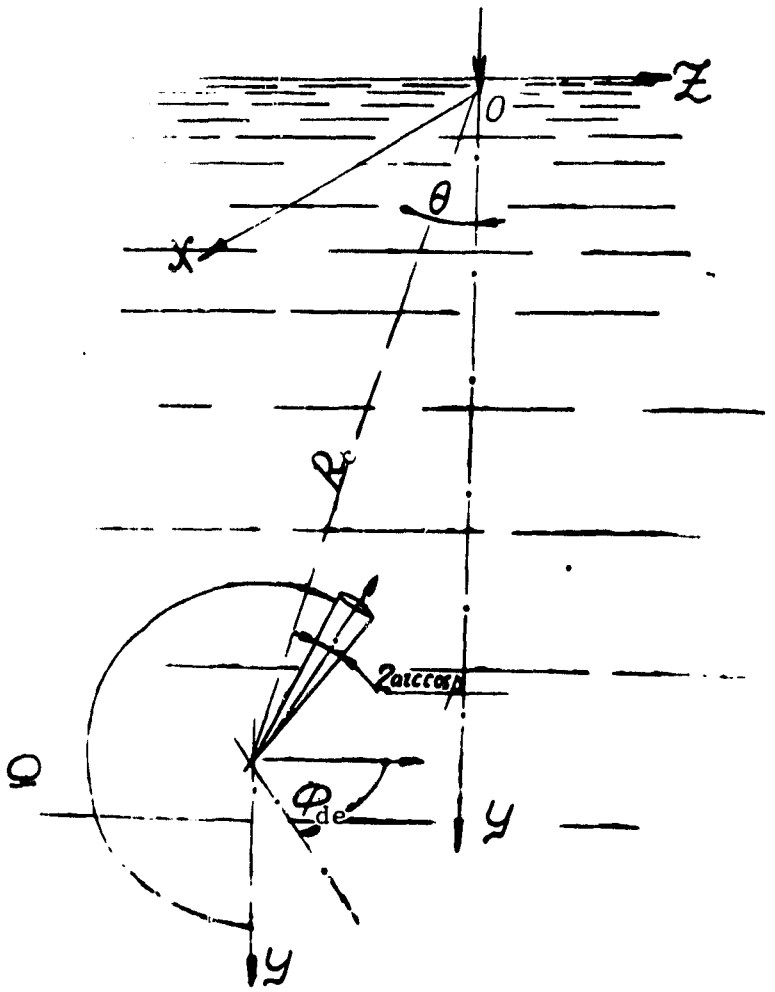

Figure 1. Plan of Task

The beginning of the coordinate system is located at the point of beam entrance into the medium. The OY axis is directed deep into the medium. /117

It is necessary to study the influence of position and orientation of the detector in space, as well as the optical properties of the medium on the temporal shape of the signal reaching the detector.

The calculations assumed that the following were constant: $\Phi_{de} = 0$, $p = 0.999$ (2.5), $v = c/n = 0.222$ m/ns, $A = 1$. Thus, this work computed the Green's functions in the system of an infinitely narrow source, a small angular aperture detector which is located at an arbitrary point in the aquatic medium and is oriented in a definite manner in space.

In order to solve the set task, a universal program was developed suitable for any computer which has a α-translator. The calculation algorithm (9, 12) was based on the method of "double local assessment" in combination with exponential transformation, in calculating the "multiple" component of the signal reaching the detector, i.e., the contributions of photons which experience two and more acts of scattering. (Calculation of a single scattering was made separately. In this case, the method of "local assessment" was also used in combination with exponential transformation).

The "grid" of points of the temporal histogram for the process of impulse diffusion is not uniform: in the beginning of the process, the temporal intervals were shorter than at the end. In all calculations, the process was traced until the onset of a "near" asymptotic regime. The entire temporal interval was divided into ten parts. The use of a BESM-6 computer made it possible to immediately calculate Ω in several directions. However, because the relative dispersion of the results depends on a number of examined trajectories, optical depth and orientation of the detector, the number of directions changed from 10 ($\tau = 5$, number of trajectories

N = 15,000 and calculation time of one variant t≈18 minutes) to 2(τ = 25, N = 25,000 and t ≈ 46 - 48 minutes). The calculations were made on a computer of the Computer Center of the Siberian Department of the USSR Academy of Sciences. It has a multiplicative sensor of pseudorandom numbers uniformly distributed in the interval (0.1). Construction of the histogram used the results with relative dispersion $\sqrt{D^2} \leq 0.3$, while the others were eliminated. It should be noted that the data with dispersion > 0.3 were less than 5%. Curves were constructed in a semilogarithmic system of coordinates in the form of the relationship lgI = f(t). On the y-axis, the numbers mark the boundary of temporal intervals of the histogram. The field of accuracy of calculation is shown by vertical segments.

The dependences of intensity of the received signal on time were computed with the following values of arguments:

$\sigma = 0{,}05;\ 0{,}123;\ 0{,}184\ [ln/\mu]$, $R_п = 100$ м;
$\Omega = 140,\ 150,\ 160,\ 170,\ 180,\ 190,\ 200,\ 210,\ 220,\ 230°$;
$\Theta = 0,\ 10,\ 20,\ 30,\ 40,\ 50°$,

with the same scattering indicatrix measured at station 347 during the trip of the /118
scientific research vessel "Im. Mendeleyev" of the Institute of Oceanography of the USSR Academy of Sciences (presented below in Figure 16). A large grid of results was obtained which makes it possible to compute Green's function (i.e., the response of the system to the effect of the δ-impulse at the inlet) of the examined system depending on the position, orientation and scattering indicator (excluding the indicatrix at this stage). This "grid" makes it possible to use interpolation to obtain Green's function or impulse transitional functions (ITF) for intermediate values of the arguments.

In order to clarify the dependence of the impulse transitional functions (ITF) on the shape of the scattering indicatrix, the following versions were computed

and $\sigma = 0.123$ 1/м, $R_c = 50$ м, $\Theta = 50°$, $\Omega = 230, 240, 250, 260$ 280°;

and $\sigma = 0.181$ 1/м, $R_c = 50$ м, $\Theta = 0°$, $\Omega = 180, 190, 200, 210$ 230°.

The main parameters of the scattering indicatrix which were used in the calculations are given below (the indicatrixes were obtained in full-scale measurements by V. M. Pavlov and O. V. Kopelevich). At angles $\Theta = 0$ and 180°, the indicatrixes were supplemented according to condition $x(0) = 2x\ (20')$, while $x(180°)$ was extrapolated. Here δ --extension of indicatrix, while Δ --decimal logarithm for ratio of brightness "forwards" to brightness "backwards."

TABLE.

Number in order	Region	Depth, m	$\bar{\gamma}$	γ^2	$\overline{\cos\gamma}$	$\overline{\cos^2\gamma}$	δ	Δ
1	Black Sea, station 100	100	0062	00361	09862	09833	321,7	6,5
2	Pacific Ocean, station 387	50	0189	0177	0.337	092	46,72	5,1
3	Sargasso Sea, station 347	300	0127	0600	079	08238	10,54	4,25
4	Pacific Ocean	100	03447	07174	0841	0852	11,58	4,68

We had in our possession results from measuring the characteristics of nonstationary light fields from a narrow-directed impulse source [10] which were made simultaneously with measurements of indicatrix numbers 3, 4 (Figure 16). This made it possible to compare the results of full-scale studies and calculations made independently of each other. The comparison was made for five characteristics of the shape of the ITF curves: widths at levels 0.5, 0.1, 0.01, position of the maximum of the curve and "asymmetry" of the curves. By asymmetry we mean the ratio of the time interval from the anterior front at the level 0.5 to the maximum to the time interval, from the maximum to the point at the dip in the curve, also at level 0.5. /119

The comparison results (after the absorption was taken into consideration and ITF's

"were convoluted" with the original signal emitted by a laser [10]) are presented in Table 1. They show that the calculated and experimental data coincide satisfactorily: the discrepancy mainly does not exceed 25%. Subsequent analysis was made based only on calculated data.

The results of calculations of all versions are presented in Tables 2 -- 26. Some of them are presented in Figures 2 - 13. The tables present the absolute brightness values of the upper lines corresponding to definite angles Ω, and in the second lines, dispersion.

In the first series (Figures 2 - 7) values are given for the shape of the impulse transitional functions (ITF) for the same distance R_c = 100 m (τ = 5, σ = 0.5 ln/m, Λ = 1), but for different mutual orientations of the receiver and the source. The second series of figures (Figures 8 - 13) contains data on the ITF for τ = 12.3 and the same orientation as in the first series. The geometric distance from the source to the detector R_c and the probability of quantum survival remain the same as in the first series. Thus, the presented data make it possible to evaluate the influence of the scattering index of the medium σ and the angles of mutual orientation of the detector-source system on the shape of the received signal.

We will examine the appearance of the obtained ITF in the example of Figure 3. The general shape of the dependence of the logarithm for intensity of the signal reaching the given detector on time is such (this is apparent in all the remaining figures) that three distinctly pronounced zones can be distinguished on it. 1--zone of increase in intensity of signal (this zone was not always "worked", for a fairly complete explanation of it it was necessary to assign extremely small quantities of the temporal intervals, which did not always coincide with other tasks of the work); 2--zone of drop in signal according to a certain complicated law; 3--

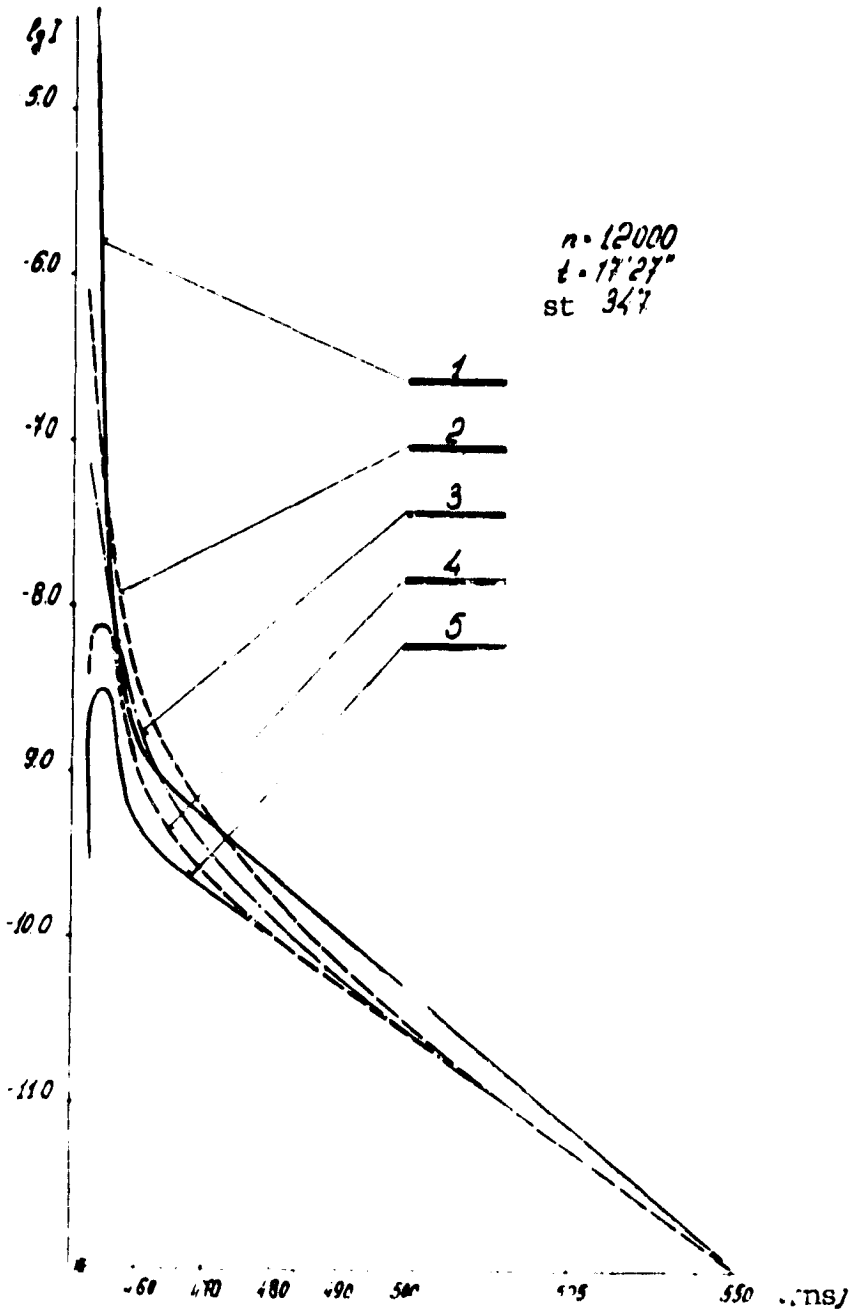

/120

Figure 2. Temporal Structure of Signal at Point R_c = 100 m, (τ = 5), Ω = 0°; 1--- Ω= 180°; 2--Ω 190°; 3-- Ω= 400°; 4-- Ω= 210°; 5--Ω = 220°.

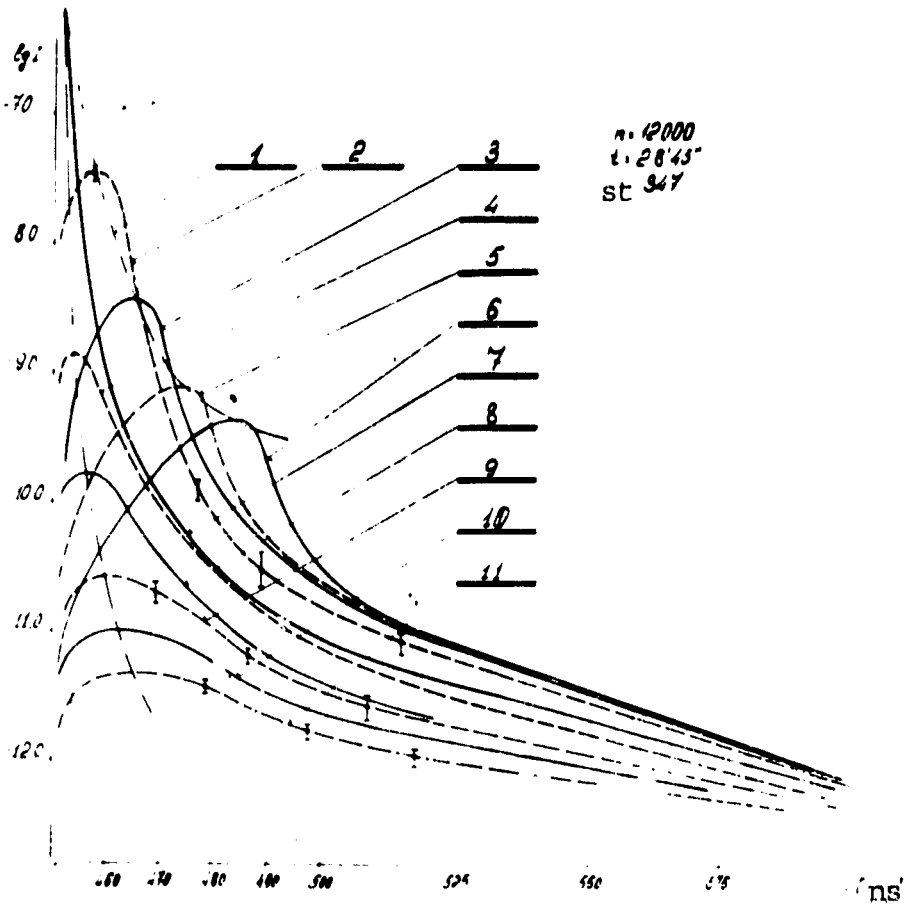

Figure 3. Temporal Structure of Signals at Point R_c = 100 m (τ = 5), θ = 10°; 1--curves of maximums; 2-- Ω = 200°, 3-- Ω = 210°, 4-- Ω = 180°; 5-- Ω = 220°; 6-- Ω = 230°, 7-- Ω = 190°; 8-- Ω = 170°, 9-- Ω = 160°; 10-- Ω = 150°; 11-- Ω = 140°.

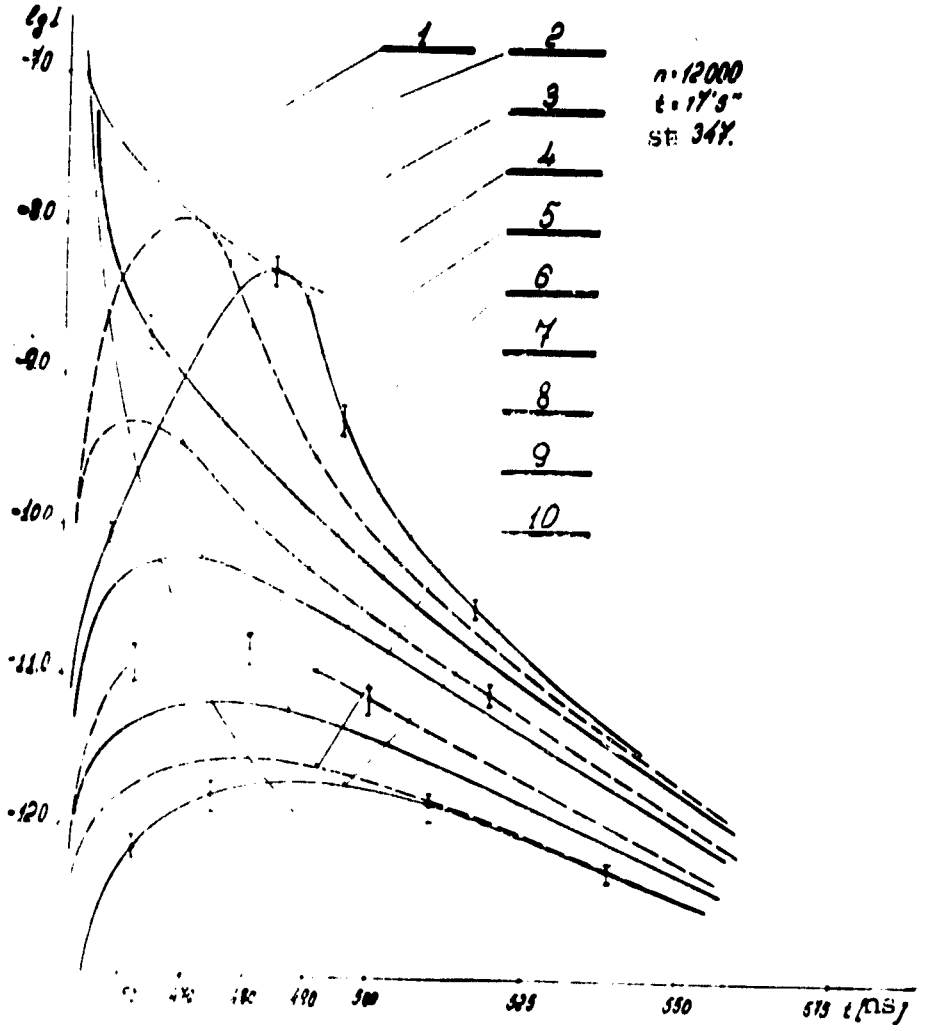

/122

Figure 4. Temporal Structure of Signals at Point R_c = 100 m (τ = 5), θ = 20°, 1--curve of maximums; 2--Ω = 200°; 3--Ω = 210°; 4--Ω = 220°; 5--Ω = 190°; 6--Ω = 180°; 7--Ω = 170°; 8--Ω = 160°; 9--Ω = 150°; 10--Ω = 140°.

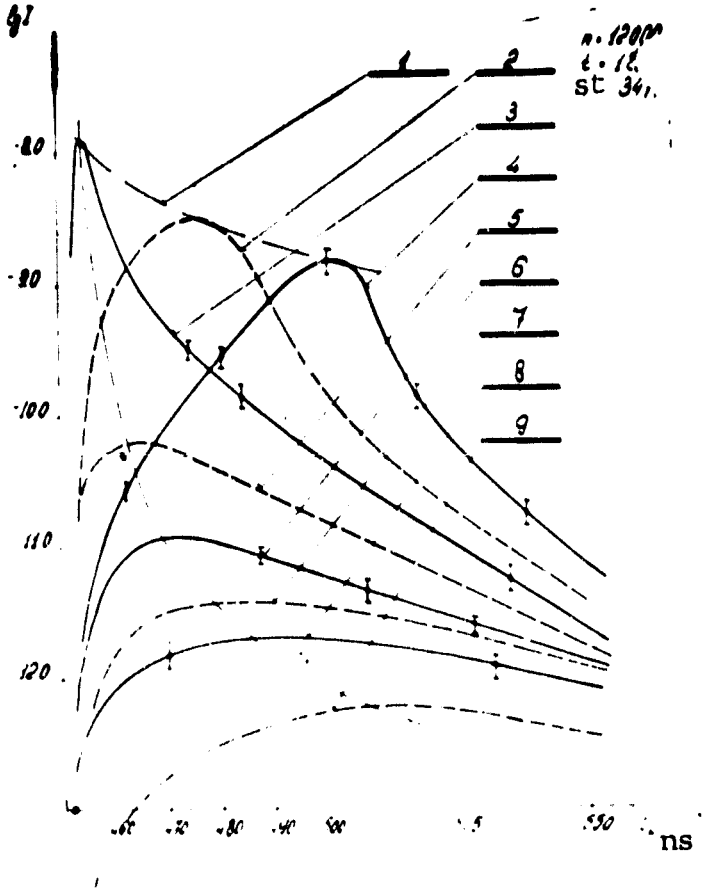

/123

Figure 5. Temporal Structure of Signals at Point R_c = 100 m (τ = 5), Ω = 30°; 1--curve of maximums; 2-- Ω = 220°, 3-- Ω = 210°; 4-- Ω = 230°, 5-- Ω = 200°; 6-- Ω = 190°; 7-- Ω = 180°; 8-- Ω = 170°, 9-- Ω = 140°.

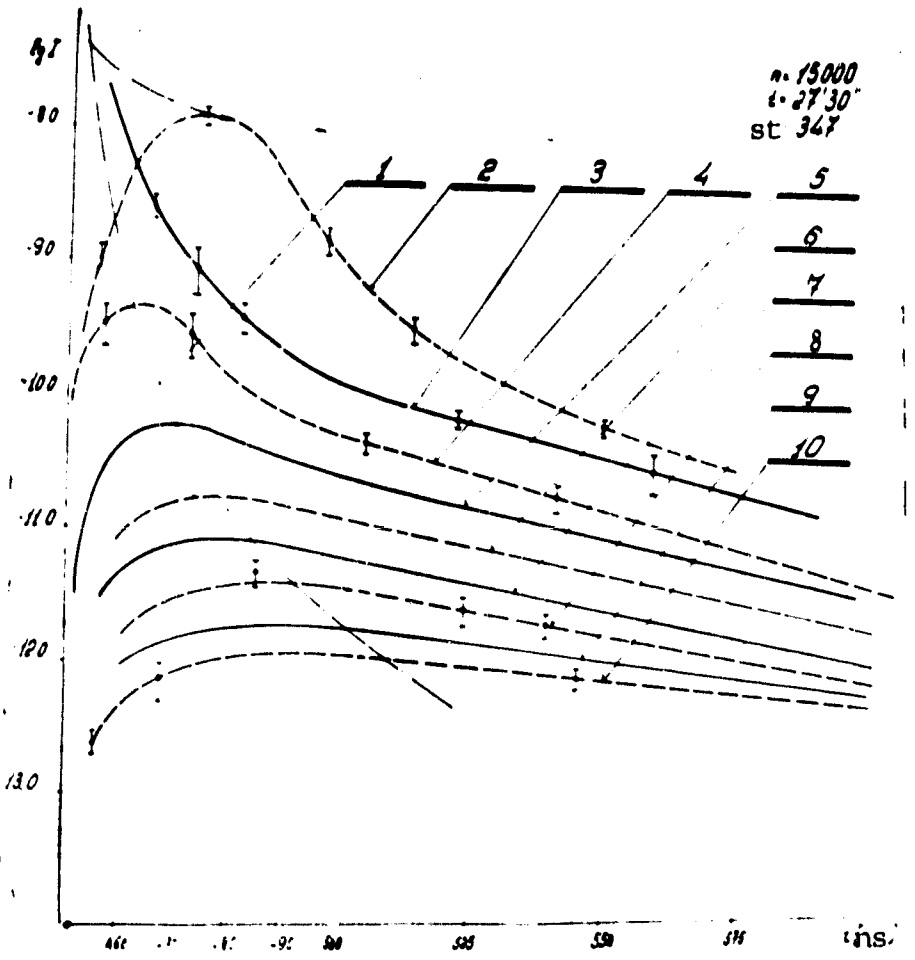

/124

Figure 6. Temporal Structure of Signals at Point R_C = 100 m (τ = 5), θ = 40°; 1---curve of maximum; 2--- Ω = 230°; 3--- Ω = 220°; 4--- Ω = 210°; 5--- Ω = 200°; 6--- Ω = 190°; 7--- Ω = 180°.

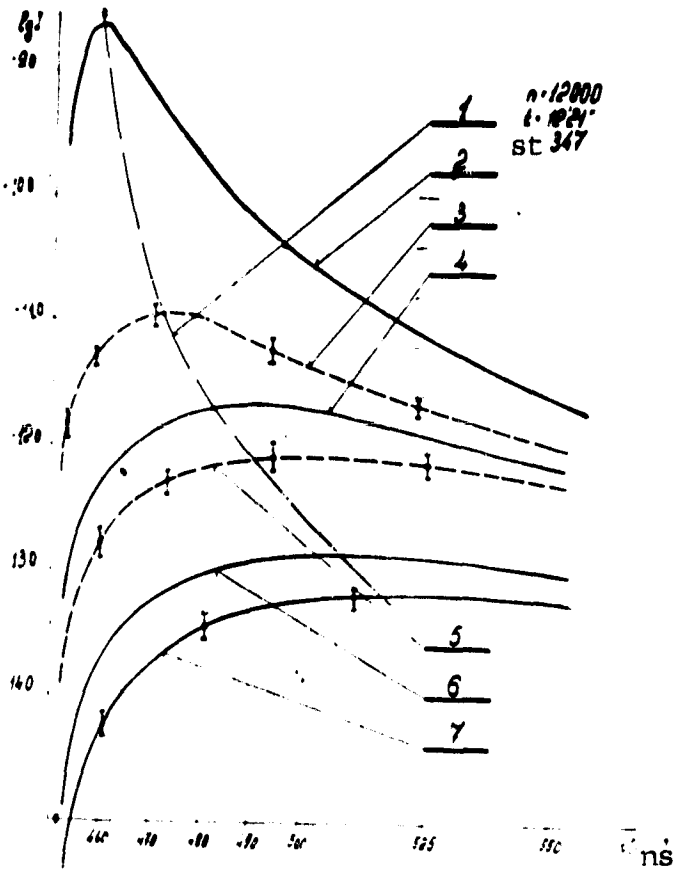

Figure 7. Temporal Structure of Signals at Point R_c = 100 m (τ = 5), Θ = 50°; 1--curve of maximums; 2-- Ω = 230°; 3-- Ω = 220°; 4--- Ω = 210°; 5--- Ω = 200°; 6-- Ω = 180°; 7--- Ω = 160°.

/125

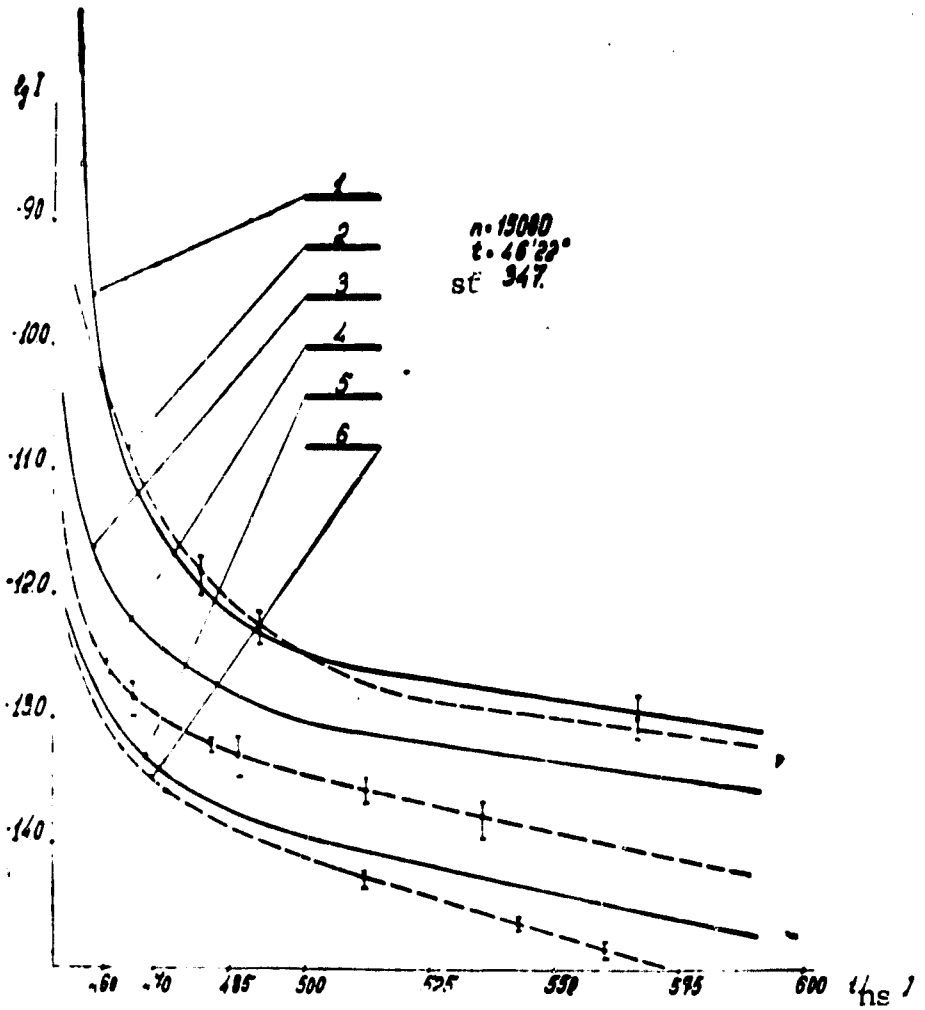

/126

Figure 8. Temporal Structure of Signals at Point R_c = 100 m (τ = 12.3), Θ = 0°; 1--Ω = 180°; 2--Ω = 190°; 3--Ω = 200°; 4--Ω = 210°; 5--Ω = 280°; 6--Ω = 250°.

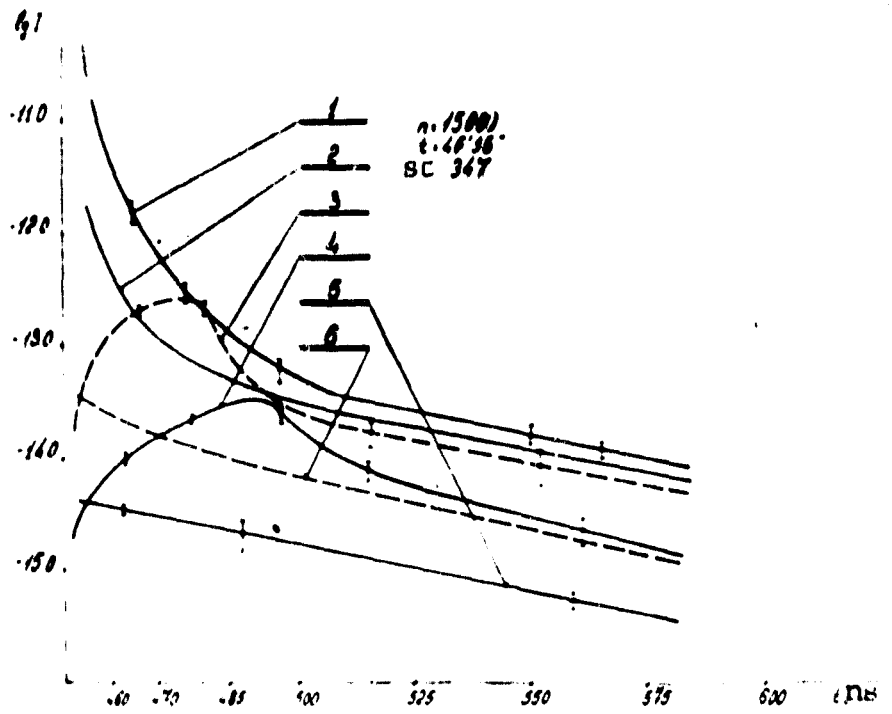

/127

Figure 9. Temporal Structure of Signals at Point R_c = 100 m (τ = 12.3); θ = 10; 1-- Ω = 190°; 2-- Ω = 180°; 3-- Ω = 220°; 4-- Ω = 240°, 5--Ω = 140°; 6-- Ω = 160°.

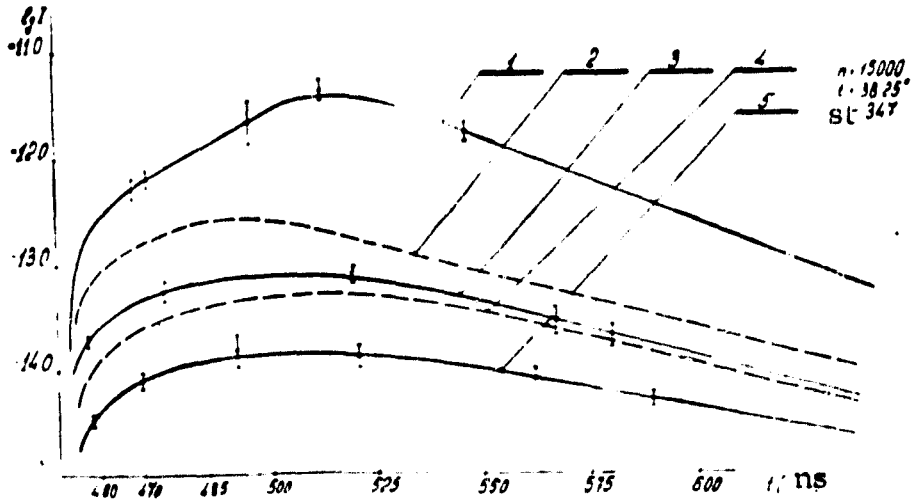

Figure 10. Temporal Structure of Signals at Point R_c = 100 m (τ = 12.3; θ = 20°; 1-- Ω = 230°; 2-- Ω = 240°; 3-- Ω = 250°; 4-- Ω = 260°; 5-- Ω = 280°.

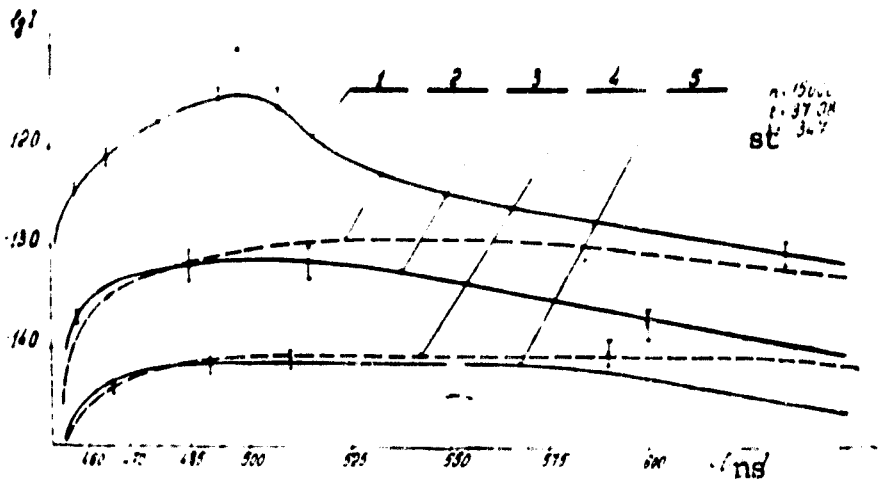

Figure 11. Temporal Structure of Signals of Point R_c = 100 m (τ = 12.3); Θ = 30°; 1--Ω = 230°; 2--Ω = 250°; 3--Ω = 180°; 4--Ω = 280°, 5--Ω = 160°. /128

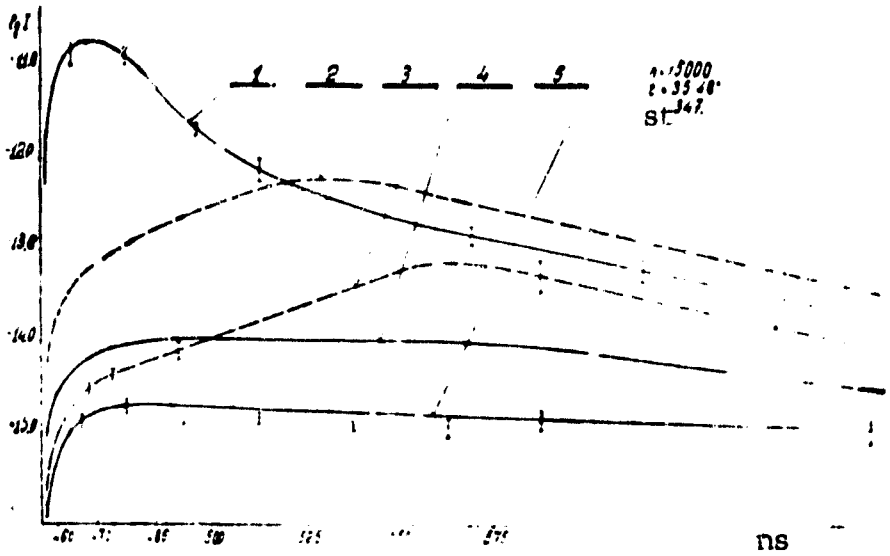

Figure 12. Temporal Structure of Signals at Point R_c = 100 m (τ = 12.3); Θ = 40°; 1--Ω = 220°; 2--Ω = 250°; 3--Ω = 280°; 4--Ω = 180°; 5--Ω = 150°.

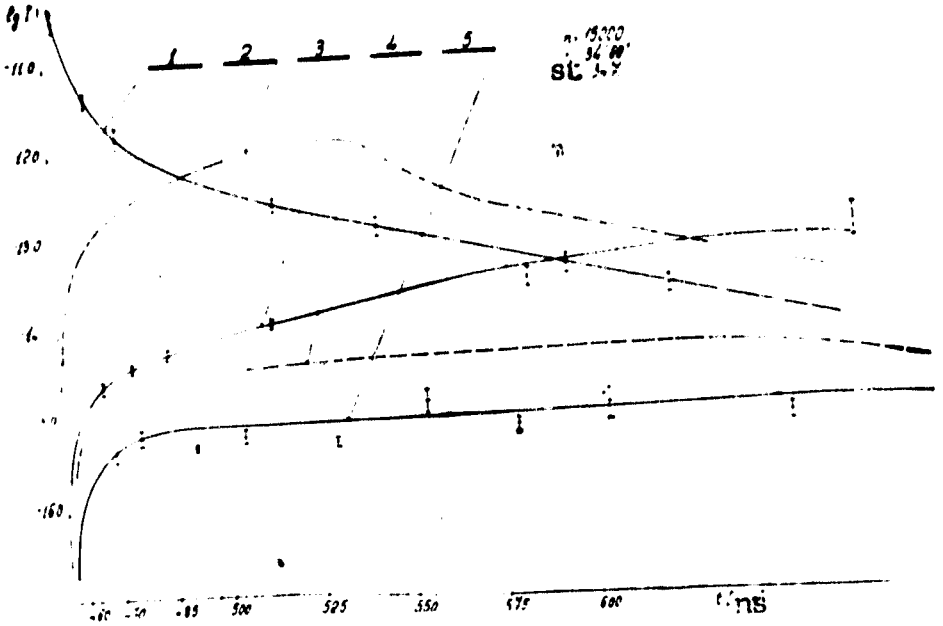

/129

Figure 13. Temporal Structure of Signals at Point R_c = 100 m (τ = 12.3), Θ = 50°; 1--Ω = 230°; 2--Ω = 250°; 3--Ω = 280°; 4--Ω = 180°; 5--Ω = 150°.

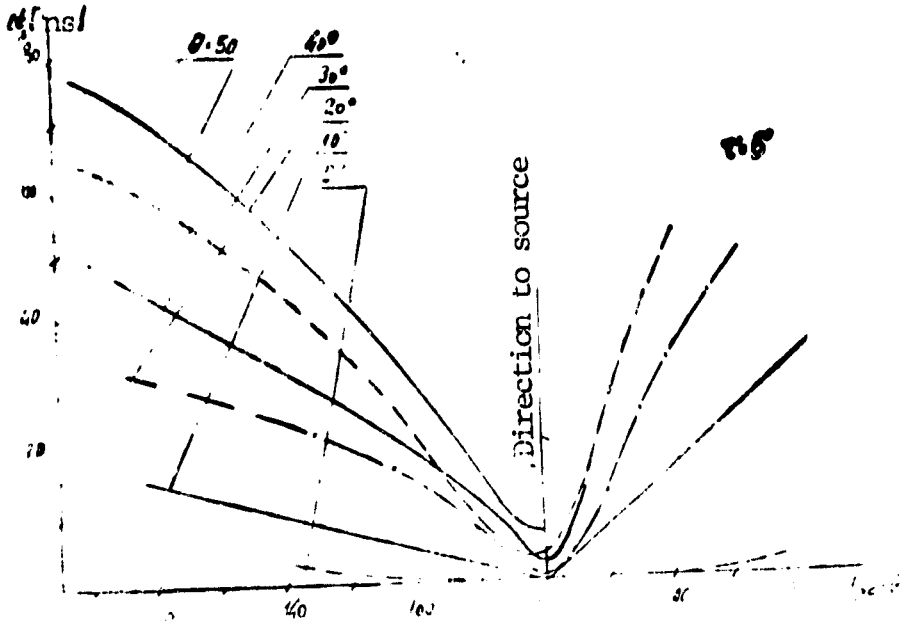

Figure 14. Dependences of Duration of Zones I and II on Geometry of Experiment: a--zone I (τ = 5), b--zone II (τ = 5), c--zone I (τ = 12.3).

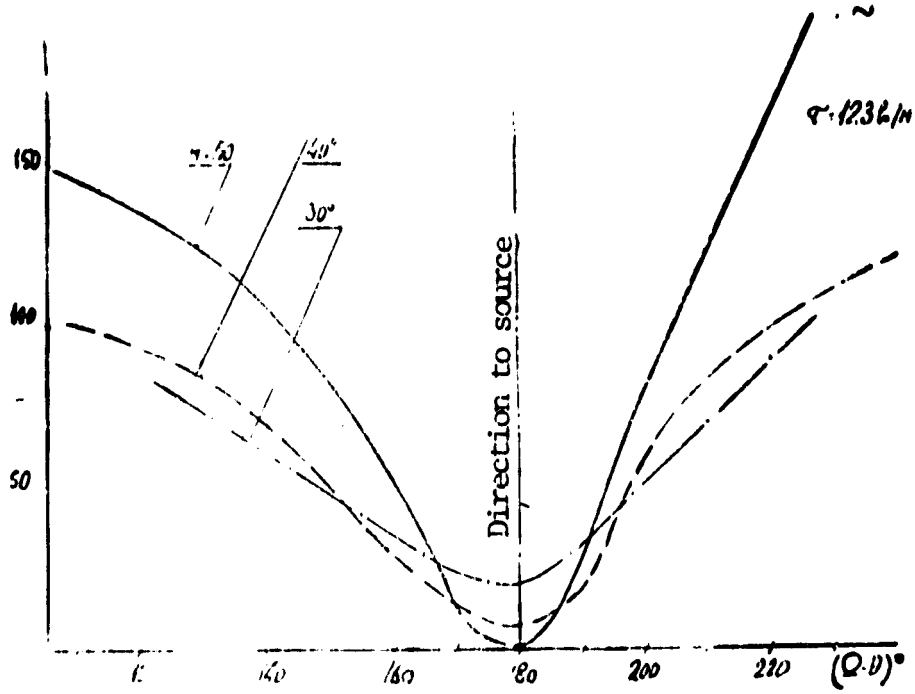

Figure 14b.

/130

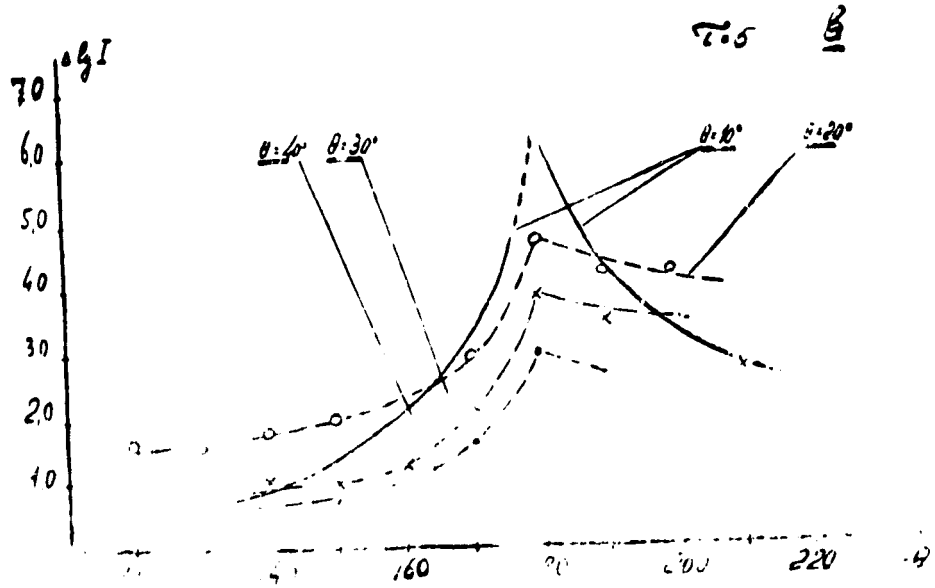

Figure 14c.

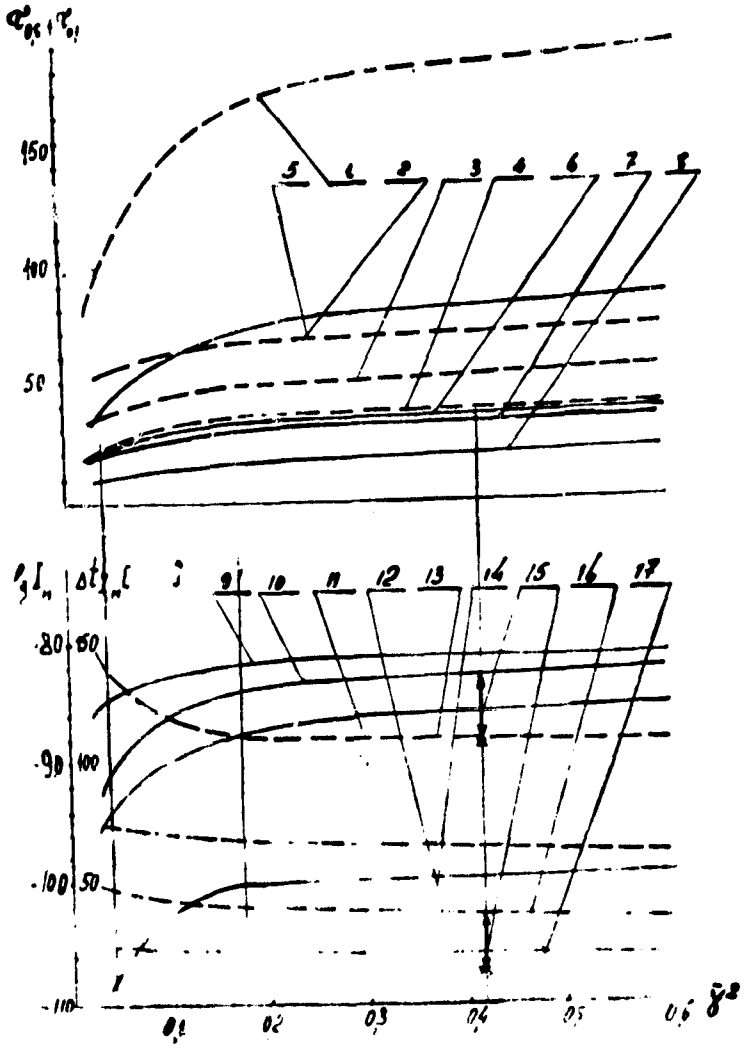

/133

Figure 15. Dependences of Parameters of Shape of ITF on: 1--$\tau_{0.1}$ Ω = 280 ; 2--$\tau_{0.1}$ Ω = 260 , 3--$\tau_{0.1}$ Ω = 250 ; 4--$\tau_{0.1}$ Ω = 240,5--$\tau_{0.5}$ Ω = 280; 6--$\tau_{0.5}$ Ω = 260; 7--$\tau_{0.5}$ Ω = 250; 8--$\tau_{0.5}$ Ω = 240, 9--$\lg I_m$ Ω = 240; 10--$\lg I_m$ Ω = 250; 11--$\lg I_m$ Ω = 260, 12--$\lg I_m$ Ω = 280; 13--Δt Ω = 280; 14--Δt Ω = 260; 15--abnormal position of points of intensity and shift in maximum, corresponding to γ^2 0.05; 16 --Δt, Ω = 250°; 17--Δt, Ω = 240°.

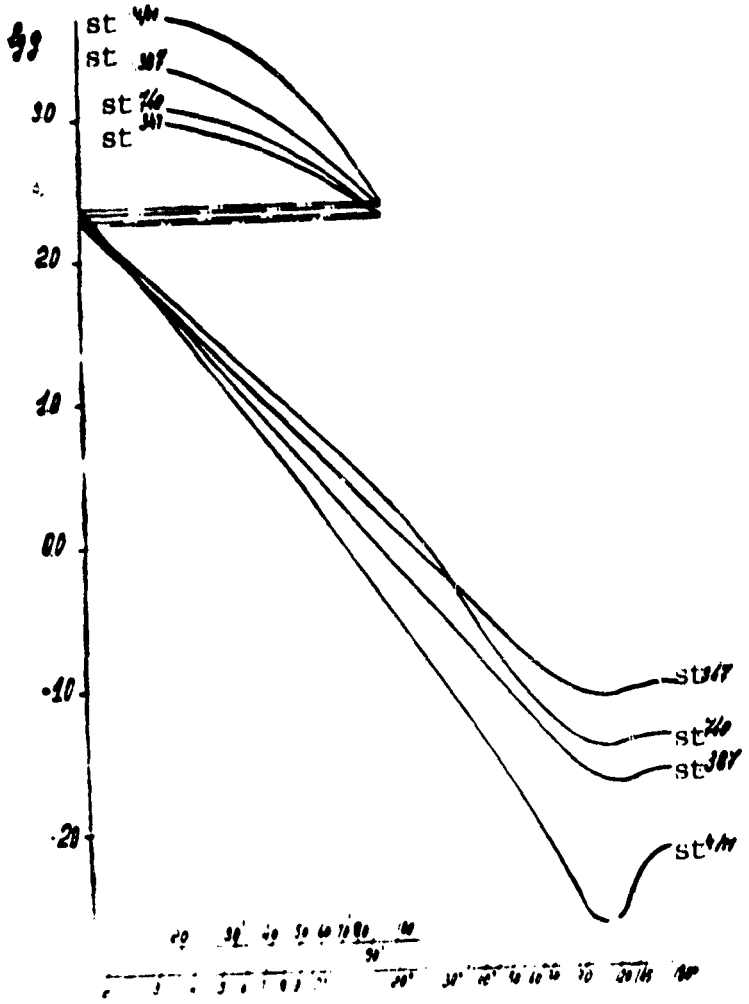

/134

Figure 16. Shapes of Scattering Indicatrixes of Sea Water, used in Calculations: 1--tangential at point corresponding to scattering angle 50° for indicatrix measured at station 740; 2--"standard" indicatrix corresponding to real indicatrix with scattering angle 50°.

zone in which decrease in signal intensity occurs according to a law close to the exponential. We will call it the "near asymptotic." It follows from theoretical solutions that with a further rise one should expect the appearance of a distant or true asymptotic regime in which temporal attenuation of the signal is subordinate to the exponential law.

The duration of the first zone (Δt_1) changes in a fairly large range of time and depends on Ω, θ and σ.

It is common knowledge (Figure 14a) that the more time passes from the beginning of the process, the higher the average order (frequency) of scattering of the photons reaching the detector. Since the interval is formed by light of small orders of scattering, then an increase in σ (with constant geometry of the experiment) or (Ω-θ) results in a decrease in the number of photons of small scattering orders which reach the detector, and consequently, decrease in the size of the signal in the /121 beginning of the process, and increase in the time interval Δt_1. For example, with σ = 0.123 1n/m and (Ω-θ) $\geq$ 215° and (Ω-θ) $\leq$ 105°, Δt_1 exceeds 150 ns. At the same time, with (Ω-θ) = 180° (the detector is directed towards the source), this interval is the minimum with σ = 0.05 1n/m and all θ $\Delta t_1 \leq$ 7 ns.

In deformation of the shape of the anterior front of the ITF curve, yet another /131 trend is observed which is traced well in the transition from one geometry of the experiment to another: characteristic changes in the shape of the curve of the anterior ITF front. If (Ω-θ) ~ 180°, then the anterior front has the shape of a flash-up with very steep elevation. With an increase in the optical distance or (Ω-θ) $<$ 180°, the anterior front is a smooth curve which is convex upwards. If (Ω-θ) $>$ 180°, then a tendency is observed for the curve of the anterior front towards "rectification," and for example, in the case θ = 50°; τ = 12.3, (Ω-θ) $\geq$ 210°

(Figure 14b) there is almost a straight section with subsequent smooth transition to the "main" curve near the maximum.

In the second zone (Δt_2), the signal is formed by photons of different orders of scattering. Their contributions are comparable in absolute quantity. Therefore, changes in mutual arrangement of the detector and source result in variation in the shape of the curve in very broad limits. In particular, a drop in the signal in this zone can be steeper than the increase in signal in the zone Δt_1 (Figures 10 - 12). This effect was also obtained in the experiment [10].

The behavior of the ITF curves in the zone Δt_2 can be approximately described by the quantity of drop in signal in a certain time interval. We selected the interval equal to 100 ns, counted from the maximum ITF. This interval usually covers part of zone III, but generally, the indicated procedure makes it possible to clarify the qualitative dependence of the average rate of change in the signal in zone II on the geometry of the experiment, θ, indicatrix, etc. As is apparent from Figure 14c, the effect of experiment geometry on the shape of the ITF in zone II is manifest most strongly with $\theta = 0°$ and $(\Omega-\theta)$ close to 180°. Increase in τ, in the same way as angles $(\Omega-\theta-180°)$ results in a decrease in the quantity of signal drop, while the curve in the limit approaches the inclined straight line.

The second zone smoothly transfers to the third zone Δt_3, the "near asymptotics," whose beginning (with fairly broad zone of transition, i.e., "blurred" boundary between zones), rapidly travels to the right on the time axis depending on θ, $(\Omega-\theta)$ and τ.

The third zone is formed by photons of large scattering orders. It is noticeable that here not only does the drop in the curve occur according to the approximately exponential law, but also (in limits of accuracy of the numerical experiments)

the exponents are very close. However, a tendency is observed towards increase in the exponent in absolute quantity with a decrease in $\sigma, 0$ and $(\Omega-0)$, i.e., with a decrease in optical distance of the point of the detector center from the beam axis. This is associated with the fact that the smaller the optical distance from the beam axis, the a) greater the contribution to the quantity of intensity of the photons of smaller orders of scattering; b) the faster the process of light emergence from the zone examined by the detector.

The tendency of the ITF curves towards convergence which is traced on all the graphs shows that the process of equalizing of the shape of the brightness body is not finished, and consequently, in addition to the three zones we obtained in numerical experiments, there is a fourth zone, distant (or true) asymptotics and drop in the ITF curve according to the exponential law. However, the extremely slow convergence of the curve does not make it possible to reach the fourth zone in the calculations. /132

In those cases where the reception point does not lie on the axis of the initiating light beam, all the ITF curves (i.e., $\lg I = f(t, \Omega = \text{const})$ are divided into two regions. The boundary between them is the ITF curve with $(\Omega-0) = 180°$: the receiver axis aimed at the "source", i.e., the point for entrance of the beam into the medium. This curve $(\Omega-0 = 180°)$ always has the acutest maximum which is located to the left of the maximum for all other curves $(\Omega-0 \neq 180°)$ and has the greatest absolute quantity. All the curves with $(\Omega-0) > 180°$ are located above this curve. All the ITF with $(\Omega-0) < 180°$ are lower. As a rule, the curves with $(\Omega-0) > 180°$ have an incline of the "near asymptotics" which is somewhat greater than the ITF with $(\Omega-0) < 180°$. In addition, an earlier emergence of the curves with lower $(\Omega-0)$ to the "near asymptotics" is observed than with greater.

One of the most important questions in studying the nonstationary narrow radiation beams in the sea is the question of the influence of the shape of the scattering indicatrix on the light field. It is extremely difficult to clarify this question in an experiment. Based on an analysis of numerical studies (Tables 19 - 26, Figure 15) one can make certain preliminary assessments. According to the suggestion of V. N. Pelevin, the influence of the shape of the scattering indicatrix on the ITF form was sought in the first approximation in the form of dependences of the ITF parameters on the second angular moments of the indicatrix which characterize the rate of photon redistribution in directions.

Figure 15 presents: in the upper part of the figure--the dependence of the width of the ITF curves at level 0.5 (dotted line) and 0.1 (solid lines), and also, in the lower part of the figure, the time of shifting of the signal maximum along the time axis (solid lines) and the logarithm of absolute values of intensity on $\bar{\gamma}^2$. The curves were constructed for cases Ω = 240, 250, 260 and 280 with θ = 50°, R_c = 50 m, σ = 0.123 ln/m, i.e., the detector was located outside the axial region of the incident radiation beam. For other θ and R_c, a similar behavior of the ITF curves occurs at different Ω.

As is apparent from Figure 15, with an increase in $\bar{\gamma}^2$, the values for the ITF width rise at level 0.5 and 0.1 (as well as 0.01), and shifts of the maximum to the right along the time axis. The absolute values of the signal maximum diminish with an increase in $\bar{\gamma}^2$. One should note that the obtained nature of behavior of the curves in Figure 15 can be predicted fairly correctly based on the model of narrow-directional radiation beam introduced in [10].

The shape of the scattering indicatrix (Figure 15) significantly influences /135
the light field in a turbid medium with $\gamma^2 \leq 0.25$. With $\gamma^2 > 0.25$, the influence of

the indicatrix is weaker: the dependence of all the examined quantities on γ^2 is almost linear.

In analyzing the behavior of the curves presented in Figure 15, yet another feature was revealed: dependences of the position of the ITF maximum and shift of it along the axis on γ^2 of time reacts sensitively to the "geometry" of the conducted experiment. This is expressed in the fact that the points corresponding to indicatrix No. 4 did not lie in those positions that they should lie with $\gamma^2 = 0.47$ in Figure 15. They are very shifted, their position is marked by crosses. Certain shifts in the corresponding points are also observed in the curves for the shift in the maximum and the ITF width at different levels, however, they are insignificant and are usually in the field of accuracy. More characteristic and clearly pronounced shifts in the points are observed in the curves of absolute value of the maximum ITF (curves 9, 10, 11 and 12 in Figure 15).

The position of the "crosses" in Figure 15 correspond to those values of γ^2 of standard* scattering indicatrix where the incline of the average section equals the incline of the real indicatrix with the scattering radiation angle given in the specific problem. For example, for indicatrix No. 4 with scattering angle 50°, the standard indicatrix has $\gamma^2 = 0.07$. Almost the same value of γ^2 is obtained in Figure 15 if the "crosses" are projected onto the corresponding curves, and then the quantity γ^2 is determined. The spread of the points, as is apparent from Figure 15, is quite permissible.

*By standard is meant that artificially constructed indicatrix which has one linear average section in the range of zenith angles.

CONCLUSIONS

1. Results are given of calculations of the ITF for different geometric situations in the ocean in the system of δ- impulses according to time and transverse dimensions: a small angular aperture detector placed in an arbitrary point of the turbid medium and oriented in a definite manner in space. All the ITF were computed for one constant hydro-optical scattering indicatrix which is characteristic for waters in the Indian Ocean.

2. The influence of the shape of the scattering indicatrix on the ITF was studied in the first approximation.

3. Consideration of other optical characteristics of the problem, coefficients of absorption, temporal form of the original signal, etc., is reduced to simple multiplication or integration of the "grid" type.

The author is sincerely grateful to K. S. Shifrin, B. A. Kargin and V. N. Pelevin for support and constant attention to this work.

BIBLIOGRAPHY

1. Romanova, L. M. "Nonstationary Light Field in a Deep Turbid Medium Illuminated by a Narrow Beam," Izv. AN SSSR, Ser. FAO, vol 5, No 5, 1969. /136

2. Romanova, L. M. "Nonstationary Light Field in Turbid Media," Teoreticheskiye i prikladnyye problemy rasseyanaya sveta ["Theoretical and Applied Problems of Light Scattering"], Minsk, 1971.

3. Delin, L. S. "Spread of Narrow Light Beam in Medium with Very Anisotropic Scattering," Izv. vuzov, ser. radiofizika, vol 9, No 1, 1969.

4. Katsev, I. L.; Zege, E. P. Vremennyye asimptoticheskiye resheniya uravneniya perenosa izlucheniya i ikh primeneniye ["Temporal Asymptotic Solutions to the Transport Equation of Radiation Under Application"], Preprint of the Institute of Physics of the USSR Academy of Sciences, Minsk, 1973.

5. Marchuk, G. I.; Mikhaylov, G. A. Metod Monte-Karlo v atmosfernoy optike ["Monte Carlo Method in Atmospheric Optics"], Novosibirsk, Nauka, 1976.

6. Gutshabash, S. B.; Ivanov, V. V. "Propagation of Brightness Wave in Optically Fit Atmosphere," Izv. AN SSSR, Ser. FAO, vol 10, No 8, 1974.

7. Gurfink, A. M. "Nonstationary Radiation Field in Semi-infinite Medium with Non-isotropic Scattering," Optika okeana i atmosfery ["Optics of the Ocean and Atmosphere"], Leningrad, Nauka, 1972.

8. Luchinin, A. R.; and Savel'yev, V. A. Izy. VUZov, Ser. radiofizika, vol 12, No 2, 1969.

9. Krekov, G. M.; Mikhaylov, G. A.; and Kargin, B. A. "Algorithms of the Monte Carlo Method to Solve the Task of the Theory of Propagation of Narrow Light Beams," Izv. VUZ ov, ser. Fizika, Nos 4, 5, 1968.

10. Gol'din, Yu. A.; Pelevin, V. N. et al. "Experimental Studies of Nonstationary Light Field in the Ocean," Gidrofizicheskiye i gidrostaticheskiye issledovaniya v Atlanticheskom i Tikhom okeanakh ["Hydrophysical and Hydrostatic Studies in the Atlantic and Pacific Oceans"], Moscow, Nauka, 1974.

11. Katsev, I. L. "Propagation of Light Impulse in Semi-infinite Isotropically Scattering Medium," ZhPS, vol 9, No 6, 1968.

12. Mikhaylov, G. A. "Use of Exponential Transform in Calculating Passage of the Monte Carlo Particles," Metod Monte-Karlo v probleme perenosa izlucheniy ["Monte Carlo Method in a Problem of Radiation Transport"], Moscow, Atomizdat, 1967.

TABLE 1. COMPARISON OF RESULTS OF PHYSICAL AND MATHEMATICAL EXPERIMENTS*

Geometric Parameters	$R_c = 50$, $\Theta = 0°$, $\tau = 9,2$, $\Lambda = 0,8$, st. 740				$R_c = 50$, $\Theta = 50°$, $\tau = 6,15$, $\Lambda = 0,67$ st. 387			
Parameter	Ω = 180	190	200	230	230	240	260	280
Shift in amplitude	16/17	18/18	18/21	16/23	30/35	40/38	72.92	130/127
Ratio %	1	100	85,8	70.5	85.8	105.2	78.4	102,5
0.5 Ratio %		9 [illegible] 0.5	13/11	19/11	32/29	40/31	48/47	74/80
0.1 Ratio %	10.5	10.5	118		110	132	102	92,5
	14.5	18. 4	27,5/23	38/29	72/63	85/70	110.96	164/196
0.01 Ratio %	9[illegible]	9[illegible].5	119.5	75.3	114.2	121.5	114.5	94,9
Asymmetry at level 0.5 Ratio %	22.[illegible]	44.47	52.55	14/24				—
	4	42	94.5	21/38	—	—		—
	5 4	8,5/9,5 / 9,5/11.5	11/14 / 9/12	10.5 8 / 131	12/20 / 3,5/17	18/22 / 14/17	22/26 / 23/23	40/34 / 44/42
		108.2	104.8	70/93	75,5	99,5	84,6	112,2

*The term "ratio %" means the ratio of data of mathematical experiments of this work to the measured [10] presented in the previous line.

/13

TABLE 2. ITF FOR CASE: ZENITH ANGLE OF RECEPTION POINT θ= 0°; SEMI-ANGLE OF TAPER OF RECEIVER γ_s = 2.5°; INDICATRIX OF STATION 347; σ = 0.05 ln/m; A = 1; R_c = 100 m; N = 12,000; c_1 = 0.025; v = 0.222 m/ns*

Time Interval / Ω	450–452	452–454	454–456	456–458	458–460	460–470	470–480	480–500	500–525	525–550
140	1.79–8 0.157	3.22–8 0.095	1.19–8 0.0789	5.03–9 0.0872	1.50–9 0.0925	7.75–9 0.0983	5.21–10 0.197	1.36–10 0.329	9.67–11 0.269	4.61–11 0.255
150	7.191–8 0.0656	7.651–8 0.066	2.115–8 0.110	1.714–8 0.280	5.276–9 0.0886	2.397–9 0.125	5.874–10 0.119	2.921–10 0.177	1.98?–10 0.199	1.965–11 0.211
160	5.385–7 0.108	1.615–7 0.0556	5.836–8 0.295	1.910–8 0.106	1.178–8 0.182	3.547–9 0.100	8.142–10 0.121	4.146–10 0.286	1.849–10 0.383	1.203–10 0.596
170	5.287–6 0.085	5.275–7 0.099	1.146–7 0.166	3.696–8 0.153	1.599–8 0.193	5.324–9 0.149	1.168–9 0.258	2.678–10 0.176	8.478–11 0.136	1.2?2–10 0.614
180	3.694–1 0.0357	3.935–7 0.125	5.406–8 0.173	1.588–8 0.134	1.120–8 0.263	4.094–9 0.457	1.822–9 0.619	7.388–10 0.438	1.688–10 0.321	1.233–10 0.584
190	946–9 0.0309	2.24–7 0.108	6.114–8 0.167	3.134–8 0.165	2.803–8 0.260	1.349–8 0.354	5.448–10 0.157	3.492–10 0.250	7.609–11 0.132	6.706–11 0.258
200	0.82–7 0.0?8	938–8 0.213	2.037–8 0.151	.230–8 0.160	7.229–9 0.157	3.796–9 0.167	7.150–10 0.113	8.590–10 0.514	9.516–11 0.262	6.344–10 0.796
210	209–8 0.0?8	852–8 0.171	6.342–9 0.0573	6.478–9 0.387	4.8?6–9 0.365	2.738–9 0.437	1.260–9 0.350	2.258–10 0.152	6.600–11 0.143	1.708–10 0.671
220	7.503–9 0.0780	1.532–9 0.0495	3.569–9 0.162	1.957–9 0.094	1.573–9 0.103	7.882–10 0.0863	4.432–10 0.355	2.044–10 0.242	1.175–10 0.281	3.745–11 0.223
230	3.425–9 0.0757	2.306–9 0.0955	1.503–9 0.110	9.842–10 0.0926	6.982–10 0.?41	3.?1?–10 0.?84	2.180–10 0.?48	1.364–10 0.274	1.036–10 0.347	2.436–11 0.122

*The order of the number is indicated from the right of the significant part of one, for example 1.79–8 means 1.79 x 10^{-8}.

TABLE 3. ITF FOR THE CASE: ZENITH ANGLE OF RECEPTION POINT = 10° , SEMI-ANGLE OF TAPER OF RECEIVER γ_s = 2.5°; INDICATRIX OF STATION 347; σ = 0.05 ln/m; Λ = 1; R_c = 100 m, N = 15,000; c_1 = 0.040; v = 0.222 m/ns.

Time Interval Ω	450—455	455—460	460—470	470—480	480—490	490—500	500—525	525—550	550—575	575—600
140	3,216—11 0,0635	5,691—11 0,1136	4,807—11 0,182	3,799—11 0,146	5,454—11 0,339	1,762—11 0,132	1,134—11 0,137	9,183—12 0,446	6,144—12 0,241	5,204—12 0,315
150	8,600—11 0,1014	1,020—10 0,0973	1,008—10 0,160	5,625—11 0,131	4,740—11 0,418	1,955—11 0,0986	2,219—11 0,189	9,252—12 0,144	9,129—12 0,269	8,320—12 0,258

Time Interval Ω	450—455	455—460	460—470	470—480	480—490	490—500	500—525	525—550	550—575	575—600
160	3,178—10 0,173	2,915—10 0,965	2,076—10 0,123	1,992—10 0,412	6,540—11 0,125		2,688—11 0,210			6,840—12 0,191
170	1,178—9 0,0503	1,961—9 0,452	4,861—10 0,0905	3,140—10 0,203	9,817—11 0,136			1,656—11 0,153	9,312—12 0,141	
180	1,270—8 0,0717	1,026—8 0,430	1,575—9 0,126	7,115—10 0,448	1,974—10 0,217	1,085—10 0,316	4,034—11 0,104	2,160—11 0,296	1,310—11 0,143	2,824—11 0,573
190	2,565—6 0,103	2,776—8 0,187	2,448—9 0,139	4,916—10 0,127	2,091—10 0,265	1,097—10 0,146	5,707—11 0,137	3,210—11 0,248	1,647—11 0,282	1,685—11 0,348
200	1,009—7 0,797	3,502—7 0,0923	1,406—8 0,101	1,253—8 0,151	3,088—10 0,132	2,567—10 0,479	8,666—11 0,172	4,096—11 0,229	2,307—11 0,290	1,062—11 0,134
210	3,219—9 0,0862	1,084—8 0,050	3,727—8 0,173	2,294—9 0,101	8,448—10 0,265	1,690—10 0,123	9,476—11 0,126	4,193—11 0,348	2,360—11 0,198	
220	5,038—10 0,0625	1,352—9 0,0728	4,911—9 0,0576	7,575—9 0,050	6,224—10 0,0983	3,222—10 0,212	1,539—10 0,380	2,605—11 0,0943	2,674—11 0,263	2,407—11 0,320
230	1,334—10 0,0803	1,301—9 0,253	8,059—10 0,138	3,065—9 0,059	3,721—9 0,435	5,721—10 0,302	1,193—10 0,178	5,066—11 0,288	3,815—11 0,414	1,501—11 0,188

TABLE 4. ITF FOR THE CASE: ZENITH ANGLE OF RECEPTION POINT ϑ = 20°, SEMI ANGLE OF TAPER OF RECEIVER γ_s = 2.5°; INDICATRIX OF STATION 347; σ = 0.05 1n/m; A = 1; R_c = 100 m; N = 12,000; c_1 = 0.025, v = 0.222 m/ns

Time interval / Ω	450—452	452—454	454—456	456—458	458—460	460—470	470—480	480—500	500—525	525—550
140	1,294—12 0,594	2,027—12 0,160	1,899—11 0,553	1,223—11 0,386	7,311—12 0,176	1,687—11 0,235	1,617—11 0,182	1,815—11 0,159	9,251—12 0,162	5,118—12 0,103
150	1,302—12 0,368	4,150—12 0,183	1,156—11 0,358	1,554—11 0,222	3,080—11 0,552	2,570—11 0,141		2,207—11 0,165	1,336—11 0,140	8,539—12 0,165
160	4,622—12 0,568	9,863—12 0,164	6,425—11 0,682	8,797—11 0,223	2,998—11 0,162	5,771—11 0,199	4,654—11 0,238	4,663—11 0,286	1,912— 0,1[illegible]	1,204—11 0,213
170	1,665—11 0,300	11—969[illegible] 0,161	1,164—10 0,434	1,028—10 0,178	1,278—10 0,284	1,319—10 0,127	1,563—10 0,294	6,803—11 0,165	2,822—11 0,130	1,253—11 0,134
180	5,496—11 0,161	2,000—10 0,206	2,662—10 0,149	3,282—10 0,162	5,103—10 0,225	5,155—10 0,225	2,415—10 0,292	9,857—11 0,132	8,989—11 0,259	1,692—11 0,172
190	8,966—10 0,127	3,671—9 0,502	3,365—9 0,243	4,967—9 0,441	1,371—9 0,128	2,286—9 0,199	6,070—10 0,257	5,272—10 0,350	1,390—10 0,280	2,981—11 0,199

Time Interval / Ω	450—452	452—454	454—456	456—458	458—460	460—570	470—480	480—500	500—525	525—550
220	6,144—7 0,171	4,517—7 0,158	9,289—8 0,166	3,217—8 0,151	1,930—8 0,279	1,002—8 0,317	1,011—8 0,121	1,639—9 0,582	7,795—11 0,118	7,453—11 0,464
200	1,535—9 0,148	1,117—8 0,220	1,470—8 0,163	5,153—8 0,356	7,182—8 0,213	1,122—7 0,21[illegible]	6,812—9 0,196	1,359—9 0,286	1,234—10 0,169	2,021—10 0,392
210	1,129—10 0,308	3,455—10 0,335	8,278—10 0,142	1,144—9 0,107	2,172—9 0,230	3,576—9 0,217	3,457—8 0,223	3,023—9 0,097	2,974—10 0,171	1,356—10 0,390
230	2,505—11 0,372	6,118—11 0,238	1,696—10 0,239	1,829—10 0,165	3,003—10 0,165	1,138—9 0,337	1,818—9 0,146	8,649—9 0,115	9,429—10 0,233	2,264—10 0,402

TABLE 5. ITF FOR THE CASE: ZENITh ANGLE OF RECEPTION POINT $\Theta = 30°$, SEMI ANGLE OF TAPER OF RECEIVER $\gamma_s = 2.5$; INDICATRIX OF STATION 347; $\sigma = 0.05$ ln/m, $\Lambda = 1$, $R_c = 100$ m; N = 12,000; $c_1 = 0.025$; $v = 0.222$ m/ns

Time interval / τ	450—452	452—454	454—456	456—458
140	4.316—14 0.193	2.425—13 0.219	1.064—12 0.708	7.416—13 0.430
150	1.226—13 0.298	2.770—13 0.200	2.897—12 0.698	1.189—12 0.260
160	2.577—13 0.110	5.929—13 0.151	4.516—12 0.442	1.539—12 0.111
170	8.430—13 0.589	1.117—12 0.074	4.003—12 0.538	4.245—12 0.201
180	1.445—12 0.138	3.584—12 0.209	1.205—11 0.185	1.372—11 0.166
190	6.696—12 0.088	2.085—11 0.084	5.808—11 0.317	4.922—11 0.152
200	1.605—10 0.385	3.123—10 0.152	6.690—10 0.447	5.120—10 0.250
210	6.665—8 0.154	1.278—7 0.355	3.785—8 0.100	3.186—8 0.313
220	1.815—10 0.290	5.656—10 0.081	4.473—9 0.614	4.169—9 0.200
230	8.348—12 0.086	4.088—11 0.224	1.049—10 0.268	2.333—10 0.269

458—460	460—470	470—480	480—500	500—525	525—550
5.613—13 0.136	1.524—12 0.178	2.440—12 0.207	4.511—12 0.243	5.254—12 0.423	4.785—12 0.346
0.122—12 0.297	3.630—12 0.331	4.121—12 0.215	3.931—12 0.116	4.784—11 0.831	4.000—12 0.162
2.426—12 0.215	5.626—12 0.203	5.347—12 0.125	8.764—12 0.317	4.379—11 0.492	5.360—12 0.205
1.741—11 0.461	1.508—11 0.330	11—999'1 0.198	1.963—11 0.313	1.414—11 0.250	1.222—11 0.328
3.167—11 0.574	3.282—11 0.278	3.278—11 0.190	2.707—11 0.117	3.095—11 0.372	2.209—12 0.140
1.300—10 0.363	1.055—10 0.194	8.386—11 0.136	1.437—10 0.518	4.580—11 0.194	2.368—11 0.269
6.346—10 0.220	4.690—10 0.174	3.615—10 0.292	1.554—10 0.252	8.014—11 0.273	2.642—11 0.166
1.204—8 0.303	3.136—9 0.152	1.392—9 0.254	2.908—10 0.200	3.076—10 0.550	5.571—11 0.180
2.414—8 0.652	2.672—8 0.100	2.985—8 0.159	2.385—9 0.221	2.514—10 0.159	2.776—10 0.468
2.758—10 0.102	9.650—10 0.196	2.818—9 0.195	1.551—8 0.216	1.410—9 0.284	1.792—10 0.228

TABLE 6. ITF FOR THE CASE: ZENITH ANGLE OF RECEPTION POINT $\vartheta = 40°$; SEMI ANGLE OF TAPER OF RECEIVER $\gamma_s = 2.5$; INDICATRIX OF STATION 347; $\sigma = 0.05$ ln/m; $\Delta = 1$, $R_c = 100$ m, N = 15,000; $c_1 = 0.040$; $\sigma = 0.222$ m/ns

Time Interval Ω	450—455	455—460	460—470	470—480	480—490	490—500	500—525	525—550	550—575	575—600
140	1.025—13 0,535	2.150—13 0,394	7,129—13 0,395	6.274—13 0,212	3.471—12 0.463	1.340—12 0,421	9.167—13 0,256	1.647—12 0.430	1.730—12 0.364	1.204—12 0.362
150	1.400—14 0.159	2.329—13 0,192	7,661—13 0.373	1.186—12 0.588	1.356—12 0.385	3,090—12 0.578	8.850—13 0.159	8.563—13 0,167	2.583—12 0,641	7.014—13 0,170
160	2.849—13 0,788	6.479—13 0.394	1,301—12 0,300	5.384—12 0.790	1.880—12 0.190	2.896—12 0,358	1.506—12 0,148	2.341—12 0.284	2.468—12 0.497	1.248—12 0,354
170	562—13 0,461	7.868—13 0.238	1.698—12 0.209		4.828—12 0.250	2.764—12 0.262	2.645—12 0.178	2.118—12 0.223	1.820—12 0.199	2.754—12 0.495
180	1.877—12 0,520	1.806—12 0.194	7.791—12 0,401	1,029—11 0,364		4.041—12 0,154	7.340—12 0.366	2.919—12 0.289	1.701—12 0,166	
190	2.532—12 0,446	1.198—11 0.404	8.877—12 0.132	2.027—11 0.353	1.726—11 0,412	1.116—11 0,443		5.707—12 0.228	3.903—12 0.416	
200		2.463—11 0.158	5.935—11 0,443	5.536—11 0.289	922—11 0,087	2.550—11 0,411		1.683—11 0.549	7.751—12 0,270	
210	1.991—10 0.346	3.604—10 0,477	4.496—10 0.435	2.819—10 0.384	3.499—11 0.142	4.783—11 0.176	4.454—11 0.210	1.902—11 0.262	1.690—11 0,496	
220	3.423—8 0,256	1.827—8 0.224	2.513—9 0.173	8.975—10 0.458	3.870—10 0.280		6.935—11 0.118		3.130—11 0.364	2.005—11 0.252
230	2.728—10 0.225	1.014—9 0.216	9.028—9 0,451	1.243—8 0.121	9.230—9 0.172	1.441—9 0.271	2.177—10 0.255	6.364—11 0.131	4.261—11 0.198	2.629—11 0.199

TABLE 7. ITF FOR THE CASE: ZENITH ANGLE OF RECEPTION POINT $\theta = 50°$; SEMI ANGLE OF TAPER OF RECEIVER $\gamma_s = 2.5$; INDICATRIX OF STATION 347; $\sigma = 0.05$ 1n/m; $\Lambda = 1$, $R_c = 100$ m, N = 12,000; $c_1 = 0.025$; $\nu = 0.222$ m/ns

Time. interval / Ω	450—452	452—454	454—456	456—458	458—460	460—470	470—480	480—500	500—525	525—550
140	2,123—15 0,396	6 102—15 0,269	1,353—14 0,140	2,183—14 0,129	2,480—14 0,148	8,411—14 0,188	3.725—13 0.383	5,010—13 0.375	4,355—13 0,183	6,141—13 0,174
150	3,561—15 0,356	1.373—14 0,152	2,836—14 0,321	3,107—14 0,194	3.801—14 0,106	2.008—13 0,559	3,391—13 0,478	1.339—12 0,640	4.625—13 0,180	5.956—13 0,154
160	4.638—15 0,333	1.810—14 0.162	2.708—14 0,120	6,827—14 0,304	5,887—14 0,217	2,787—13 0,433	3,750—13 0.261		6.675—13 0,182	7,002—13 0.147

Time Interval / Ω	450—452	452 454	454—456	456 - 458	458—460	460—470	470—480	480—500	500—525	525—550
170	1833—15 0 331	2,771—14 0.133	6,049—14 0,214	1,206—13 0,506	9 472—14 0,158	3 666—13 0,380	6.527—13 0 318	1.570—12 0,315	9,259—13 0,204	1.516—12 0,446
180	1 633—14 0 244	4.032—14 0 118	1,083—13 0,163	1.437—13 0,149	2.900—13 0.297	7.836—13 0 337	1.056—12 0,196	3 669—12 0,546	1 248—12 0.123	1,088—12 0,112
190	3 851—14 0.176	1,927—13 0.311	3.599—13 0,319	1,213—12 0,464	6 698—13 0.190	1 422—12 0.254	3.888—12 0.432	3.180—12 0.246	2.208—12 0.111	3,390—12 0,297
200	1.242—13 0.138	4 480—13 0,141	7.670—13 0.102	1 683—12 0,322	4,075—12 0.449	5,300—12 0.271	4 922—12 0,203	8,471—12 0.370	4 343—12 0,153	7.491—12 0.308
210	8 994—13 0,303	1.991—12 0.094		7,113—12 0,201	6,698—12 0,197	1 551—11 0.279	2 204—11 0.437	1 766—11 0.188	1 226—11 0.209	1 387—11 0.263
220	1.362—11 0 217	3 336—11 0.194		5,058—11 0.115	5 197—11 0.266	1 123—10 0,285	9.729—11 0.249	5,927—11 0.276	4 164—11 0,355	2.173—11 0,207
230	5 840—9 0,150	9 959—9 0 170		1,038—8 0.321	1.278—8 0 466	3 805—9 0,295	8.875—10 0 401	5.116—10 0,346	8.544—11 0,210	4.683—11 0.135

TABLE 8. ITF FOR THE CASE: ZENITH ANGLE OF RECEPTION POINT θ = 0 °; SEMI ANGLE OF TAPER OF RECEIVER γ_s = 2.5; INDICATRIX OF STATION 347; σ = 0.123 1n/m; A = 1, R_c = 100 m, N = 15,000; c_1 = 0.0984 ν = 0.222 m/ns

Time interval / Ω	450–460	460–470	470–485	485–500	500–525	525–550	550–575	575–600	600–650	650–700
180	4.993—8 0.125	7.008—12 0.398	1.555—12 0.344	4.654—13 0.294			1.187—13 0.368	9.516—14 0.304	1.898—13 0.421	5.201—14 0.418
190	1.528—10 0.020		1.209—12 0.324	5.899—13 0.260	1.830—13 0.175	1.356—13 0.245	9.202—14 0.329	6.762—14 0.181		2.746—14 0.321
210	5.195—12 0.017	5.799—13 0.068	3.200—13 0.240	1.111—13 0.175	8.146—14 0.238	5.253—14 0.422	4.224—14 0.281	6.785—14 0.450		1.426—14 0.296
230	9.566—13 0.014	1.544—13 0.031	6.305—14 0.104	5.252—14 0.362	2.802—14 0.226	1.719—14 0.327	2.408—14 0.480	6.771—15 0.146		5.269—15 0.191
250	3.677—13 0.019	8.365—14 0.031	2.940—14 0.063	1.386—14 0.093	8.649—15 0.136	5.896—15 0.199	5.711—15 0.431	5.108—15 0.458	3.828—15 0.320	7.571—15 0.407
280	1.955—13 0.016	5.502—14 0.023	2.357—14 0.092	9.992—15 0.482	5.514—15 0.155	2.379—15 0.110	1.473—15 0.118	1.990—15 0.258	1.302—15 0.236	1.237—15 0.456

TABLE 9. ITF FOR THE CASE: ZENITH ANGLE OF RECEPTION POINT $\Theta = 10°$; SEMI ANGLE OF TAPER OF RECEIVER $\gamma_S = 2.5$; INDICATRIX OF STATION 347; $\sigma = 0.123$ln/m; $A = 1$, $R_c = 100$ m, N = 15,000; $c_1 = 0.0984$, $v = 0.222$ m/ns

Time Interval Ω	450—460	460—470	470—485	485—500	500—525	525—550	550—575	575—600	600—650	650—700
140	4.359—14 0.044	3.648—14 0.084	2.294—14 0,097	2.256—14 0.344	2.950—14 0.485		5.620—15 0.145		9.228—15 0.325	1.216—14 0.143
160	3.215—13 0.048	2.003—13 0.121	1.449—13 0.242	7.142—14 0.207	5.055—14 0.299	3.112—14 0.170	2.677—14 0.229	2.091—14 0.409	1.954—14 0.283	2.215—14 0.281
180	9.853—12 0.061	1.838—12 0.105	6.143—13 0.109	2.531—13 0.141	2.837—13 0.300	9.7—13 0.298	7.548—14 0.200	1.769—13 0.425		1.394—14 0.126
200	1.943—10 0.509	1.630—11 0.214	3,022—12 0.206	6.430—13 0.182		1.[illegible]—13	200—13 0.189	7.911—14 0.235	5.575—14 0.250	3.534—14 0.287
220	6.550—13 0.034	2.122—12 0.046	2.241—12 0.097	2.029—13 0,176	1.753—13 0.274	5.[illegible]—14 0.260	8.639—14 0.296	5.809—14 0.393	3.152—14 0.176	1.985—14 0.476
240	7.960—14 0.083	1.070—13 0.076	2.329—13 0.070	3.491—13 0.136	1.381—13 0.216	9.68—14 0.469	0.296 575—600	1.213—14 0.202	1.384—14 0.631	1.385—14 0.474

TABLE 10. ITF FOR THE CASE: ZENITH ANGLE OF RECEPTION POINT $\vartheta = 20°$; SEMI ANGLE OF TAPER OF RECEIVER $\gamma_s = 2.5$; INDICATRIX OF STATION 347; $\sigma = 0.123$ ln/m; $A = 1$, $R_c = 100$ m, N = 15,000; $c_1 = 0.0984$, $v = 0.222$ m/ns

Time interval / Ω	450–460	460–470	470–485	485–500	0.284	525–550	550–575	575–600	600–650	650–700
230	1 681—13 0 066	5 234—13 0 249	6,437—13 0,178	2 276—12 0,564	500—525 4,449—13	1,724—13 0.245	1.437—13 0.281		2 703—14 0.167	3 733—14 0 391
240	4.786—14 0.083	1.374—13 0,203	2,210—13 0,377	1,862—13 0,173	0.257 2.911—13	7 256—14 0 283	4.037—14 0.233	3.916—14 0.282	1.858—14 0.164	
250	1.890—14 0.069	5.709—14 0.336	5.719—14 0,181	6.341—14 0,129	0,127 8.331—14	8.020—14 0.104	2.929—14 0.355	2.058—14 0 260		2 704—14 0.466
260	8,577—15 0.073	2.212—14 0.200	2 866—14 0,223		0,149 5.255—14	3.921 —14 0.174	2.922—14 0 153	1.328—14 0.204	6.575—15 0.211	1.357—14 0.342
280	3.424—15 0.080	0.010—14 0.404	7,835—15 0.129	1.598—14 0,401	0.461 1 344—14	5 603—15 0.133	8 068—15 0.259	5.109—15 0.101	4.220—15 0,119	3.044—15 0.252

TABLE 11. ITF FOR THE CASE: ZENITH ANGLE OF RECEPTION POINT $\vartheta = 30°$; SEMI ANGLE OF TAPER OF RECEIVER $\gamma_s = 2.5$; INDICATRIX OF STATION 347; $\sigma = 0.123$ ln/m; $\Lambda = 1$, $R_c = 100$ m, N = 15,000; $c_1 = 0.0984$; $\nu = 0.222$ m/ns

Time interval / Ω	450–460	460–470	470–485	485–500	500–525	525–550	550–575	575–600	600–650	650–700
150	1.578—15 0.106	5.271—15 0.214	6.836—15 0.263	5.320—15 0.246	5.612—15 0.305	3.758—15 0.244	6.897—15 0.547			1.735—15 0.259
180	2.032—14 0.070		6.871—14 0.357	5.099—14 0.449	7.272—14 0.456	2.333—14 0.468	1.485—14 0.350	1.705—14 0.303	3.169—15 0.423	7.345—15 0.205
230	3.433—13 0.243	9.472—13 0.220	1.813—12 0.188	3.316—12 0.318	2.572—12 0.574	1.556—13 0.130	1.417—13 0.264	9.128—14 0.374	9.217—15 0.132	5.844—14 0.405
250	1.438—14 0.160	3.626—14 0.086	7.015—14 0.138	5.733—14 0.097	1.320—13 0.268		7.860—14 0.222	7.649—14 0.487	8.960—14 0.294	4.043—14 0.367
280	1.515—15 0.293	3.963—15 0.112	7.026—15 0.226	6.423—15 0.139	7.806—15 0.203	6.877—15 0.193		8.951—15 0.343	1.061—13 0.356	5.093—15 0.146

TABLE 12. ITF FOR THE CASE: ZENITH ANGLE OF RECEPTION POINT $\theta = 40°$; SEMI ANGLE OF TAPER OF RECEIVER $\gamma_s = 2.5$; INDICATRIX OF STATION 347; $\sigma = 0.123$ 1n/m; $\Lambda = 1$, $R_c = 100$ m, N = 15,000; $c_1 = 0.0964$ $\nu = 0.222$ m/ns

Time interval / Ω	450 -460	460–470	470—485	485—500	500 - 525	525—550	550 -575	575—600	600—650	650—700
150	3.915—16 0.230	1.350—15 0.152	2.010—15 0.154	1.486—15 0.132	1.491—15 0.159	1 248—15 0.135	1 228—15 0.276	1 467—15 0.249		1.141—15 0.431
180	4.025—15 0.260	9.151—15 0 184	8.930—15 0 137	9.203—15 0.265	8.813—15 0 273	4.422—15 0 184	7.092—15 0.358	9.480—15 0.405	9 967—15 0.394	3.680—15 0.185
230	1 141—12 0,227	1 575—11 0.575	1.310—11 0.184	2.457—12 0.157	7.365—13 0.357	1 677—13 0.172	1 412—13 0 328	1 611—13 0 461	6.001—14 0.272	
280	1.476—14 0.147	5.407—14 0.110	9.712—14 0.117	2.377—13 0.393	4.506—13 0 486	5.161—13 0.224	3.036—13 0.260	1.682—13 0.307	1 456—13 0.498	4.080—14 0.208
250	7.400—16 0 124	3.117—15 0.135	4.231—15 0.112	8 132—15 0.198		8.053—15 0 210	1.043—14 0 219	5 328—14 0 490	1.467—14 0.356	1 702—14 0.233

TABLE 13. ITF FOR THE CASE: ZENITH ANGLE OF RECEPTION POINT $\theta = 50°$; SEMI ANGLE OF TAPER OF RECEIVER $\gamma_s = 2.5$; INDICATRIX OF STATION 347; $\sigma = 0.123$ 1n/m; $A = 1$, $R_c = 100$ m, $N = 15,000$; $c_1 = 0.0984$ $v = 0.222$ m/ns

Time Interval Ω	450—460	460—470	470—485	485—500	500—525	525—550	550—575	575—600	600—650	650—700
150	7.099—17 0.119	5.011—16 0.238	7.072—16 0.205	5.119—16 0.104	6.617—16 0.168	5.254—16 0.116	1.293—15 0.367	3.360—16 0.246	9.795—16 0.466	6.279—16 0.272
180	1.868—15 0.649	1.998—15 0.258	2.551—15 0.206	2.534—15 0.190	1.773—15 0.156	2.179—15 0.186	9.003—15 0.578	1.919—15 0.478		2.556—15 0.278
230	3.946—11 0.336	1.439—12 0.360	1.594—12 0.312	3.292—13 0.190	2.406—13 0.170	1.268—13 0.278	4.366—14 0.158	3.924—14 0.227		8.259—14 0.640
250	4.055—14 0.280	1.006—13 0.101	2.506—13 0.172	4.725—13 0.272	1.090—12 0.207	1.105—12 0.333	2.037—13 0.138	9.51—13 0.543	1.363—13 0.416	1.777—13 0.443
280	7.364—16 0.233	2.652—15 0.136	4.239—15 0.108	5.669—15 0.124	1.156—14 0.155	1.185—14 0.145	4.459—14 0.415	2.732—14 0.249	2.011—14 0.220	7.491—14 0.488

TABLE 14. ITF FOR THE CASE: ZENITH ANGLE OF RECEPTION POINT $\Theta = 0°$; SEMI ANGLE OF TAPER OF RECEIVER $\gamma_s = 2.5$; INDICATRIX OF STATION 347; $\sigma = 0.184$ 1n/m; $\Lambda = 1$, $R_c = 100$ m, $N = 15{,}000$; $c_1 = 0.15$; $v = 0.222$ m/ns

Time Interval / Ω	452—460	460—475	475—490	490—510	510—540	540—570	570—600	600—650	650—700	700—750
140	7.03—15 00071	4.32—16 0037	1.076—16 0.121	7.45—17 0072	1.397—18 0293	6.41—18 0303	4.39—18 0239	.	2.58—18 0167	3.83—18 033
150	1.77—14 00066	1.61—14 02	2.67—16 0218	1.13—16 0305	5—16 0315	8.1—17 0.213	8.38—17 0295	1.16—16 0309	3.87—17 0181	
160	5.—14 00098	4.85—15 0127	8.88—16 0224			1.93—16 0244	1.32—16 0215	1.46—16 0246		1.26—16 0355
170	1.82—13 00138		1.84—14 0189			2.29—16 0169	1.95—16 0428	1.32—16 0291	9.81—17 0289	6.5—17 0305
180	8.16—14 0167	1.02—14 0042	2.92—15 0191		1.3—15 0312	9.7—16 0492	5.32—16 04909	4.83—16 0462	3.11—16 0491	1.3—16 0424
190	3.1—13 00177	2	3.52—15 0.42		8.6—16 131	3.02—16 043	2.35—16 0364	3.1—16 04	1.13—16 027	7.84—17 0355
200	3.24—14 0223	2.47—14 0217	1.06—14 0324		42—16 1155	9.3—16 0432		2.45—16 0356	1.52—16 0497	1.18—16 0477

Time Interval / Ω	452—460	460—475	475—490	490—510	510—540	540—570	570—600	600—650	650—700	700—750
210	1.02—14 00072	7.04—16 00615	3.2—16 0369	1.66—16 0248	1.89—16 0252	1.25—16 0238	9.82—17 0226	5.1—17 0162		
220	4.10—15 000876	3.5—16 0041	1.11—16 005	1.06—16 0488	3.66—17 0228			6—17 0359	2.73—17 0362	
230	1.88—15 000919	2.17—16 00295	6—17 003	3.87—17 02	1.98—17 0195	2.39—17 022	2.28—17 0232	3.26—17 029	2.04—17 0557	2.63—17 036

TABLE 15. ITF FOR θ=10°, R_c = 100 m; σ = 0.184 ln/m; STATION 347; N = 15,000;

Time Interval Ω	452—460	460—475	475—490	490—510	510—540	540—570	570—600	600—630	630—700	700—750
140	0175—16 0039	6.39—17 00685	3.25—17 0086	2.069—17 0125	.145—17 0156	1.967—17 0437	1.168—17 0383	1.54—17 0329	1.69—17 0291	
150	2.42—16 00455	1.18—16 00502	7.39—17 0171	4.52—17 0282	4.39—17 0266		1.87—17 0214	2.86—17 0252		
160	6.86—16 0042	3.5—16 0099	1.52—16 0138	8.68—17 0157			8.29—17 0477	8.42—17 0259	3.98—17 0184	
170	2.84—15 00531	8.95—16 0119	6.5—16 045	3.14—16 0281	1.8—16 0342	2.35—16 0358	1.4—16 3479		.04—16 0263	8.26— 021
180	2.34—14 0066	4.96—15 0255	1.86—15 0239			3.66—16 0293	1.356—16 0236	—16 03	3.82—16 454	5.49 019
190	2.53—12 0248	1.247—14 0073	3.89—15 0241		6.57—16 0321	4.97—16 0231		1.35— 0158		8.3— 0203
200	.27—13 018	9.36—14 019		8.45—16 0138			2.65—16 0351	1.91 0364		0.65
210	9.53—14 0086	1.14—14 0106	1.14—15 0204	5.32—16 0259	6.59—16 0456	3.1—16 0271	4.43—16 0312	2.31—16 0284	3.5—16 039	
220	1.37—15 00336	4.54—14 00654	7.42—16 01	3.18—16 0295	2—16 0124			1.00—16 0206		9.2 0252
230	4.10—16 00361	7.1—16 00855	1.15—15 00528	8.92—17 0097	3.2—16 0202		5.92—17 0294	1.3—16 0289		4.68— 0222

/155

TABLE 16. ITF FOR $\theta = 20°$, R_c = 100 m; σ = 0.184 ln/m; STATION 347; N = 15,000; c_1 = 0.15

Time Interval / Ω	452—460	460—475	475—490	490—510	510—540	540—570	570—600	600—650	650—700	700—750
140	1.58—17 0076	2.06—17 0077	1.12—17 0093	1.33—17 0203		6.51—18 011	9.89—18 0295	7.66—18 02596	3.91—18 0252	
150	3.58—17 0295	3.7—17 0275	2.55—17 0125	2.01—17 0203	1.1—17 013	9.43—18 0217		1.37—17 044		1.27—17 0445
160	7.44—17 0663	7.18—17 0673	7.55—17 0387	2.77—17 0141	1.8—17 028	2.3—17 0252	1.27—17 0308	1.57—17 0496		9.—18 0223
170	2.23—15 0057	2.91—15 001	1.26—16 018	9.5—17 0222	5.65—17 0248	6.85—17 0358		7.2—17 0449	2.38—17 0202	3.34—17 0322
180	9.18—16 0063	7.77—16 0139		2.11— 023		4.46—16 0475	2.94—16 0487	8.45—17 0217	5.4—16 0366	3.87—17 0272
190	7.52—15 0072	3.06—15 0187	1.49—15 0297	8.42—16 021	5.25—16 0286	1.87—16 018	2.065—16 0393		3.81—17 0147	5.05—17 0371
200	7.28—15 032	1.51—14 0415	4.84—15 0259	1.134—15 0178	1.79—16 0128		2.08—16 0209	1.62—16 0202	5.43—17 0179	6.41—17 0262
210	2.2—15 0121	3.23—14 018		1.13—15 0131	7.72—16 0246	3.9—16 025	3.68—16 03	1.46—16 0182	1.003—16 0263	1.76—16 34
220	1.7—16 09	9.—15 021	2.63—15 0292	1.41—15 0258	9.29—16 0657	5.59—16 0333	4.56—16 0399	1.81—16 0189	1.08—16 0217	1.88—16 380
230	2.17—15 0076	7.59—16 018	2.15—15 039	1.81—15 0262	1.79—15 0298	1.112—16 0165	4.84—17 0203			7.6—17 0279

TABLE 17 TTF FOR θ = 30°, R_c = 100 m; σ = 0.184 ln/m; STATION 347; N = 15,000;

Time Interval Ω	452 – 460	460 – 475	475 – 490	490 – 510	510 – 540	540 – 570	570 – 600	600 – 630	630 – 700	700 – 750
140	8.65 – 17 0111	1.41 – 16 0159	1.1 – 16 0372	6.67 – 17 0462	5.23 – 17 0344	7.02 – 17 0365	8.32 – 17 0318	7.01 – 17 053	2.37 – 17 0176	5.93 – 17 0564
150	4.65 – 18 0181	7.75 – 18 0108	7.64 – 18 9	5.3 – 18 0281	2.93 – 18 0163	1.95 – 18 0163	3.45 – 18 0305	3.25 – 18 0188	1.88 – 18 0205	
160	6.66 – 18 0092	1.32 – 17 0116	8.76 – 18 0136	7.06 – 18 019	3.16 – 18 0145	4.32 – 18 0262		1.29 – 18 0183		
210	1.24 – 17 0079	2.15 – 17 0099	1.54 – 17 0214	1.111 – 17 0235	6.6 – 18 016	1.098 – 17 037	1.11 – 17 0355	1.37 – 17 0275		
220	3.35 – 17 0113	4.53 – 17 0128	3.6 – 17 0266	1.68 – 17 0116	9.41 – 18 0125	3.41 – 17 0478	2.77 – 17 0279	2.57 – 17 0273	1.48 – 17 0448	
230	8.65 – 17 0111	1.41 – 16 0169	1.1 – 16 0372	6.66 – 17 0462	5.23 – 17 0344	7.02 – 17 0365	8.32 – 17 0318	7.01 – 17 053	9.37 – 17 0176	5.93 – 17 0564

TABLE 18. ITF FOR $\theta = 50°$, R_c = 100 m; σ = 0.184 ln/m; STATION 347; N = 15,000;

Time Interval / Ω	452–460	460–475	475–490	490–510	510–540	540–570	570–600	600–650	650–700	700–750
140	1.073–18 0133	[illegible] 011	2.23–18 0121	2.15–18 0103	2.61–18 0297	1.775–18 0161	2.85–18 035	1.4–18 0164	1.49–18 0135	[illegible] 0249
150	2.72–18 0179	6.04–18 0197	5.09–18 0101	5.89–18 [illegible]	4.41–18 0172	4.65–18 0231	2.75–18 016			
160	4.84–18 0142	1.05–17 0098	1.02–17 014[illegible]	1.05–17 0237	6.94–18 0173	1.16–17 040	8.4–18 0232	5.65–18 0172		
180	1.13–17 0115	2.28–17 0082	2.28–17 0125	[illegible] 022	2.007–17 0396	2.35–17 0296	1.21–17 0286	1.14–17 0192		
190	3.63–17 0136	6.4–17 0212	4.75–17 0149	4.18–17 0275	4.4–17 0235	4.63–17 0275		2.27–17 0174	1.68–17 0264	
200	1.66–16 0135	1.93–16 0205	1.2–16 [illegible]		8.9–17 0152	8.31–17 180		5.–17 0257	2.34–17 019	
210	1.62–15 [illegible]	8.51–16 0161	4.42–16 0179	3.96–16 0186		1.17–16 0201	1.25–16 0204	9.66–17 0232		9.2–17 0299
220	1.1–15 0189	1.54–14 0253	1.55–11 0197	2.51–17 0124		5.25–16 0225		3.03–16 0295	1.25–16 01997	6.6–17 017

TABLE 19.

ITF for $\Theta = 50°$, $R_C = 50$ м, $\sigma = 0{,}123$ in/м, $N = 15\,000$, $C_t = 0{,}0984$, ST. 347

Time Interval Ω	—240	240—260	260—280	280—300	300—325	325—350	350—375	375—400	400—425	425—400
230	8.176—9 0.163	5 924—10 0.322	5,80—11 0.177	3.075—11 0 192	1 541—11 0 161	1 576—11 0 331	7 9 2—12 0 205	3.882—12 0.265	2 182—12 0.131	1 [illegible]—12 0.197
240	1.22—9 0.281	5 114—9 0.171	1.504—10 0.119	9 658—11 0 279	2 752—11 0.256	1 647—11 0 191		6 20—12 0 183	3 [illegible]42—12 0 126	3.56—12 0 237
250	1 075—10 0 148		.73—9 .223	2.314—10 0 304	4,91—11 0 170	4 935—11 0 242	1 16—11 0 160	8 54—12 0 257	7 168—12 0.229	1.46—12 0 170
260	2.02—11 0.159	1 315—10 0.150	5.19—10 0 284	9 51—10 0.198	8 60—11 0 082	5 142—11 0 261	1 80—11 0 136	1 548—11 0 307	1 128—11 0 [illegible]82	3.80—12 0.150
280	2.137—12 0.147	9.762—12 0 209	2,921—11 0 206	2.183—11 0 125	5 812—11 0.158	9 582—11 0 129	5 76—11 0 [illegible]51	2.78—11 0 352		1 01—11 0.366

TABLE 20.

ITF for $\Theta = 50°$, $R_C = 50$ м, $\sigma = 0{,}123$ in/м, $N = 15\,000$, $C_t = 0{,}0984$, ST387.

Time Interval Ω	—240	240—260	260—280	280—300	300—325	325—350	350—375	375—400	400—425	425—450
230	4,596—9 0.256	9.88—11 0.303	1 823—11 0 377	4,43—12 0.498	382—13 0 [illegible]34	[illegible]48—12 0 420	5 [illegible]97—13 0 [illegible]62	7 70—13 0 383		3 047—13 0.443
240	2.59—9 0 366	2.516—9 0.126	6.48—11 0.412	1.06—11 0.366	2 33—12 0 [illegible]34	7 [illegible] 0 [illegible]21			1 67—13 0 389	
250	7.59—11 0 252	7,125—10 0.193	2 512—9 0.338	3.07—11 0.244	6 09—12 0 215		1 [illegible]51—13 0 [illegible]456	1 61—12 0 [illegible]564	6 84—13 0 421	
260		7.53—11 0 177	4.67—10 0.344	1,02—9 0.448		[illegible] 0 [illegible]232			1 621—12 0 406	581—12 0 235
280	6.25—13 0.213	7 43—12 0 368	2 98—11 0 334	2.696—11 0.364	3 80—11 2 [illegible]19	1 [illegible]234—11 0 [illegible]268	1 [illegible]61—11 0 237	[illegible]882—11 1 [illegible]89	1 240—11 0 [illegible]351	

/161

TABLE 21. ITF FOR $\theta = 50°$, $R_c = 50$ m; $\sigma = 0.123$ ln/m; STATION 740: N = 15,000; $c_1 = 0.0984$

Time Interval / Ω	—240	240—260	260—280	280—300	[illegible]	325—350	350—375	[illegible]	[illegible]	425—450
[illegible]	2.83—10 0.092	5.76—11 0.407	1.946—11 0.273	[illegible] 0.215	[illegible] 0.294	[illegible] 0.476	2.87—12 0.451	[illegible] 0.252		
[illegible]	3.91—10 0.182	1.334—10 0.193	5.51—11 0.285	1.437—11 0.462		[illegible]	1.00—12 0.477		[illegible] 0.345	

Time Interval / Ω	—240	240—260	280—300	260—280	300—325	325—350	350—375	375—400	400—425	425—450
250	1.43—10 0.208	1.33—9 0.114	1.14—10 0.238	3.22—11 0.190	1.34—11 0.246	5.624—12 0.271	5.464—12 0.451	1.41—12 0.269		
260	1.57—11 0.126	5.81—10 0.283	5.62—10 0.185	7.29—11 0.106	2.51—11 0.165	1.92—11 0.320	6.000—12 0.417	3.63—12 0.292		
280	1.244—12 0.419	1.02—11 0.240	[illegible] 0.202		1.20—10 0.268	5.37—11 0.271	2.33—11 0.228		1.185—11 0.357	

TABLE 22.

ITF for $\Theta = 50°$, $R_c = 50$ м. $\sigma = 0.123$ in м, $N = 15\,000$, $C_t = 0.0984$, Sr. B.S.

Time Interval / Ω	—240	240—260	260—280	280—300	300—325	325—350	350—375	375—400	400—425	425—450
230	6.338—10 0.196	3.014—12 0.346	2.201—13 0.264	4.019—14 0.229	1.910—14 0.343	4.340—15 0.184		1.025—15 0.195	2.097—15 0.327	
240	2.938—10 0.132	4.516—10 0.095	1.452—12 0.190	1.544—13 0.210	5.570—14 0.191	8.861—15 0.207		1.684—15 0.519	2.264—15 0.332	1.628—15 0.355
250		7.080—11 0.189	5.00—10 0.416	1.489—12 0.151	1.402—13 0.265	5.687—14 0.499		4.957—15 0.462		3.164—15 0.455
260	3.855—12 0.592	3.2—12 0.551	4.719—11 0.376	1.684—13 0.192	3.015—13 0.436	1.[illegible]—13 0.173		1.80[illegible]—14 0.50	[illegible]—14 0.496	
280		8.431—14 0.193		1.219—12 0.366	1.347—12 0.783	[illegible]—11 0.[illegible]	1.352—13 0.140	7.226—[illegible] 0.150	1.361—13 0.294	7.84[illegible] 0.262

TABLE 23.

ITF for $\Theta = 0°$, $R_c = 50$ м. $\sigma = 0.184$ in м, $N = 12\,000$, $C_t = 0.15$, Sr. 347.

Time Interval / Ω	—230	230—240	240—250	250—260	260—270	270—280	280—290	300—325	325—350	350—400
180	4.155—6 0.051	3.775—10 0.542	4.751—11 0.472	1.038—11 0.424	1.089—11 0.294		3.028—12 0.355			[illegible]48 0.2[illegible]
190	1.320—8 0.0132		3.346—11 0.298	8.722—12 0.167	7.342—12 0.280	7.968—12 0.368	3.352—12 0.339	3.297—12 0.347	1.01—12 0.228	6.[illegible]—13 0.254
200	1.637—9 0.012	2.225—10 0.470	1.676—11 0.161	5.41—12 0.128	6.468—12 0.271		4.185—12 0.365	2.179—12 0.275	2.055—12 0.185	7.63—13 0.197
210	4.575—10 0.014	3.775—11 0.085	1.015—11 0.207	4.678—12 0.276		2.723—12 0.261	1.974—12 0.338	1.032—12 0.280	8.568—13 0.304	4.534—13 0.169
239	8.94—11 0.031	1.044—11 0.057	3.541—12 0.146	1.569—12 0.139	9.925—13 0.266	6.810—13 0.223	0.441	7.689—13 0.165	[illegible]—13 [illegible]	4.791—13 0.258

TABLE 24. ITF for $\theta=0°$, $R_c=50$ м, $\sigma=0.184$ ln м, N = 15 000, $C_1=0.15$, Sr. 387.

Time Interval Ω	—230	230—240	240—260	260—280	280—300	300—325	325—350	350—375	375—400	400—450
180	1.791—5 0.419	2.418—10 0.247	1.362—11 0.372	9.430—13 0.286		8.56—14 0.258		6.451—14 0.498	3.818—14 0.366	2.928—14 0.421
190	3.114—8 0.037	1.80—10 0.227	1.154—11 0.338	5.70—13 0.227		7.12—14 0.223	8.93—14 0.453	4.990—14 0.310		
200	2.75—9 0.046	1.01—9 0.728	2.185—11 0.414	1.65—12 0.411	5.74—13 0.161	2.9—13 0.488	1.174—13 0.496	8.481—14 0.426		
210	6.56—10 0.071	1.40—10 0.346	2.42—11 0.512		2.28—13 0.187	2.151—13 0.432	9.19—14 0.521	4.77—14 0.353	1.512—14 0.359	3.858—14 0.313
230	8.55—11 0.027	2.482—11 0.174	6.6—12 0.341		3.08—13 0.253	1.88—13 0.223		1.45—14 0.231	2.572—14 0.254	2.79—14 0.433

TABLE 25. ITF for $\theta=0°$, $R_c=50$ м, $\sigma=0.184$ ln м, N = 15 000, $C_1=0.15$, St740.

Time Interval Ω	230	230—240	240—260	260—280	280—300	300—325	325—350	350—375	375—400	400—450
180	0.0[illegible]	0.2[illegible]	0.281	0.806	1.395—12 0.248	8.81—13 0.245	2.52—13 0.209	1.76—13 0.322	2.352—13 0.495	1.148—13 0.426
190	0.0[illegible]	0.332	0.131	0.197	0.262	0.321	3.9[illegible]—13 0.337	4.0—13 0.528	1.05—13 0.251	1.152—13 0.403
200	6.22—9 0.026	2.41—10 0.154	3.22—11 0.214		1.15—12 0.172		5.33—13 0.374	6.84—13 0.358	1.934—13 0.509	1.537—13 0.374
210	1.95—10 0.026	7.03—11 0.111	1.47—11 0.133	7.05—12 0.213	1.015—12 0.187	1.273—12 0.338	1.017—12 0.492		1.798—13 0.519	
220	5.32—11 0.019	1.52—11 0.261	4.385—12 0.2[illegible]	1.85—12 0.[illegible]30		3.71—13 0.264	3.706—13 0.195		2.856—13 0.392	2.667—13 0.479

TABLE 26. ITF FOR $\theta = 0°$, $R_c = 50$ m; $\sigma = 0.184$ ln/m; STATION B.S; N = 15,000; $c_1 = 0.15$

Time interval / Ω	—230	230—240	240—260	260—280	280—300	300—325	325—350	350—375	375—400	400—450
180	7.86—5 0.098	1.026—11 0.284	8.62—14 0.277	1.45—14 0.349	2.43—15 0.256		2.915—16 0.138	1.72—15 0.453	1.225—16 0.202	1.902—16 0.426
190	6.064—8 0.043	7.86—11 0.365	7.4—13 0.482	7.03—15 0.311	2.03—15 0.287				1.101—16 0.245	1.195—16 0.290
200										
210	7.86—10 0.05		1.53—12 0.336	1.97—14 0.206	7.35—15 0.370		2.43—16 0.113			2.74—16 0.494
230	1.232—10 0.204	1.76—11 0.368	6.56—13 0.131	1.02—13 0.371	1.396—14 0.473	1.696—15 0.218			1.509—15 0.457	

CONSIDERATION OF TEMPORAL CHARACTERISTICS OF EQUIPMENT IN EXPERIMENTAL STUDIES OF NONSTATIONARY LIGHT FIELDS

GOL'DIN, YU. A., PELEVIN, V. N.

Determination of Green's function of a nonstationary problem G(t) with experimental data can be simplified by selecting the corresponding measurements. It is shown that calculation of G(t) does not require knowledge of the temporal characteristics of individual elements of the measurement system. It is sufficient to determine the shape and amplitude of the "original pulse" f(t) in the work which contains all the information regarding temporal characteristics of the measurement system as a whole. The reception and recording units of the studied and reference pulses must be identical.

One of the methods for studying nonstationary light fields (NLF) making it possible to solve the task more generally is the method of determining Green's function G(t), that is, spatial-temporal distribution from a source yielding a δ-impulse in time [1,2]. The brightness sources used in the experimental studies emit impulses of finite duration, while the receiving-recording equipment has a finite frequency transmission band. It introduces distortion into the recorded temporal changes of brightness. As a result, the temporal course of signal P(t) recorded at a certain point differs from the unknown Green's function G(t).

The shape of the light impulse of the source $f_0(t)$, the impulse transitional function of the reception-recording equipment h(t), and the shape of the recorded impulse P(t) are linked to G(t) by the integral equation:

$$P(t) = \int\int f_0(t - \tau_2 - \tau_1) G(\tau_1) h(\tau_2) d\tau_1 d\tau_2 \qquad (1)$$

Solution to Equation (1) makes it possible to obtain G(t) in principle from experimental data.

This study (without concerning the methods for solving (1)) will examine how to simplify the task of determining G(t) by selecting the correct measurement plan.

P(t) is the result of the successive action of the impulse of the scattering medium source and the measurement system. If the medium and the measurement system are linear, then the final result, that is the amplitude and shape P(t),

does not depend on the sequence of actions [3]. It is natural that this assertion refers to the sequence of mathematical operations. It is impossible to experimentally permutate the order of passage by the impulse of the medium and the measurement system, since the light impulse is transformed into an electrical impulse in the photoreceiver at the inlet of the reception-recording system.

We will write:

$$P(t)=\int_0^t\left[\int_0^t f_0(t-\tau_2-\tau_1)G(\tau_1)d\tau_1\right]h(\tau_2)d\tau_2= \tag{2}$$

$$=\int_0^t\left[\int_0^t f_0(t-\tau_2-\tau_1)h(\tau_2)d\tau_2\right]G(\tau_1)d\tau_1$$

Taking into consideration (2), one can write

$$P(t)=\int_0^t f_1(t-\tau)G(\tau)d\tau, \tag{3}$$

$$f_1(t)=\int_0^t f_0(t-\tau)h(\tau)d\tau. \tag{4}$$

$f_1(t)$ is the source impulse recorded by the employed reception-recording system directly at the source outlet in the absence of a scattering medium. We will call $f_1(t)$ the original impulse of the measurement system. The original impulse contains all the information regarding the temporal characteristics of the measurement system as a whole. One can formally consider that the source emits the impulse $f_1(t)$, while the reception-recording system is ideal.

Expressions (3, 4) make it possible to draw a number of conclusions which are important for practice.

Finding G(t) by solving (1) does not require separate analysis of $f_0(t)$ and h(t). It is sufficient to determine the form and amplitude of the original impulse $f_1(t)$. Consequently in making measurements, one should record as the reference impulse not the impulse emitted by the source $f_0(t)$, but the original impulse of the system $f_1(t)$. The systems of reception and recording of the studied and reference impulse therefore must be identical.

The functions $f_0(t)$ and $h(t)$ are included in the expression which determines $f_1(t)$ equivalently. It is impossible to obtain a significant decrease in the duration $f_1(t)$, by only reducing $f_0(t)$ or $h(t)$. In fact, if for example, the duration of $h(t)$ is much greater than the duration of $f_0(t)$, then the appearance of $f_1(t)$ determines precisely $h(t)$. Further decrease in the duration $f_0(t)$ with preservation of $h(t)$ practically will not alter the appearance of $f_1(t)$. In this respect, it is expedient to make the duration of the source impulse and temporal resolution of the reception-recording system roughly equal.

Requirements for duration $f_1(t)$ are determined by the extent of $G(t)$ at the assigned level which must be recorded, and by the quantity of error in measuring the duration of the studied impulse at this level. In fact, with an increase in duration $f_1(t)$, the quantity of absolute error in determining the duration of the impulse $P(t)$ rises at the assigned level. With a certain duration $f_1(t)$, the quantity of error is compared with the quantity of differences in form $P(t)$ and $f_1(t)$. Information regarding the medium is completely lost and it is not possible to determine $G(t)$ from (1). Detailed study of the accuracy of transformation (3) depending on experimental errors were made in [2].

BIBLIOGRAPHY /168

1. Romanova, L. M. "Nonstationary Light Field in Turbid Media," Teoreticheskiye i prikladnyye problemy rasseyaniya sveta ["Theoretical and Applied Problems of Light Scattering"], Minsk, 1971.

2. Gol'din, Yu. A.; Gashko, V. A.; Karlsen, G. G.; Pelevin, V. N., and Shifrin, K. S. "Experimental Studies of Nonstationary Light Fields in the Ocean," in Gidrofizicheskiye i gidrooptricheskiye issledovaniya v Atlanticheskom i Tikhom okeanakh ["Hydrophysical and Hydro-optical Studies in the Atlantic and Pacific Oceans"], Nauka, Moscow, 1974.

3. Beletskiy, A. F. Osnovy teorii lineynykh elektricheskikh tsepey ["Fundamentals of the Theory of Linear Electrical Circuits"], Svyaz', 1967.

USE OF THE PROPERTIES OF THE SPATIAL STRUCTURE OF NONSTATIONARY LIGHT FIELD TO CONDUCT EXPERIMENTAL STUDIES. YU. A. GOL'DIN and V. N. PELEVIN /168

It is shown that properties of the spatial structure of a nonstationary light field can be used to reduce the experimental studies.

It was noted in publication [1], that the task of forming a nonstationary light field of scattering medium can be reduced in the general form to finding at different points of the given medium, the temporal distribution of brightness from the source which emits a narrow-directional light beam which is sufficiently short in time so that it can be interpreted as a δ-impulse, i.e., finding Green's function of the process G. Here we will examine the question of how one can reduce the number of measurements in studying the spatial structure of a nonstationary light field in an assigned medium, by using the ratios which link $G(\vec{r}, \vec{n}, t)$ for certain pairs of $\vec{r}$ and $\vec{n}$. The link of $G(\vec{r}, \vec{n}, t)$ for certain pairs of $\vec{r}$ and $\vec{n}$ can be obtained by using, first, the properties of symmetry of the light field structure, and secondly, the ratio of optical reciprocity. We will first examine the properties of symmetry.

In order to describe the position of the brightness meter and its orientation in relation to the source, we will introduce a coordinate system which is presented in Figure 1. The source is placed in the beginning of the coordinates. The original radiation of the source spreads in direction $\vec{n}_0$. The position of the detector is determined by the length of the radius-vector r, polar angle α and azimuth angle ϕ. The value $\alpha = 0°$ corresponds to direction $\vec{n}_0$. Orientation $\vec{n}_1$ is determined by the polar angle β and the azimuth angle ϕ. With $\beta = 0°$, the detector is aimed at the source. The value $\phi = 0°$ corresponds to the case where $\vec{n}_0$ and $\vec{n}_1$ lie in one plane, /169 while n_1 with $\beta < 180° - \alpha$ is aimed to the side from the axis of the original light beam.

There is axial symmetry of the structure of the field in relation to the axis of the light beam from the source. This means that $G(\vec{r}, \vec{n}, t)$ does not depend on the quantity ϕ. Therefore, with the assigned value $\vec{r}$, it is sufficient to make /170

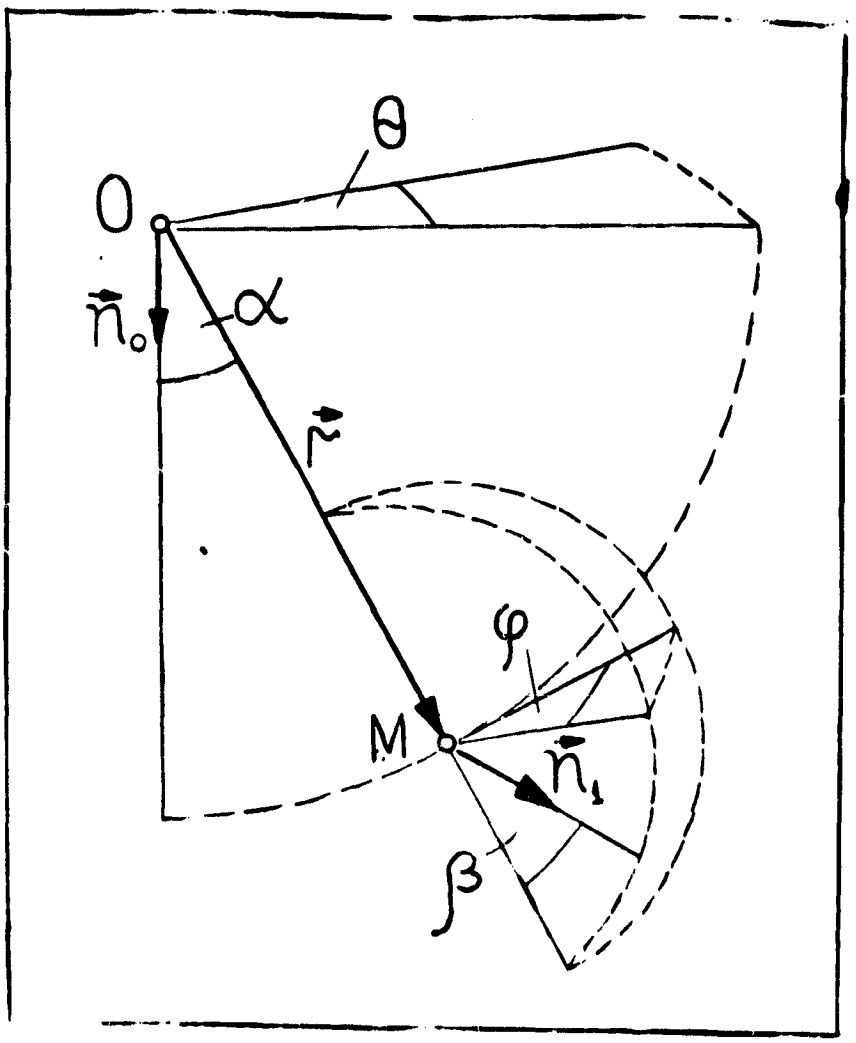

Figure 1. System of Coordinates Introduced to Describe Position of Brightness Meter-Receiver and its Orientation in Relation to Source. Explanation in text.

measurements for one random value of θ, changing the quantity α from 0° to 180°.

In addition, symmetry occurs in relation to the plane formed by $\vec{n}_0$ and $\vec{r}$, that is $G(r_1, \alpha_1, \beta_1, \varphi_1, t) = G(r_1, \alpha_1, \beta_1, -\varphi_1, t)$. As a consequence of this, it is sufficient to make measurements for the quantities β and ϕ which change in the same way as α, in limits from 0° to 180°.

Consideration for the properties of symmetry for α, β, and ϕ makes it possible to reduce the volume of measurements necessary for each medium made with assigned detail four-fold. The possibility of further reduction in the number of measurements is associated with the use of the ratio of optical reciprocity [2].

We will formulate a theorem for optical reciprocity of the NLF case as follows: in a stationary medium, the value of Green's function at point $\vec{r}_1$ in direction $\vec{n}_1$ at moment of time t_1 governed by point source located at point $\vec{r}_0$ and emitting impulse $\delta(t_0 - t)$ at moment of time t_0 in direction $\vec{n}_0$ coincides with the value of Green's function at point r_0, in direction $-\vec{n}_0$, at moment of time t_1, governed by a point source located at point $\vec{r}_1$ and emitting the impulse $\delta(t_0 - t)$ at moment of time t_0 in direction $-\vec{n}_1$.

$$G(\vec{r}_1, \vec{n}_1, t_1; \vec{r}_0, \vec{n}_0, t_0) = G(\vec{r}_0, -\vec{n}_0, t_1, \vec{r}_1, -\vec{n}_1, t_0)^{1)} \tag{1}$$

Ratio (1) is correct in a stationary linear medium which generally can be non-uniform and have a boundary of random shape. We will now obtain the first corollary we need for the theorem of optical reciprocity which makes it possible to reduce the number of measurements with unchanged position of the source. In deriving this corollary, we assume that the medium is uniform and boundless.

In a uniform boundless medium, Green's function does not depend on the position of the source-receiver system in space, but is only determined by the position of the receiver in relation to the source and the mutual orientation. Taking this into consideration, we transform correlation (1). The function in the right side of (1) corresponds to a case where the source is located at point $\vec{r}_1$ and emits in direction $-\vec{n}_1$. We will turn the source-receiver system by 180° around the middle of a segment

1)The arguments and parameters in the first group to the point with a comma refer to the receiver, the second--to the source.

which connects the source and the receiver. After this turn, the source will be at point $\vec{r}_0$. Then by two turns of the system around point $\vec{r}_0$ and around the straight line which connects the point $\vec{r}_0$ and $\vec{r}_1$, we superpose the direction of spread of /171
the original radiation source with $\vec{n}_0$. In this case the receiver will be located at a certain point $\vec{r}_2$ with direction $\vec{n}_2$.

We will write

$$G(r_0, -n_0, t_1, r_1, -n_1, t_0) = G(r_2, \bar{n}_2, t_1, r_0, n_0, t_0) \tag{2}$$

It follows from (1) and (2):

$$G(r_1, \bar{n}_1, t_1, r_0, n_0, t_0) = G(r_2, n_2, t_1, r_0, n_0, t_0) \tag{3}$$

$\bar{r}_1$ and r_2, as well as $\bar{n}_1$ and $\bar{n}_2$ are unequivocally linked. It is convenient to write this link by passing to the relative system of coordinates introduced above, associated with position and orientation of the source. In this system of coordinates, ratio (3) can be written in the form

$$G(r_1, \alpha_1, \beta_1, \varphi_1, t-t_0) = G(r_2, \alpha_2, \beta_2, \varphi_2, t-t_0) \tag{4}$$

with

$$r_1 = r_2, \ \alpha_1 = \beta_2, \ \beta_1 = \alpha_2, \ \varphi_1 = \varphi_2$$

Thus, in a uniform boundless medium, Green's function does not change with mutual permutation of the values for angles α and β.

Ratio (4) is also the unknown first consequence of the theorem of optical reciprocity.

In a real case of a limited medium, ratio (4) is fulfilled in that time interval t^*-t_0, where the influence of the boundaries on the appearance of Green's function is still not manifest, or is negligible. If measurements of the function $G(r, \alpha, \beta, \phi,$

$t-t_0$) are made in the indicated time interval, then it is sufficient to obtain data only for $\alpha \leq \beta$, or $\beta \leq \alpha$. Consequently, the necessary volume of measurements is reduced another two-fold.

The size of the time interval t^*-t_0 is defined by the position of the source in relation to the receiver, and their mutual orientation, as well as by the position and orientation of the entire source-receiver system in relation to the boundary of the medium.

Experimental studies of NLF in the sea were done from a surface ship. In this case, it was very difficult to place the entire source-receiver system at a great depth far from the boundary and to guarantee strict mutual correlation of the source and receiver and control of their operation and recording. In practice, either the source or the source and the receiver must be located at a small depth near the ship. In this case, the minimum influence of the boundary to the greatest moment in time can be guaranteed by an experimental plan in which the receiver and the source are located on a vertical bench, perpendicular to the water surface. In the case of a horizontal bench, traveling in parallel to the surface at a shallow depth, in the majority of /172 experimental siutations the value t^* will be significantly smaller.

Generally speaking, the question of the influence of boundaries with different position and orientation of the source-receiver system is very important. But study of this question is a subject of a special work. In this work, where we are only studying a case of uniform unlimited medium, measures must be taken for the maximum decrease in this influence. It is therefore necessary to use vertical optical bench and to limit the interval of values of angle α, such that the original light beam from the source located under the surface does not fall on the boundary.

The relationships obtained above refer to the functions $G(\bar{r}, \bar{n}, t; \bar{r}_0, \bar{n}_0, t_0)$. It is necessary to take into consideration that the experiment does not directly measure $G(\bar{r}, \bar{n}, t; \bar{r}_0, \bar{n}_0, t_0)$, but the received signal $P(\bar{r}_1, \bar{n}_1, t_1, S_1, \gamma_1; \bar{r}_0, \bar{n}_0, t_0, S_0, \gamma_0)$ whose quantity also depends on the "geometrical" parameters of the source and the receiver: S_0, γ_0, S_1, γ_1. We will consider that the emitting surface of the source and the input pupil of the receiver are round, while the beam patterns of the source and the receiver are axisymmetrical. Then all the correlations of symmetry are also maintained for $P(\bar{r}_1, \bar{n}_1, t_1, S_1, \gamma_1; \bar{r}_0, \bar{n}_0, t_0, S_0, \gamma_0)$. In this case, one should take for $\bar{r}_0$ and $\bar{r}_1$ the coordinates for the centers of the emitting surface and the input pupil of the receiver, and for $\bar{n}_0$ and $\bar{n}_1$, the directions of the beam axis and the visual field of the receiver respectively. We will further speak precisely in this sense of the position and orientation of the source and receiver.

The ratio of optical reciprocity (1) as applied to the functions $P(\bar{r}_1, \bar{n}_1, t_1, S_1, \gamma_1, \bar{r}_0, \bar{n}_0, t_0, S_0, \gamma_0)$ needs additional conditions. Taking into consideration the dependence of the function $P(\bar{r}_1, \bar{n}_1, t_1, S_1, \gamma_1; \bar{r}_0, \bar{n}_0, t_0, S_0, \gamma_0)$ on the "geometrical" parameters of the source and receiver, we obtain a second consequence of the theorem of optical reciprocity which links these functions.

In order to obtain $P(r_1, \bar{n}_1, t_1, S_1, \gamma_1, \bar{r}_0, \bar{n}_0, t_0, S_0, \gamma_0)$, it is necessary to integrate $G(\bar{r}_1, \bar{n}_1, t_1,; \bar{r}_0, \bar{n}_0, t_0)$ according to ar[illegible] the emitting surface of the source S_0 and the inlet pupil of the receiv[illegible] S_1, and according to directions in limits of the beam pattern of the source γ_0 and [illegible]ver γ_1.

We will write

$$\frac{R_0 K}{W_0^*} \int_{S_1} dS_1 \int_{\gamma_1} d\gamma_1 \int_{S_0} dS_0 \int_{\gamma_0} d\gamma_0 G(\bar{r}_1', \bar{n}'_1, t_1, \bar{r}'_0, \bar{n}'_0, t_0) = \tag{5}$$
$$= P(r_1, n_1, t_1, S_1, \gamma_1, r_0, n_0, t_0, S_0, \gamma_0),$$

where dS_1--element of the surface of the input pupil of the receiver located around the point with coordinate $\bar{r}_1'$, $d\gamma_1$--element of solid angle in visual field of receiver around the direction $\bar{n}_1'$, dS_0--element of emitting surface of source around a point with coordinate $\bar{r}_0$, $d\gamma_0$--element of solid angle in light beam from source around the direction $\bar{n}_0'$, B_0--brightness of source, and K--sensitivity of receiver.

We will also integrate the right and left parts of ratio (1). The integral from the left part coincides with (5). The integral from the right part can be written in the form:

$$\frac{B_0 K}{W_0} \int_{S_0} dS_0 \int_{\gamma_0} d\gamma_0 \int_{S_1} dS_1 \int_{\gamma_1} d\gamma_1 G(\bar{r}_0', -\bar{n}_0', t_0; \bar{r}_1', -\bar{n}_1', t_0) = \tag{6}$$
$$= P(r_0, -n_0, t_0, S_0, \gamma_0; r_1, -n_1, t_0, S_1\gamma_1)$$

where dS_0--element of surface of input pupil of receiver located around the point with coordinate $\bar{r}_0'$, $d\gamma_0$--element of solid angle in visual field of receiver around the direction $-\bar{n}_0$, dS_1--element of emitting surface of source around the point with coordinate $\bar{r}_1'$, and $d\gamma_1$--element of solid angle in light beam from source around direction $\bar{n}_1'$. In (6), the limits of integration over the areas and the beam patterns of the receiver and the source changed places in relation to (5).

After comparing (5) and (6), we obtain the unknown second corollary of the theorem of optical reciprocity.

The signal from the source with brightness B_0, area of emitting surface S_0, and original divergence of the beam γ_0 located at point $\bar{r}_0$ and directed to $\bar{n}_0$, recorded by the receiver with area of the input pupil S_1 and by the angle of the visual field γ_1 located at point $\bar{r}_1$ and directed towards $\bar{n}_1$, coincide with the signal from the source with the same brightness B_0 with area of the emitting surface S_1 and initial discrepancy of the beam γ_1 located at point $\bar{r}_1$ and directed towards $-\bar{n}_1$, recorded by /174

the detector with the same sensitivity K, area of the input pupil S_0 and angle of visual field γ_0, located at point $\bar{r}_0$ and directed towards $-\bar{n}_0$:

$$P(\bar{r}_1, \bar{n}_1, l_1, S_1, \gamma_1; \bar{r}_0, \bar{n}_0, l_0, S_0, \gamma_0) = \\ = P(\bar{r}_0, -\bar{n}_0, l_1, S_0, \gamma_0; \bar{r}_1, -\bar{n}_1, l_0, S_1, \gamma_1) \tag{7}$$

It is easy to understand the meaning of (7), if one takes into consideration that the ratio of optical reciprocity (1) is correct for any pair of points at the input pupil of the detector and the emitting surface of the source, and any pair of directions in limits of the angle of the visual field of the detector and the initial discrepancy of the beam. We will take the points lying on the boundaries and the extreme directions of the beam pattern. After the use of ratio (1), these points and directions change places. Therefore, the boundary of the emitting surface of the source becomes the boundary of one pupil of the detector; the boundary of the pupil of the detector becomes the boundary of the emitting surface of the source, while the beam pattern of the source and the detector also change places with a change in directions to the opposite.

Generally speaking, a similar link will also occur in the case of a source and detector with arbitrary shape of the emitting surface and input pupil, and arbitrary distribution of brightness and sensitivity by areas and angles.

From the corollaries 1 and 2 it is easy to obtain corollary 3 of the theorem of optical reciprocity. We will write corollary 3 in the relative system of coordinates presented in Figure 1.

In a uniform unlimited medium, the quantity of the function $P(r, \alpha, \beta, \phi, S, \gamma_1, l_0, S_0, \gamma_0)$ will not change during mutual permutation of angles α and β, on the condition that the area of the emitting surface of the source and the input pupil of the detector are equal, while the angular beam pattern of the source and the detector

coincide:

$$P(r_1, \alpha_1, \beta_1, \varphi_1, t, S_1, \gamma_1; t_0, S_0, \gamma_0) = P(r_2, \alpha_2, \beta_2, \varphi_2, t, S_1, \gamma_1; t_0, S_0, \gamma_0) \quad (8)$$

with $r_1 = r_2$, $\alpha_1 = \beta_2$, $\beta_1 = \alpha_2$, $\phi_1 = \phi_2$

and $S_0 = S_1$, $\gamma_0 = \gamma_1$.

The remarks regarding the quantity of the temporal interval $t^* - t_0$ in which (4) is fulfilled in the case of a limited medium and which were made after corollary 1 remained correct for (8). In practice, S_0 and S_1, as well as γ_0 and γ_1 usually differ. If the differences are not great, ratio (8) is approximately fulfilled. Where the /175 degree of approximation is on the magnitude of experimental errors, ratio (8) can be successfully used to reduce the number of measurements. The degree of approximation depends on the size of the "geometric" parameters and on the structure of the studied light field. Therefore the possibility of using correlation (8) must be determined separately for each specific case.

BIBLIOGRAPHY

1. Gol'din, Yu. A. Gashko, V. A.; Karlsen, G. G.; Pelevin, V. N.; Shifrin, K. S. "Experimental Studies of Nonstationary Light Fields in the Ocean", Gidrofizicheskiye i gidrooptycheskiye issledovaniya v Atlanticheskom i Tikhom okeanakh ("Hydrophysical and Hydrooptical Studies in the Atlantic and Pacific Oceans"), Moscow, Izd-vo, Nauka, 1974.
2. Kadomtsev, B. B. "Function of Influence in the Transport Theory of Radiant Energy", DAN SSSR, vol 113, No 3, 1957.

APPLICATION OF THE METHOD OF SUPERPOSITION TO COMPUTING GREEN'S FUNCTION OF A NONSTATIONARY LIGHT FIELD CREATED BY A BROAD DIRECTIONAL LIGHT BEAM

PELEVIN, V. N., GOL'DIN, YU. A., SHITOV, B. V.

Experimental data on the structure of a nonstationary light field of a narrow beam in the sea are used to calculate Green's functions for a field formed by an extended directed source which emits a δ-pulse in time.

It is noted in publication [1] that based on experimental data regarding the structure of a narrow beam created by a short-pulse laser in the sea, one can solve

different problems by the method of superposition. This publication presents examples of using this method to compute Green's functions of a nonstationary light field (NLF) formed in the sea by an infinitely extended, directed light source.

As an estimate, the calculations used experimental data regarding the structure of the NLF of a narrow beam in planes perpendicular to its axis that were obtained on the tenth trip of the scientific research vessel "Dmitriy Mendeleyev" in the Indian Ocean (1976). The measurement technique has been described in detail in [2]. It essentially consists of the following. A light pulse λ = 530 nm with duration at half-altitude $t_{0.9}$ = 3 - 4 ns, and energy 3 mJ, divergence 20' was generated by a laser on an AIG with Q-switched Na by an electro-optical DKDR valve and doubling of frequency in a nonlinear crystal $LiNbO_3$. The detector was ELU-FL01 which operates in a logarithmic regime with small signals. In a linear regime, the signal is recorded by photographing on the screen of a broad band oscillograph which has a transmission band of ~ 100 MHz. When a 160 m cable is used the temporal resolution of the equipment as a whole is characterized by duration of the original pulse of the system at level 0.5 comprising 6 ns (the original pulse of the system is called the /176
pulse recorded by the reception-recording equipment directly at the source outlet, without influence of the environment). The laser was placed on board the ship. In order to eliminate the influence of the surface, the beam was introduced into the water through a periscope device. The hermetically sealed detector was equipped with a cosine collector which permits determination of the temporal change in irradiance in the given point of the NLF according to the shape of the received signal.

Both the periscope device with laser, and the detector were placed on an outboard, vertically-oriented cable photometric bench which made it possible to change distance l between the point of beam entrance into the water and the detector illuminator in the range 0 - 150 m. The rotation angle of the laser beam to the vertical

α and angle of inclination of the detector axis to the vertical β were established remotely, according to the measurement program. The measurement plan is shown in Figure 1. Measurements were made in an optically u m layer of ocean water with the following characteristics: ε = 0.1δ m^{-1}; λ = 0.75.

Changes in α, β and l were made simultaneously during the measurements with preservation of the following ratios. $\alpha = \beta$(axes of the beam and their detector are parallel), $l = z/\cos\alpha$, where z is unchanged for one cycle of measurements. The mutual position and orientation of the source and the detector were thus changed so that the detector-irradiance gage seems to make a forward movement from the beam axis in a plane perpendicular to the axis which was located at distance z from the point of beam entrance into the water (see Figure 1b). Measurements were thus made of the distribution of irradiance in planes perpendicular to the axis of the narrow beam, with seven values of z from 25 to 100 m, with spacing 12.5 m. The values of the angles $\alpha = \beta$ changed discretely from 0° to 50° with spacing 2.5°.

The signal was very small at all levels with $\alpha = \beta > 50°$, therefore it may not be considered during superposition. The amplitude and shapes of the received signals $P_{\alpha,z}(t)$ were recorded.

The measured values of $P_{\alpha,z}(t)$ were used to compute the integral of superposition. In this case, the appropriate weights and temporal shifts in the signals in relation to each other were introduced. In order to compute the weights of temporal shifts, we will take into consideration that a broad pulse light beam which entered the medium with z = 0 can consist of a set of narrow beams. The number of narrow beams on a ring is proportional to its area $rdr = z\,tg\alpha \times \frac{dz}{\cos^2\alpha}$; this is the weight one should use to form the experimental pulses $P_{\alpha,z}(t)$. Time lag in different components is determined by the difference in the lengths of the path from the point of beam entrance into the water to the detector, and comprises, in relation to the pulse

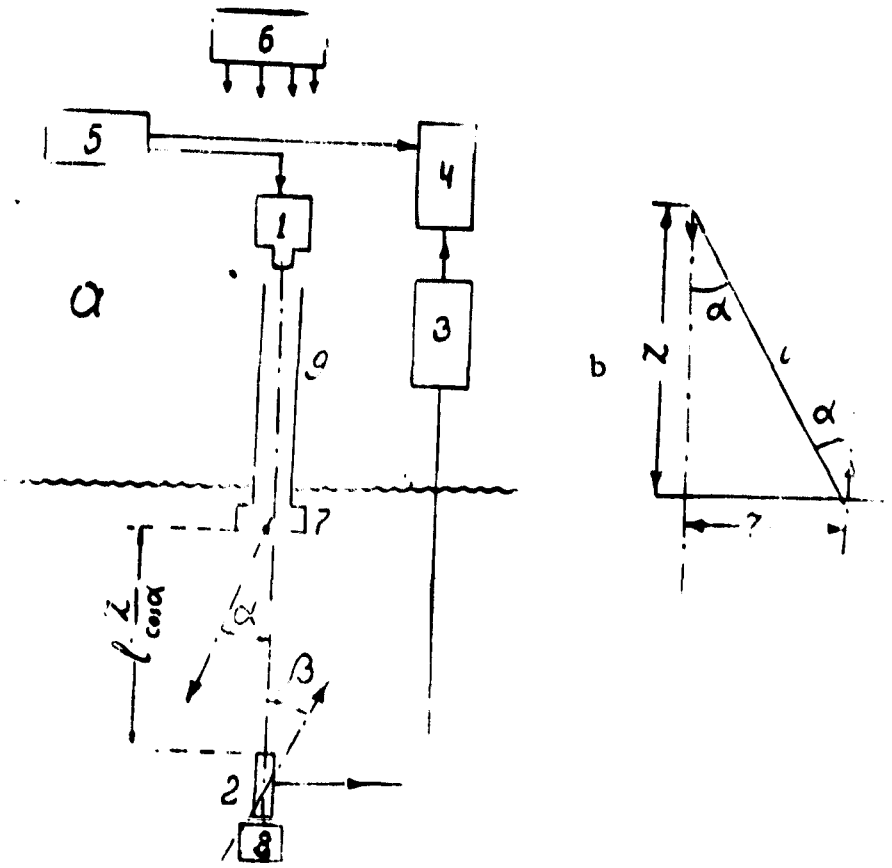

Figure 1. Measurement Plan

Key:

a. block diagram of equipment
1. laser
2. photoreceiver
3. attenuator
4. register
5. pulse generator
6. power block
7. device for remote control of turning laser beam
8. turning device of receiver
9. periscope
b. equivalent measurement plan used for superposition

which arrived first, a quantity $\frac{n(l-z)}{c} - \frac{nz(\sec\alpha - 1)}{c}$, where n is the refraction index of water, and c is wind velocity. The superposition integral can be presented /177 as follows:

$$P_1(t) = \int_0^{\alpha_2} P_2\left[t - \frac{nz(\sec\alpha - 1)}{c}\right] \cdot \frac{z\,\mathrm{tg}\,\alpha}{\cos^2\alpha}\,d\alpha,$$

where t is counted from its beginning for each received pulse. In light of the discrete measurements, the integral was replaced by the sum for the indicated value α.

The calculated values of α were taken in the middle of the measurement intervals indicated above.

Figure 2 presents signals which were mutually correlated in amplitude and temporal shift, and adopted with different α for one distance z = 100 m. They illustrate the obtained experimental material. The maximum value of the signal $P_{0.100}$ is adopted as 1. It is apparent that as the detector moves in the plane which is perpendicular to the axis of the narrow beam, away from the axis, the pulses not only diminish in amplitude and are shifted on the time axis, but also become more diffuse in time. /178

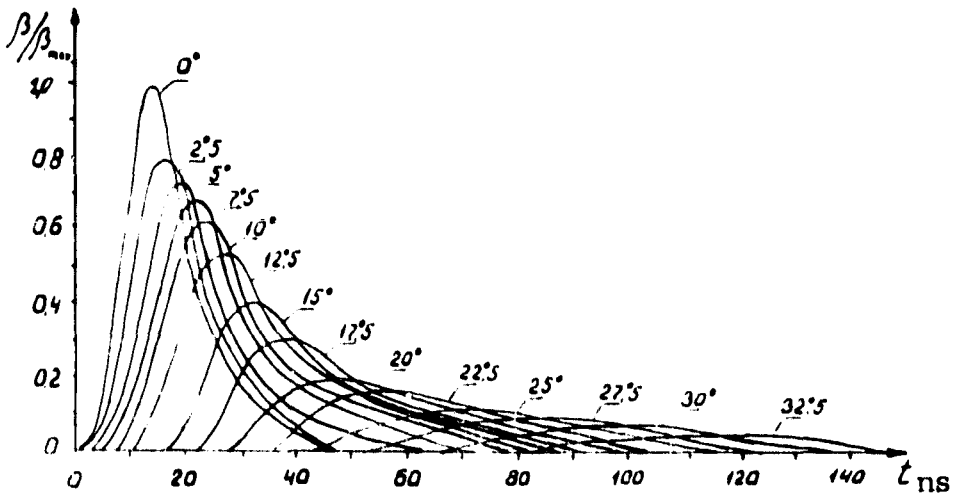

Figure 2. Signals Received with z = 100 m and Different α (α values indicated next to curves)

Figure 3 presents the same pulses multiplied by weight, proportional to the area of the corresponding "ring." It is evident that despite the fact that the greatest value of the signal in Figure 2 corresponded to $\alpha = 0°$, after consideration of the weights, the greatest contribution is made by the angle $\alpha = 10 - 17.5°$. The curves presented in Figure 3 were graphically summed. The superposition pulse $P_{100}(t)$ that was obtained as a result of summation and which was normed for one , is designated by a solid line. The shape of $P_{100}(t)$ corresponds to the temporal course of irradiance

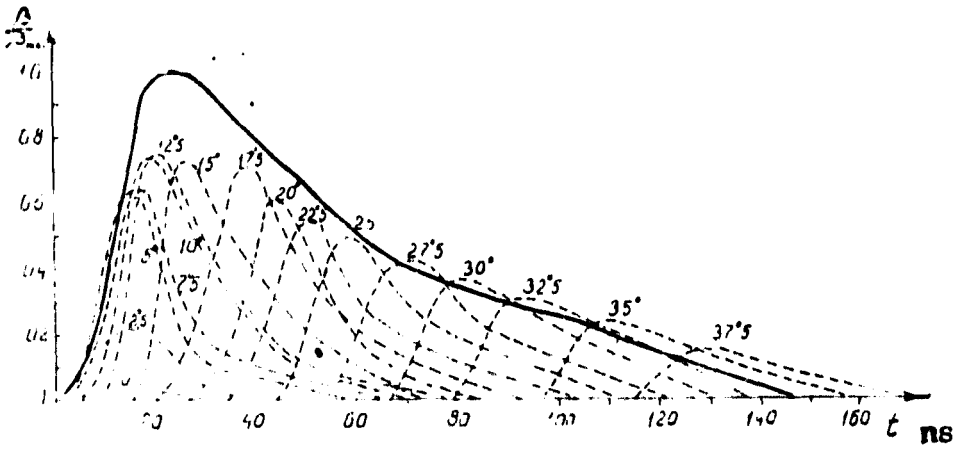

Figure 3. Measured Signals Multiplied by Corresponding Weight and Shifted in Time. The solid curve is the result of their superposition.

at level 100 m in a nonstationary field which is created by a broad light beam with the given shape of the original impulse and in the given ocean waters.

The same processing was done for other distances of z. The $P_z(t)$ values which were normed for one in the maximum are presented in Figure 4. The pulses depicted in Figure 4 are not Green's functions, since the original pulse in the experiment was noticeably different from the δ - pulse. In order to compute Green's functions it is necessary; strictly speaking, to solve the Fredholm integral equation as described in [1]. However, in our case, taking into consideration the features of the expected /179 Green's functions, one can attempt to use a simple method of selection.

In fact it is obvious that with duration of the received pulse considerably exceeding the original, the shape of the received pulse coincides with Green's function with high accuracy.

As the duration of the received pulse and its convergence to the original diminish, the difference in the received pulse from Green's function rises. We will use the method of selection which consists of the fact that the received pulse with /180

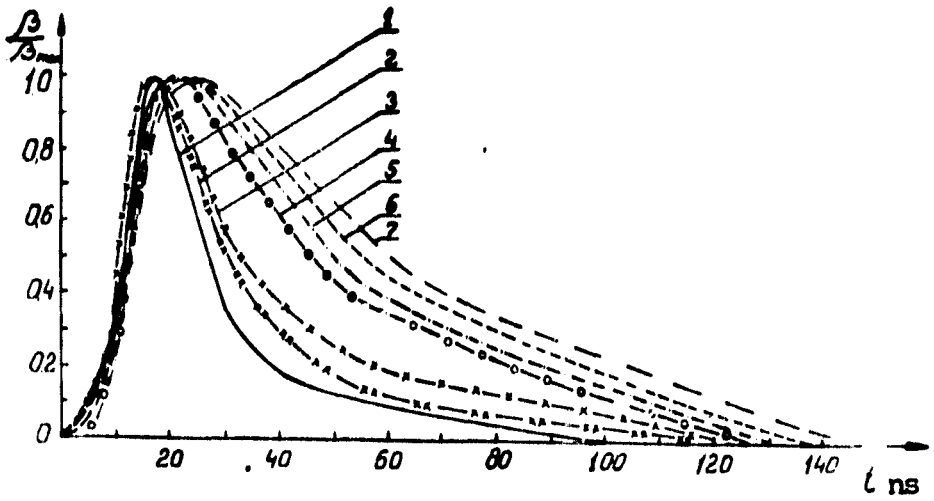

Figure 4. Results of Superposition at Different L

Key:

1. L = 25 m
2. 37.5
3. 50
4. 62.5
5. 75
6. 87.5
7. 100 m

different "compression coefficients" k, i.e., $f_k(t) = P$ which is "compressed" along the time axis is used as a preferable shape of Green's function. Then the curves $f_k(t)$ are convoluted with initial pulse in accordance with the integral:

$$P_k(t) = \int_0^t P_0(t-\tau) f_k(\tau)\, d\tau$$

The obtained pulses $P_k(t)$ are compared with the received pulse. It is shown in Figure 5 that at level 100 m with compression coefficient k = 0.95, the shape of the computed pulse $P_{0.9}(t)$ is close to the received pulse. The width of both pulses at level 0.5 coincides exactly. This operation of selection which requires short machine time, was carried out for all pulses presented in Figure 4. The table of the obtained values for compression coefficient k is presented below, while the appearance of Green's functions evaluated in this manner is presented in Figure 6.

Z, м	100	87,5	75,0	62,5	50	37,5	25
к	0,95	0,9	0,8	0,7	0,6	0,5	0,4

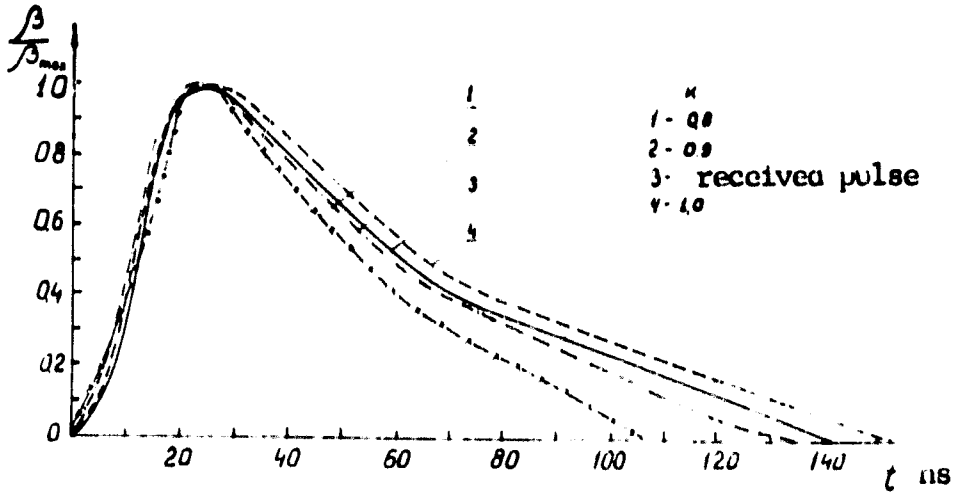

Figure 5. Comparison of Received Pulse (solid line) with Results of Convolution of Proposed Functions Characterized by Different k (k values indicated on field of figure).

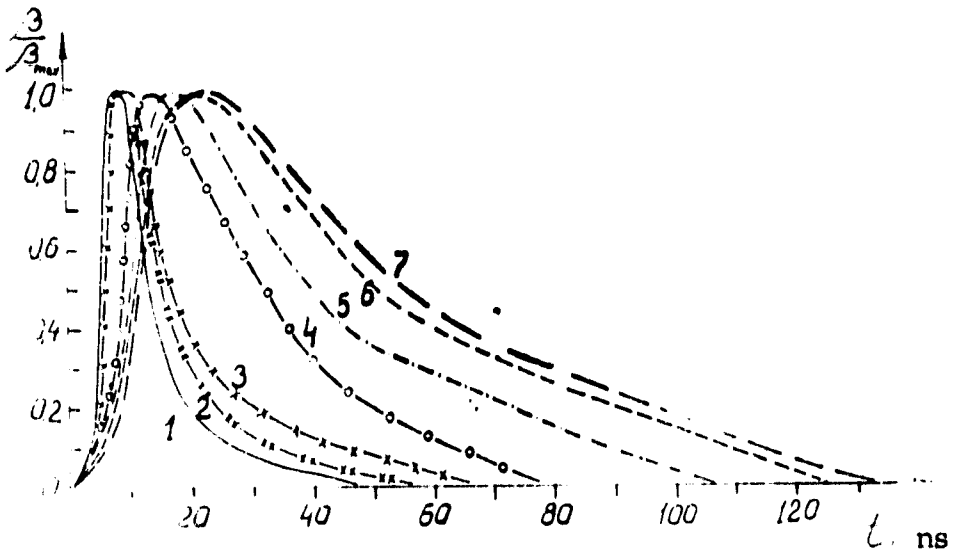

Figure 6. Green's Functions of Broad Beam at Different Distances of z

Key:

1.	z = 25 m	5.	75
2.	37.5	6.	87.5
3.	50	7.	100 m
4.	62.5		

The indicated method of selection is simple and can apparently be used to process material of mass measurements of NLF in the sea, in order to evaluate the main parameters of Green's functions. A certain criterion for correctness of selection is coincidence of the results of convolution of the selected and the original pulses with t[illegible] measured. The area of applicability of the selection method and the accuracy of the results can be established only by comparing with the accurate resolution of the Fredholm equation. This will be the result of a special examination. /181

Thus, the Green's functions of the NLF created by a broad light beam which is a δ - impulse in time are computed and presented in Figure 6. These functions have the physical meaning of temporal relationship of irradiance of an area perpendicular to the direction of beam propagation. The widths of Green's functions according to the half-altitude $\Delta\tau_{0.5}$ ns are presented in the table.

[illegible]	100	[illegible]	[illegible]	[illegible]	[illegible]	[illegible]	[illegible]
$\Delta\tau_{0.5}$	16	39	31	21	16	10	7

The transition to sea media with other values of absorption (i.e., other parameters of photon survival) can be made as indicated in [3].

BIBLIOGRAPHY /182

1. Gol'din, Yu. A.; Gashko, V. A.; Karlsen, G. G.; Pelevin, V. N.; and Shifrin, K. S. "Experimental Studies of Nonstationary Light Field in the Ocean," Gidrofizicheskiye i gidrooptricheskiye issledovaniya v Atlanticheskom i Tikhom okeanakh ["Hydrophysical and Hydrooptical Studies in the Atlantic and Pacific Oceans"], Moscow, Izd-vo, Nauka, 1974.

2. Gol'din, Yu. A.; Bachernkov, V. V.; Vortman, M. I.; Zudkov, P. I., Kagayn, V. E.; Makarov, Yu. A.; and Pelevin, V. N. "Experimental Study of Propagation of Short Light Pulses in Sea Water," Opticheskiye issledovaniya v okeane i v atmosfere nad okeanom ["Optical Studies in the Ocean and in the Atmosphere Above the Ocean"], P. P. Shirshov Institute of Oceanology of the USSR Academy of Sciences, 1975.

3. Pelevin, V. N. Eksperimental'noye issledovaniye svetovykh poley v okeane ("Experimental Study of Light Fields in the Ocean"), author's abstract of dissertation for defense of scientific degree of doctor of physical-mathematical sciences, Moscow, 1978.

EQUIPMENT AND TECHNIQUE FOR STUDYING SPREAD OF MONOCHROMATIC RADIATION IN SEA WATER

ABRAMOV, O. I., YEREMIN, V. I., KARLSEN, G. G., LOBOV, L. I., POLOVINKO, V. V.

This article describes equipment with submersible source of monochromatic radiation. It describes the technique for studying the laws of propogation of UV-radiation in a sea and for studying attenuation of monochromatic radiation with wavelengths 0.53 and 0.35 μm by great masses of sea water. Results of full-scale studies in the Black Sea are presented. It is shown that when UV-radiation spreads in sea water, considerable transformation of UV-radiation occurs in the visible spectral region. A brief analysis is made of the findings.

Study of the laws governing the spread of monochromatic radiation through large masses of sea water is an important task of hydro-optics and is of great importance in solving applied problems. To conduct these studies from a ship in the open sea, the V. I. Lenin Electrical Engineering Institute developed equipment consisting of a submergible source of monochromatic radiation (SMR), receiver and auxiliary units.

The SMR is a unified design with a head of emitters (double laser with λ=0.53 μm and λ= 0.35μm), power block, cooling block and commutation block (Figure 1). The structure is inside a hermetically sealed box which maintains outer pressure of over 50 atm. Quartz illuminators and rotating prisms are in the box end section to generate laser radiation. The head of emitters (Figure 2) consists of a bench holding a laser in a ruby and a laser on glass with neodymium. Both lasers operate in a monopulse regime with doubling of the generation frequency on CPD crystals. There is a photoreceiver on the bench to receive the reference signal and to monitor the laser radiation and the color filters which intercept radiation of the main harmonics (1.06 μm and 0.69 μm) and transmit radiation of the second harmonics (respectively 0.53 μm and 0.35 μm).

All the optical-mechanical lasers to be adjusted are securely fastened to the bench. This excludes the need to use special adjustment mechanisms. This /183 method of attachment significantly increases the service life and

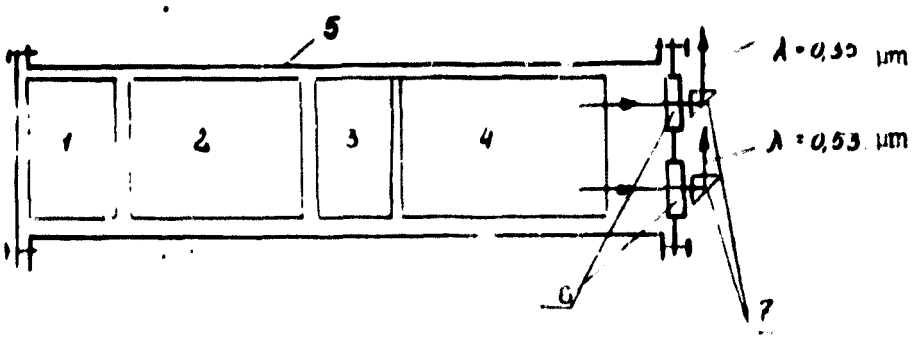

Figure 1. Block Diagram of SMR
Key:
1. cooling block
2. power block
3. commutation block
4. head of emitters
5. illuminators
6.7. turning prism

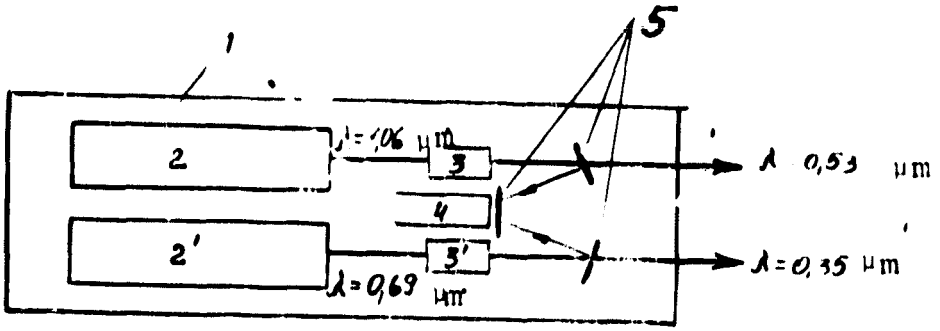

Figure 2. Head of Emitters
Key:
1. bench
2. laser on glass with neodymium
2! laser on ruby
3,3'. CPD (carbcxypeptidase)
4. photoreceiver
5. light filters

reliability of the laser operation under expedition conditions. Both lasers operate from a common power block and use a common cooling block. A commutation block is used to turn on the ruby or neodymium laser.

For remote control and monitoring of the operation, the SMR uses a special control panel which has an actuating circuit, monitoring device, circuit for regulating

the radiation power, and circuit for controlling the commutation block The control panel is connected to the SMR by a multiple-strand KSK 6 cable or KSB-8 cable.

The developed SMR can operate both under surface conditions (the SMR is located on board), and under water conditions (the SMR is lowered into the water with the help of a winch and cable) at depths to 500 m, with the following parameters of the radiation pulses: tracking frequency f = 0.1 - 1 Hz, λ = 0.53 μm, P_i = 0.2 - 1.4 MW, λ = 0.35 μm, P_i = 0.1 - 1 MW. The maximum average consumed power is 500 W. /184

The receiver consists of a photo receiver - spectroanalyzer, power block, control panel and indication block. The photo receiver (Figure 3) uses an FEU-97 photo multiplier and optical attachment with quartz lens and diaphragm in a focal plane which guarantees visual angle of the photo receiver of 3.5°.

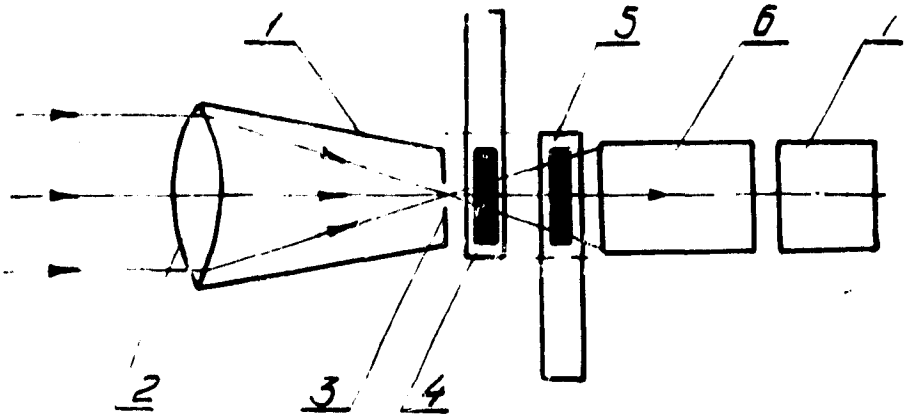

Figure 3. Plan of Photo Receiver-Spectroanalyzer

Key:

1. attachment
2. quartz lens
3. diaphragm
4. drum with neutral light filters
5. drum with color light filters
6. FEU-97
7. preamplifier

It should be noted that experimental studies of the laws governing the spread of radiation of artificial sources through large masses of sea water are associated with measurements of optical signals which change during the study in a large dynamic

range (up to 12 orders). This is a very labor-intensive task which requires a great deal of time. This is explained by the fact that the attenuators, neutral light filters made of NS type glass usually used in these studies have high nonuniformity of the spectral characteristics, especially in the short-wavelength region. This makes it necessary to have labor-intensive conversions. In addition, the lack of very dense neutral filters also complicates these studies.

In order to increase the efficiency and reliability of these studies, the V. I. Lenin All-Union Electrical Engineering Institute developed and manufactured neutral /185
light filters with transmission coefficient 10^{-1}, 10^{-2}, etc., up to 10^{-8} with nonuniform transmission coefficient in the visible and UV regions (up to 0.3 μm) of no more than ±20%. A drum with these filters is attached in front of the PM cathode. In order to guarantee the possible study of the spectral composition of radiation used by the photoreceiver, a drum of changeable colored light filters is used. It is also installed in front of the PM cathode. The color filters are combinations of series colored glasses. These combinations were selected so that the total spectral characteristics had the narrowest possible transmission bands, and the maximums were separated the most uniformly from each other and corresponded to the most important wavelengths in the visible and UV regions, including wavelengths of SMR radiation.

A broad-band pre-amplifier was installed in the photoreceiver. It can be used with low levels of the signals. The pre-amplifier was turned on remotely from the control panel, where, in addition, the main amplifier and the current control circuit of the PM gating were also located. A recording oscillograph S8-7A was used as the indication block. Depending on the selected regime, signals are fed directly to its input with loading of the PM or amplified by one or both amplifiers.

The PM divider is powered with the help of a series source of the type VS-23. The photoreceiver is connected to the control panel and the power block by two

coaxial cables. On the 8th Black Sea trip of the scientific research weather ship "Viktor Bugayev" tests were conducted on this set of equipment, and attenuation of monochromatic radiation was studied with $\lambda = 0.53$ μm and $\lambda = 0.35$ μm by large masses of sea water. In addition, studies were made of the spectral transformation of UV-radiation with $\lambda = 0.35$ μm during passage through different masses of sea water.

The location of equipment on the ship is presented in Figure 4. The control panel of the SMR, oscillograph, power block and control panel of the photoreceiver, as well as auxiliary equipment were installed in the ship laboratory. The photo-receiver was attached to the bulwark on a special rotating device which permitted the photoreceiver to be aimed at any angle to the surface of the sea. The SMR can be lowered into the water with the help of a winch and pulley on a cable to depth 500 m.

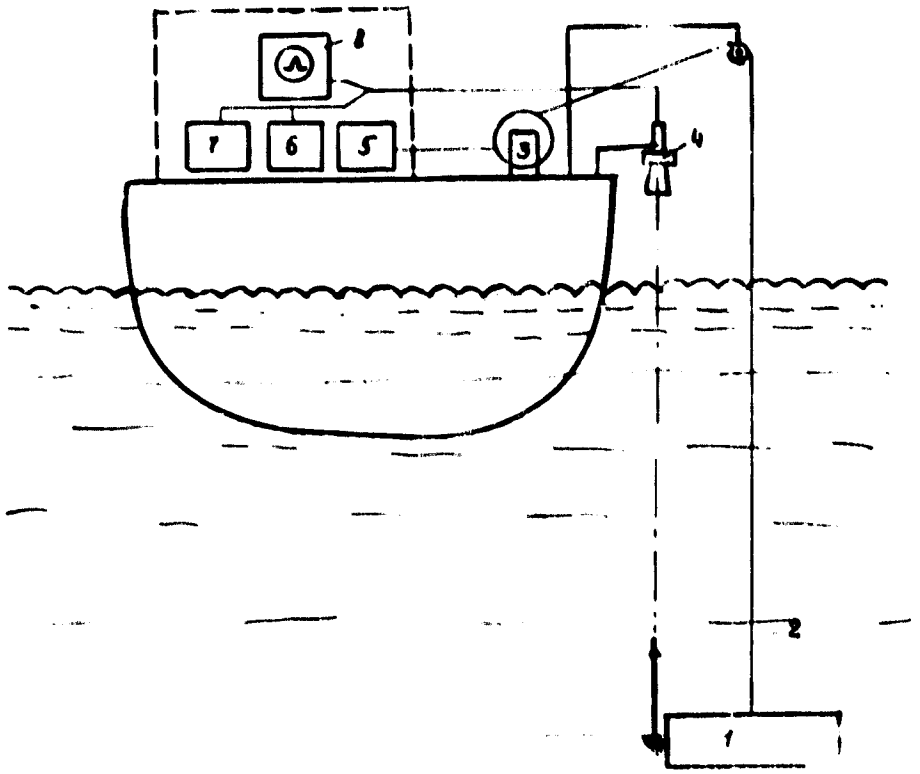

Figure 8. Arrangement of Equipment On Board Ship
[key on next page]

Figure 8. (key)

1. SMR
2. cable
3. winch
4. photoreceiver-photoanalyzer
5. control panel for SMR
6. power block of photoreceiver
7. control panel of photoreceiver
8. oscillograph

During study of attenuation of monochromatic radiation of water masses, the SMR is lowered to depth h_1. The rotating prisms direct the laser radiation upwards. The neodymium laser with $\lambda = 0.53$ μm is turned on. The photoreceiver which is fastened to the bulwark is aimed at the region of emergence of the radiation of the submerged SMR from the water. Using drums, a color filter is installed with maximum transmission at $\lambda = 0.53$ and neutral filter which guarantees operation of the PM in a linear regime. The operator measures the amplitude of the received signals on the oscillograph screen. /186

The same operations are done when the ruby laser is turned on with $\lambda = 0.35$ μm. Then the SMR is lowered to depth H_2 and the indicated measurements are repeated. Curves for the dependence of the amplitude of received signals on the depth of SMR submersion are plotted with regard for the coefficient of attenuation of the neutral filters. Figure 5 presents these curves, obtained in the Black Sea waters in the region of the Bosporus.

In the study of the spectral transformation of the UV-radiation, the technique mainly remains the same. In this case, only the ruby laser with $\lambda = 0.35$ μm operates in the SMR. Measurement of intensity of the radiation emerging from the water is done not only in the UV region of the spectrum, but also in the visible region by replacing the colored filters in the photoreceiver. Specifically, in this case we used filters with the following wavelengths of the transmission maximum: /187

$\lambda = 0.35$ μm, $\lambda = 0.42$ μm, $\lambda = 0.46$ μm, $\lambda = 0.5$ μm, $\lambda = 0.54$ μm, with band width at level 0.5 about 15 - 35 nm. Measurements were also made without color filters.

In this case the PM can record radiation in a broad spectral range, according to the spectral characteristics of the photocathode. Figure 6 presents dependences of the intensity of the spectral components of the radiation emerging from the water on the depth of SMR submersion, obtained in the same waters.

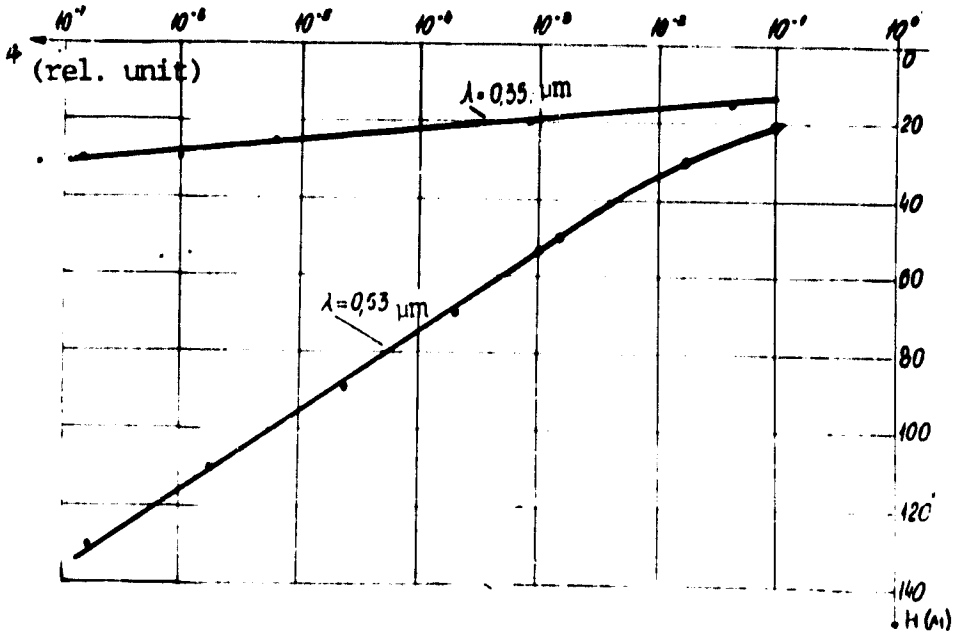

Figure 5. Dependence of Intensity of SMR Radiation Emerging from Water on Depth of Submersion.

Figure 7 presents a family of spectra of the radiation emerging from the water at different depths of submersion of SMR.

Attenuation curves (Figure 5) agree fairly well and supplement analogous data that we previously obtained using a submersible photoreceiver and a surface SMR with close parameters of the radiation pulses. The most interesting are the results of studying the spectral transformation of UV-radiation. This transformation is based on known phenomena of combination scattering and photoluminescence of sea water [1, 2], however the examined experimental data from the submersible SMR were obtained /188

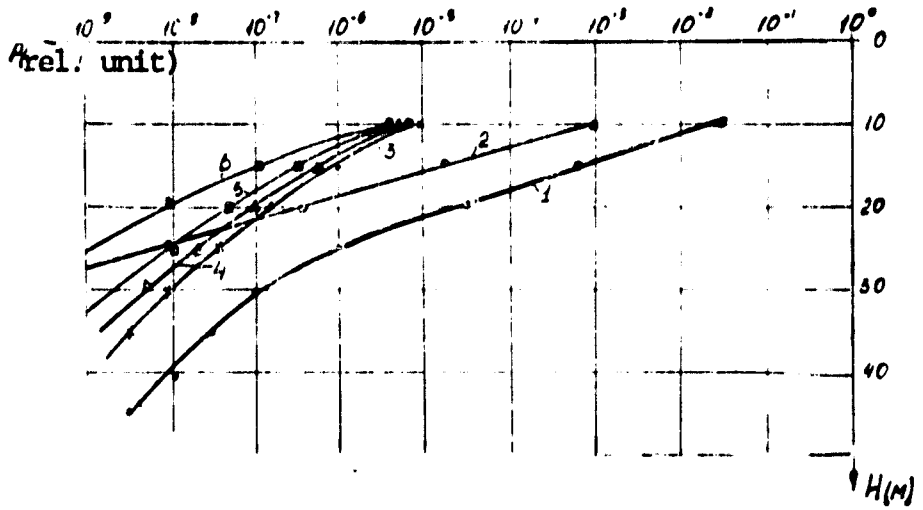

Figure 6. Dependence of Intensity of Components in Spectrum of Radiation Emerging from the Sea and Depth of SMR Submersion (λ = 0.35 μm)

Key:

1. without color filters
2. λ = 0.35 μm
3. 0.54
4. 0.5
5. 0.46
6. 0.42

for the first time (we did not encounter information on similar works in the literature). Based on the curves presented in Figures 6 and 7, one can draw a number of preliminary conclusions. When UV-radiation spreads in the mass of sea water, considerable transformation of the UV radiation into the visible region occurs. The transformed radiation during its further spread is attenuated in different sections of the spectrum in a different manner. This is determined by the various spectral coefficients of attenuation of sea water in these sections. Both of these processes occur continuously and simultaneously. Consequently, the spectrum of the radiation emerging from the water mass, generally depending on the set of parameters and factors, is determined to a considerable measure by the intensity of FMV [expansion unknown] and spectral transmission of sea water.

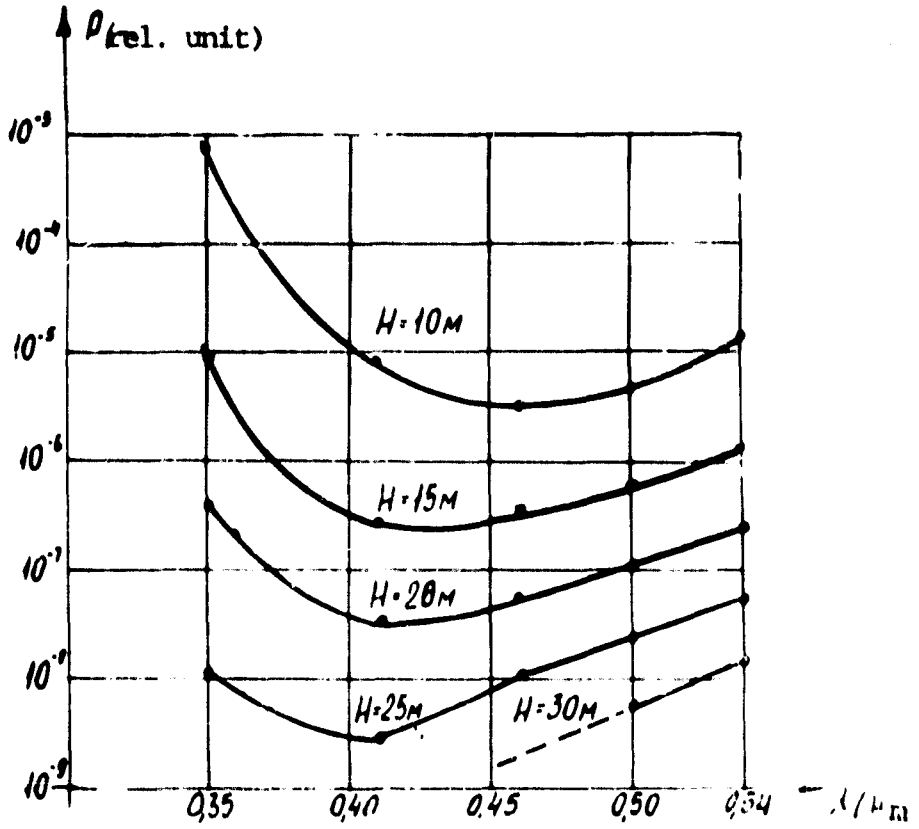

Figure 7. Spectrum of Radiation Emerging from Water with Different Depths of SMR Submersion (λ = 0.35 μm)

It is quite understandable that similar discussions make it possible to qualitatively explain the relationships in Figures 6 and 7 only in the first approximation. They do not take into consideration at all the possible nonlinear phenomena in the zone of high intensity of laser UV-radiation, change in hydro-optical properties of water with depth, spatial characteristics of radiation, and a number of other factors.

On the other hand it is clear that the obtained experimental data on the transformation of monochromatic UV-radiation during spread in the mass of sea water bear a large volume of information on properties of water on the route of spread. For complete processing of similar data additional studies are required and correction

of the technique for conducting studies. It is evident, however, that these /189
studies on the transformation of UV-radiation are of importance and can enter the arsenal of modern methods and means of studying the World Ocean.

It should be noted that when spectral studies are made of light fields in the ocean from artificial and natural sources, it is necessary to take into consideration possible spectral transformation in a number of cases.

Further improvement in the equipment must be aimed at improving the resolution of the photoreceiver-spectroanalyzer, automation of the measurement processes, stabilization of the spatial position of the SMR in the submerged state, and development of remote control over the mechanism for turning the rotating SMR prisms. This will significantly expand the potentialities of the equipment and will make it possible to conduct studies of the spatial characteristics of the brightness body.

BIBLIOGRAPHY /190

1. Kizel', A. A.; Rakhmetov, M. I. "Blue Luminescence of Liquids," Ucn. zap. tadzn. gos. un-ta, No 4, 1955.

2. Karabashev, G. S., Zangalis, K. P.; Solov'yev, A. M., and Yakubovich, V. V. "New Data on Photoluminescence of Sea Water," Izd. AN SSSR, FAO, 7, No 1, 1971.

III. APPLICATION OF OPTICAL METHODS FOR STUDYING BIOLOGICAL AND HYDROLOGICAL CHARACTERISTICS OF THE SEA /191

EVALUATION OF CHLOROPHYLL CONTENT IN THE UPPER SEA LEVEL BY MEASURING THE COLOR INDEX. AFONIN, YE. I., VERSENEVA, G. P., KRUPATKINA, D. N., LI, M. YE., MAN-KOVSKIY, V. I., SOLOV'YEV, M. V.*

*Marine Hydrophysical Institute of the Ukrainian SSR Academy of Sciences, A. Kovalevskiy Institute of Biology of Southern Seas of the Ukrainian SSR Academy of Sciences.

A correlation expressed by a linear regression equation in a double logarithmic scale is found from 175 simultaneous measurements of the color index and chlorophyll concentration in water samples taken on a ship. The analysis includes data obtained in the Atlantic Ocean and adjacent seas which have a large range of change in the chlorophyll concentration. Possible use of the results from measuring color index from the ship for a rapid evaluation of the biological productivity of the studied region is shown.

Noncontact optical methods for determining the content or organic substances in the ocean have been developed in recent years. It was shown in [1] that the sea water color is influenced by the phytoplankton pigments. The authors [2] measured the radiation spectrum ascending from the sea from an airplane. Spatial inclination of the ascending radiation showed a correlation with the content of phytoplankton pigments, whose concentration was measured from a ship on the same route as the airplane.

The authors of [3] obtained a quantitative link between the chlorophyll content a and the radiation brightness emerging from the sea in two close spectral sections (λ_1 = 443 nm and λ_2 = 525 nm). They found a linear correlation between the logarithm of chlorophyll concentration a and the difference between radiation intensities emerging from the sea at given wavelengths. Water samples in which the chlorophyll content a was determined were taken from 0 to 10 m.

Study [4] used a small amount of statistical material during shipboard measurements to obtain a linear relationship between average chlorophyll content a, b and c in the upper 30-meter water layer and the parameter a which is close to the ratio of spectral brightness coefficients of the sea with wavelength λ_1 = 430 nm and λ_2 = 502 nm at which measurements were made.

Publication [5] further developed the idea of determining chlorophyll content in sea water by an optical method from a ship. By using a two-flux approximation and experimental data on the specific chlorophyll absorption and coefficients of absorption of clean sea water with λ_1 = 462 nm and λ_2 = 537 nm, the authors obtained a correlation between the chlorophyll content in the water and the ratio of the co- /192
efficients of diffuse reflection with these wavelengths. The coefficients of diffuse reflection, in turn, were computed from experimental data by measuring the ratios of brightness of the sky with two wavelengths and brightness of the sea with the same wavelengths. The total concentration of chlorophyll a, b and c in the samples was determined by the standard method and averaged for the depth of the translucent layer. The analysis included 18 measurements of chlorophyll content in the samples and 62 optical analyses. A correlation graph was obtained which links the chlorophyll concentration determined by two methods. The maximum discrepancy does not exceed 1.8-fold and is comparable to the spread of analyses of chlorophyll concentrations of different samples taken at one station.

The spectral distribution of brightness of light emerging from the sea was measured in [6] using a monochromator through a vertical shaft in the bottom of the ship. It also recorded the spectrum of radiation falling on the sea surface. An analysis was made of the quotient from dividing these two spectral distributions, called the conditional coefficient of sea brightness. The authors of the publication found a link between the position of the second maximum of spectral distribution of the conditional coefficient of brightness and the concentration of chlorophyll. However, the correlation of relative depth of dip in the curve of this distribution at λ = 430 nm was higher. A comparison was made of the optical data with average total chlorophyll content a, b, c, and pheophytin for three levels (0, 10 and 25 m). The results of 19 measurements were used to obtain a correlation coefficient of 0.88.

The chlorophyll concentration a and c was determined by the standard spectrophotometric method according to the technique presented in [8].

A special experiment was conducted to verify the rate of water exchange in the shaft. A logarithmic photometer-transparency meter was submerged into the shaft. Its readings were continuously recorded by a self-recorder. The water in the shaft was further clouded by pouring in a certain quantity of milk. It was established that in calm weather with ship velocity of 16 knots, water exchange in the shaft occurred in 30 - 40 minutes. This was noted by restoration of the transparency meter readings. With wave action of 3 - 4 points, this time was reduced to 10 - 15 minutes. Consequently, comparison of the color index with the measured chlorophyll concentration should be done in a time interval of ~30 minutes before taking of the sample. During this time the readings of the color index gage must be averaged.

Parallel measurements of the chlorophyll content in the upper layer of the ocean and the color index were also made on the 15th and 16th trips of the scientific research vessel "Akademik Vernadskiy." The 175 joint measurements which were included in the analysis were made in the following regions: Black Sea (42 samples), Mediterranean Sea (37 samples), eastern part of the North Atlantic Ocean near the coast of Africa (61 samples), Sargasso Sea (23 samples), central region of the tropical Atlantic Ocean (7 samples), Caribbean Sea (5 samples). The measurements covered regions with very low (≤ 0.1 mg x m^{-3}) and high (~10 mg x m^{-3}) chlorophyll concentrations. The analysis did not include measurements made in shallow water near the coastline and in regions of river run-off, since in these cases, the presence of a considerable quantity of terrigenous particles made distortions in the quantity of the color index.

The measurement results are presented in Figures 1 and 2. Figure 1 shows the dependence of the chlorophyll concentration a on the quantity of the color index, while Figure 2 shows the same dependence for total chlorophyll concentration in c. The data are plotted on the graph in a double logarithmic scale.

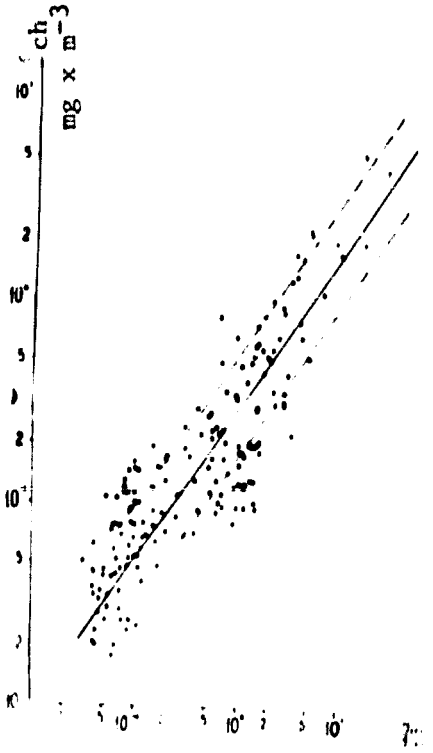

Figure 1. Ratio Between Concentration of Chlorophyll a in Upper Layer of Sea and Color Index

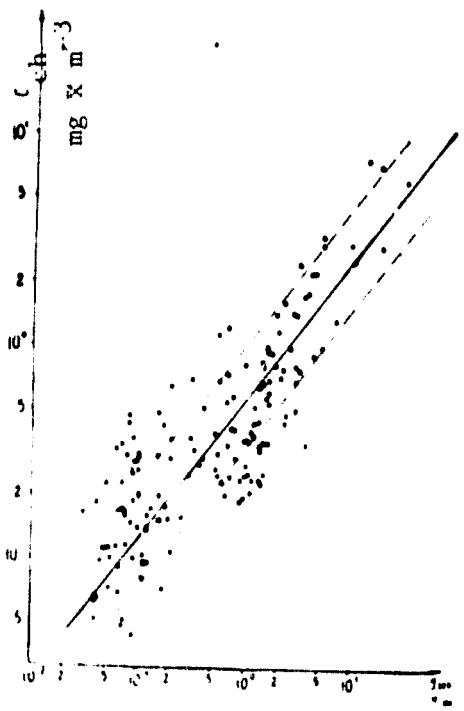

Figure 2. Ratio Between Total Concentration of Chlorophylls a and c in Upper Layer of Sea and Color Index

Coefficients of linear correlation were computed for both distributions. They were equal to 0.86 ($\pm$ 0.04) and 0.83 ($\pm$ 0.05) respectively. The 95% confidence intervals are shown in parentheses.

The regression equations which provide an estimate of the average concentration /194
of chlorophyll with the assigned quantity of the color index look like

and $$\lg c_a = -0.53 + 0.71 \lg J_c$$
$$\lg c_{ac} = -0.21 + 0.66 \lg J_c$$

where c_a and c_{ac}--concentration of chlorophyll a and the sum of a and c respectively, expressed in mg x m^{-3}, J_c--color index in dimensionless units. During graduation of the color index gage, the color index of the screen made of a white sheet of Whatman drawing paper illuminated by the sun and scattered light of the sky on a cloudless day was taken as one. The instrument was graduated in hours, close to noon. The screen was located at an angle close to 90° in relation to the incident solar light.

In the figures, the dotted line shows lines which designate the sampling stan- dard deviation of the measured values of chlorophyll concentration from the pre- /195
dicted, which is determined in each case by the corresponding regression equation.

The nature of spread of the points on the graphs is such that under the most unfavorable conditions, concentrations of chlorophyll which relate to each other as 1:6 for chlorophyll a and 1:10 for the sum of chlorophylls can correspond to the same value of the color index. On the boundary of the sampling standard deviation, this ratio is 1:1.8 to one side of the regression line, i.e., in 70% of the cases, the measured chlorophyll concentration differs from the predicted given by the regression equation, by not more than 1.8-fold. One can name several reasons for the spread of points on the x-axis. First of all, the measurements of chlorophyll concentration were only made in the most upper layer of the sea, while the effective

thickness of the water from which the light is collected and is recorded by the instrument, is 25 - 30 m according to the estimates of publication [4] for clean ocean water. In more turbid water, this thickness diminishes. Secondly, the water in addition to phytoplankton has particles of another type, detritis, mineral suspension, which change the color index, by distorting information regarding the chlorophyll. Thirdly there are method errors in determining the concentration of phytoplankton pigments. In our opinion, the contribution to spread of points for this reason is not definitive, since error in determining the concentration of pigments by the spectrophotometric method is ~10% with concentrations of pigments up to 10 mg x m^{-3} and increases to 20% with concentrations less than 5 mg x m^{-3} [9].

Spread of points of the same order was obtained in publication [10]. It presents the experimental result of simultaneous analysis of the ratio of coefficients of diffuse reflection with two wavelengths λ_1 = 430 nm and λ_2 = 560 nm, and total concentration of chlorophyll a and pheophytin a. The authors of publication [10] present a theoretical calculation which agrees with the spread of points obtained in the experiment. In this case they indicate that in addition to selective absorption by phytoplankton pigments, the ratio of coefficients of diffuse reflection can be significantly influenced by parameters of back-scattering of the marine suspension.

In summarizing, one can stress that extensive statistical material was used to obtain a correlation between the chlorophyll content in the upper sea level and the color index. In estimating the chlorophyll concentration from the quantity of the color index in 70% of the cases, it does not differ by more than 1.8-fold from the predicted provided by the corresponding regression equation obtained from experimental data. The suggested method was verified in different regions of the ocean

which strongly differ in level of trophicity, and can be used as a fast method for estimating the biological productivity of regions during motion of a ship.

In conclusion, the authors are grateful to V. A. Basharin and V. N. Voskresen- /196 skiy for help in the work.

BIBLIOGRAPHY

1. Yentsch, C. S. "The Influence of Phytoplankton Pigments on the Color of Sea Water," Deep-Sea Res., vol 7, No 1, 1960, pp 1 - 9.

2. Clarke, L.; Ewing, G. C.; Lorenzen, C. J. "Spectra of Back-Scattered Light from the Sea Obtained from Aircraft as a Measure of Chlorophyll Concentration," Science, vol 167, No 3921, 1970, p 1119.

3. Arvesen, J. C.; Weaver, E. C.; and Millard, I. P. "Rapid Assessment of Water Population by Air-Borne Measurements of Chlorophyll Content," AIAA, Paper No 71, 1971, p 1097.

4. Shifrin, K. S.; Sud'bin, A. I.; Bekasova, O. D.; et al. "Study of the Link Between Chlorophyll Content and Brightness of Light Emerging from the Sea," TROPEKS-72, Leningrad, Gidroneteoizdat, 1974.

5. Novogrudskiy, B. V.; Shifrin, K. S. "Measurement of Chlorophyll Concentration from a Ship by Optical Method," Gidrofizicheskiye i opticheskiye issledovaniya v Indiyskom okeane ["Hydrophysical and Optical Studies in the Indian Ocean"], Moscow, Nauka, 1975.

6. Pelevin, V. N.; Byalko, A. V.; Bekasova, O. D., and Tsvetkova, A. M. "Determination of Chlorophyll Concentration from the Spectrum of Radiation Emerging from the Sea," Gidrofizicheskiye i opticheskiye issledovaniya v Indiyskom okeane, Nauka, 1975.

7. Li, M. Ye., Martynov, O. V. "Certain Results of Studying Color Index in the Sea," Morskiye gidrofizicheskiye issledovaniya ["Marine Hydrophysical Studies"], No 1 (72), Sevastopol', Izd. MGI AN USSR, 1976.

8. UNESCO Determination of Phytosynthetic Pigments in Sea Water, 1966, pp 11 - 69.

9. Berseneva, G. P.; and Finenko, Z. Z. "Quantitative Analysis of Chlorophylls a and c in Marine Plankton Algae with the Help of Paper Chromatography," Okeanologiya, 15, No 1, 176, 1975.

10. Morel, A.; and Prieur, L. "Analysis of Variations in Ocean Color," Limnol. Oceanogr. 22, No 4, 1977, pp 709 - 722.

EVALUATION OF CHLOROPHYLL CONCENTRATION IN THE SEA BY THE SPECTRUM OF OUTGOING RADIATION FOR WATERS WITH HIGH CONTENT OF DISSOLVED ORGANIC MATTER.

V. I. BURENKOV, A. P. VASIL'KOV, B. F. KEL'BALIKHANOV and L. A. STEFANTSEV

A technique is suggested for evaluating chlorophyll content from the spectral relationship of the brightness coefficient for productive waters with a high content of dissolved organic substance. This technique considers absorption by the substance to the red spectral region. It is shown that the radiation spectra from the sea can be confidently used to separate the low- and highly-productive regions.

Study [1] has suggested a method for evaluating the chlorophyll content in sea water by the outgoing radiation spectrum. Chlorophyll content based on this method is proportional to the so-called "chlorophyll dip" in the spectrum of the sea brightness coefficient $\rho(\lambda)$. For waters with a high quantity of dissolved /197 organic matter, the chlorophyll absorption band is masked by intensive absorption of dissolved organic matter and the "chlorophyll dip" can be altogether missing, despite the large chlorophyll content. [2] has developed a technique for evaluating chlorophyll concentration from the spectrum $\rho(\lambda)$ which is suitable for relatively clean ocean waters. This work, based on material from the Black Sea expedition of the Oceanography Institute of the USSR Academy of Sciences in 1978, suggests a technique for evaluating the chlorophyll content by the spectrum $\rho(\lambda)$ for productive waters with a high content of dissolved organic matter. Measurements of the spectral brightness coefficient of the sea and vertical attenuation index were made from onboard the ship in the Gulf of Odessa in July 1978.

The gage for spectral brightness coefficient of the sea is a spectrophotometer to measure the spectral density of radiation brightness emerging from the sea B_m, spectral density of sky brightness at the zenith B_H, and spectral radiation of the sea surface E_o in the spectral range 400-700 nm with resolution 2.5 nm. The sea brightness coefficient is expressed by the formula

$$\rho = \frac{n^2}{T_1 T_2} \cdot \frac{B_m - RB_H}{E_o} \qquad (1)$$

Here n is the refraction index of light by water, R = 0.02-- is the Fresnel coefficient of light reflection with normal incidence, T_1--transmission coefficient by the interface air-water of the diurnal light flux, T_2--transmission coefficient of the interface water-air of light diffusely reflected by the sea mass at the zenith.

Figure 1 presents typical spectra for the brightness coefficient of the sea for the Gulf of Odessa, and also for comparison presents spectral relationships of the coefficient of brightness obtained in July 1978 in the regions of Kerch' and the southern coast of the Crimea. It is directly apparent that the spectra significantly differ from each other: the maximum $\rho(\lambda)$ is shifted from 480 - 490 nm for water near the southern coast of the Crimea to 570 nm for waters of the Gulf of Odessa. This change was also noted well visually: the color of the sea changed from blue to yellow-brown in the Gulf of Odessa. Shift in the maximum $\rho(\lambda)$ towards large λ is also accompanied by a significant decrease in the values $\rho(\lambda)$ in the short wavelength region of the spectrum.

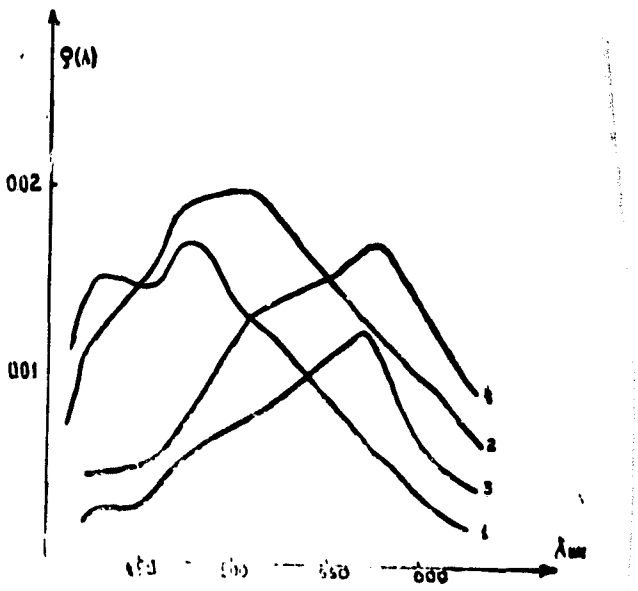

Figure 1. Spectral Dependence of Brightness Coefficient $\rho(\lambda)$:1.for measurements in region of the southern shore of Crimea; 2. in region of Kerchenskiy Strait; 3,4. region of the Gulf of Odessa

For the spectra of $\rho(\lambda)$ measured in the Gulf of Odessa, the "chlorophyll dip" was only recorded in the region $\lambda \sim 440$ nm in individual cases. The absence (in the /198
limits of experimental error) of a "chlorophyll dip" in the majority of measured spectra apparently can be explained by the excessively high absorption of dissolved organic matter. On its background, absorption of chlorophyll and pigments is in the limits of experimental error. In fact, the simultaneous measurements of the index of vertical attenuation $\alpha(\lambda)$ showed that water in the Gulf of Odessa is characterized by extremely high values of the absorption index $\varkappa(\lambda)$--Figure 2 (absorption index is determined according to α by the formula $\varkappa = 0.8\alpha$). Such large values of $\varkappa(\lambda)$ are not only associated with high bioproductivity of the waters, but also the efflux of yellow substance from the rivers (Southern Bug, Dniepr), washing of yellow substance from the shores and sludge(the depth of the Gulf of Odessa does not exceed 20 - 25 m). The spectral curve $\varkappa_B(\lambda)$ for absorption of substance contained in the sea water is approximated well by the relationship

$$\varkappa_B(\lambda) = \varkappa_B(440)e^{-\gamma(\lambda-440)} \qquad (2)$$

with coefficient $\gamma = 0.0145$ nm^{-1} close to the value $\gamma = 0.015$ nm^{-1} presented in Yerlov [3].

In order to link the brightness coefficient with the primary hydro-optical /199
characteristics, we will use a formula obtained in [4]

$$\rho(\lambda) = \frac{\sigma_{180}(\lambda)}{2\varkappa(\lambda)} \qquad (3)$$

where $\sigma_{180}(\lambda)$--value of the scattering index for 180°. Based on formula (3), an estimate was made of the spectral relationship of $\sigma_{180}(\lambda)$ according to the measured relationships $\varkappa(\lambda)$ and $\rho(\lambda)$. These calculations showed that essentially for all measured spectra $\rho(\lambda)$ in limits of the experimental error, $\sigma_{180}(\lambda)$ does not depend on λ--Figure 3. For comparison, Figure 3 presents the relationship $\sigma_{180}(\lambda) \sim \lambda^{-1.45}$

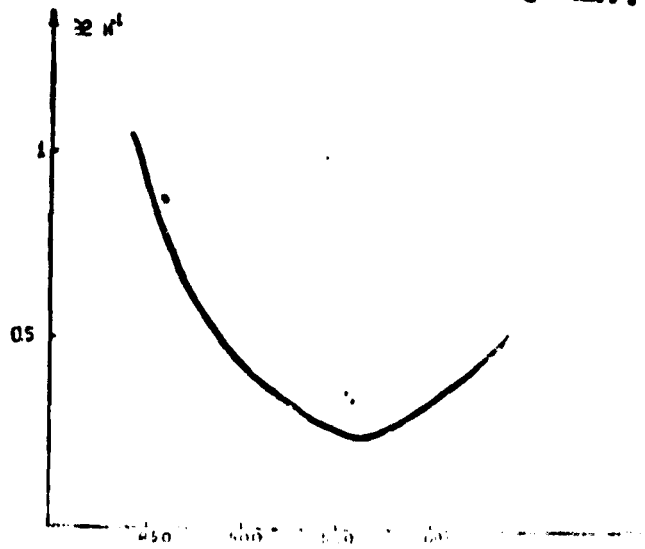

Figure 2. Spectral Dependence of Absorption of Light by Sea Water $\varkappa(\lambda)$ in the Gulf of Odessa

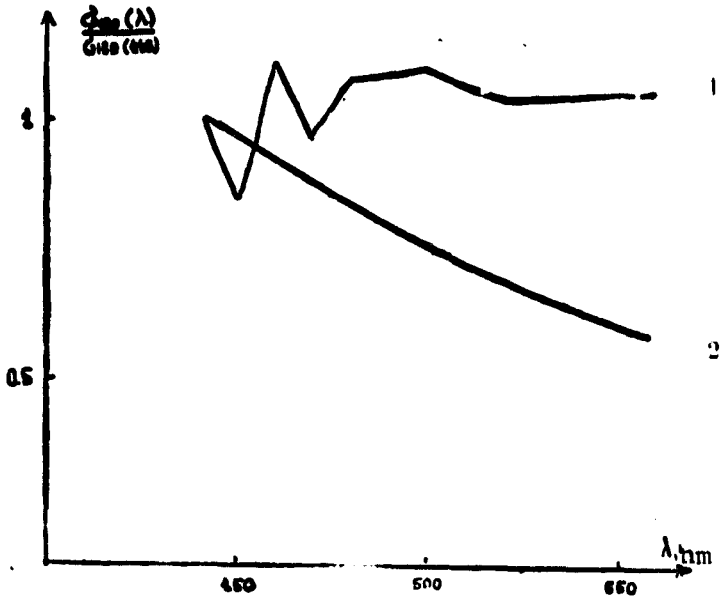

Figure 3. Spectral Dependences of Back-Scattering $\sigma_{180}(\lambda)$: 1) for measurements of spectra $\rho(\lambda)$ $[\sigma_{180}(\lambda) \sim \varkappa(\lambda)\rho(\lambda)]$; 2) curve $\sigma_{180}(\lambda)_{\lambda}$-1.45

suggested in [2]. It corresponds to back-scattering by primarily small particles. This is generally fulfilled for the open ocean. Near shores and in the presence of river debris, the content of large suspended matter can be significantly higher. It apparently plays a decisive role in back-scattering. The findings confirm these considerations, since large particles scatter light nonselectively.

On the assumption of $\sigma_{180}(\lambda)$ = const, we have from (3)

$$\rho(\lambda) \sim \varkappa^{-1}(\lambda) \qquad (4)$$

Figure 4 compares the measured spectral relationship $\rho(\lambda)$ and that calculated by (4) based on the experimentally obtained curve $\varkappa(\lambda)$. The curves in Figure 4 are superposed at λ = 570 nm. This is the wavelength which corresponds to the maximum measured spectrum $\rho(\lambda)$. As is apparent from the figure, the curves coincide with good accuracy. /20

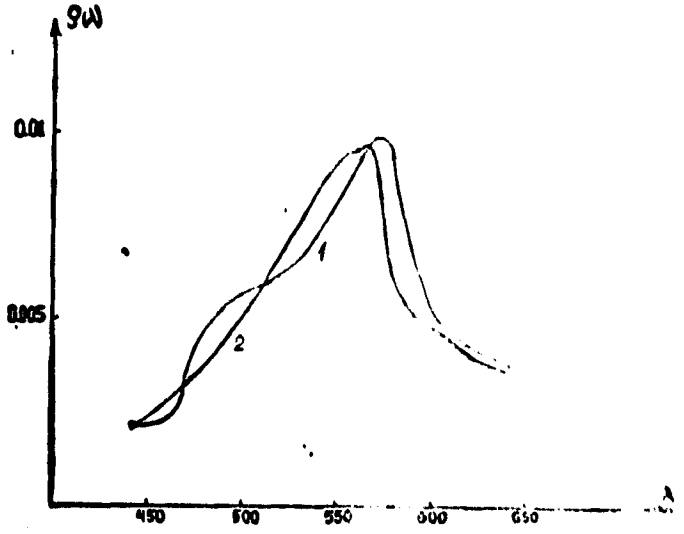

Figure 4. Dependences of Brightness Coefficient $\rho(\lambda)$: 1. measured in region of Gulf of Odessa; 2. curve $\rho(\lambda) \sim \varkappa(\lambda)^{-1}$

Thus, the waters of the Gulf of Odessa are characterized by excessively large values of absorption by substance which is contained in the sea water, and nonselectivity of back-scattering. These experimental facts and the correlation between the chlorophyll concentration and the value $\varkappa_B(\lambda)$, (λ = 450 - 470 nm) from publication [5] were the basis for the suggested technique. It follows from (4) (λ = 450 - 470 nm in the further presentation)

$$\frac{\rho(600)}{\rho(\lambda)} = \frac{\varkappa_w(\lambda)}{\varkappa_w(600)+\varkappa_*(600)} \qquad (5)$$

where $\varkappa_*$--absorption index of clean water. In (5) with λ = 450 - 470 nm, absorption by clean water is ignored, and it is a distinctive feature of the technique that absorption by substance is taken into consideration all the way to λ = 600 nm. Assuming in accordance with (2) that $\varkappa_B(600) = \varkappa_B(\lambda)e^{-\gamma(600-\lambda)}$, we have from (5)

$$\varkappa_B(\lambda) = \varkappa_w(600)\left|\rho(\lambda)/\rho(600) - e^{-\gamma(600-\lambda)}\right|^{-1} \qquad (6)$$

By having the values of $\varkappa_B(\lambda)$ from (6), and by using the correlation relationship from (5), the chlorophyll concentrations were computed from the measured spectra of the brightness coefficient. Table 1 presents the calculated and measured chlorophyll concentrations c_{ch} in different regions of the Gulf of Odessa, as well as the measured values of $\rho(\lambda)$, used to restore the values $\varkappa_B(\lambda)$. We note that the calculated values of c_{ch} somewhat changed depending on the reference point wavelength λ in (6). The values in Table 1 were averaged for three reference wavelengths λ = 450, 460, and 470 nm. /201

The findings do not make it possible to correctly evaluate the accuracy of determining c_{ch} by spectra $\rho(\lambda)$, although in individual cases the coincidence of the measured and calculated c_{ch} is good. (We note that the accuracy of the calculation is apparently determined to a considerable degree by the correlation relationship [5] obtained under different conditions). Nevertheless, the measurements make it possible

TABLE 1. VALUES OF BRIGHTNESS COEFFICIENT $\rho(\lambda)$ MEASURED IN DIFFERENT REGIONS OF THE GULF OF ODESSA, AND CORRESPONDING VALUES OF MEASURED AND CALCULATED CHLOROPHYLL CONCENTRATIONS IN mg/m^3

Number	Time	Concentration of Chlorophyll Measured	Concentration of Chlorophyll Calculated	$\frac{\lambda}{(\rho)\lambda}$	420	440	460	480	500	520	540	560	580	600	620
11.7.78	16.00—17.00	0,52	1,1		1,09	1,02	1,04	1,21	1,43	1,62	1,82	1,98	2,01	1,62	1,28
12.7.78	13.00—14.00	0,89	0,95		0,20	0,32	0,42	0,70	0,83	0,93	1,03	1,08	1,09	0,61	0,29
12.7.78	14.30—15.00	0,76	0,92		0,25	0,27	0,44	0,59	0,70	0,87	1,05	1,23	1,16	0157	0,34
12.7.78	16.30—17.00	1,73	1,8		0,42	0,49	0,70	1,0	1,24	1,33	1,43	1,65	1,67	1,32	1,00
16.7.78	16.00—16.30	1,76	2,0		0,50	0,51	0,54	1,07	1,40	1,55	1,73	2,12	2,27	1,48	1,17

to state that this region refers to the highly productive. Thus, studies made in recent years have shown that the spectra of radiation emerging from the sea can be confidently used to separate low-and high-productive regions [1, 2, 6]. It is further expedient to establish gradations in water productivity which could be reliably separated by measurements of $\rho(\lambda)$.

BIBLIOGRAPHY /203

1. Pelevin, V. N. "Evaluation of Concentrations of Suspended Matter and Chlorophyll in the Sea by Spectrum of Outgoing Radiation Measured from a Helicopter," Okeanologiya, vol 18, No 3, 1978.

2. Burenkov, V. I.; Gurevich, I. Ya.; Kopelevich, O. V.; and Shifrin, K. S. "Brightness Spectra of Outgoing Radiation and Their Change with Observation Altitude," Opticheskiye metody izucheniya okeanov i vnutrennikh vodoyemov ["Optical Methods of Studying Oceans and Internal Reservoirs"], Novosibirsk, 1978.

3. Yerlov, N. Opticheskaya okeanografiya ["Optical Oceanography"], Moscow, Mir, 1970.

4. Golubitskiy, B. M.; Levin, I. M.; and Tantashev, M. V. "Brightness Coefficient of Semi-Infinite Layer of Sea Water," Izv. AN SSSR, FAO, No 11, 1974.

5. Kopelevich, O. V.; and Burenkov, V. I. "Link Between Spectral Values of Indices of Absorption of Light by Sea Water, Pigments of Phytoplankton and Yellow Substance," Okeanologiya, vol 17, No 3, 1977.

6. Bekasova, O. B.; Kopelevich, O. V., and Sud'bin, A. I. "Determination of Optical Properties of Sea Water, Content of Chlorophyll and Suspended Matter in Surface Layer of Ocean by Spectral Values of Brightness of Ascending Radiation," Okeanologiya, vol 19, No 2, 1979.

AIRCRAFT RECORDING PHOTOMETER OF SEA SURFACE BRIGHTNESS.

YEFIMENKO, I. D. NOVIKOV, V. S. PELEVIN, V. N.

An aircraft recording photometer of sea surface brightness in FAR-1 and FAR-2 modifications is described. The first modification makes it possible to record distribution over the sea surface of the brightness coefficient ρ at λ = const with frequency to 100 Hz. This corresponds to resolution on the surface on the order of a few meters.

The second modification records the ratio $\rho\lambda_1/\rho\lambda_2$ with the same frequency. The instrument permits long-range evaluation of concentration of suspended matter and chlorophyll in the surface layers of the sea, and also determination of the optical water index.

It is indicated in [1] that measurements of the brightness coefficient of the sea $\rho\lambda$ in the short wavelength region of the spectrum, or the ratio of the brightness coefficients of the sea in two spectral regions can be used to determine the optical index of the water type. It, in turn, makes it possible to obtain information about the characteristics of light attenuation in these waters.

A number of publications [2 - 5] have focused attention on the fact that the ratio of coefficients $\rho\lambda$ in two spectral regions can be used to evaluate the chlorophyll concentration in the upper layer of sea water. It is noted in [6] that in the coastal zone of the sea above the shelf, the $\rho\lambda$ values at $\lambda \cong 600$ nm are proportional to the concentration n_{sus} of suspended substance in the interval n_{sus} from 0 to 8 - 9 mg/l.

This far from complete list of the potentialities for long-range spectrometry results in the need to construct a photometer which records $\rho\lambda$ or the $\rho\lambda_1/\rho\lambda_1$ ratio

in current time, without subsequent numerical processing of the measurement data. This requires equipment division of two signals into each other.

The use of a photometer on an airplane or helicopter stipulates fairly high fast-response, the possibility of recording a signal with frequency of several tens of hertzes.

This article describes two modifications of a developed photometer (aircraft recording) designated below as FAR-1 and FAR-2. These modifications are respectively designed to record $\rho\lambda$ with fixed wavelength λ and $\rho\lambda_1/\rho\lambda_1$ ratio for two previously selected sections of the spectra, with frequency of the meterings to 100 Hz. In order to guarantee this fast-response, both photometers use two photomultipliers each with identical characteristics and a system of automatic signal division into each other with recording of information on magnetic tape, and parallel, for visual control of measurements on board the carrier, on a pen self-recorder.

The course of the FAR-1 rays is shown in the plan of Figure 1, and the external appearance in Figure 2. Two optical systems made as identical as possible are placed in a tube 500 mm long and 60 mm in diameter. One of the lenses 2 (left in Figure 1) is aimed downwards for observation of the sea brightness at the nadir, the second 2' is aimed at a plate made of frosted glass horizontally arranged and illuminated by the light of the sun and the sky. Lenses (2 and 2'), interference light filters (3 and 3') and photo detectors FEU-62 (4 and 4') of both channels are identical in characteristics. Since there are no two completely identical photomultipliers, their characteristics are converged by balancing the voltage on both dividers.

A white frosted plate 5 is graduated in relation to the white Lambert reflector, so that the actual right channel yields a signal U_y which is proportional to brightness of the latter B_0, while the left channel provides a signal U_x which is proportional

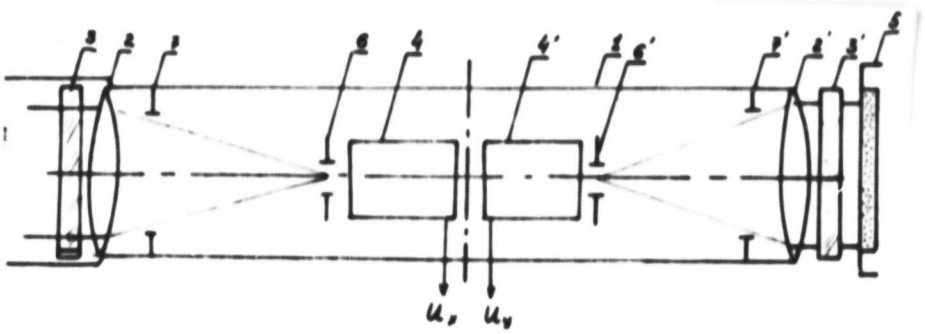

Figure 1. Plan of Course of Beams in FAR-1
Key:
1. housing in gimbal mount
2,2'. lenses
3,3'. interference light filters
4,4'. FEU-62
5. plate made of frosted glass
6,6'. diaphragms of visual field
7,7'. diaphragms of light force

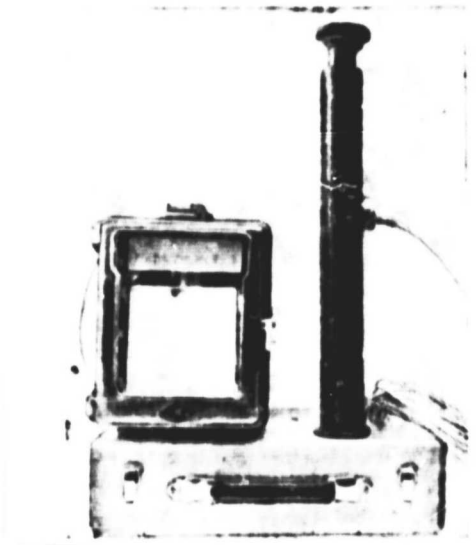

Figure 2. External Appearance of FAR-1--sensor, recorder block and power block

to brightness of the sea at the nadir $B^{\downarrow}$. Both photofluxes are intensified by a preamplifier and are fed to the signal divider (Figure 3). It is constructed according to a plan for transformation of one of the signals to the frequency of pulse tracking, while the other--to the duration of these impulses with subsequent separation of the constant component of a number of pulses with the help of low frequency filter (LFF). /205

The resulting signal which is proportional to the U_x/U_y ratio is intensified in power and fed to the pen of the self-recorder N- 384-1. The self-recorder is made so that it guarantees movement of paper with velocity to 1 m/min. Both modulated signals are recorded in parallel on a two-track cassette tape recorder.

With this plan of measurements, we are actually recording the brightness ratio of the sea B to the brightness of the white plate B_0, while $\rho\lambda$ should be computed according to formula [6]:

$$\rho_\lambda = \frac{B_\lambda - 0{,}02\, B_{\uparrow\lambda}}{B_{0\lambda}} \qquad (1)$$

where $B_{\uparrow\lambda}$ --brightness of the sky at the zenith. The error which develops when the term $0.02\, B_{\uparrow\lambda}$ is ignored, depends on λ and the weather conditions, and according to our measurement data over the Baltic Sea, it is the quantity given in Table 1.

It is apparent from the table that in the long wavelength region of the spectrum /207 at $\lambda \geq 560$ nm, the brightness of reflection of the sky by the water-air boundary in clear sunny weather can be ignored, assuming in this case an error that does not exceed 10% (for turbid waters of the Baltic Sea). In overcast weather, this error increases (see table).

With measurements of $\rho\lambda$ in a shorter wavelength region, one should continually take into consideration the contribution of the term $0.02\, B_{\uparrow\lambda}$. For this purpose it is necessary to periodically remove the frosted glass and conduct a simultaneous recording of brightness of the sea and the sky. The plan for the course of rays in the photometer of FAR-2 modification is similar to that shown in Figure 1, but in this case, both brightness meters are aimed downwards (see external appearance of FAR-2 in Figure 4). The instrument is based on series-produced field binoculars which make it possible to aim both lenses at the same section of the surface. Both channels differ only in wavelength of transmission λ_1 and λ_2 of changeable interference

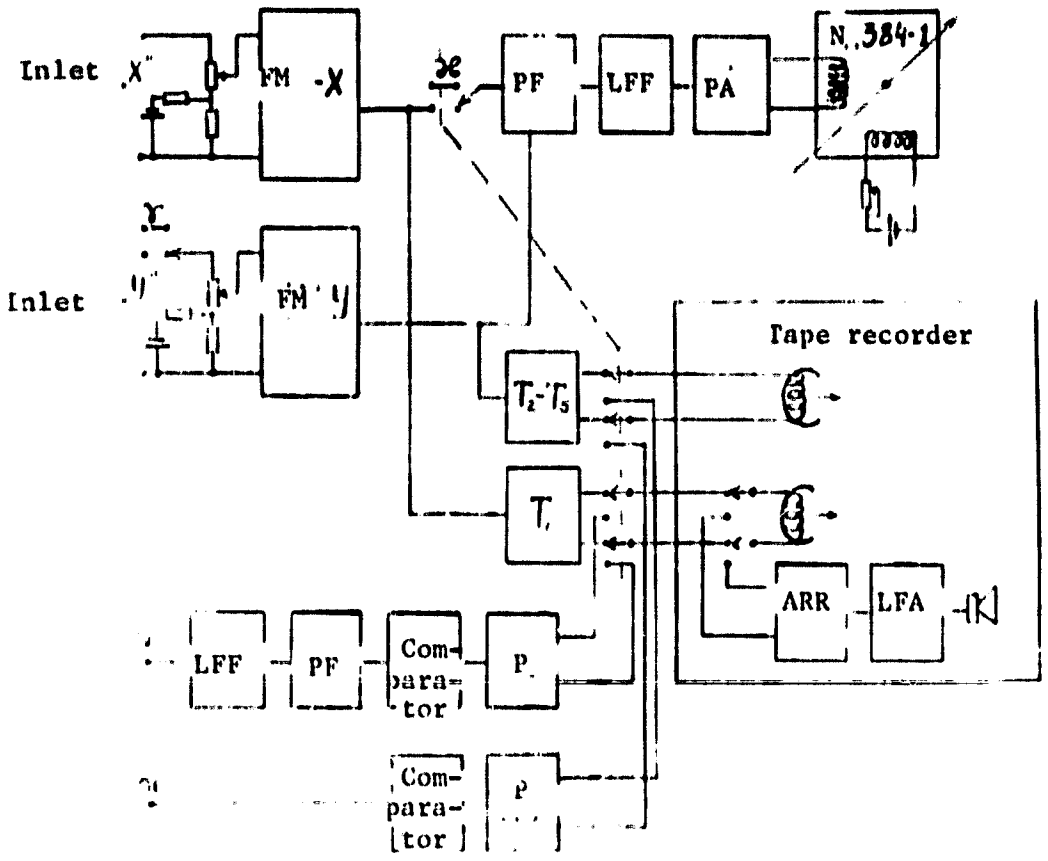

/206

Figure 3. Block Diagram of Divider of Signals and Recorders

Key:

1. FM-"x"--frequency modulator of channel "x"
2. PF--pulse former
3. LFF--low frequency filter
4. PA--power amplifier
5. FM-"y"--frequency modulator of channel "y"
6. P--preamplifier
7. ARR--amplifier of reproduction recording
8. LFA--low frequency amplifier
9. T_1 + T_5--triggers

light filters installed at the inlet.

The systems of balancing the PM sensitivity, division of two signals and /208
recording are the same as in -1. Both instrument modifications were gimbal-mounted outside the cabin of the helicopter. This made it possible to photometer

TABLE 1. DEVIATION OF QUANTITY $\frac{B_{T\lambda}}{B_{\rho\lambda}}$ FROM $\rho\lambda$ ACCORDING TO (1)

λ nm	Weather conditions	
	0°	П
369÷383	35—45%	35—45%
426÷457	25—30%	30—35%
558÷695	7—10%	15—25%

the sea strictly at the nadir regardless of the angles of heeling and pitching of the helicopter.

Figure 4. External Appearance of FAR-2, Optical Sensor, Recorder Block and Power Block

Order of calibrating the aircraft recording photometer. Graduation of the FAR-1 uses a portable "optical bench" 150 cm long and shown in Figure 5. Two reflecting mirrors are installed on the ends of the bench, while a photometric lamp PZh type is installed in the center on a rod 75 cm long.

The optical FAR-1 block is installed in the middle of the bench. Frosted glasses are put on both lenses. A lamp is turned on, and mirrors direct the light to both channels of the instrument so that the light spot completely covers the frosted

attachment. By balancing the voltage on both PM through potentiometers, one should attain similar readings in both channels (i.e., at the outlet of the instrument signal $U_x/U_y = 1$). By reducing voltage on the photometric lamp, one should reach equality of the readings in both photomultipliers in broad limits of illumination at the inlets.

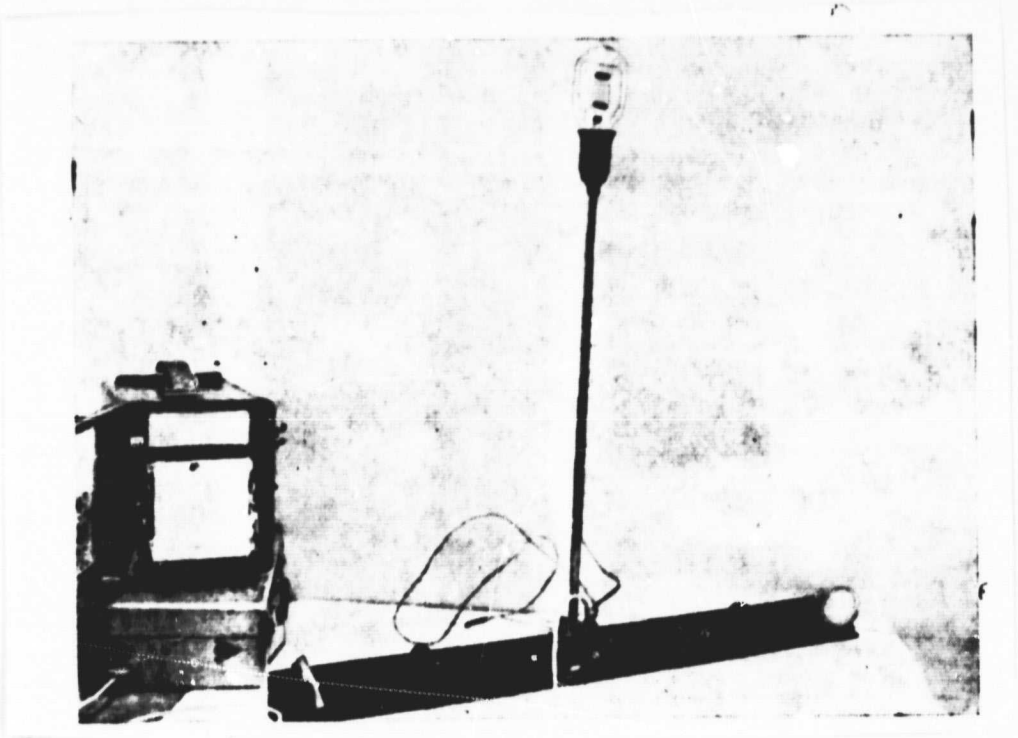

Figure 5. External Appearance of Graduated Bench for FAR-1

During calibration of FAR-2, its optical sensor is aimed at a uniformly illum- /20
inated surface, since the visual fields of both FAR-2 channels coincide. After initially installing similar light filters on both channels, the same readings are achieved with different level of illumination of the shield. Then two working light filters are installed, and with illumination of the white shield by solar light, equality of both signals is again established. Now the instrument readings during flight over the sea will equal the $\rho\lambda_1/\rho\lambda_2$ ratio with error that is mainly determined

by lack of consideration for mirror reflection of the color of the sky by the surface. The quantity of this error can be estimated with the help of the table presented below.

The design of the instruments is shown in Figures 2 and 4. The weight of the optical blocks is not more than 1 kg each. The autonomous power block (completely independent of the on-board circuit) with batteries weighs 5 kg. The overall dimensions are 400 x 100 x 150 mm. The electronic circuit of the recorder, the tape recorder and the system for recording the operator's voice are mounted on the body of the self-recorder N-384-1, and are located inside its housing. The weight of this recording block is 4 kg and the overall dimensions are 200 x 150 x 280.

MAIN SPECIFICATIONS

1. Range of signal change C_x--40 db.
2. Range of signal change C_y--30 db.
3. Error in the recording channel no more than 0.5%.
4. Range of recording frequency 0 - 100 Hz, i.e., spatial resolution during flight of airplane at velocity 1000 kg-m/h--3 meters.

An example of realization of instrument readings during testing over the sea is given in Figure 6.

BIBLIOGRAPHY /210

1. Pelevin, V. N. "Spectral Characteristics of the Field of Solar Radiation in the Sea and Above its Surface," in this collection, 1979.
2. Pelevin, V. N.; Lokk, Ya. F.; and Kel'balikhanov, B. F. "Photometer to Measure Spectral Brightness of Radiation Emerging from the Sea and Results of its Testing Under Full-Scale Conditions," in Opticheskiye issledovaniya v okeane i v atmosfere nad okeanom ["Optical Studies in the Ocean and in the Atmosphere Above the Ocean"], P. P. Shirmov Institute of Oceanology of the USSR Academy of Sciences.

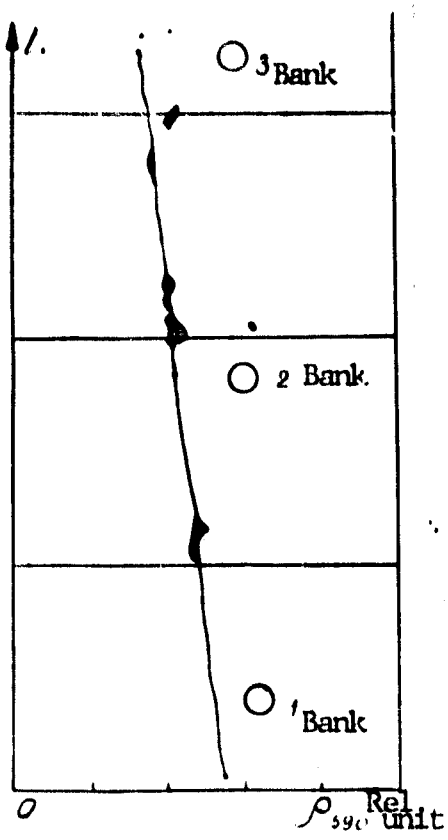

Figure 6. Example of Realization Obtained by FAR-1 Photometer. The photometer is installed on the prow of the ship following from the depth of the Gelendzhik Gulf (first bank) to exit from the gulf into the open sea (third bank). Interferences caused by foam on the surface are visible.

3. Clarke, L.; Ewing, G. C.; and Lorenzen, C. J. "Spectra of Back-Scattered Light from the Sea Obtained from Aircraft as Measure of Chlorophyll Concentration," Science, 1970, 167, No 3921, p 1119.

4. Shifrin, K. S.; Sud'bin, A. I.; Bekasova, O. D.; et al. "Study of the Link Between Chlorophyll Content and Brightness of Light Emerging from the Sea," Tr. TROPEKS-72, ["Works of TROPEKS-72"], Leningrad, Gidrometeoizdat, 1974.

5. Neuymin, G. G.; Li, M. Ye.; and Zakirchenko, Yu. I. "Water Color Index of the Caribbean Sea and Adjoining Region of the Atlantic Ocean," Issledovaniye Karibskogo morya ["Study of the Caribbean Sea"], Izd. MGI AN USSR, Sevastopol', 1974.

6. Pelevin, V. N. "Estimate of the Concentrations of Suspended Matter and Chlorophyll in the Sea from Spectrum of Outgoing Radiation Measured from a Helicopter," Okeanologiya, vol 18, No 3, 1978.

POSSIBLE EVALUATION OF THE DISTRIBUTION OF YELLOW SUBSTANCE IN SEA WATER FROM THE SPECTRA OF OUTGOING RADIATION. PELEVIN, V. N, GRUZEVICh., A. K., AND LOKK, YA. F.

The authors compared the values for the ratio of brightness coefficient of the sea $\rho\lambda$ at λ = 369 nm and λ = 590 nm and the concentration of "yellow substance" in the sea, expressed in optical units. The distribution of this ratio for the water area of the Gulf of Riga is constructed from the measurement data from a helicopter on 18 and 19 September 1977.

The Baltic summer expedition of 1977, as well as the 1975 - 1976 expeditions [1 - 3] made simultaneous measurements of the spectra of radiation emerging from the sea and the concentrations of chlorophyll, suspended matter and light-absorbing dissolved substances of organic origin ("yellow substance") contained in the water samples. This work presents data which evaluate the possible determination of the quantity of "yellow substance" in the water from values of the brightness coefficient of the sea $\rho\lambda$.

It is common knowledge that the spectral course of $\rho\lambda$ in a two-stream approximation is described by the formula [4, 5, et al.]:

$$\rho_\lambda \sim \frac{\beta\lambda}{\varkappa\lambda + \beta\lambda}. \qquad (1)$$

where $\beta\lambda$--back-scattering index, $\varkappa\lambda$--index of absorption of light by the medium. The absorption index of light by sea water in the visible and ultraviolet spectral regions can be presented in the form of the sum of the following components [3]: /211

$$\varkappa = \varkappa_c + \varkappa_{pigm} + \varkappa_{ys} + \varkappa_{non} \qquad (2)$$

where $\varkappa_c$--index of absorption by clean water, $\varkappa_{pigm}$--by pigments of phytoplankton, $\varkappa_{ys}$--by yellow substance, $\varkappa_{non}$--particles of suspension which nonselectively absorb light.

We will examine the spectral course of the absorption indicators of light by clean water, by phytoplankton pigments and by substances of organic origin dissolved

in water (Figure 1). It is apparent from the figure that absorption of light by yellow substance in the short wavelength region of the spectrum exceeds absorption by other components. In turn, it follows from (1) that large concentrations of yellow substance must result in a decrease in values of $\rho\lambda$ in the blue and near ultraviolet regions of the spectrum.

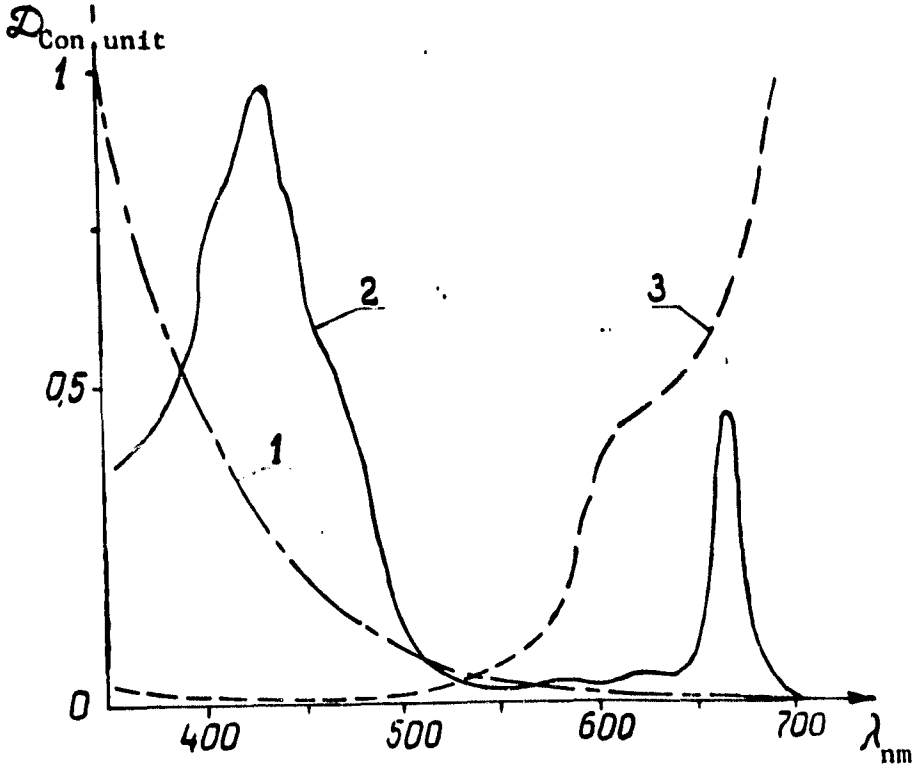

Figure 1. Typical Spectral Course of Absorption Indicator of Light of "Yellow Substance" (1), Phytoplankton Pigments (2) and Clean Water (3).

However, in many cases an increase in concentration of yellow substance in sea /212 water occurs simultaneously with an increase in the concentration of suspended matter. As a consequence $\beta\lambda$ rises. The rise in $\beta\lambda$ in formula (1) compensates for the increase in $\varkappa\lambda$, and as a result, the correlation $\rho\lambda$ with concentration of yellow substance may not be observed. At the same time, an increase in $\beta\lambda$ with a rise in concentration of suspended matter occurs over the entire spectrum. This makes it

very useful to examine the $\rho\lambda_1/\rho\lambda_2$ ratio for two separate sections of the spectrum. This ratio depends to a considerably lower degree on the change in the suspended matter concentration. In this case, λ_1 should be selected in the short wavelength region of the spectrum, where absorption of light by yellow substance dominates over other components, while λ_2--in the longer wavelength region where absorption by dissolved organic matter is insignificant. In addition, after using the $\rho\lambda_1/\rho\lambda_2$ ratio, one can significantly decrease the dependence of this photometered quantity on the phytoplankton pigments. For this purpose, λ_1 should be selected in the near ultraviolet region, while λ_2 in the yellow. Then the blue-green band of absorption of chlorophylls and accompanying pigments of phytoplankton will mainly be located between these spectral sections.

In the analysis of the experimental data we used the results of photometering of the water area of the Gulf of Riga from a KA-26 helicopter on 18 and 19 September 1977. Photometering was done in eight spectral sections λ_1 = 369, 386, 426, 458, 556, 590, 664 and 690 nm with width of the spectral interval $\Delta\lambda \cong 10 - 15$ nm. At the same time, water samples were taken in certain points of the gulf from the surface for laboratory analysis of the content of suspended matter, chlorophyll and yellow substance. The photometering data were used to compute the $\rho\lambda$ values according to the formula [5]:

$$\rho_\lambda = \frac{B_{\downarrow\lambda} - 0{,}02B_{\uparrow\lambda}}{B_{0\lambda}}, \qquad (3)$$

where $B_{\downarrow\lambda}$--brightness of the sea observed at the nadir, $B_{\uparrow\lambda}$--brightness of the sky at the zenith, $B_{0\lambda}$ --brightness of the horizontal light scatterer illuminated by the sun and light of the sky.

It should be noted, that according to our measurements from a low-flying helicopter, the contribution of light of the sky, mirror-reflected by the water-air boundary, in the near UV-spectral region is very significant. For a cloudless sky it is 50 - 70% of the observed brightness of the sea. Because of this circumstance, changes

in brightness of the sea in the blue and near ultraviolet regions must be made with special caution, while calculations of $\rho\lambda$ are accompanied by mandatory consideration of Fresnel's correction in formula (3).

The content of yellow substance in the samples was evaluated according to the technique described in [6]. As a parameter characterizing the concentration of dissolved substances of organic origin, the indicator of absorption by yellow substance was selected at short wavelength boundary of the spectral region of photometering at λ = 369 nm, i.e., $^{\times}_{ys369}$. The $^{\times}_{ys369}$ values were computed from measurement results of optical density of evaporated water samples on the "Spekord" spectrophotometer. /213

A total of 25 samples were taken. It was found that over the water area of the Gulf of Riga, the $^{\times}_{ys369}$ values vary in limits from 1.0 to 3.5 m^{-1} (with natural base), while for the Daugava and Pyarnu Rivers it is 2.8 - 14.0 m^{-1}.

Preliminary examination of the measurement results confirmed that the absolute values of ρ_{369} do not correlate with the concentration of yellow substance $^{\times}_{ys369}$ in the corresponding samples. We therefore further relied on the ratio ρ_{369}/ρ_{590}, where the wavelengths 369 nm and 590 nm were selected according to the considerations presented above. In this case one can expect that at least in limits of the restricted water area, the ρ_{369}/ρ_{590} and $^{\times}_{ys369}$ values will correlate among themselves.

We will trace the distribution of ρ_{369}/ρ_{590} over the water area of the Gulf of Riga (Figure 2). For this purpose, the rate of change in the quantity ρ_{369}/ρ_{590} was divided into six intervals which are marked on the map by conventional designations. This made it possible to isolate the following regions in the Gulf of Riga:

I. Central part of the gulf and Irbenskiy Strait, through which water exchange with the Baltic Sea mainly occurs. Here the quantity of ρ_{369}/ρ_{590} ratio changes from 0.9 to 1.35, while to the southwest of the Ruhnu Island it even exceeds these values.

II. Vast spaces of the north and east sections of the Gulf of Riga characterized by values $0.6 < \rho_{369}/\rho_{590} \leq 0.9$.

III. Southern part of the water area of the gulf, its eastern coast and zones of shallow water around Rukhnu and Kikhnu Islands with values ρ_{369}/ρ_{590} from 0.4 to 0.6 inclusively.

IV. Sections with values $\rho_{369}/\rho_{590} < 0.4$ in the vast southeast zone of the gulf and in the Pyarnu Strait where the currents carry away highly productive water of large rivers Liyelupe, Daugava, Gaui and Pyarnu. To the southeast of the mouth of the Daugava River the ratio ρ_{369}/ρ_{590} diminishes to 0.3 and even less.

It should be noted that the large range of change in the ρ_{369}/ρ_{590} ratio (5-fold and more) on a comparatively limited water area of the Gulf of Riga and the positively traced geographic laws governing its distribution make this quantity very useful in studying the hydrological regime of the gulf.

The limited number of samples taken does not make it possible to make a reliable correlation between the concentration of yellow substance and the quantity of the ρ_{369}/ρ_{590} ratio. However we attempted to determine the nature of this link. It was found that for clarity it is more convenient to use the opposite correlation, i.e., ρ_{590}/ρ_{369}. The values x_{ys369} were divided into three groups according to the site of water sample taken in limits of the sections referring to a certain gradation in the quantity ρ_{369}/ρ_{590} (Figure 2). For each group the average values x_{ys369} and ρ_{590}/ρ_{369} and their standard deviations were computed. The obtained relationship is indicated in Figure 3. The standard deviations of the comparable quantities was also noted here. It is easy to see that the concentration of yellow substance in the surface waters of the Gulf of Riga rises with an increase in ρ_{590}/ρ_{369} ratio. With high concentrations of yellow substance this dependence has a roughly linear nature.

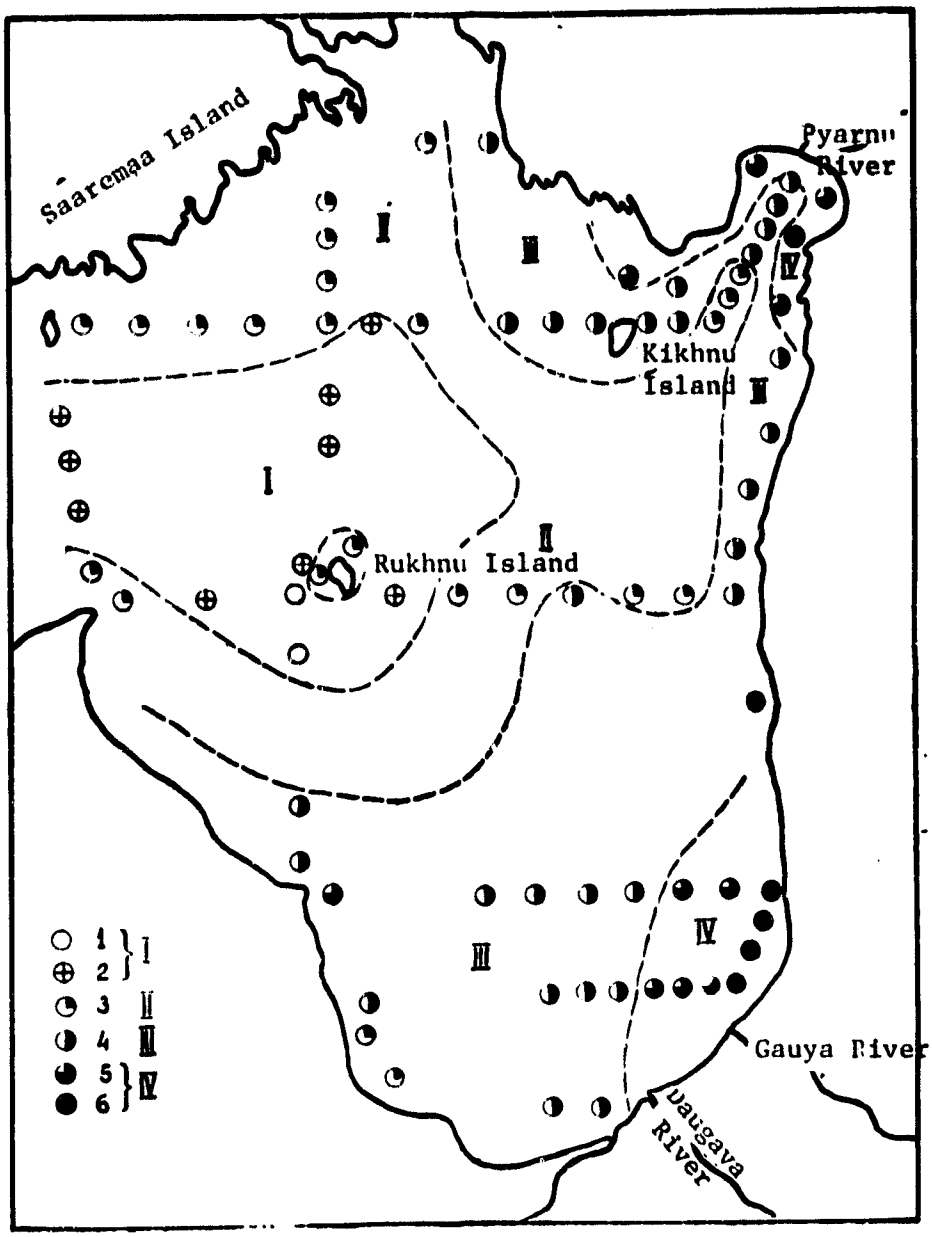

/414

Figure 2. Distribution of Values ρ_{369}/ρ_{560} over Water Area of the Gulf of Riga According to Data of Flight on 18 and 19 September 1977.

Key.

1. $1.35 < \rho_{369}/\rho_{560}$
2. $0.9 < \rho_{369}/\rho_{560} \leq 1.35$
3. $0.6 < \rho_{369}/\rho_{560} \leq 0.9$
4. $0.4 < \rho_{369}/\rho_{560} \leq 0.6$
5. $0.33 < \rho_{369}/\rho_{560} \leq 0.4$
6. $\rho_{369}/\rho_{560} \leq 0.33$

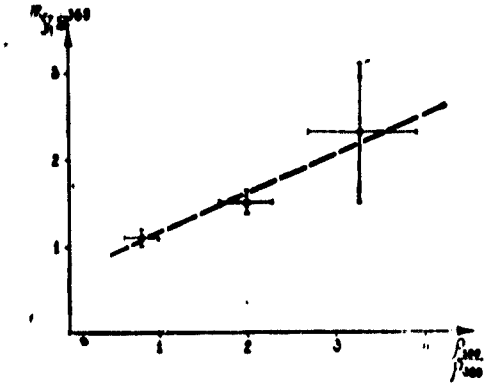

Figure 3. Comparison of Concentration of "Yellow Substance" χ_{ys369} and Ratio of the Coefficients of Brightness ρ_{590}/ρ_{369} for a Number of Water Areas in the Gulf of Riga. The average values and the standard deviation from the averages by samplings are plotted.

The basic possibility of developing a long-range method for evaluating the content of dissolved substances of organic origin in sea waters follows from the presented data. However, in order to pinpoint the detected links, and to evaluate the accuracy of the method and influence of other , possibly unconsidered factors, it is necessary to further collect experimental data and perfect the measurement technique.

It is also required that an explanation be found for the fact that for the rivers Daugava and Pyarnu which contain a very large quantity of suspended matter and dissolved organic substances, the regression obtained for the waters of the Gulf of Riga (Figure 3) is not maintained.

BIBLIOGRAPHY

1. Pelevin, V. N.; Lokk, Ya. F., Kel'balikhanov, B. F. "Photometer to Measure Spectral Brightness of Radiation Emerging from the Sea and Results of its Tests Under Full-Scale Conditions," Opticheskiye issledovaniya v okeane i v atmosfere nad okeanom ["Optical Studies in the Ocean and in the Atmosphere Above the Ocean"], P. P. Shirshov Institute of Oceanology of the USSR Academy of Sciences, Moscow, 1975. /216

2. Lokk, Ya. F., Pelevina, M. A.; Tenson, Yu. "Study of Chlorophyll Distribution from a Helicopter," Tezisy I s'yezda sovetskikh okeanologov ["Summaries of Reports of the First Congress of Soviet Oceanographers"], USSR Academy of Sciences, Moscow, 1977.

3. Pelevin, V. N.; Pelevina, M. A.; Kel'balikhanov, B. F. "Study of the Spectra of Radiation Emerging from the Sea from a Helicopter," in Opticheskiye metody izucheniya okeanov i vnutrennikh vodoyemov ["Optical Methods of Studying the Oceans and Internal Reservoirs"], Izd. Nauka, Siberian Department of the USSR Academy of Sciences, Novosibirsk, 1978.

4. Ivanov, A. P. Fizicheskiye osnovy gidrooptiki ["Physical Fundamentals of Hydrooptics"], Izd. Nauka i tekhnika, Minsk, 1975.

5. Pelevin, V. N. "Evaluation of the Concentration of Suspended Matter and Chlorophyll in the Sea from Spectrum of Outgoing Radiation Measured from a Helicopter," Okeanologiya, vol 18, No 3, 1978.

6. Pelevina, M. A. "Technique and Results of Measuring Spectral Absorption of Light by Dissolved Organic "Yellow" Substance in Waters of the Baltic Sea," in this collection, 1978.

METHOD FOR LOCATING DISTURBED SEA-SURFACE BY DIVERGING LIGHT PULSE. PELEVIN, V. N.

A new method is suggested for sea surface location by a diverging short IR-light pulse. It is shown that widening of a pulse reflected by the surface makes it possible to evaluate the dispersion of deviations in the elements of the disturbed surface. The method is tested during location of the surface of the Baltic Sea from a helicopter flying at altitudes 100 - 500 m.

There are different methods for light-location of a disturbed sea surface which have the purpose of evaluating its different geometrical characteristics [1 - 3, et al.]. When the sea is illuminated at acute angles to the horizontal, the profile of the wave is restored according to the shape of the reflected pulse [1]. During location of the sea surface from a helicopter, by directed short pulse at changing angles to the vertical, depending on the amplitude of the reflected signal on the angle of location, the distribution function for the inclinations of the surface elements is determined [2].

There is theoretical substantiation for the method of surface location by a vertically directed short pulse, in which the distribution dispersion of the surface altitude is evaluated from the temporal expansion of the reflected pulse [3, et al.].

This work provides substantiation and description of experimental verification of the new method. It consists of locating the surface of the sea by a very diverging short IR-like pulse. It is shown that widening of the pulse reflected by the surface carries information about dispersion of the inclinations of the surface elements, and with high wind velocities, also about the quantity of foam on the sea surface.

The method is based on the following concepts regarding the process of IR-pulse reflection by the sea surface.

1. When the water surface is illuminated by laser radiation with wavelength $\lambda = 1.06$ μm, the primary percentage of the back-scattered signal is created by light which is mirror-reflected by the air-water interface, and namely, the areas oriented perpendicularly to the direction of the superposed source-receiver. Light $\lambda = 1.06$ μm which enters under the surface, is intensively absorbed by water, therefore the percentage of light which is diffusely reflected by the mass is relatively low. /217

2. The intensity of the signal reflected by the surface is proportional to the value of the distribution function of the inclinations $Q(\eta_x, \eta_y)$ with arguments that correspond to the angles of surface location from a helicopter. The course of the functions $Q(\eta_x, 0)$ for different dispersions of inclinations σ^2 (i.e., different "irregularity" of the surface) is shown in Figure 1. The distribution functions based on experimental data are assumed to be normal. It is easy to see that change in dispersion in inclinations results in a noticeable change in the value of the function Q, and this means, also the intensity of the reflected signal, both with angles of location θ close to 0°, and with angles on the order of 10 - 20° (depending on the value of dispersion σ^2). Foam on the surface is scattered according to Lambert's law.

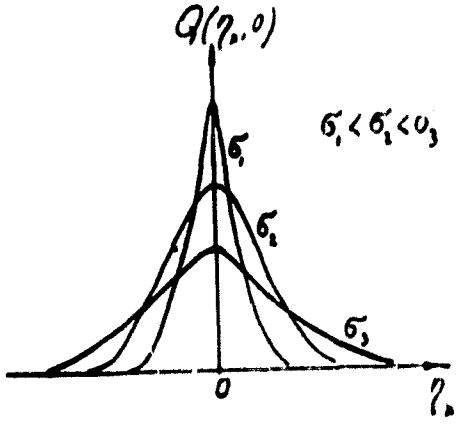

Figure 1. Course of the Functions $Q(\eta_x, 0)$ for Different Versions of Inclinations σ^2.

We will make theoretical substantiation of long-range methods for determining dispersion of inclinations of elements of the sea surface according to one reflected pulse of a laser. The laser beam was defocused in limits of the angle $\pm\psi$ from the vertical (ψ = 16 - 20°). The angular diagram of the receiver of reflected radiation corresponds to the same taper. The axis of the light beam is vertical, like the axis of the receiver. Reflection of light from different sections of the surface creates a shift in the reflected pulses in time because of difference in the path through air, depending on the angle of inclination of the incident radiation. This effect creates expansion of the pulse. The influence of dispersion of elevations is not taken into consideration. According to expansion of the reflected pulse, dispersion of inclinations of the surface elements is computed.

The calculated formulas were derived as follows. Assume that the laser pulse /218 with energy q J is uniformly distributed in limits of solid angle Ω. The temporal course of the pulse is described by the function $p(\tau)s^{-1}$, and $\int p(\tau)d\tau = 1$. Then the power of the light which spread in the element of solid angle $d\omega$--see Figure 2,-- equals $qp(\tau)\cdot\frac{d\omega}{\Omega}$ W. After reflection from the surface, each of the elements of the beams will be partially directed towards the receiver which has input area S and is located next to the source at altitude h from the surface. The axis of the visual field of the receiver is vertical. Its angular aperture corresponds to the same

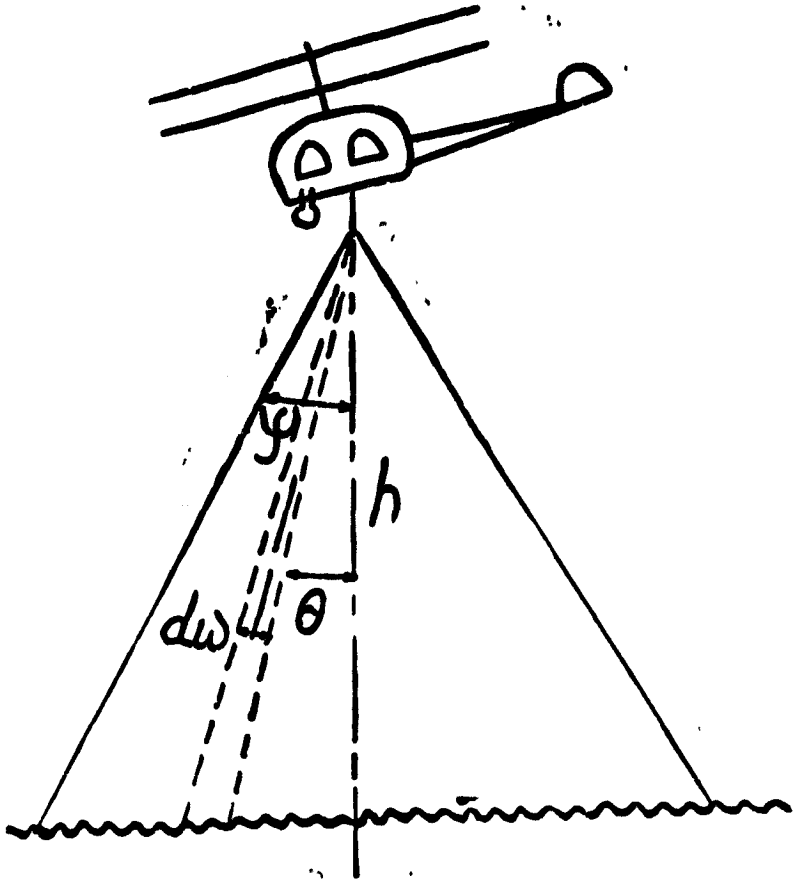

Figure 2. Plan of Location of Disturbed Sea Surface by Short Diverging IR-Pulse from Helicopter.

solid angle $\Omega = 2\pi(1 - \cos\Psi)$. A percentage of radiation equal to $y(0)$ will return to the receiver from each of the elementary beams, where 0--angle of inclination of elementary beam to the vertical. This percentage will reach the receiver with time lag equal to $\phi(0)$. As a result, the power of the received signal will be /419

$$m(\tau) = \int_{\Omega} \frac{q}{\Omega} \cdot y(\theta) \cdot p[\tau - \varphi(\theta)] \cdot d\omega \qquad (1)$$

With conical configuration of the incident beam $d\omega = 2\pi d\cos\theta$.

We will examine what appearance the functions $y(0)$ and $\phi(0)$ have. The probability of development of a reflecting area in the zone of incidence of the elementary beam is described in the distribution function of the inclinations. We will

consider it not to be different from the normal:

$$Q(\eta_x, \eta_y)) = = \frac{1}{2\pi\sigma_x\sigma_y} \times e^{-\frac{\eta^2_x}{2\sigma^2_x} - \frac{\eta^2_y}{2\sigma^2_y}} \tag{2}$$

Here $\eta_x = \operatorname{tg}\Theta_x$; $\eta_y = \operatorname{tg}\Theta_y$; Θ_x and Θ_y--angles of inclination of the perpendicular in relation to the vertical, in two mutually perpendicular planes. The probability of incidence of the reflected beam in the receiver, correspondingly equals

$$\frac{1}{4} Q(\eta_x, 0) \cdot \Delta 0 \tag{3}$$

where $\Delta 0$--solid angle at which the input opening of the receiver is observed from the center of the area. The multiplier 1/4 takes into consideration the change in direction of the reflected beam in relation to that which falls on the two-fold angle of incidence. From obvious considerations (see Figure 2):

$$\Delta 0 = \frac{s\cos\Theta}{(h/\cos\Theta)^2} = \frac{s}{h^2} \cdot \cos^3\Theta, \text{ from which} \tag{4}$$

$$y(\Theta) = F_r \cdot \frac{1}{4} \Theta(\eta_x, 0) \cdot \frac{s}{h^2} \cos^3\Theta \tag{5}$$

F_r--coefficient of Fresnel's reflection for beams falling perpendicularly on the water surface (equal to 0.02). As a result

$$y(\Theta) = 0{,}02 \frac{1}{8\pi\sigma_x\sigma_y} \exp\left(\frac{\operatorname{tg}^2\Theta}{-2\sigma^2_x}\right) \frac{s}{h^2} \cos^3\Theta \tag{6}$$

The function $\phi(\Theta)$ is determined from geometric considerations according to the difference in courses of the vertical and inclined beams:

$$\varphi(\Theta) = \frac{2}{c}\left(\frac{h}{\cos\Theta} - h\right) = \frac{2h}{c}(\sec\Theta - 1) \tag{7}$$

Now the shape of the received signal is generally equal to:

$$m(\tau) = \int_{\Omega} \frac{q}{\Omega} \times \frac{2\pi \cdot 0{,}02}{8\pi\sigma_x\sigma_y} \exp\left(\frac{\operatorname{tg}^2\Theta}{2\sigma^2_x}\right) \frac{s}{h_2} \cos^3\Theta) \times \tag{8}$$

$$\times P\left[\frac{2h}{c}(\sec\Theta - 1) - \tau\right] d\cos\Theta$$

/220

where the trigonometric function Θ is unequivocally linked to τ. If the function P which stands under the integral is δ --function, the integration is simplified: all the multipliers with change in the variables are removed from the integral sign.

We take into consideration that

$$\int a(x)\delta[\Phi(x)-\tau]dx=\frac{a(x_0)}{\Phi'(x_0)}. \tag{9}$$

It follows from (8) and (9)

$$m(\tau)=0{,}02\,\frac{q\cdot s\cdot c}{8\pi\Omega\cdot\sigma_x\sigma_y h^3}\left(\frac{1}{\frac{c\tau}{2h}+1}\right)^5\exp\left(-\frac{c\tau}{h\cdot 2\sigma_x}-\frac{c^2\tau^2}{4h^2\sigma_y^2}\right)$$

By introducing the equipment constant into the quantity $A=0{,}02\,\frac{qsc}{8\pi\Omega}$, we obtain the following dependence of the shape of the reflected pulse on σ_x, σ_y and h:

$$m(\tau)=A\,\frac{1}{\sigma_x\sigma_y h^3}\left(\frac{1}{\frac{c\tau}{2h}+1}\right)^5\exp\left(-\frac{c\tau}{h2\sigma_x^2}-\frac{c^2\tau^2}{8h^2\sigma_y^2}\right) \tag{10}$$

It is apparent that the main parameter which $m(\tau)$ depends on, equals $\frac{c\tau}{2h}=t$. Its meaning is that this is the dimensionless time where a unit corresponds to the time for passage by light of double distance between the flying object and the nearest point of the sea surface. We will pass to the variable t:

$$m(t)=A\,\frac{1}{\sigma_x\sigma_y h^3}\left(\frac{1}{t+1}\right)^5\exp\left(-\frac{t}{\sigma_x^2}-\frac{t^2}{2\sigma_y^2}\right) \tag{11}$$

This is Green's function which describes reflection of the diverging δ - pulse from the disturbed surface. We now take into consideration that, starting with a certain wind velocity, the wave crests collapse and foam forms on the surface of the sea. We will designate the percentage of the surface covered by foam as ξ_1, and the coefficient of reflection of foam as ξ_2. The product $\xi=\xi_1\times\xi_2$ is the equivalent percentage of surface which reflects according to Lambert's law with albedo 1. The strength of light reflected by the Lambert surface illuminated by beam $q\cdot p(\tau)\frac{d\omega}{\Omega}$,

in direction of the receiver equals:

$$dI = \frac{\cos\Theta}{\pi} \xi \cdot q \cdot p(\tau) \frac{d\omega}{\Omega} \tag{12}$$

while the level of the received signal

$$dI\Delta 0 = \frac{1}{\pi} \xi q p(\tau) \frac{d\omega}{\Omega} \frac{\pi}{4^2} \cos^4\Theta. \tag{13}$$

The signal received from the foam is obtained by integration

$$m_1(\tau) = \frac{\xi q}{\pi\Omega} \frac{s}{h^2} \int_{\Omega} p\left|\frac{2h}{c}(\sec\Theta - 1) - \tau\right| \cos^4\Theta d\omega . \tag{14}$$

If $p(\tau)$ -- δ-function, then $m(\tau)$ --pulse transitional function:

$$m_1(\tau) = -\frac{\xi qs}{\pi\Omega h^2} \cdot 2\pi \int p\left|\frac{2h}{c}(\sec\Theta - 1) - \tau\right| \cos^4\Theta d\cos\Theta = \tag{15}$$

$$= -\frac{\xi qs}{\pi\Omega h^2} \cdot 2\pi \left(\frac{c\tau}{2h}+1\right)^{-4} \cdot \frac{1}{\Phi'_{\cos}} = \frac{\xi}{8} \cdot C \cdot (t+1)^{-6},$$

where $C = \frac{qsc}{\Omega h^3}$.

The temporal course of this function, as we see, does not depend on the quantity of foam, but only on the altitude h, while its shape expressed through dimensionless time is invariable.

On the whole, consideration for foam on the surface results in summation of the two ITF obtained above. We will compare their amplitudes (having dimensionality of power):

$$m_{\max} = \frac{0{,}02qSc}{8\pi\sigma_x\sigma_y\Omega} \cdot \frac{1}{h^3} . \tag{16}$$

$$m_{1\max} = \frac{1}{8}\frac{qSc}{\Omega} \cdot \frac{1}{h^3} \tag{17}$$

We note that with $\sigma_x \sigma_y \to 0$, i.e., in complete calm, the amplitude m_{1max} will not at all approach ∞, since in this case S cannot be considered a finite quantity.

The order of the quantity $\sigma_x\sigma_y$ for those wind velocities when foam develops, is $\sigma_x\sigma_y = 0.01$, while the numerical multiplier before the expression for m_{max} about 0.08 --

this quantity will almost always be greater than ξ. It follows from here that the amplitude of the reflected signal will always be formed by the mirror reflection from the area, and not by diffused scattering by foam. However, drop in the pulse with some noticeable quantity of foam will be governed by the latter. One can judge the quantity of foam on the water surface from the degree of widening of the pulse.

We will examine in more detail the case of low wind velocities in which foam-formation is insignificant.

Calculation of the values for the width of the function $m(\tau)$ in them with level 0.5, e^{-1}, 0.1 and 0.01 from the maximum, resulted in values presented in the table for different flight altitudes. The dependence of σ_x^2 on W is given from [4].

TABLE OF WIDTH OF REFLECTED PULSE IN ns.

h м	W м/s	2,6	7	Level
	σ_x^2	0,005	0,0075	
50		1,2	2,4	0,5
		2,0	4,0	e^{-1}
		3,8	7,6	0,1
		7,7	16,5	0,01
100		2,3	4,7	0,5
		4,0	8,0	e^{-1}
		7,6	16,3	0,1
		15,5	31	0,01
200		4,7	9,4	0,5
		8,0	16	e^{-1}
		15,3	30,6	0,1
		31	62	0,01
300		7,1	14,1	0,5
		12	24	e^{-1}
		23	45,9	0,1
		46,5	93	0,01

By using the data of this table, or formula (11) one can estimate the dispersion of surface deviations (with wind velocities not exceeding 7 m x s^{-1}) by widening of the short light signal reflected by the surface.

In the Baltic summer expedition of 1977, an experimental verification was made of the method. A system including a laser on AIG with Nd and receiver with high temporal resolution was used as the helicopter lidar. The laser beam was defocused by the lens in limits of~ 20° to the side and the receiver had the same visual field. Measurements were made at $\lambda = 1.06$ μm.

The measurements of the dispersion of inclinations of the surface elements /223 according to temporal expansion of the reflected pulse were made at different flight altitudes (from 100 to 500 m). An example of the obtained pulses is given in Figure 3, which schematically presents the initial pulse (1) and the pulse reflected from the surface from altitude 200 m (2). There is a noticeable increase in the width of the reflected pulse because of the more gently sloping decline. With an increase in flight altitude, a further expansion of the pulse is observed which corresponds to the presented theory. Evaluation of dispersion of the inclinations yielded the quantity $\sigma_x^2 = 0.05 - 0.006$. This approximately corresponds to that calculated in [4] with the given wind velocity. It should be stipulated that wind velocity was measured not directly at the point of observation, but on the shore, a distance of several kilometers. This circumstance does not make it possible to use the experimental results to evaluate the accuracy of the method. It is further necessary to make simultaneous measurements of wave action by long-range and contact methods.

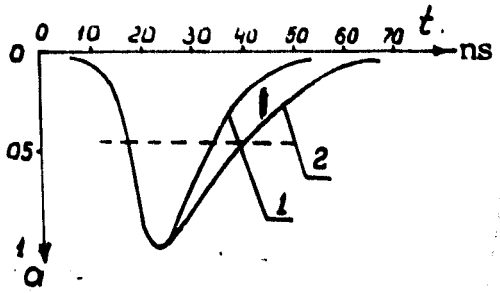

Figure 3. Example of Obtained Pulse Reflected by the Sea Surface (2) and Illustrated Together with the Original Pulse (1).

BIBLIOGRAPHY

1. Zakharov, V. M.; Pavlov, V. N.; and Rokotyan, V. E. "Determination of Geometrical Elements of the Sea Surface with the Help of a Laser Locator," Trudy TsAO, No 105, 1973.

2. Gol'din, Yu. A.; Kagayn, V. E.; Kel'balikhanov, B. F.; Pelevin, V. N. "Location of Disturbed Sea Surface with the Help of Lasers from a Helicopter," Opticheskiye metody izucheniya okeanov i vnutrennikh vodoyemov ["Optical Methods of Studying the Ocean and Internal Reservoirs"], Izd-vo Nauka, Siberian Department of the USSR Academy of Sciences, Novosibirsk, 1978.

3. Gurevich, G. S. "Laser Method of Determining Certain Statistical Characteristics of Sea Wave Action," IV Vsesoyuznyy simpozium po lazernomu zondirovaniyu atmosfery. Tezisy doklaqov ["Fourth All-Union Symposium on Laser Sensing of the Atmosphere, Summaries of Reports"], Tomsk, 1976.

4. Pelevin, V. N.; and Burtsev, Yu. G. "Measurement of Inclinations of Elementary Surfaces of a Disturbed Sea," in Opticheskiye issleqovaniya v okeane i atmosfere nad okeanom ["Optical Studies in the Ocean and Atmosphere Above the Ocean"], P. P. Shirshov Institute of Oceanology of the USSR Academy of Sciences, Moscow, 1975.

LASER METHOD OF MEASURING DISPERSION OF DEVIATIONS OF DISTURBED SEA SURFACE. STEMKOVSKIY, A. I. /224

A method is suggested for measuring the dispersion of inclinations of a disturbed sea surface with the help of a laser located on a flight craft. It consists of comparing power of two pulses of nanosecond duration reflected from the sea surface at different angles. Calculations of the optimal measurement conditions are presented.

Publications [1, 2, 3, 9] have established the appearance of statistical distribution of surface elements of a disturbed sea according to the values of deviations. The value of dispersion of this distribution is necessary in order to solve a number of tasks of acoustics and optics of the sea, in particular, to calculate light fields under a disturbed sea surface [6].

In order to determine the dispersion of deviation, radar [5] and aerial stereophotography of the sea surface are used [7]. However, it is common knowledge that radar methods have lower resolution as compared to optical, while processing of aerial stereophotographs requires considerable time expenditures.

Publication [4] describes a method for determining dispersion of deviations by the increase in duration of the diverging laser pulse of infrared light of nanosecond duration during reflection from the sea surface.

This article describes a method for determining the dispersion of deviations based on a comparison of the powers of two laser IR-pulses of nanosecond duration reflected by the sea surface at two different angles. The sources of the pulses and the receiver were arranged next to each other on board a flight vehicle. The original pulse was divided with the help of a divider into two. One pulse was aimed on a vertical towards the surface ($\theta_1 = 0$), while the second at angle θ_2 (see the figure). Consequently, the reflected pulses fall on the receiver at a different time. So that the pulses are not superposed on the oscillogram, and so that they can be compared in amplitude, it is necessary for the difference in the paths traversed by the pulses to exceed their duration. Since this difference in the course is determined by the size of the angle θ_2, the following conditions are placed on it

$$\left(1+\frac{c\cdot\tau}{2h}\right)\cdot\cos\theta_2<1 \qquad (1)$$

where c--light velocity;

τ --duration of pulses;

h--altitude of source of radiation and receiver above the sea. For example, with τ = 10 ns and h = 100 m, the angle $\theta_2 \geq 8.5°$.

The amplitude values for the powers of the first and second pulses after reflection are determined as follows:

$$m_1=\frac{1}{4}q_1\cdot F_h\cdot Q_1(0;\ 0)\cdot\Delta\theta_1 \qquad (2)$$

$$m_2=\frac{1}{4}q_2\cdot F_h\ Q_2(\eta_x;\ \eta_y)\cdot\Delta\theta_2 \qquad (3)$$ /225

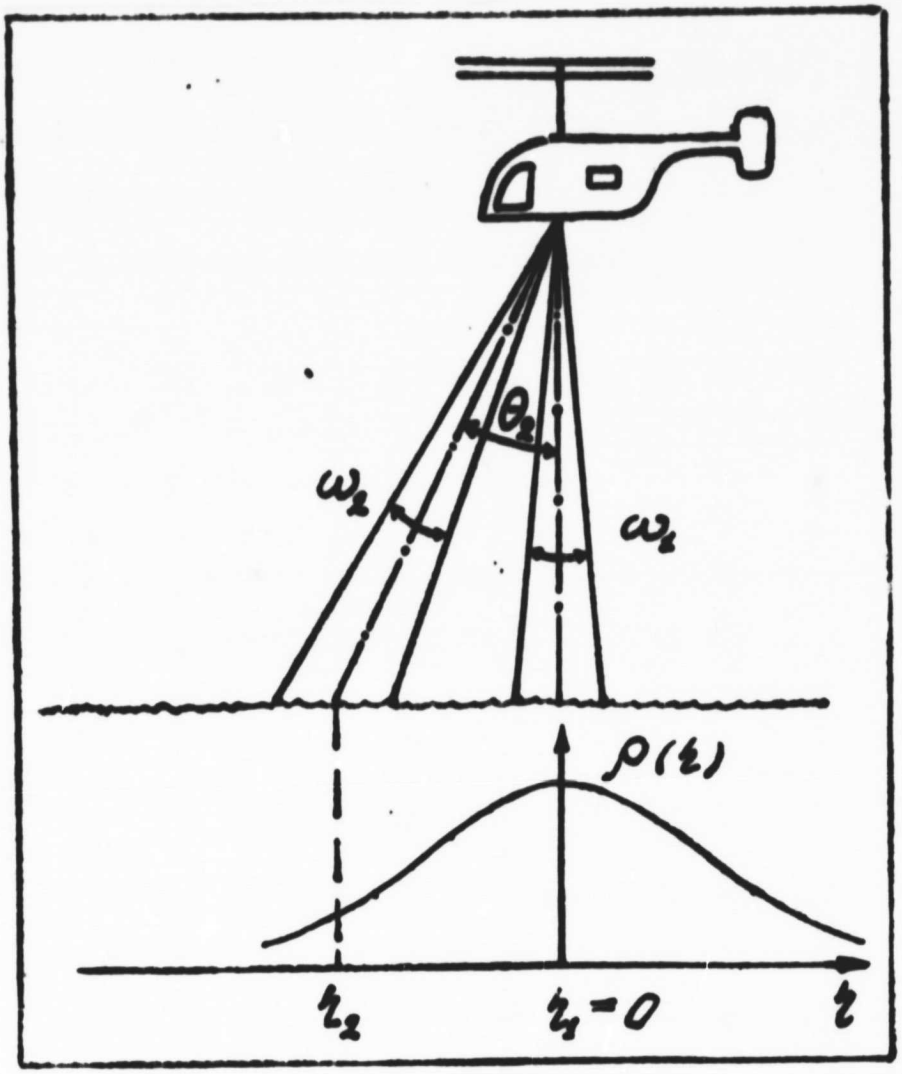

Figure 1. Plan of Sensing Sea Surface and Distribution of Deviations in Sensing Plane. Here $\rho(\eta)$ designates the distribution in direction of wind $Q(\eta_x; 0)$ or transverse $Q(0; \eta_y)$.

where q_1 and q_2--powers of pulses before reflection; F_n--coefficient of reflection according to Fresnel,

$Q(\eta_x; \eta_y)$--density of probability of distribution of deviations which has the appearance (3) suggested in [9] and pinpointed in [2].

$$Q(\eta_x; \eta_y) = \frac{1}{2\pi\sigma_x\sigma_y} \cdot \exp\left[\frac{\eta_x^2}{2\sigma_x^2} - \frac{\eta_y^2}{2\sigma_y^2}\right], \quad (4) \qquad /226$$

where $\eta_x = tg\Theta_x$; $\eta_y = tgQ_y$; Q_x and Q_y--angles of inclinations from vertical in two mutually perpendicular planes, one of which is oriented in direction of the wind;

σ_x^2 and σ_y^2--dispersions of deviations;

$\Delta 0_1$ and $\Delta 0_2$--solid angles at which the inlet opening of the receiver is visible from the reflection point.

$$\Delta 0_1 = \frac{S_{re}}{h^2}; \qquad \Delta 0_2 = \frac{S_{re} \cdot \cos^3\Theta_2}{h^2},$$

where S_{re}--area of input opening of the receiver.

Assuming that at the sites of reflection of the pulses, the dispersions are the same, we will write a logarithm for the ratio of (2) to (3) in the form

$$\frac{\eta_x^2}{2\sigma_x^2} + \frac{\eta_y^2}{2\sigma_y^2} = \ln \frac{m_1}{m_2} + \ln k + 3\ln \cos\Theta_2, \tag{5}$$

where k designates the ratio q_2/q_1.

Determination of the unknown quantity (σ_x, σ_y) from equation (5) is possible when wave action is isotropic $\sigma_x^2 = \sigma_y^2$, or the direction of the wind is known. In the latter case, we will assume either $\eta_x = 0$, or $\eta_y = 0$. The following equation will be common for these cases

$$\frac{\eta_x^2}{2\sigma^2} = \ln \frac{m_1}{m_2} + \ln k + 3\ln \cos\Theta_2 \tag{6}$$

which contains only one unknown, designated as σ^2.

During photographic recording of pulses from the oscillograph screen, and subsequent processing of the oscillograms, it is convenient to select the parameter k such that

$$\ln k + 3\ln \cos\Theta_2 = 0$$

With $\Theta_2 = 10°$, the parameter k = 1.05. Then $\sigma^2 = \frac{\eta_2^2}{\ln m_1 - \ln m_2}$

It will be convenient to use this expression in logarithmic reception of the signals.

Measurement of σ^2 can be automated by controlling the quantity of parameter k such that the condition $\ln \frac{m_1}{m_2}=0$ is fulfilled all the time. In this case, from /227 (6) by using the correlations

$$\cos\Theta_2=\frac{1}{\sqrt{1+\eta_2^2}};\quad \ln(1+\eta_2^2)\approx\eta_2^2,$$

we obtain

$$\sigma^2=\frac{\eta_2^2}{2\ln k-3\eta_2^2}.$$

We will trace the dependence of the power of the second impulse on the altitude, with regard for the fact that

$$\eta_2^2=\left(1+\frac{c\tau}{2h}\right)^2-1. \tag{7}$$

This equality can be obtained from the condition (1). It is apparent from it that the relationship between η_2^2 and h with $h \gg c\tau$ is inversely proportional. Thus, with low altitudes, the angle Θ_2 must be large. The power of the second impulse in this case will be small because of the low probability of reflection at large angles. With high altitudes the power will also be low, since it diminishes inversely proportional to the square of the altitude. Consequently, there is an altitude at which the second pulse has the maximum power on the condition of separate reception with the first impulse.

We will rewrite equation (3) in the form

$$m_2\sim h^{-2}\cdot(1+\eta_2^2)^{-\frac{3}{2}}\cdot\exp\left[\frac{\eta_2^2}{2\sigma^2}\right]$$

We will replace in it η_2 according to (7) and will solve the task for finding the extreme. As a result, we can pass to the equation

$$t^3+2t^2+(1+\sigma^2)t-2\sigma^2=0$$

where $t = c\tau/2h$. Since $\sigma^2 \ll 1$, we can write

$$t^3+2t^2+t-2\sigma^2=0.$$

The only actual root of this equation lies in the interval $[\sigma^2;\sigma]$. Because of the smallness of the root, it can be found from the equation

$$t-2\sigma^2=0$$

from which

$$h_0 \approx \frac{c\tau}{2\sigma^2},$$

where h_0--optimal altitude of sensing. With τ = 10 ns, h_0 = 50 m for $\sigma^2 = 14.6 \times 10^{-3}$ (wind velocity W = 6.0 m/s); h_0 = 280 m for $\sigma^2 = 2.7 \times 10^{-3}$ (W = 1.8 m/s). The value of σ^2 here and below is taken from [2].

We will examine the basic sources of errors in this method. Random error of /228 measurements of dispersion can be computed according to the following formula

$$\frac{\Delta\sigma^2}{\sigma^2} = \frac{4\cdot\Delta\theta_2}{\sin 2\cdot\theta_2} + \frac{2}{\ln z}\cdot\frac{\Delta k}{k} + \frac{2}{\ln z}\cdot\frac{\Delta\left(\frac{m_1}{m_2}\right)}{\left(\frac{m_1}{m_2}\right)}, \quad (8)$$

where

$$z = \frac{m_1}{m_2}\cdot k\cdot\cos^3\theta_2 = \exp\left[\frac{\eta_2^2}{2\sigma^2}\right]$$

Inz = 2 with optimal values h and η_2.

It is apparent from (8) that instability of the source does not influence the accuracy of determining dispersion. Decrease in measurement accuracy can occur because of fluctuations in the quantities m_1 and m_2, which may be observed during reflection of the entire incident power of the beams from small angles of the disturbed surface. It is known from [3, 10] that these fluctuations diminish both with an increase in the illuminated area and with a rise in irregularity of the sea surface. Thus, sufficient measurement accuracy of dispersion can be reached by

reducing the level of fluctuations with an increase in divergence of the beam or increase in the measurement altitude. By knowing the law for distribution of fluctuations and the dependence of the parameters of this distribution on the dimensions of the reflecting field and the characteristics of wave action, one could compute the optimal solid angle ω_1 and ω_2 occupied by the beam. However, the authors did not know this information.

The second factor which significantly influences the accuracy of dispersion measurement is foam on the sea surface. When there is foam, part of the reflected signal will be governed by reflection from the mirror areas, and part by the diffused reflection in the foam. For both pulses one can write

$$\mu_1 = (1-\xi_1)\cdot m_1 + \xi_1 \cdot m_1'$$
$$\mu_2 = (1-\xi_1)\cdot m_2 + \xi_1 \cdot m_2'$$

where ξ_1--percentage of surface covered by foam.

For signals from foam which we will consider a Lambert emitter, expressions are obtained (see [8])

$$m_1' = \frac{\xi_2}{\pi}\cdot q_1 \cdot \Delta\Theta_1 \cdot \overline{\cos}_1\delta$$
$$m_2' = \frac{\xi_2}{\pi}\cdot q_2 \cdot \Delta\Theta_2 \cdot \overline{\cos}_2\delta$$

where ξ_2--coefficient of foam reflection;

$\overline{\cos}_1\delta$ and $\overline{\cos}_2\delta$--average cosines of reflection. With $\sigma^2 = 0$ $\overline{\cos}_1\delta = 1$ and $\overline{\cos}_2\delta = \cos\Theta_2$ must be true.

We will find the ratio of μ_1 to μ_2, and will transform it to the following /229

$$\frac{\mu_1}{\mu_2}\cdot k\cdot\cos^3\Theta_2 = \frac{Q_1 + V\cdot\overline{\cos}_1\delta}{Q^2 + V\cdot\overline{\cos}_2\delta} = Z$$

where

$$V = \frac{1}{\pi}\frac{\xi_2}{F_r}\cdot\frac{\xi_1}{1-\xi_1}.$$

If Z is presented in the form of $\exp\left[\frac{\eta_3^2}{2\sigma_\eta^2}\right]$, then

$$\sigma_p^2 = \frac{\gamma_3^2}{2\sigma_p^2 Z},$$

where σ_p^2--pseudodispersion of deviations, since this quantity is not the dispersion of true distribution of deviations, and depends on the parameter V, dispersion of true distribution of σ^2 and the size of the angle θ_2. Tables I and II illustrate the dependence of the pseudodispersion on ξ_1 and θ_2. We assume $\xi_2 = 1$ and $F_h = 0.02$.

TABLE I. WITH $\overline{\cos_1\delta} = 1$, $\overline{\cos_2\delta} \approx 1$, $\sigma_2 = 5{,}4 \cdot 10^{-3}$ & $\theta_2 = 6°$.

ξ_1 (%)	1	5	10	20	30
σ_η^2/σ^2	1.04	1.15	1.36	1.80	2.20

The limiting value ξ_1 according to [11] equals 30%.

TABLE II. WITH $\sigma_2 = 7{,}9 \cdot 10^{-3}$ & $\xi_1 = 10\%$.

θ_2	6°	7°	8°	9°	10°
σ_p^2/σ_η^2	1.27	1.61	1.72	1.84	2.00

CONCLUSIONS AND RECOMMENDATIONS

1. The examined method for determining dispersion of deviations is adopted if the distribution of deviations is subordinate to a normal law, i.e., the wind velocities are not too great.

2. With nonisotropic wave action, the plane of sensing (plane in which both beams lie) must be oriented initially in the direction of the wind, and then in a transverse direction to it. /230

3. The azimuth of these two directions can be determined from the maximum and minimum signal reflected at angle θ_2, during rotation of the sensing plane.

4. There is an optimal altitude which depends on the dispersion of deviations at which it is recommended that measurements be made.

5. In order to reduce systematic error introduced by foam in measurement of dispersion, it is recommended that sensing be done with the smallest possible angles.

6. Measurement of dispersion can be done with the help of a laser of continuous action, covering vertical and inclined beams in turn.

In conclusion the author expresses his gratitude to Vadim Nikolayevich Pelevin for statement of the task and discussion of the results.

BIBLIOGRAPHY

1. Tsiplukhin, V. F.; Martsinkevich, L. M. "Study of Probability Characteristics of Inclinations of Disturbed Sea Surface," FAO, vol 9, No 7, 1973.

2. Pelevin, V. N.; and Burtsev, Yu. G. "Measurement of Inclinations of Elementary Surface Areas of a Disturbed Sea," Opticheskiye issledovaniya v okeane i v atmosfere nad okeanom ["Optical Studies in the Ocean and in the Atmosphere Above the Ocean"], works of the Institute of Oceanography of the USSR Academy of Sciences, 1975.

3. Lebed'ko, Ye. G.; Pokrovskiy, Yu. P.; Porfir'yev, L. F. et al. "Probability Characteristics of Reflection of Pulse Optimal Signals from Disturbed Water Surface," Priborostroyeniye, No 8, 1976, pp 109 - 113.

4. Pelevin, V. N. "Method of Locating Disturbed Sea Surface by Diverging Light Pulse," this collection, 1979.

5. Gernaker'yan, A. A. et al. Radiolokatsiya morskoy poverkhnosti ["Radiolocation of the Sea Surface"], 1978.

6. Kozlyaninov, M. V.; Kopelevich, O. V.; Ochakovskiy, Yu. Ye.; and Pelevin, V. N. "Modern Problems of Sea Optics," Teoreticheskiye i prikladnyye problemy rasseyaniya sveta ["Theoretical and Applied Problems of Light Scattering"], ed. by B. I. Stepanov and A. P. Ivanov, 1971.

7. Martsinkivich, L. M. "Study of Statistical Characteristics of Deviations of a Disturbed Sea Surface from Aerial Surveys of Stereophotography of Waves," Meteorologiya i gidrologiya, No 11, 1970.

8. Sapozhnikov, R. A. Teoreticheskaya fotometryia ["Theoretical Photometry"], 1977.

9. Cox, Ch; and Munk, W. "Slopes of the Sea Surface Deduced from Photographs of Sun Glitter," Bull. of the Scripps Inst. of Oceanogr., 1956, vol 6, No 9.

10. Jelalian, A. V. "Sea Echo at Laser Wavelengths," Proceedings of the IEEE, vol 56, No 5, 1968.

11. Ross, D. B.; and Cardone, V. "Observation of Oceanic Whitecaps and Their Relation to Remote Measurements of Surface Wind," J. Geophys. Res, 79(3), 1974, pp 444-452.

MEASUREMENT OF CURVATURE DISTRIBUTION OF SURFACE ELEMENTS OF A DISTURBED SEA. YU. G. BURTSEV, AND V. N. PELEVIN /231

Estimates are given for the curvature of small sections of a disturbed sea surface obtained by the method of photographing a system of flashes when the sea is illuminated by an artificial light source.

Measurements of the curvature of small sections of a disturbed water surface were first made by A. Scooly [1] under laboratory conditions. We used the method of A. Scooly in measurements on the sea.

The essence of the method is photographing with a short time lag a system of flashes created on the surface of the sea by a light source of finite dimensions. Orientation of the photo equipment and the course of the beams are identical [2]. Primary processing of the materials consists of measuring the distribution of density spots on the film according to the dimensions with the help of a microscope. The curvature of the reflecting surface elements is further computed with the help of the formula

$$g = \frac{RLf}{2H^2} \qquad (1)$$

where g--dimension of flash on the film;

R--radius of curvature of the surface element forming the flash,

L--diameter of the light source,

f--focal distance of the camera,

H--altitude of the camera above the sea surface.

Measurements were made in the open sea from a ship, from a fixed scaffold at a distance to 400 m from the shore, near the shore from a pontoon during implementation of the "Chernomor" program in the southern department of the Institute of Oceanography of the USSR Academy of Sciences. During the experiments, measurements were made of the density functions of the probability $P_W(R^{-1})$ for distribution of surface elements by curvature R^{-1} with different values of wind velocity W above the surface, in the interval 1.0 - 8.0 m/s.

Distributions $P_W(R^{-1})$ have the appearance of curves with one maximum whose position depends on wind velocity of the surface. The maximum of the curves does not go beyond the limits of the range of values of curvature 4 - 7 x 10^{-2} cm^{-1}. This corresponds to the radii of curvature 25 - 14 cm. The distributions are asymmetrical. The right branches (region of larger values of curvature) are more gently sloping.

The average values of curvature R_{cp}^{-1} increased with a rise in wind velocity. With W > 3.5 m/s, the experimental points are satisfactorily described by the regression line

$$R_{cp}^{-1} = (-1{,}26 + 2{,}3W) \cdot 10^{-2} \cdot см^{-1}, \qquad (2)$$

obtained by the method of least squares. The standard deviations for values of curvature σ_K with W > 3.5 m/s increased linearly with wind velocity. The regression line /232 obtained by the method of least squares corresponds to the relationship

$$\sigma_K = (-4{,}13 + 1{,}23W) \cdot 10^{-2} \cdot см^{-1} \qquad (3)$$

The equations of linear regression computed by A. Scooly for the quantity R_{cp}^{-1} with σ_k indicate the more rapid increase in the quantity with the increase in wind velocity. Since the experimental conditions of A. Scooly in this work significantly differ, while as far as we know no other experiments have been made to measure curvature of elements of the sea surface, then it is not possible to make satisfactory comparison of the data.

Measurement errors in $P_W(R^{-1})$ when working according to this technique are formed of a) erroneous measurements of g on the microscope; b) errors caused by the use of a simplified expression; c) errors developing because of inaccurate value of the altitude of the camera above the disturbed surface.

Evaluation of the quantity of these errors yielded as a sum the error of computing R_{cp}^{-1} for the given range W not exceeding 30% of the measured quantity.

BIBLIOGRAPHY

1. Scooly, A. H. "Curvature Distribution of Wind-Created Water waves," Trans. Amer. Geophys. Union, vol 36, No 2, 1955.

2. Pelevin, V. N.; and Burtsev, Yu. G. "Measurement of Inclinations of Elementary Areas of the Surface of a Disturbed Sea," in Opticheskiye issledovaniya v okeane i v atmosfere nad okeanom ["Optical Studies in the Ocean and in the Atmosphere Above the Ocean"], Institute of Oceanology of the USSR Academy of Sciences, Moscow.